DEVELOPMENTS IN D.C. DISC MACHINES

Design, construction and performance of permanent magnet axial field motors for traction applications

by

M.R.N. ALI

A Thesis submitted to the University of Warwick for the degree of Doctor of Philosophy based upon research conducted in the Department of Engineering

January 1985

CONTENTS

LIST OF TABLES

LIST OF FIGURES

Acknowledgements

I would like to express my thanks to the following:

To my wife for her continual support and encouragement and my children for their smiles and cheerfulness in times of stress.

To my Academic Supervisor, Mr. A.E. Corbett, for his encouragement, assistance and patience throughout my period of study.

To my friends for their academic support, particularly Chris Roerig, Colin Anscomb and Selami Söylemez.

To all members of the Engineering Department Workshop for their assistance with construction of the motor, particularly Mr. David Thompson.

To Mrs. Penny Mead for converting my manuscript from Arabic English to English English.

To Mr. Michael G. Gould for his photographs which have brought my thesis to life.

Finally, to the many others, too numerous to name here, who have willingly given my their help and advice.

Summary

Axial-field permanent magnet motors have been shown to offer improved efficiency and power density compared with conventional machines. The different aspects of the advantages of permanent magnet disc armature motors have been demonstrated.

A technique is described by which the magnetic circuit is then designed for optimum motor efficiency. The development of criteria for the selection of machine parameters leads to a computer program that produces a realistic design given only the desired power, speed, and voltage as input data. An analytical model has been established to quantitively predict the degree to which the permanent magnet field is demagnetised by the armature current.

A new method for armature construction (skeleton armature) is described which is more satisfactory than encapsulation for the necessary mechanical strength and rigidity.

The high power to weight and high power to volume allows novel locations to be considered for the drive motor within the vehicle, and a new design of axle-mounted twin-rotor machine will also be described. Such relocation, together with belt reduction gear, reduces the weight and power losses associated with other transmission components.

The construction of a vehicle test facility to evaluate the performance of electric and hybrid vehicles is described. The Nova series hybrid vehicle was tested on the rig. The trials showed that the losses in belt drive transmissions were less than those in a conventional transmission.

List of Principal Symbols

Symbols represented as strings of capital letters usually refer to those used in a computer program or associated output.

a	number of parallel paths in a D.C. machine
A	brush contact area
Ac	specific electric loading
α, ALPHA	ratio of pole arc to pole pitch
ARMCRT	armature current
Bi,j	flux density at position (i,j) in polar co-ordinates
Bm,BM	magnet flux density
Bw	magnet flux density at working temperature
Bs	magnet flux density at sub-zero temperature
Br	remanance on demagnetisation curve
C, CRTDSY	current density in armature conductors
C_B	battery capacity
C_D	vehicle drag coefficient
C_c,COILS	number of coils in a D.C. machine
d_1,D1	inner active diameter of disc armature motor
d_2,D2	outer active diameter of disc armature motor
η,EFF	efficiency
E,EP	generated e.m.f.

F_1	tyre rolling resistance
F_2	aerodynamic drag
FRR	flux return ring
G,GAUGE	gauge of wire used in armature
GAP	magnetic airgap length
H_g	magnetising force in airgap
H_m,HM	magnetising force in magnet
I	(armature) current
L,LAY	number of layers of armature conductors
LC,LCOEFF	leakage coefficient
LF,LFACT	loss factor
l_g	length of magnetic airgap
l_m,LMAG	length of magnet
LOSS	electrical losses in disc armature motor
MAGDSY	density of magnetic material
MECHLO	mechanical loss
M_v	mass of road vehicle
μ_o	permeability of free space
μ_r	relative permeability
n	rotational speed, rev/min
w	rotational speed,
p,POLES	number of poles in a D.C. machine
P	power output (gross)
PATHS	number of parallel paths in a D.C. machine
ϕ,PHI	flux per pole
PWRWGT	ratio of motor power to motor weight, power density

ρ	resistivity of copper, density of air
R_a, RAPM	armature resistance
r_1	inner active radius of disc armature motor
r_2	outer active radius of disc armature motor
SF	space factor
T	mechanical torque
TEMP	armature temperature at which motor performance is calculated
THICK	thickness of flux-return ring
T_r	rated torque
TURNS	turns per coil
TOTWGT	total weight of motor
v	speed of road vehicle
V	voltage
V_b	brush voltage drop
WGTFRR	weight of flux-return ring
WGTMAG	weight of magnet
WGTNAP	weight of"non-active parts"
WGTWIR	weight of copper used in armature winding
W_m	mechanical loss
W_e	eddy current loss in armature copper
z.%	number of conductors in an armature
z_i	ideal number of conductors

Chapter 1 Introduction

Oil is running out. It will not be long before this, one of our most precious assets, will pass its supply peak and will start to decline in available volume.

It has powered the greatest technological revolution in history; it is the life-blood of the manufacturing and transport industries, and factors other than short-term commercial interests should decide how remaining supplies are used.

In 1973, OPEC countries took action to conserve oil to ensure that future generations are not left without, and this action will be increased by both producers and consumers during this next decade.

A full study[1] of the problem of reducing petrol consumption shows that it is in the transport sector, in particular road transport, (where 79% of the petrol is used), that the largest petrol saving will be made.

The goal of reducing the amount of petroleum demand in road transportation, can

be achieved by transferring some of the demand to more plentiful energy sources such as coal or nuclear sources. Electric vehicles can satisfy this requirement because all their energy needs may be obtained from central electricity power stations which may use these alternative fuels. However, the energy advantage of electric cars is obtained at the expense of several performance characteristics. Range, acceleration, hill climbing ability and usually maximum speeds are reduced compared with those obtained by conventionally powered vehicles.

A hybrid vehicle which uses two sources of energy has the potential of reducing petroleum dependence to a lesser degree than an electric vehicle but its performance is more like the conventional vehicle than that of the poorer performing electric vehicle. Furthermore, the hybrid vehicle can still operate as an all-electric vehicle, but at lower performance levels. Until recently, hybrid vehicles were designed to reduce emissions, rather than to minimise petroleum

consumption. However, the present interest in hybrids is because of the reduction in on-board petroleum consumption. Therefore, nowadays hybrid vehicles have been designed to serve as transitions between conventional and the all-electric vehicle. Thus, manufacturers of certain hybrid vehicles will allow a gradual change-over in manufacturing processes. As progress is made, these hybrids will be built with smaller and smaller engines and will use batteries of gradually increasing capacity. Hence, the hybrid vehicle is essentially an all-electric vehicle loaded with an ideal battery system which, in this case, is represented by the on-board engine generator set. Therefore, the engine generator is a temporary solution until the promised breakthrough in traction-battery design occurs.

The impression thus gained, is that the only current problem is the development of a high performance traction-battery. This is inaccurate because the existing electric and hybrid vehicle consists of limited

production vehicles, various experimental vehicles and conversions of conventional vehicles. The component quantities required have not been sufficient to justify extensive development by manufacturing industry. Consequently, designers have had to adapt and modify equipment that was originally not designed for electric and hybrid vehicle applications. This is particularly true for propulsion systems, while electric motors having sufficient power for electric and hybrid vehicles were designed for industrial applications for which weight, size, and part-load efficiency are not critical factors, and for which considerations such as long-life are more important than initial cost. As a result, available traction motors are expensive, inefficient at low power levels, their power density is not optimised, and transmissions are designed around the operating parameters of petrol powered engines. The result is that propulsion systems found in existing electric and hybrid vehicles are characterised by performance below theoretical expectations.

The need is thus demonstrated when considering the design of any new electric and hybrid vehicles of not being restrained by having to use existing I.C.E. vehicle components. However, it is economically much more viable to take as the basis for an electric vehicle some I.C.E. vehicle for which mass production capabilities are already available.

This conflict of requirements is overcome at Warwick University[2,3] by developing a disc motor and transmission that is efficient and will also fit into an existing I.C.E. vehicle chassis with the minimum modification.

Development of the axial-field,[4,5] permanent magnet, DC disc motor has demonstrated significant improvements over conventional machines in terms of efficiency and power density, giving the machine good potential for application in electric and hybrid vehicles. Furthermore, the short axial length and high power/volume ratio of the machine facilitates the design of compact traction systems.

The essential difference between the DC disc motor and its conventional counterpart

lies in the disposition of the active conductors and the working magnetic flux: in the disc motor the magnetic flux is parallel to the shaft and the active conductors are perpendicular to it. This configuration lends itself well to high pole number designs, and the heavy steel yoke of conventional machines is replaced by thin-section steel flux return rings and a light alloy frame. Using permanent magnets it is practicable to employ a coreless armature construction which further promotes weight saving and means that no iron is subject to varying magnetic flux. The absence of iron losses and elimination of the requirement for excitation power are both helpful in the quest for high efficiency.

A twin armature disc motor with differential action has been developed for the drive of an experimental hybrid sports car. This machine comprises a common magnetic circuit which houses two disc armatures, each armature mechanically driving an independent output shaft which transmits power to a road wheel through belt-reduction gearing, thereby

eliminating the need for a mechanical differential gear. The twin armature motor and belt reduction gears have been carefully designed to fit within the limited span between the two road wheels in the space usually occupied by the differential rear axle drive.

Figure 1.1 shows a disc motor employing magnets of the alnico type (Hycomax III). Specifying Hycomax III allows for a moderately high air-gap flux density which leads to very high motor efficiency. Unfortunately the cost of alnico material has increased quite dramatically during the course of the project owing to a large increase in the world price of cobalt, and it is considered that building a traction motor using magnet material of this type will not become widespread in such an application.

In contrast, the cost of ferrite materials is low enough to make its use viable in spite of its low remanence and energy density. For this reason, a machine using ferrite magnets, as shown in Figure 1.2 has been developed. Significant savings in weight and cost result

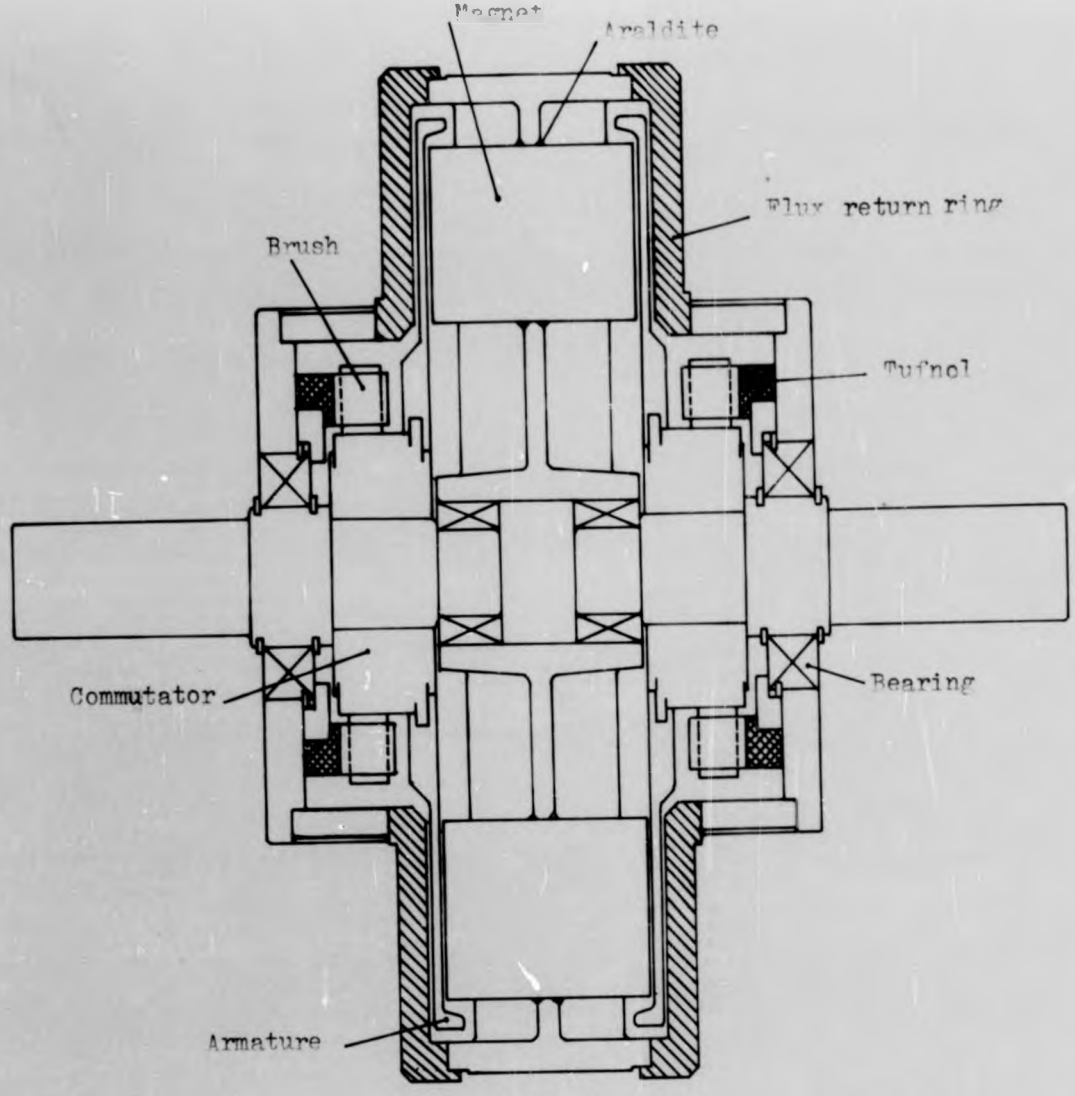

Fig. 1.1 : Twin Rotor Disc Motor using Vycomax 111

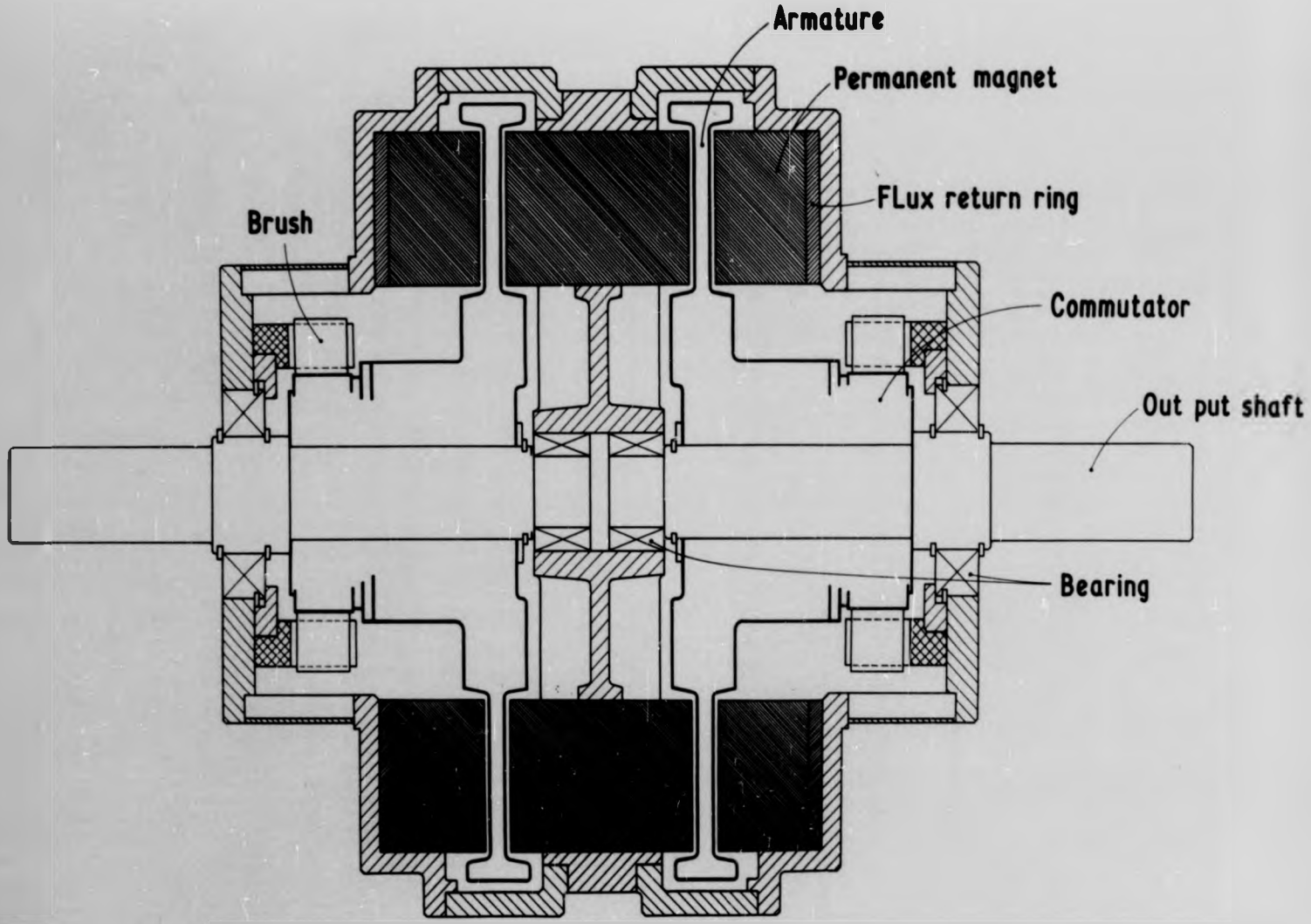

Fig. 1.2 : Twin Rotor Disc Motor using Feroba 111

from adopting the twin-rotor arrangement rather than two separate motors. The vehicle also employs a disc-armature generator having many parts which are common to the motor, as shown in Figure 1.3.

The development of criteria for the selection of all machine parameters has made it beneficial to reappraise the design methods available and highlight aspects of design and performance peculiar to this type of machine.

The principles of the machine have been studied at great length and comparable attention needs to be paid to the magnet behaviour of the machine especially when applied to electric traction. There have been no reliable methods of determining the losses involved and their relationship to the performance of the machine. This is an aspect which required extensive investigation. Although illustrated here for this novel topology for application as a traction motor, the procedures and criteria described could equally be applied to the design of motors for

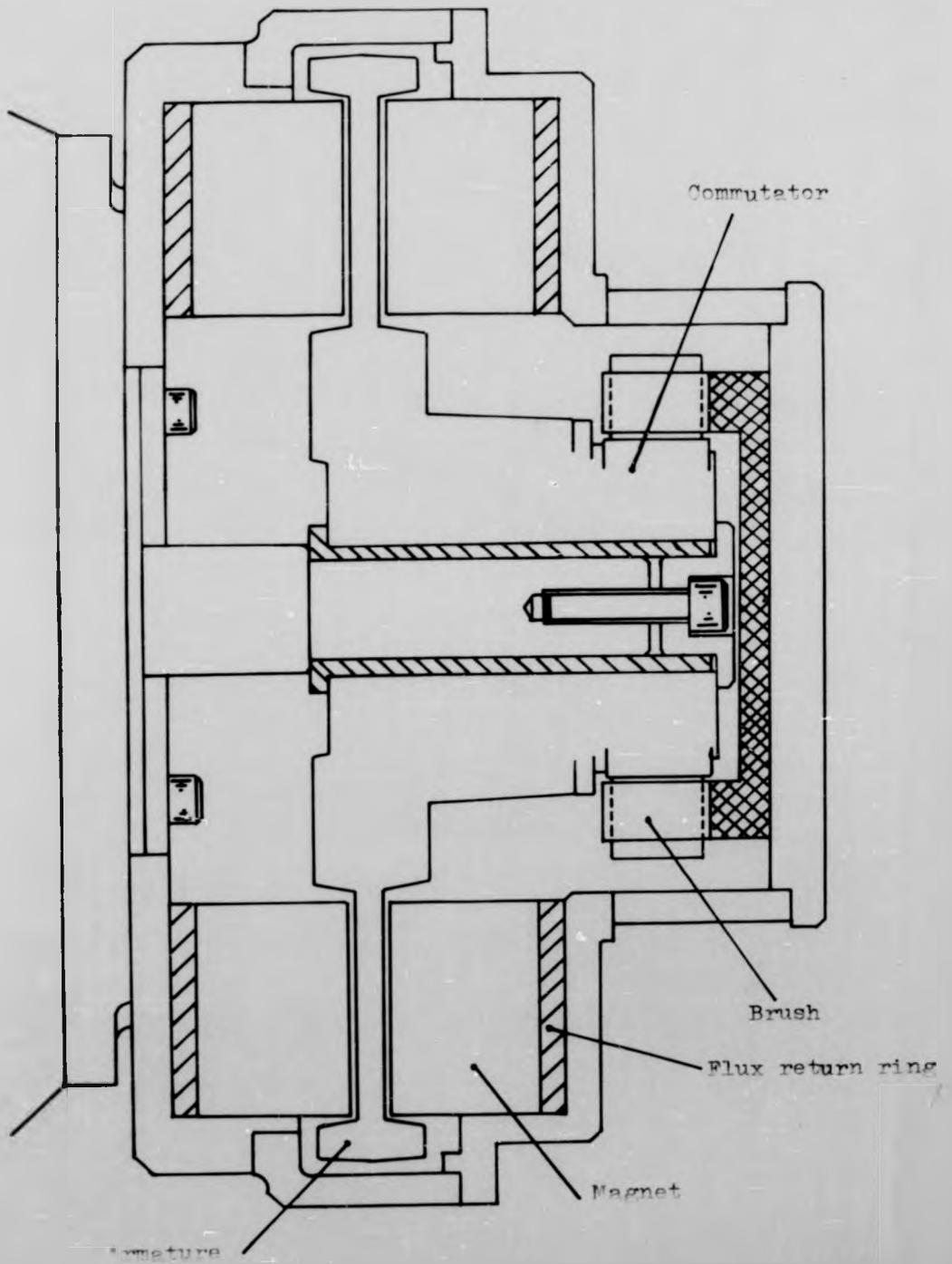

Fig 1.3 - Disc Armature Generator

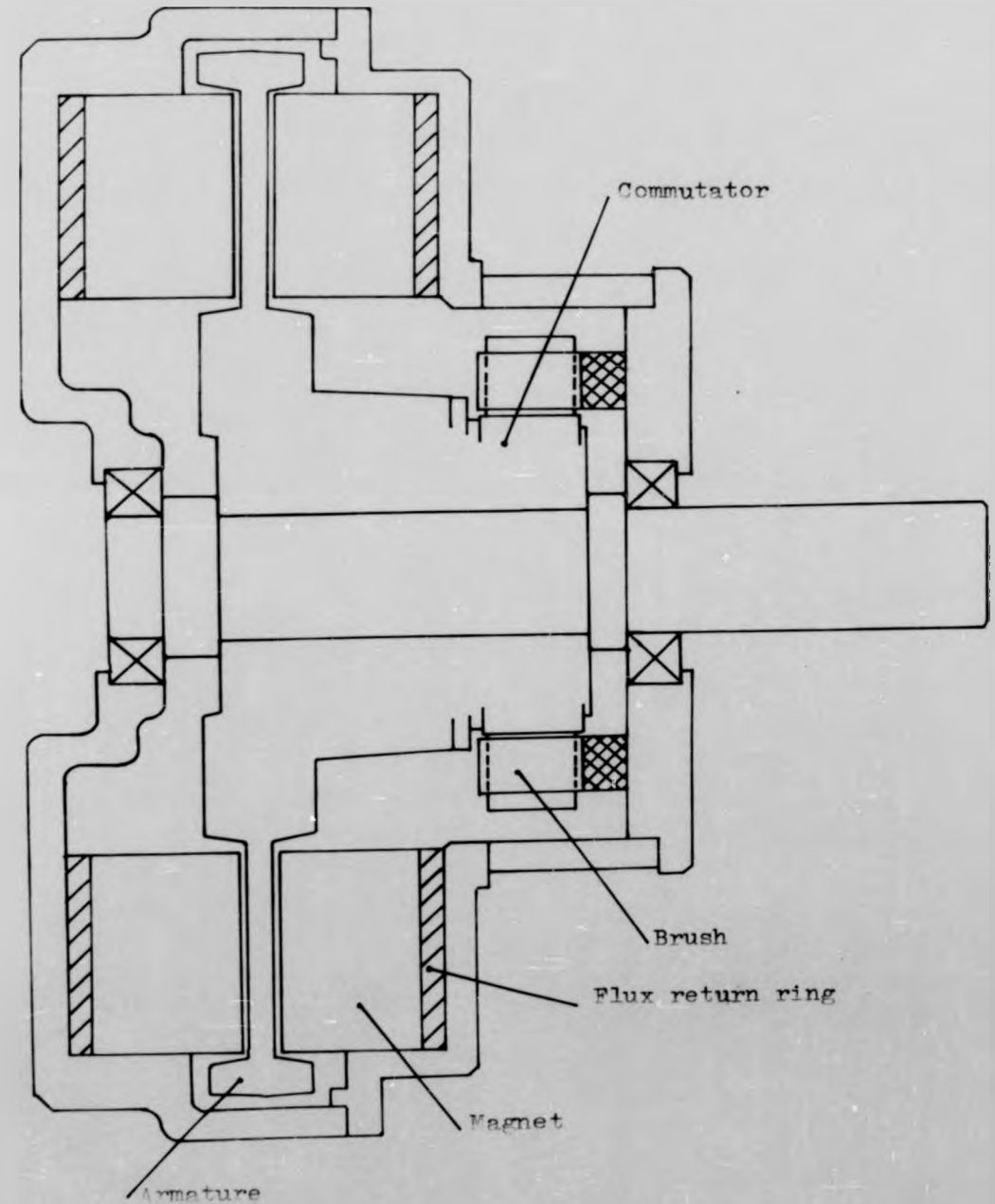

Fig. 1.4 : Single Version Disc Motor

any application. The result is given for a single version motor as shown in Figure 1.4 the measured performance of which compared favourably with predicted performance.

Chapter 2 Principles of the Machine

2.1 Introduction

The axial field DC machine is one of the first machines devised to convert electrical power into mechanical power. Its origin can be traced to disc-type machines conceived and tested by Michael Faraday, the experimenter who formulated the fundamental concepts of electromagnetism. The machine was a copper disc rotated by a spindle in an axially directed permanent-magnetic field, with sliding contacts (brushes) at the edge and centre of the disc, for introducing and/or picking off electrical power as shown in Figure 2.1. Faraday's primitive design was quickly improved, and the multipolar version, in which a winding is rotated in the magnetic field of successive N-S pole-pair, soon followed.

In recent years, the use of DC machines has become almost exclusively associated with applications where the unique characteristics of the DC motor (e.g. high starting torque for traction motor application) justify its cost, or where portable equipment must be run from a DC (or battery) power supply.

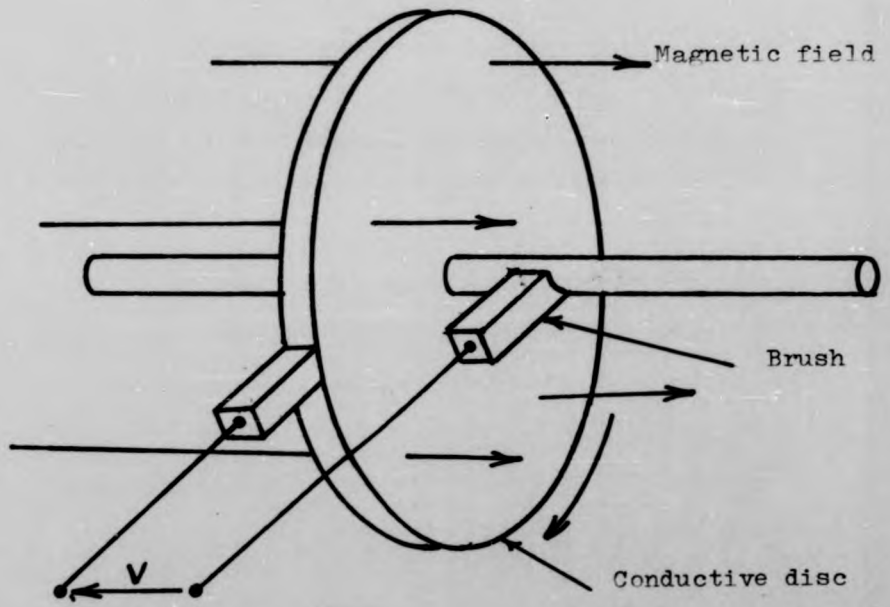

Fig. 2.1 : Schematic of Faraday's disc

The ease with which the DC motor lends itself to speed control has been recognised. Compatibility with the new thyristor (SCR) and transistor amplifiers, plus better performance due to the availability of new improved materials in magnets, brushes and epoxies, has also revitalised interest in DC machines. The need for new high-performance motors with highly sophisticated capabilities has produced a super-abundance of new shapes and sizes quite unlike DC machines of a decade ago.

Most industrial motors have multipolar field systems and a cylindrical shape. There are, however, several other possible forms such as the disc, the linear and the tubular. Further, the homopolar field arrangement (the type of machine built by Faraday) has been developed to provide large current at low voltage for electro-chemical processes. The homopolar shape lends itself to the use of superconducting field windings, by means of which very high working flux densities can be achieved. But whatever the topology of the machine, and be it homo- or multi-polar, the

essential requirement is that a current flows in a direction at right-angles to that of the flux of a permanent or electromagnet in such a way as to utilise most effectively the mechanical force developed by flux-current interaction. The relation between the cylindrical, disc and linear forms is brought out in Figure 2.2 in terms of the conversion region, i.e. the gap between the fixed and moving members. If the cylindrical gap region (a), shown with its d- and q- axes and armature current directions, has its front radius contracted and its rear radius expanded, it becomes the disc form (b); and if, instead, it is cut axially and 'unrolled' the result is the flat linear form (c); and finally if (c) is 're-rolled' into a tube, the linear tube shape (d) is obtained.

Fig. 2.2 : Forms of d.c. machine

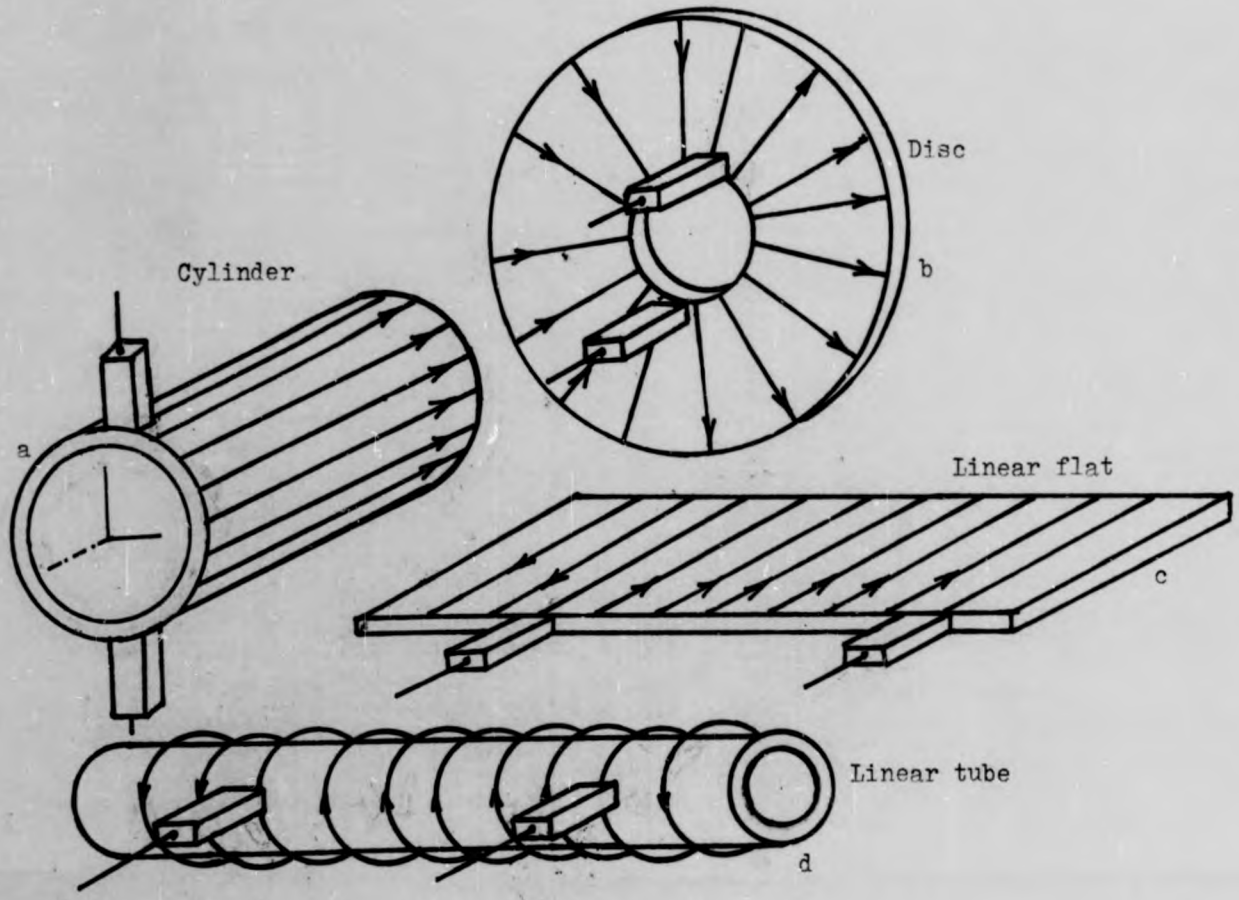

2.2 Improving Efficiency and Performance

In DC motors, power is wasted due to losses associated with the iron core. In conventional designs, these losses are reduced by laminating the rotor core, thus elimination of these losses must serve to increase the motor efficiency. Furthermore, for traction applications, operation at high efficiency over a wide load range is necessary with high power/weight ratio. Meeting these requirements has been accomplished by a variety of designs. Maximising the developed torque and power of the conventional DC machine by use of the new magnetic material has been one method of approach, whilst other types reflect more fundamental changes. Amongst these latter types are those having an iron-less rotor construction. Elimination of all iron losses in this type of motor is accomplished by combining all of the iron structure with the permanent magnet assembly, so that the flux return circuit is stationary on the remote side from the magnets, and inserting the core-less armature conductors into the air-gap.

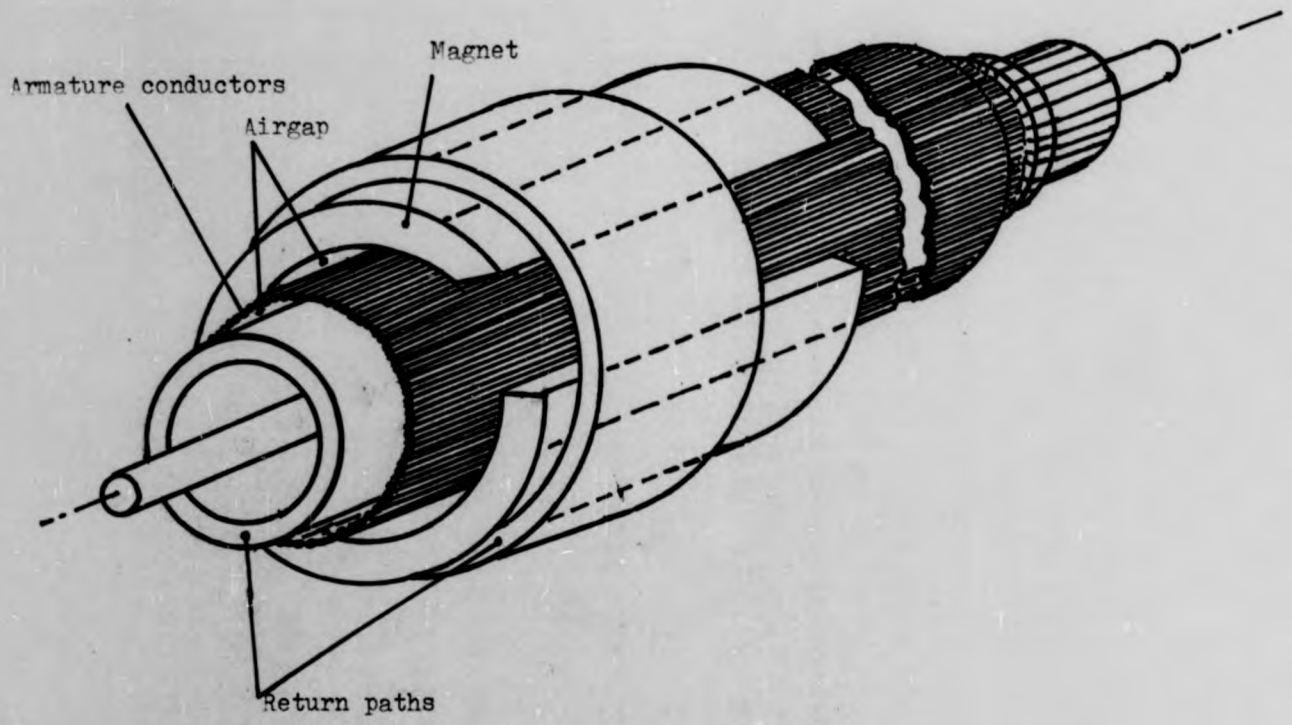

Fig. 2.3 : Shell armature motor

The iron-less (or moving coil) structure design of the present era has followed two general paths: the flat disc armature and the hollow ("shell" or "cup") armature. The two structures are shown in Figures 2.4 and 2.3. Both units have a multitude of conductors which move in a magnetic field. The armature structure is supported mainly by non-magnetic materials and the active conductors are therefore moving in an air-gap with a high magnetic flux density.

The shell-type armature (Figure 2.3) consists of a cylindrical, hollow rotor which is fabricated to form a rigid shell structure by bonding copper or aluminium coils or skeins by the use of polymer resins and fibreglass and other structural members. This method offers considerable flexibility in design since the manufacturer can offer a variety of wire sizes, turns per coil, and diameter and length options.

Due to the unique construction of shell (cup) armature motors which is fixed at one end to the shaft by a plastic disc which also carries the

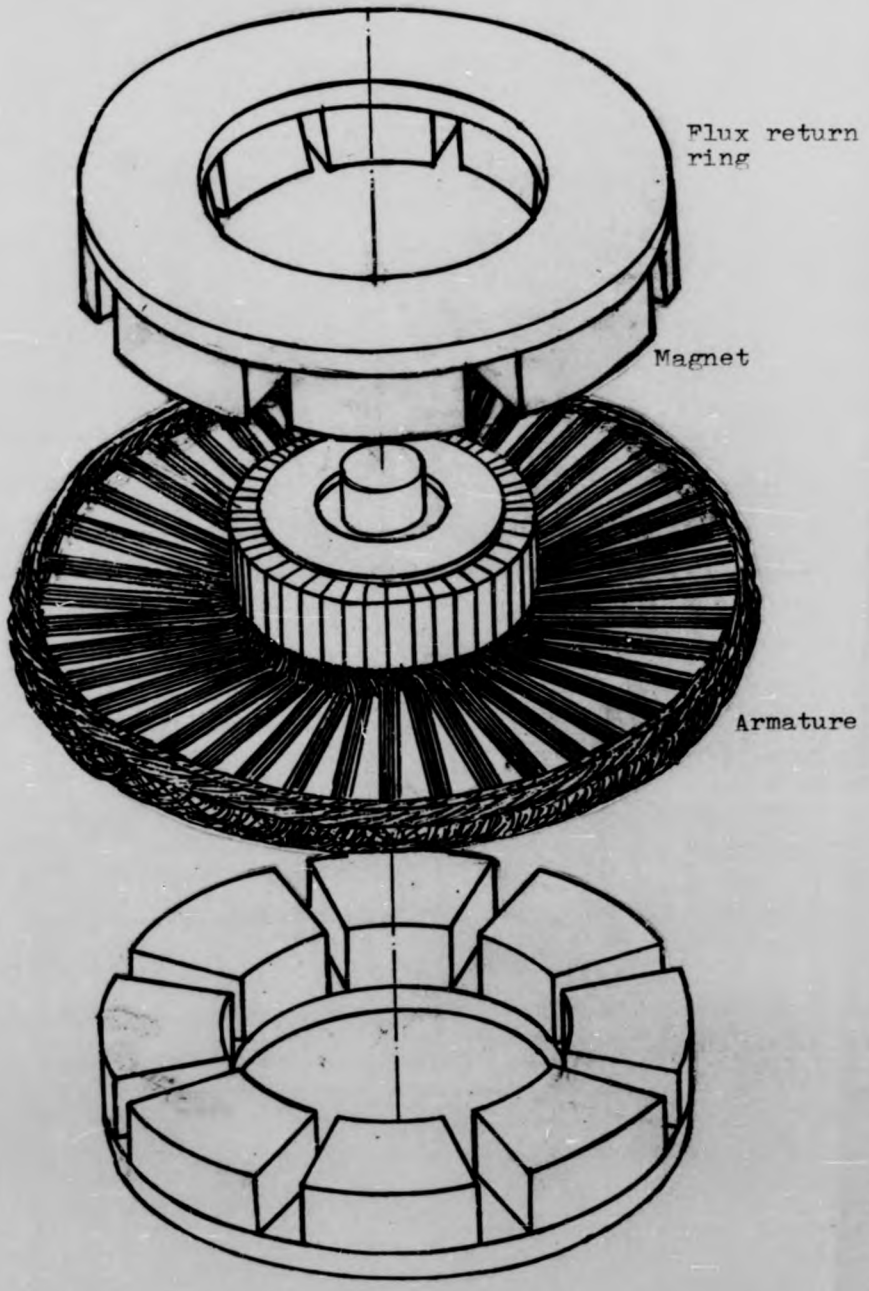

Fig. 2.4 : Disc armature motor

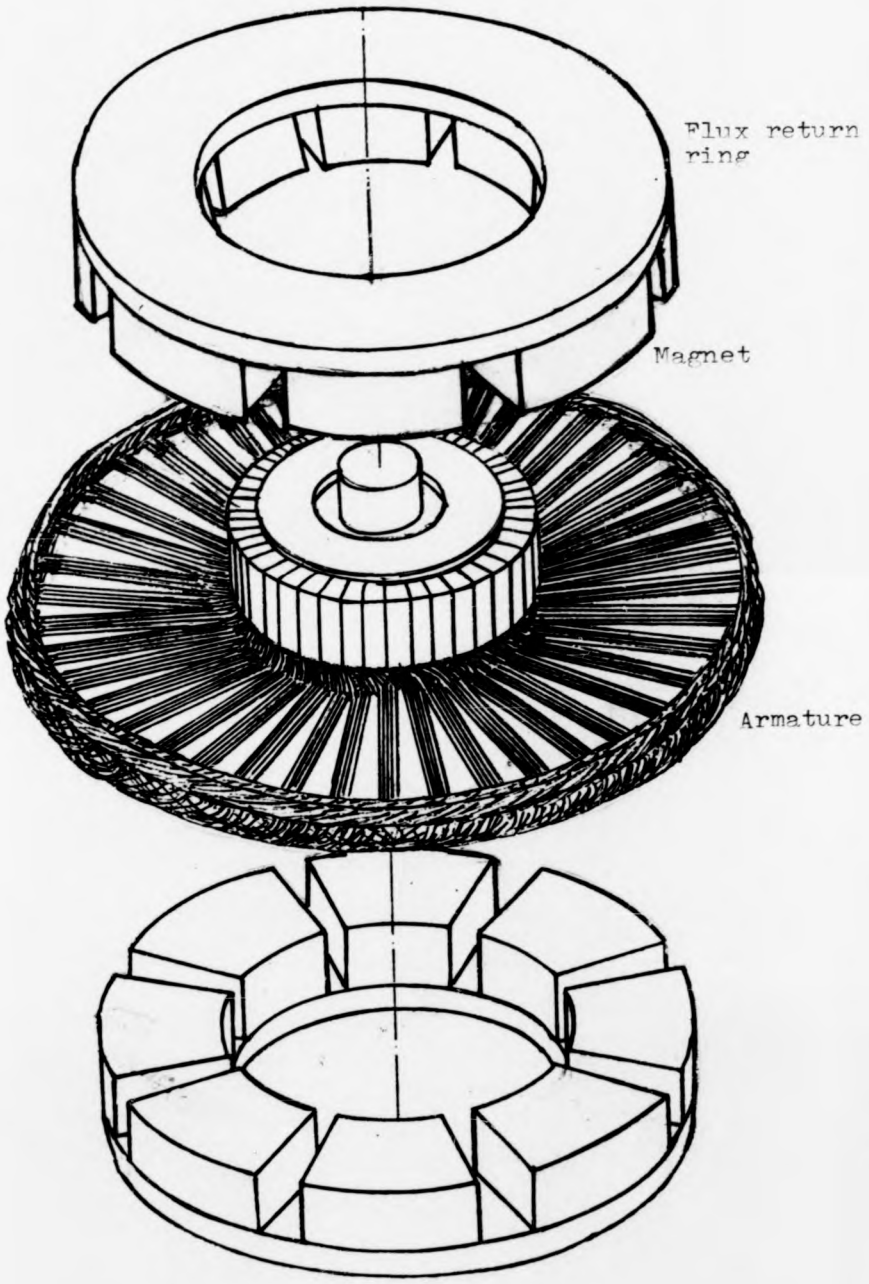

Fig. 2.4 : Disc armature motor

cylindrical commutator, and since plastic parts deflect under torque, the instant velocities of various parts are different, which results in angular vibrations which may cause problems to the user.[6.7] This phenomenon has the effect of limiting the size of this type of motor to under one horsepower. It is found that the cylindrical shell construction of the armature has low mechanical stability, and this limits the overload capability considerably. It is considered that it may not sustain the environmental conditions particularly shock and vibration required in road traction especially if subjected to any emergency overload.

This conflict of requirements is overcome by developing a new motor. This new motor is an axial field DC machine, with a permanent magnet field system. The disc armature motor differs from other axial field machines primarily in respect of its rotor's construction. The active conductors lie radially, and the wire-wound coils are arranged in various ways to give a convenient number of layers. This is

traditionally any even number.

The coils and commutator are given mechanical rigidity by encapsulating in epoxy resin (Figure 5.15) or wrapping with heat-curing glass-fibre tapes and dipped in varnish to give a "skeleton" construction, but since no iron is included in the rotor, an air-gap length of a few millimeters results. This, however, is easily overcome by using permanent magnets of relatively high coercivity.

There are many advantages that result from this particular motor design, and most are found to be desirable in the electric vehicle application. There being no iron in the armature, there will consequently be no core losses. Bearing losses also are very small since there is no thrust force. The efficiency of the disc-armature motor can therefore be very high, dependent upon the copper losses of the armature winding, and hence upon the motor's designed operating voltage and speed.

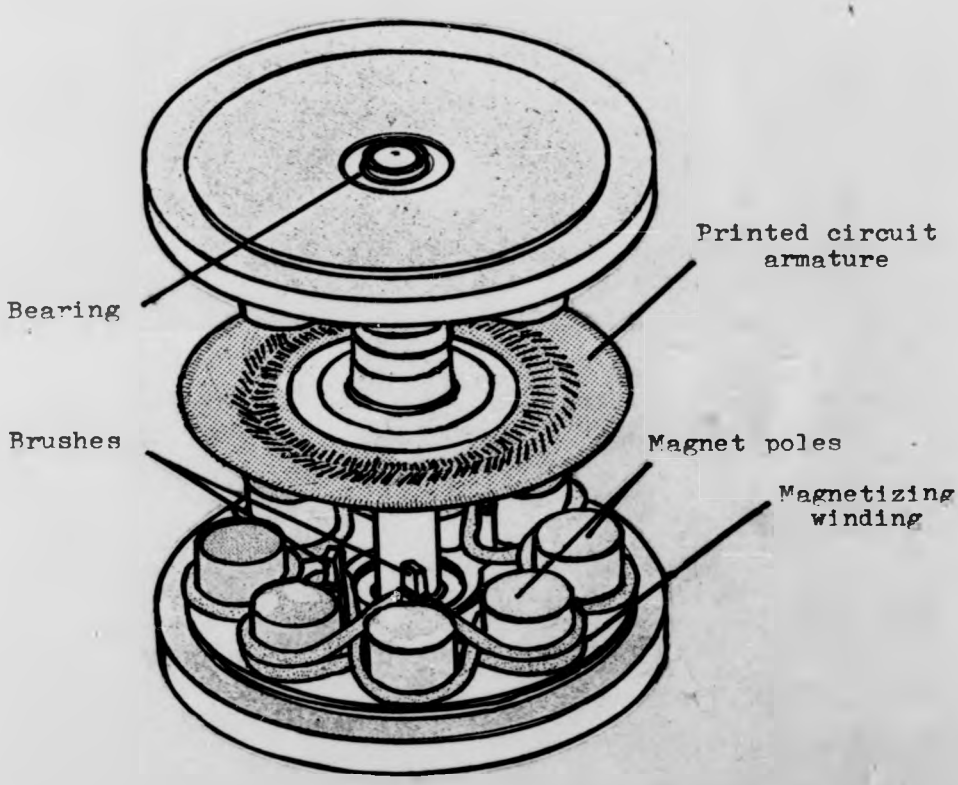

Fig. 2.5 : Printed circuit motor

The topology of the disc-armature motor shown in Fig. 2.4 is similar to that of the printed circuit machine shown in Figure 2.5 However, in the development of this new machine, modelling of the magnet system has produced a design that gives a much improved flux per pole, using poles shaped as segments of a toroid (Figure 2.4). It is especially important to use an accurate model of the permanent magnet materials to achieve optimum performance of this type of machine, due to its unusually large air-gap. It is also particularly pertinent to use new designs of a machine based upon such a model, since these more advanced magnet materials are most often directly substituted for older types in conventional machines, with the result that their superior properties are not fully utilised.

That the disc-armature motor's pole design gives an increased pole surface area than that used in most printed circuit machines is not the sole difference between the two. The more conventional winding of the disc armature motor allows it to sustain normal traction and overload currents, conditions under which printed circuit motors have frequently been found to burn out.

2.3 Calculation of Magnetic Field Distribution in the Air Gap

More often the designer requires to calculate the field and possibly the field gradient produced by the magnet at some point outside the magnet or in a gap.

In theory magnets were regarded as made up of many tiny current loops. The atomic view of the origin of magnetism is very important theoretically, for understanding the behaviour of magnetic materials, but for calculating external fields, continuous models usually suffice.

The most realistic model is to suppose that each element of volume dv inside the magnet constitutes a magnetic dipole which has a dipole moment[8] Jdv, where J is the average polarisation within the element. According to elementary magnetostatics, the potential at a point P at distance r meters from this dipole, in a direction defined by an angle θ, as shown in Figure 2.6

$$\varphi = \frac{J.\cos\theta.dv}{4\pi.\mu_o.r^2} \qquad 2.1$$

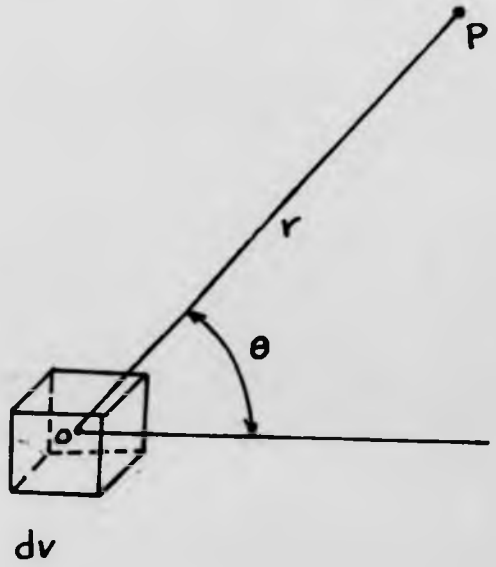

Fig. 2.6 : Magnet volume element

The magnetising force in the direction of the line joining between the dipole and point P is

$$H_{op} = -\frac{d\nu}{dr} = \frac{2J \cdot \cos\theta \cdot dv}{4 \mu_o \cdot r^3} \qquad 2.2$$

In theory it is possible to integrate Equation 2.2 over the volume of any magnet, if the distribution of J is known, and then, if flux density is required μ_o is omitted from the denominator of Equation 2.2. In practice, the integration can only be carried out numerically. This method is probably the most promising one for estimating the fields produced externally by magnets in which J, although not uniform, has a distribution which is known or can be guessed. Unfortunately, the mathematics associated with this model tend to be rather complicated. The mathematics can often be simplified by using a pole model. The choice of this method made on criteria of the ease with which it permits the correct result to be calculated. It actually involves very crude approximations. The assumption of the pole method is that if dipoles are placed end to end

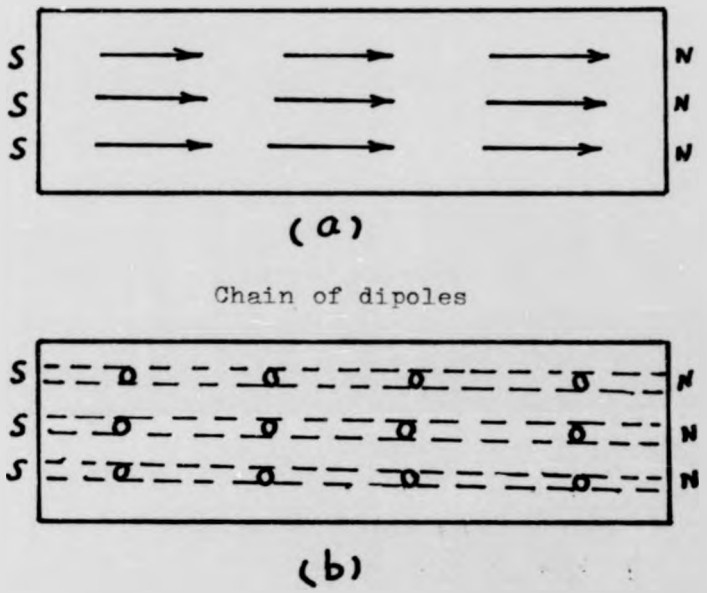

Fig. 2.7 : Pole models

in a chain (Figure 2.7.a) the N pole of one dipole neutralises the S pole of the next, and only one N pole and one S pole are left at the ends of the chain. The same concept arises just as naturally from current loops (Figure 2.7.b). Each current loop is regarded as one turn in a long thin solenoid. A long thin solenoid is equivalent to a needle shaped magnet with an N pole at one end and an S pole at the other. Therefore, it is quite suitable to treat a magnet, which is made in homogeneous materials, as having a uniform distribution of poles on its end face-plan i.e. the surface pole strength, J, has a constant value on the magnet's face, and is zero on its sides. This is a reasonable approximation for the high-coercivity anistropic magnet used in disc armature motor applications, where the direction of magnetisation is along the normal on the magnet face-plan. As stated above, the pole strength on area dA on a surface whose normal makes zero angle to the direction of the surface polarisation, is J dA. Then the potential at distance r from such a small element, as shown in Figure 2.8 is:

in a chain (Figure 2.7.a) the N pole of one dipole neutralises the S pole of the next, and only one N pole and one S pole are left at the ends of the chain. The same concept arises just as naturally from current loops (Figure 2.7.b). Each current loop is regarded as one turn in a long thin solenoid. A long thin solenoid is equivalent to a needle shaped magnet with an N pole at one end and an S pole at the other. Therefore, it is quite suitable to treat a magnet, which is made in homogeneous materials, as having a uniform distribution of poles on its end face-plan i.e. the surface pole strength, J, has a constant value on the magnet's face, and is zero on its sides. This is a reasonable approximation for the high-coercivity anistropic magnet used in disc armature motor applications, where the direction of magnetisation is along the normal on the magnet face-plan. As stated above, the pole strength on area dA on a surface whose normal makes zero angle to the direction of the surface polarisation, is J dA. Then the potential at distance r from such a small element, as shown in Figure 2.8 is:

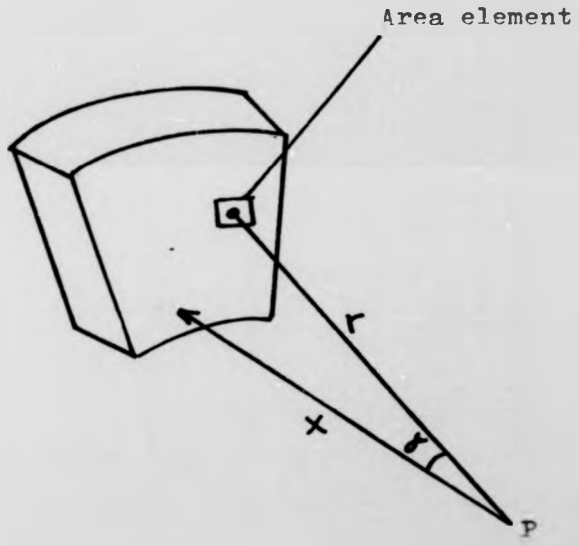

Fig. 2.8 : Magnet segment for field distribution

$$\varphi = \frac{J}{4\pi.\mu_o.r}\, dA \qquad 2.3$$

and the magnetising force H is given by the following differentiation from Equation 2.3

$$H = -\frac{d\varphi}{dr} = \frac{J}{4\pi.\mu_o.r^2}\, dA \qquad 2.4$$

If only the axial direction is considered, integration over the whole pole face yields

$$H_x = \int \frac{J.\cos\gamma}{4\pi.\mu_o.r^2}\, dA \qquad 2.5$$

Where γ is the angle between the normal at magnet surface and the line joining dA to point P. To obtain B in Tesla multiply by μ_o and so eliminate μ_o from the denominator.

The armature winding is formed in discrete layers, each lying in a radial plane in front of the pole's face. If the winding is reduced to

individual conductors, and each conductor to elements that lie in such a plane at radial and angular positions denoted by subscripts i and j, then the air-gap flux density $B_{i,j}$ in the axial direction is given by

$$B_{i,j} = \int \frac{J \cdot \cos\gamma}{4\pi . r^2} dA \qquad 2.6$$

Complications arise in the pole method, when problems with non-uniform magnetisation are met, since the poles can no longer be supposed to be situated on the surface of the magnet.

The advantage of replacing dipoles with poles is that the field due to dipoles obeys an inverse cube law, and depends on the angle between the direction of the dipole and the line joining it to the point at which the field is required, while the field due to a pole obeys a simple inverse square law and is directed along the line joining the pole to the point. So, the significance of Equation 2.6 is that the field

in the air-gap can be calculated without reference to a potential distribution on the pole face. The magnet polarisation J exists only on the pole face and is not dependent upon radial or angular position. The drawback to Equation 2.6 is that the remaining integration can only be performed by numerical means, and it will only be possible to find a discrete field distribution. Modern computers have made numerical integration a reasonable proposition and the method is probably the most promising one for estimating the fields produced externally by magnets in which J, has uniform and known distribution.

2.4 Working Equations

2.4.1 EMF Equation

The disc armature, Figure 2.9 of effective outer and inner diameters d_2 and d_1, rotate in an average air-gap flux density $\overline{B}$ at angular speed w. Consider an element of armature conductor of radius r and radial length dr. It moves at peripheral speed w.r and its motional EMF is:

$$de = \overline{B}.w.r.dr \qquad 2.7$$

The conductor EMF between diameters d_2 and d_1 therefore:

$$= \overline{B}.w \int_{\frac{1}{2}d_1}^{\frac{1}{2}d_2} r dr = \frac{1}{8} (d_2^2 - d_1^2) \overline{B}.w \qquad 2.8$$

If Z_s are the number of conductors in series between the brushes, so that

$$Z_s = \frac{Z}{a} \qquad 2.9$$

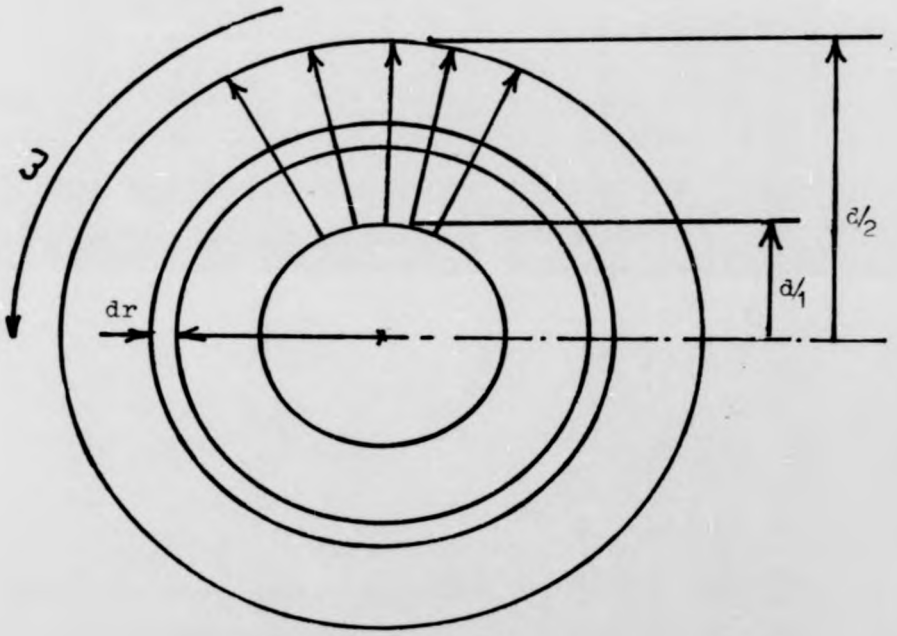

Fig. 2.9 : Disc armature

Where a is the number of parallel paths through the armature and Z the total number of armature conductors. Thus:

$$E = \frac{1}{8} \bar{B}.w.\frac{Z}{a}.(d_2^2 - d_1^2) \qquad 2.10$$

Where E is the total armature EMF. Equation 2.10 is often the most useful for determining the EMF generated in a disc armature machine. However, the flux per pole. ϕ, may be written as:

$$\phi = \bar{B}.\pi. \frac{(d_2^2 - d_1^2)}{4\ p} \qquad 2.11$$

Where p is the number of poles. Therefore, the EMF may be expressed as:

$$E = \frac{\phi.p.w.Z}{2\ \pi.\ a} \qquad 2.12$$

But

$$w = \frac{2\ \pi.n}{60} \qquad 2.13$$

Where n is the rotational speed in rev/min.
Thus:

$$E = \frac{\phi.p.n.Z}{60\ a} \qquad 2.14$$

Equation 2.14 is the familiar EMF equation for a d.c. machine.

2.4.2 Torque Equation

If the armature conductor carries a current of I_c, the interaction force on the element dr of the conductor is:

$$dF = \bar{B}.I_c.dr \qquad 2.15$$

Developing a torque

$$dT_c = \bar{B}.I_c.r.dr \qquad 2.16$$

Where T_c is the torque due to a single armature conductor, Equation 2.16 integrates between the limits d_2 and d_1 to give:

$$T_c = \frac{1}{8}(d_2^2 - d_1^2)\bar{B}.I_c \qquad 2.17$$

But $I_c = \frac{I}{a}$ 2.18

Therefore Equation 2.17 becomes:

$$T_c = \frac{1}{8} (d_2^2 - d_1^2) \bar{B}.\frac{I}{a} \qquad 2.19$$

And the total armature torque, T is:

$$T = \frac{1}{8} (d_2^2 - d_1^2) \bar{B}.\frac{I}{a}.z \qquad 2.20$$

2.4.3 Power Equation

It can be shown easily that the converted power of the electric motor (including disc motor), P, is:

$$P = T.w \qquad 2.21$$

Substituting for T from Equation 2.20

$$P = \frac{1}{8}(d_2^2 - d_1^2)\,B.\frac{I}{a}.Z.w \qquad 2.22$$

Let A_c be the specific electric loading, i.e. ampere-conductor divided by meters of armature winding at radius $\frac{d_1}{2}$, therefore:

$$A_c = \frac{I_c.Z}{\pi.d_1} = \frac{I.Z}{a.\pi.d_1} \qquad 2.23$$

Substitute for I and w in Equation 2.22 from Equation 2.23 and 2.13 thus:

$$P = \frac{\pi^2.B.A_c.n.(d_2^2 - d_1^2)\,d_1}{240} \qquad 2.24$$

2.4.4 Relationship Between d_2 and d_1 for Maximum Power

From Equation 2.24 power can be written as:

$$P = k(d_2^2 - d_1^2)\,d_1 \qquad 2.25$$

Where k is a constant. For maximum power:

$$\frac{dP}{dd_1} = k\,(d_2^2 - 3d_1^2) = 0 \qquad 2.26$$

And this is zero only when:

$$d_2^2 = 3\, d_1^2 \qquad 2.27$$

and $$d_1 = \frac{d_2}{\sqrt{3}} \qquad 2.28$$

Substituting in Equation 2.24:

$$P = \frac{\pi^2\, \bar{B}\, A_c\, n\, d_2^3}{360\sqrt{3}} \qquad 2.29$$

Thus the power output available from disc armature motors is approximately proportional to the cube of the outer active diameter.

2.5 Design Fundamentals of Permanent Magnet

In this section the basic concepts of permanent magnet design along with some specific information on their applicability to axial field machine configuration are set forth.

The designer of magnetic circuits should normally aim to produce the required flux in the air-gap at minimum cost. Since permanent magnet material is much more expensive than the type of soft iron or mild steel used in permanent magnet assemblies, minimising the cost is often equal to minimising the volume of permanent magnet used.

Fig. 2.10 shows part of a typical magnetic circuit (for a disc armature motor). It consists of two permanent magnet halves with total length lm, two mild steel return rings and a relatively large air-gap, lg, which accommodates the total armature thickness with suitable running clearances between it and the pole faces. Correspondingly the mmf supplied by the permanent

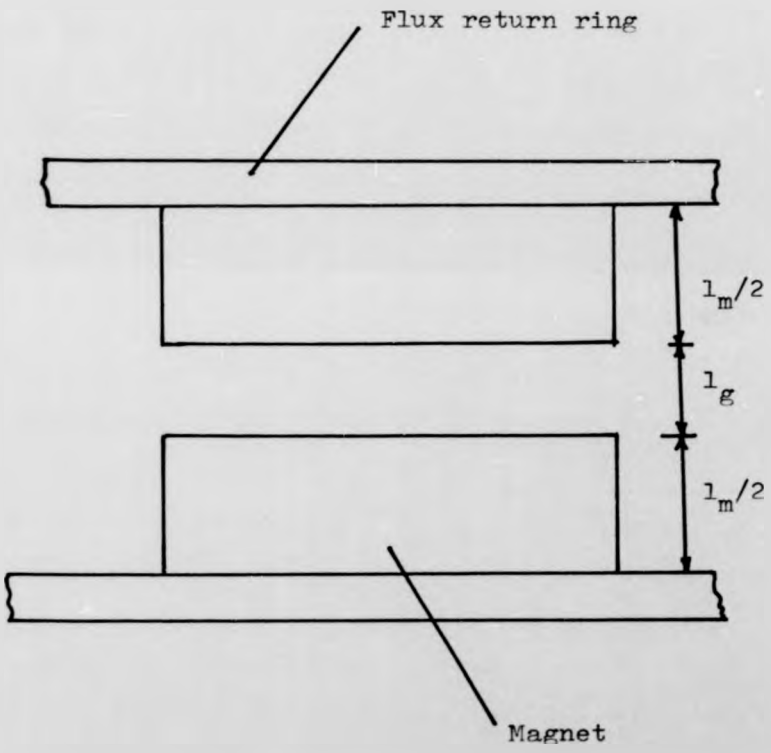

Fig. 2.10 : Magnetic circuit of disc armature motor

magnet is equal to that expended across the air-gap, i.e. the total magnetomotive force in the circuit equal to zero. This theory is true only when using a correction factor, LF, the loss factor, which accounts for the mmf lost in the reluctance of any joints or in any steel parts of the circuit that cannot be regarded as having infinite permeability, therefore:

$$Hm.Lm = LF.Hg.lg \qquad 2.30$$

Where Hm and Hg are the magnet and air-gap magnetising force. The value of the loss factor, generally varies from 1.2 to 1.3 and it requires some experience to estimate. On the other hand, the flux in the permanent magnet material is equal to the sum of the flux in the gap and the leakage flux, which is wasted because it returns by some path other than through the gap. Consequently, the permanent magnet flux density, Bm, is greater than the air-gap flux density, Bg. This leakage is usually accounted for by introducing

a leakage coefficient, LC such that:

$$Bg = \frac{Bm}{LC} \qquad 2.31$$

The leakage coefficient, LC, is generally rather difficult to evaluate. The specific case for disc armature motors is covered in Section 3.4. Now, since by definition:

$$Hg = \frac{Bg}{\mu_o} \qquad 2.32$$

Therefore, from Equation 2.31 and 2.32, air-gap magnetisation becomes:

$$Hg = \frac{Bm}{LC\ \mu_o} \qquad 2.33$$

By substituting for Hg from Equation 2.33 in Equation 2.30, lm becomes as:

$$lm = \frac{LF.Bm.lg}{LC.\mu_o.Hm} \qquad 2.34$$

Equation 2.34 completes the calculation of magnet length. This concludes the first part of the design problem.

In dealing with permanent magnet design, interest is centred only on the demagnetising curve. Fig. 2.11 shows the demagnetision curve of a permanent magnet material having previously been fully magnetised. On the right hand side of Fig. 2.11 a product of Bm Hm has been plotted against the value of B. There is one particular working point on the demagnetisation curve for which the product BH is a maximum. This maximum is referred to as (BH) maximum and is a useful characteristic of the material. It has the dimensions of energy per unit volume (Jm^{-3}) and is generally called the maximum energy product. If the values of Bm and Hm corresponding to the (BH) maximum are used in determining lm, the design will also be for minimum magnet volume.

Now, if the term $\frac{Bm}{Hm}$ of Equation 2.34 is

algebraically expressed as a function of lm and lg with a constant of proportionality $\frac{LC}{LF}\mu_o$, then Equation 2.34 becomes as:

$$\frac{Bm}{Hm} = \frac{LC}{LF}\mu_o.\frac{lm}{lg} \qquad 2.35$$

For the specific design of DC disc motors $\frac{LC}{LF}$ approaching to unity, then Equation 2.35 can be written:

$$\frac{Bm}{Hm} = \mu_o \frac{lm}{lg} \qquad 2.36$$

This equation shows how to design a magnet with the correct length so that it will work at the optimum (BH) maximum point, which is given by the intersection P of a line OA of slope defined by Equation 2.36 and the demagnetising curve in Fig. 2.13. Incidentally, given the demagnetisation curve, the (BH) maximum point can be quickly approximated by drawing lines parallel to the axes through the

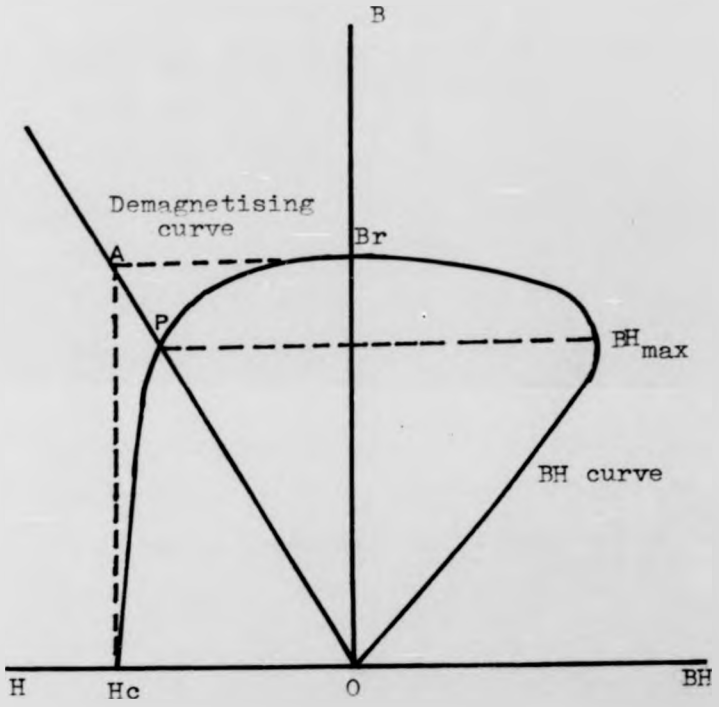

Fig. 2.11 : Demagnetization and BH versus B curves

Br and Hc points to intersect at A forming a rectangle A Br O Hc. The diagonal OA of this rectangle is approximately the unit permeance line given by Equation 2.36. This construction is not quite accurate but gives a very good approximation to (BH) maximum. In a practical design, there may well be other factors as well as minimum magnet volume to be taken into consideration as discussed in Chapter 4. It must be stressed that this discussion relates to a magnet assembly that is magnetised to saturation after assembly and is not subjected to permeance changes or to substantial current m.m.fs under working conditions.

It will be noted that the factors which determine the load line slope are geometrical and are dependent on the size and disposition of the magnetic circuit but are independent of the demagnetisation curve, thus working values of Bm and Hm for another magnet material with the same dimensions and disposition would be given

by the intercept of the same load line with the new demagnetisation curve. The application of this single load line to the whole volume of permanent magnet material is usually a reasonable approximation with magnets of modern material with uniform cross-section and flux-path length.

From the above discussion, it is evident that the minimum volume of magnet material to fulfil a motor specification is obtained by a design in which the magnet working points are at a point on the demagnetisation curve for $(BH)_{max}$. But, as mentioned earlier, the desirable working point is likely to be higher than B_m for $(BH)_{max}$ due to secondary considerations, e.g. with ferrite magnets, protection against sub-zero temperature changes and difficulty in producing and utilizing optimum dimensions.

3.1 Design Procedure

In order to design a d.c. axial-field permanent magnet motor, one needs to know the output power required, the operating voltage, the speed specification and the choice of magnet material. Having specified these, a suitable starting point for the design procedure would be to consider the diameter of the machine.

It has been shown in Chapter 2 that the total mechanical power from a disc armature motor is proportional to the cube of the diamater and the equation expressing this relationship is:

$$EI = 1.58 \times 10^{-2}\, n.d_2^3.\bar{B}.A_c \qquad 3.1$$

Where $\bar{B}$ and A_c are the specific magnetic and electric loadings respectively, d_2 is the outer active diameter to be calculated. E and I are the armature e.m.f. and current, and n is the motor speed in rev./min.

This equation is used in the calculation of the most appropriate diameter. It would, however, be more convenient to express $\bar{B}$, the magnetic loading, in terms of the flux density of the magnet rather than that in the air gap. This may be achieved by incorporating the leakage coefficient, LC, and the ratio of pole arc to pole pitch. Therefore the depletion of B_m in a magnet to $\bar{B}$ in the air gap is considered to occur in two stages. Leakage flux from a magnet's sides gives flux density Bg in the gap adjacent to the pole face, which then spreads across the gap over a pole pitch to $\bar{B}$ thus:

$$\bar{B} = \frac{\alpha}{LC} . B_m \qquad 3.2$$

Where B_m is the magnet's flux density. Accordingly equation 3.1 is now written:

$$IE = \frac{1.583 \times 10^{-2} \; n. \; .B_m . A_c . d_2^3}{LC} \qquad 3.3$$

With A_c defined at diameter d_1 as:

$$A_c = \frac{Z . I}{\pi . a . d_1} \qquad 3.4$$

Where a is the number of parallel paths and Z is the number of active conductors.

As the conductors are more tightly grouped towards the inner active radius and as end windings exist at a radius less than $\frac{d_1}{2}$, a space factor, SF, is defined to ensure that it will be possible to accommodate the end windings. SF is kept approximately constant and less than "1" for all disc armature motors and it is defined as:

$$SF = \frac{Z.G}{L.\pi.d_1} \qquad 3.5$$

Where G is the gauge of wire in mm used and L the number of layers in the armature winding.

Substituting for Z of Equation 3.4 from Equation 3.5. A_c becomes:

$$A_c = \frac{SF.I.L}{a.G} \qquad 3.6$$

Ignoring for the moment mechanical losses, IE may be taken as equal to P, then the outer

diameter d_2 is given by rearranging Equation 3.1 as:

$$d_2 = \left[\frac{P.\ a.G.LC}{1.583 \times 10^{-2}.n.\alpha.Bm.SF.I.L} \right]^{\frac{1}{2}} \quad 3.7$$

The values of LC, and SF remain approximately constant from machine to machine. Suitable values are assigned, and L is initially taken as 2 to simplify the armature construction. This leaves only the number of parallel paths, gauge of wire, magnet flux density and armature current to be determined for the evaluation of d_2. Until recently, the magnet operating flux density was chosen at its maximum energy density. A new approach to specify the working point for the magnet is used here. This will favour a point higher than BH max due to consideration of protecting the magnet against sub-zero temperature change and obtaining greater output.

The steps to specify the magnet working point according to this new approach are as follows: The initial step is to choose the BH max point on the BH curve of the magnet under

consideration with the condition that the curve is obtained under the lowest expected temperature to which the magnet (motor) will be subjected through its service time. If it happens that the point is on the non-linear part of the curve, then the value of B is increased by moving it further up on the curve until a value on the linear part is reached. This is necessary to ensure reversible losses due to changes in temperature. (The theory behind this will be explained in more detail in the next chapter.)

The next step is to draw a line between this point and the origin. This line represents the magnet load line for the motor magnet. Obviously, this line cuts all demagnetization curves which are drawn under different higher temperatures. Two of these curves are the BH curve at room temperature (usually supplied by magnet manufacturers) and the BH curve at working temperature. (the temperature where the motor runs continuously at its rated power and current).

Fig. 3.1 shows three demagnetizing curves

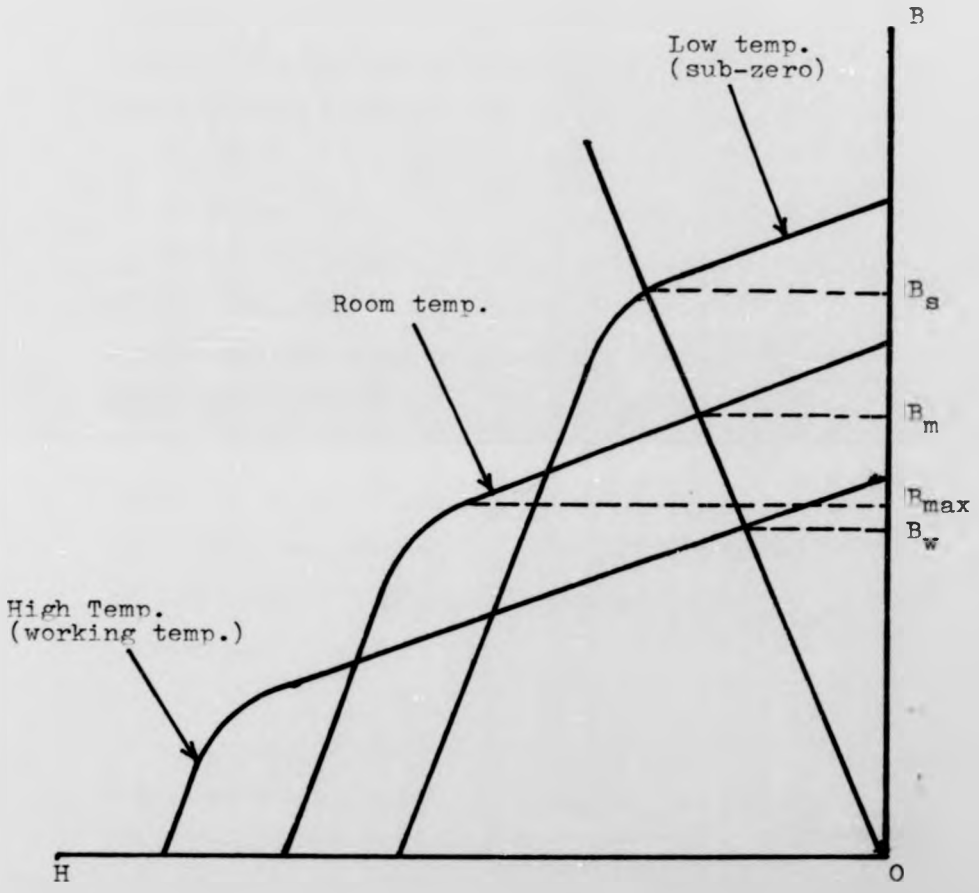

Fig. 3.1 : Demagnetisation curves under different temperatures

for a magnet which are obtained under the lowest temperature, room temperature and working temperature, where B_s . B_m and B_w are the flux densities which are appointed by the load line respectively. Here we start to use B_w instead of B_m in Equation 3.1 to calculate machine diameter and speed. On the other hand, B_m will be used later to calculate the magnet length, l_m, and weight. Although higher flux densities are guaranteed by this method which would reduce A_c, this would be at the expense of magnet weight. While this represents a departure from the BH max ideal, it allows designs to be determined accurately.

To minimize the design dependence on the demagnetization curve, B_w is derived from B_m. This is possible because the usual working temperature of the magnet in disc armature motors are within the linear temperature range i.e. when magnets are heated or cooled, there is an increase or decrease in magnetization which is recoverable when the magnet returns to its original temperature.

This change is found by multiplying the temperature coefficient by the change in temperature from its room value, so that the general equation becomes:

$$B_{t2} = B_m - \frac{TC}{100} B_m \Delta t \qquad 3.8$$

where $\Delta t = t_2 - t_{room}$

TC here is the average value for the reversible temperature coefficient, t_2 is the magnet final temperature and B_{t2} is the flux density at t_2 temperature. When Equation 3.8 used to calculate the specific flux density B_w it becomes

$$B_w = B_m - \frac{TC}{100} B_m (t_2 - 22) \qquad 3.9$$

As the terminal voltage, V, is known, E is initially taken as a fraction of this. Therefore the current may be determined from the relationship:

$$P = EI \qquad 3.10$$

The number of parallel paths, gauge of wire, armature current and current density (current per unit area of armature conductor) are related by the equation:

$$I = \frac{a.C.\pi.G^2}{4} \qquad 3.11$$

Where C is the current density in A/mm^2, as G is specified in mm, C is given a value which ensures that the temperature of the armature at continuous running with rated current condition, is compatible with the heat deflection temperature of the epoxy resin system employed for encapsulating the winding. This leaves the wire gauge and number of parallel paths to be determined. Initial design assigns 'a' the lowest possible value (2 for a double-layer wave winding), the corresponding ideal value of G is hence calculated, and the standard wire gauge above this value is selected. The value of d_2 may now be calculated.

Equation 3.7 shows that d_2 is proportional

to the number of parallel paths 'a', the wire gauge G, and the inverse of layers number $\frac{1}{L}$.

Hence, one can increase or decrease d_2 by suitable modification to a, G and L until desired values are reached. This is useful in cases where restriction on the overall diameter DØ is specified. The difference between DØ and d_2 which is occupied by the casing, its clearance with the rotor, and the end-winding, is estimated initially as 20% of DØ, i.e., d_2 is equal to 0.8 DØ. This restricted diameter can be produced by adjusting the calculated diameter as stated above.

Having established d_2, Equation 2.29 may be used to find d, and thus the two principal dimensions of the machine are known. Before any further step into design procedures, a comparison between the wire gauge G and the calculated diameter d_2 is necessary, to check that there is no appreciable mismatch of the actual physical sizes. Equation 3.11 shows that for a given armature current the value

of G can be reduced by increasing the value of a. This may be done by choosing other armature connection patterns, e.g. a duplex wave winding which has 4 parallel paths, or simple lap winding which has parallel paths equal to the number of poles. The number of parallel paths in the latter can be doubled by using duplex lap. Theoretically this is possible, but in practice, the duplex winding (wave or lap) is undesirable because of the high circulating current due to the high number of short circuited coils under commutation. This problem is solved by connecting two simple windings (wave or lap) to the commutator in parallel (see Chapter 5). This makes the number of parallel paths twice that in the simple winding which has the effect of reducing the wire gauge, but on the other hand, it increases the number of layers.

The next step is to select an initial number of poles. Specifying this in early design procedures was empirical and based on a compromise and allowed to increase with the diameter of the machine. Experience shows that if the number of poles is too small, the flux return rings become

heavy and the end-windings of the armature become bulky. If the number of poles is too large, the number of armature coils and the number of commutator segments become very high; the brushes become thin in section and the distance between brushes of opposite polarity become very small. However, the actual value is not critical as this number will be verified through calculations incorporating the machine parameters at a later design stage (see Section 3.4). Eight or ten poles may be taken as a preliminary number.

The next step is to select the minimum number of coils per pole per layer, which ensures that a feasible winding arrangement will result. This also should be not less than five, to ensure that commutation power losses are not significant. From this the minimum number of coils is calculated taking into account the type of winding under consideration (wave, lap, etc). An ideal number of conductors, Z_i, for the machine may be calculated from:

$$n = \frac{E.a.60}{\phi.Z.p} \qquad 3.12$$

When $\emptyset$ is calculated from B_m. d_2. d_i. α and p. This ideal value. Z_i may be expressed as:

$$Z_i = \frac{360a.E.LC.10^{-6}}{n.\alpha.B_m.\pi.d_2^2} \qquad 3.13$$

With d_2 expressed in mm. Generally this will be a non-integral value and it is used with the number of coils, to find the number of turns per coil which will yield the number of armature conductors nearest to Z_i, by taking the integral ratio of the relationship

$$\text{Turns/coil} = \frac{Z_i}{2 \text{ x coils}} + 0.5 \qquad 3.14$$

There are a number of design criteria that are now commonly employed in axial-field machines. It assumes a drum commutator is used, with a brush diameter of $0.6\, d_1$, so that the

$$\text{segment width} = \frac{0.6\,\pi.d_1}{\text{segments}} \qquad 3.15$$

To ensure that the brush width is at least greater than the segment width, we state that the

$$\text{brush width} = 1.5 \text{ segment width} \qquad 3.16$$

With a typical current density of $120 mA/mm^2$, and a full set of brushes, brush length will be:

$$\text{brush length} = \frac{I \times 10^2}{9p \times \text{segment width}} \qquad 3.17$$

Following normal practice, it is possible to accommodate the brushgear without it protruding beyond the normal casing dimensions, then a face commutator is selected. This usually occurs only in machines with the longer, low coercivity magnetic materials e.g. alnico.

3.2 Design Check

The best way to check the design specification against the original specification is by accurate prediction of the rated power, speed, torque and efficiency. In order to carry out such a performance prediction, the losses within the machine must be taken into account.

With an iron free armature core losses are eliminated. Armature reaction effects can be considered negligible in machines of this type which leave only the copper losses, brush voltage drop loss and mechanical loss to be estimated. The copper losses are taken as the I^2R due to armature resistance and the eddy current loss of the copper conductor, We, to calculate I^2R, the armature resistance, R_a has to be calculated first. The layout of a typical winding with full-pitch coils is shown in Figure 3.2. In order to derive the armature resistance, it may be assumed that the end-windings lie approximately at diameter D2 and D1 so that one turn has the length:

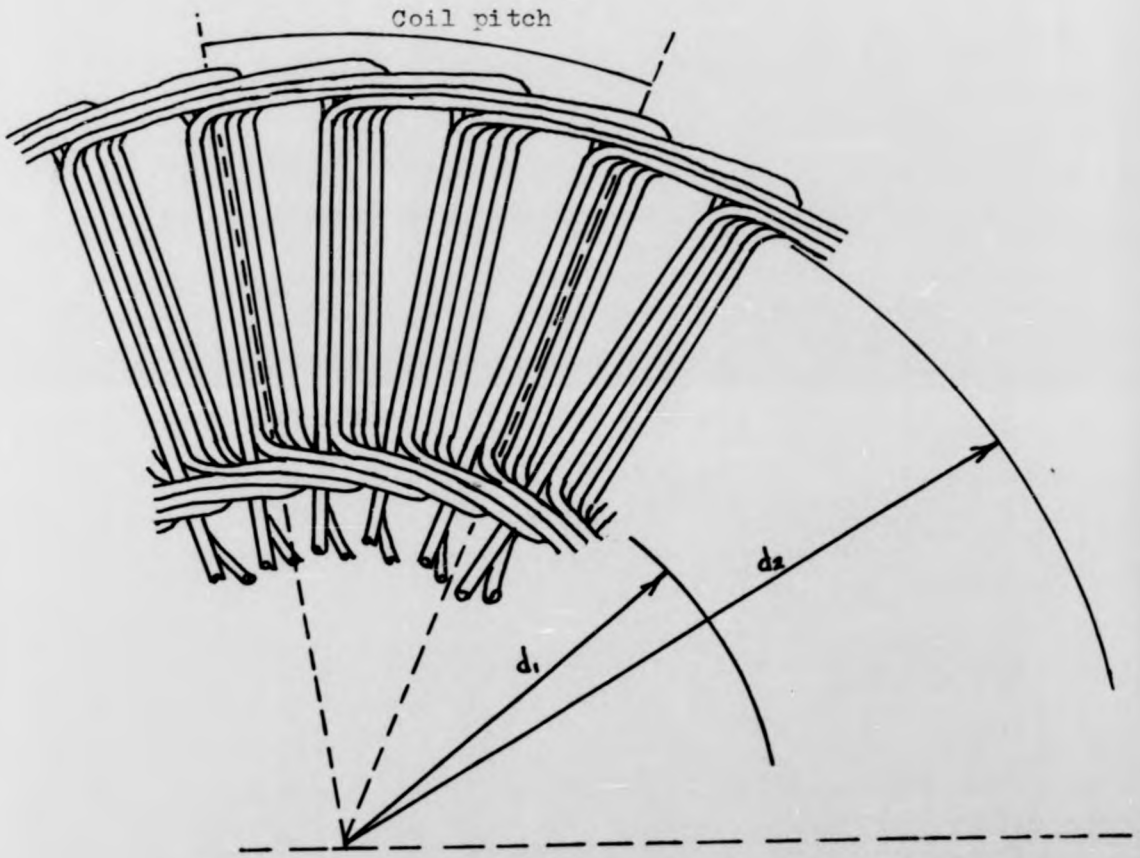

Fig. 3.2 : A double-layer winding arrangement

$$(D2 - D1) + \frac{\pi}{p}(D2 + D1)$$

To this 25% is added as an allowance for the unequal length of the coil sides and end-windings, and also includes a suitable length of conductor for connection to the commutator.

If at normal operating temperature, the resistivity of the copper winding is taken as ρ_{ot} and the round conductor has an area $\frac{\pi.G^2}{4}$. with Z conductors in the winding, and 'a' parallel paths, the armature resistance is found to be:

$$R_a = \frac{2\,\rho_{ot}.Z \times 1.25}{\pi.a^2.G^2}\left[(d_2 - d_1) + \frac{\pi}{p}(d_2 + d_1)\right] \qquad 3.18$$

According to B.S. 1727 and using Equation 2.28, Equation 3.18 becomes:

$$R_a = \frac{2 \times 2 \times 10^{-8}\ Z\ 1.25\ d_2}{\pi.a^2.G^2}\left(0.422 + \frac{4.955}{p}\right) \qquad 3.19$$

Using Equation 3.19 I^2R may easily be evaluated.

The next step is to calculate the eddy-current loss in the copper conductor. It is obvious that the armature winding is rotating in the main magnetic field of the stator, and will be subject to a loss due to eddy current. This loss can be limited by subdividing the conductors and transposing the strands. It can be shown that the eddy-current loss (Chapter 5) is taken as:

$$W_e = n^2 \left[1.422 \times 10^{-12} Z.D_2 \left(\frac{G^2 . .Bm.p}{LC} \right)^2 \right] \qquad 3.20$$

Where W_e is the eddy-current loss in the armature copper conductors, if n, is the rotational speed in rev/min, D_2 and G in mm, W_e will be in watts.

To find brush voltage drop loss, a constant voltage drop per brush pair may be assumed. This is then multiplied by the armature current to give the associated power loss.

Next the mechanical losses in the machine have to be determined. In earlier days, the

designer made an estimate of these losses based on experience. For more general design procedure, an alternative approach has been developed which enables a reasonable assessment of mechanical losses to be made. The new assessment does not require a detailed specification of the mechanical layout of the machine. In fact, it is independent of the machine layout.

Experience gained in the operation of earlier machines has been used to advantage in the creation of such an assessment which makes it possible to develop an empirical equation to predict the mechanical losses. This analysis made use of results from the light run test of the prototypes that have already been built and tested. These results relate to conditions of varying speed and applied voltage where the motor does not drive any additional mechanical load. The input power is calculated from the product of current and voltage. From this product, is subtracted the I^2R loss and the brush voltage drop loss with the remaining power taken as the mechanical loss for the

particular machine at this operating speed. It is assumed that brush friction, windage and bearing friction are the only mechanical losses to be considered. These are assumed to depend on the outer diameter D_2, armature rated current I and rotating speed n. The dependance of the mechanical loss on these variables are evaluated to yield the final expression for mechanical losses in a disc armature motor.

$$W_m = \left(\frac{D_2^{2.64}}{59600} + \frac{0.0496\ I}{0.155} \right) \times 10^{-4} \times n^{1.304} \qquad 3.21$$

Where W_m is the total mechanical loss, D_2 is the outer active diameter in mm, I the rated current in Amps, and n the rotational speed in rev/min, W_m will then be expressed in watts. The formula may be used to predict the performance of any disc armature motor. Reference 10 illustrates the derivations of this formula and its accuracy.

Having determined the armature resistance and the expected losses in a motor, a new value

for the generated e.m.f. is calculated from:

$$E = V - IR_a - V_b \qquad 3.22$$

Where V_b is the voltage drop due to the brushes and is given a suitable value from manufacturers' data. The rated motor speed found directly from Equation 3.12 and the rated power output of the motor P_r, may now be calculated from:

$$P_r = EI - W_m - W_e \qquad 3.23$$

Where W_m and W_e are the mechanical and eddy current losses in watts respectively.

Finally, the torque and efficiency are found from:

$$T_r = \frac{60\ P_r}{2.\pi.n} \qquad 3.24$$

$$\text{and } \eta = 1 - \frac{W_m + I^2R_a + V_b.I + W_e}{V.I} \qquad 3.25$$

Where T_r is the rated torque in Nm and η the efficiency of the motor.

3.3.1 Computer Techniques

The advent of the digital computer not only eliminated many long and tedious hand calculations, but also made possible optimisation techniques which were not previously attempted. It is to this type of application, where a set of calculations may be performed many times over, that the computer is ideally suited. The design parameters of a motor, for example, could be given some initial values; from these the expected performance is calculated and compared with the required performance, and finally the design parameters are modified in some way to try and improve the agreement between required and calculated performance. The whole procedure is then repeated until the agreement is close enough for practical purposes. Methods of this nature form the basis of many design programs or design "software".

When applied to the design of rotating electrical machines, an added advantage is that changes in the design parameters (numbers of poles or coils, wire gauge, etc) may be made readily,

quickly assessed, and it is possible for a program to consider a wide range of these values in the search for the optimum design. The accuracy of the final design obviously depends on the mathematical relations used in the computer program.

Once the software is written, the next step is to run it in the most convenient way. Perhaps the most basic and familiar method was to punch out the program on cards, add cards containing the necessary data input (power and speed required, size limitations, etc.) and then allow a computer operator to handle the actual run. Information from the program (the required design parameters) will normally be printed out on the central line-printer and returned to the designer for consideration. A faster method entailing more user involvement is to write an "interactive" computer program and then use a remote terminal. Here, the designer types in his requirements and the program is executed immediately with the results displayed on the terminal screen, and also printed out if

required. An important benefit of this technique is the facility to alter any of the design specifications whilst at the terminal and the effect of any changes may be assessed a few seconds after it is made. All the software described here is of this interactive nature.

A further advantage of using the computer is its ability for graphical representation. This enables design results to be considered in a more meaningful form and a wealth of software has been written[10] (by others!) and some incorporated into the design procedure which will give the predicted performance curve. Graphical output may be seen at the terminal or, more usually, as a hard copy from a plotting device. Of all the benefits that the digital computer can bring to a design process it is the time saved that is most apparent. To consider two or three design alternatives, even with the aid of a calculator, can be a long process. The computer program that has been used covers some 40 different alternatives in

less than seven seconds of computer time, although the hard copy will take slightly longer to produce. With the introduction of low-cost, micro-processor-based desk top computers it has become viable for even small companies to have such design facilities in-house.

3.3.2 Software Development

The development of computer programs suitable for the design of axial field d.c. machines has taken place over a period of years with continued refinement and updating of the routines.

The first program[11] was written in 1970 using the language Algol 60. It enabled the designer to specify the majority of the motor design parameters as input data with the program calculating other design parameters and the predicted performance. The input data sheet is illustrated in Table 3.1. When values are assigned to the listed parameters, the program performs the calculations and produces the results. Examples of this form of output are shown in Table 3.2 which illustrates the design parameters of a motor. The operation of the program requires the Algol instruction to be supplied on punched cards with the actual run supervised by a member of the computer unit staff. The output from the program generated on the

UNIVERSITY OF WARWICK

School of Engineering Science

TYPE 2A DISC-ARMATURE MOTOR DESIGN - DATA SHEET.

Design specification	Machine design No.	
	Output power, watts	
	Voltage, volts	
	Speed, rev/min	
Design data	Internal diameter, d_1 mm	
	External diameter, d_2 mm	
	No. of poles.	
Magnetic circuit data	B_m, Tesla	
	H_m A/M	
	Double or single magnets	
	Leakage coefficient	
	Loss factor	
	Pole-arc/pole-pitch	
	Airgap, mm	
	Magnet density	
	Max flux density in MS, T	
Electric circuit data	No. of parallel paths	
	No. of coils	
	No. of turns/coil	
	Diameter of wire (bare) mm	
	Current density, A/mm^2	
	Space factor	
	Armature temperature, ^oC.	
	Wt. of non-active parts, kg	
	Mechanical loss, watts	
	Performance graphs (T or F)	

Table 3.1 : Original C.A.D. input data sheet

DISC-ARMATURE MOTOR DESIGN

DESIGN NO: 6

DESIGN SPECIFICATION

OUTPUT: 2500 WATTS
VOLTS: 84V
SPEED: 3000 R.P.M.

DESIGN DATA

D2 = 230 MM
D1 = 140 MM
NO OF POLES = 12
TERMINAL VOLTAGE = 84 VOLTS

MAGNETIC CIRCUIT DATA

BM = .286 TESLA
HM = 50500.0 A/M
LEAKAGE COEFFICIENT = 1.27
LOSS FACTOR = 1.27
USEFUL FLUX/POLE = .000368 WEBERS
POLE PITCH/POLE ARC = .75
MAGNET LENGTH = 22.5 MM
MAGNET WEIGHT = 4.15 KGMS
THICKNESS OF FRR = 3.94 MM
FRR WEIGHT = 1.61 KGMS
AIR GAP = 10.0 MM
MAGNET DENSITY = 4.70 GMS/CC
MAXIMUM FLUX DENSITY OF MILD STEEL = 1.32 TESLA
DOUBLE OR SINGLE MAGNETS = 2

ELECTRIC CIRCUIT DATA

NO OF PARALLEL PATHS = 4
NO OF COILS = 122
NO OF TURNS/COIL = 5
NO OF CONDUCTORS = 1220
WIRE DIAMETER = 1.22 MM
WIRE WEIGHT = 1.52 KGMS
CURRENT DENSITY = 8.00 AMPS/MM**2
ARMATURE CURRENT = 37.41 AMPS
I**2R LOSSES = 229.7 WATTS
SPACE FACTOR = .84
NO OF LAYERS = 5
TEMPERATURE = 75.0 DEGREES C.
ARMATURE RESISTANCE = .164 OHMS
INDUCED EMF = 77.86 VOLTS

Table 3.2 : Design parameters for 2.5kW motor

WEIGHT OF NON ACTIVE PARTS = 12,0 KGMS
TOTAL WEIGHT = 19,28 KGMS
MECHANICAL LOSS = 100 WATTS
SPEED = 3467,4 R,P,M,
POWER = 2812 WATTS
TORQUE = 7,75 NM
POWER/WEIGHT = 145,8 WATTS/KGM
EFFICIENCY = ,895

PERFORMANCE SPECIFICATIONS

CURRENT DENSITY AMP/MM*2	ARMATURE CURRENT AMPS	SPEED RPM	POWER WATTS	TORQUE NM	EFFICIENCY
2	9,352	3672,5	671,20	1,75	,854
3	14,03	3638,3	1046,0	2,75	,888
4	18,70	3604,1	1413,7	3,75	,900
5	23,38	3569,9	1774,2	4,75	,903
6	28,06	3535,7	2127,4	5,75	,903
7	32,73	3501,6	2473,6	6,75	,900
8	37,41	3467,4	2812,5	7,75	,895
9	42,08	3433,2	3144,3	8,75	,889
10	46,76	3399,0	3468,8	9,75	,883
11	51,44	3364,8	3786,2	10,7	,876
12	56,11	3330,6	4096,4	11,7	,869
13	60,79	3296,4	4399,5	12,7	,862
14	65,46	3262,2	4695,3	13,7	,854
15	70,14	3228,1	4984,0	14,7	,846
16	74,82	3193,9	5265,5	15,7	,838

TIME = 0002 02

Table 3.2 (continued) : Design parameters for 2.5kW motor

lineprinter would be returned after a short time. As well as the results presented in tabular form, there is also the option of graphical representation on a plotting device. Typical examples of this graphical output are given in Figure 3.3.

Although this program was of great value, it had the obvious limitation that as it was only a calculating routine, the majority of design parameters had to be specified at the start. Unique results are calculated from each set of inputs. There was no guarantee that the predicted performance will match the desired specification, or that an optimum design had been produced. Several attempts were needed to generate a result close enough to the original specification.

Thus, it was decided to improve on this by introducing the self parameter variations and the interactive facilities to allow extensive investigation of the effects of parameter change on expected performance of the machine, with the designer still able to make changes according to his experience. Work on improving this resulted

Fig. 3.3 (a): Computer produced curve

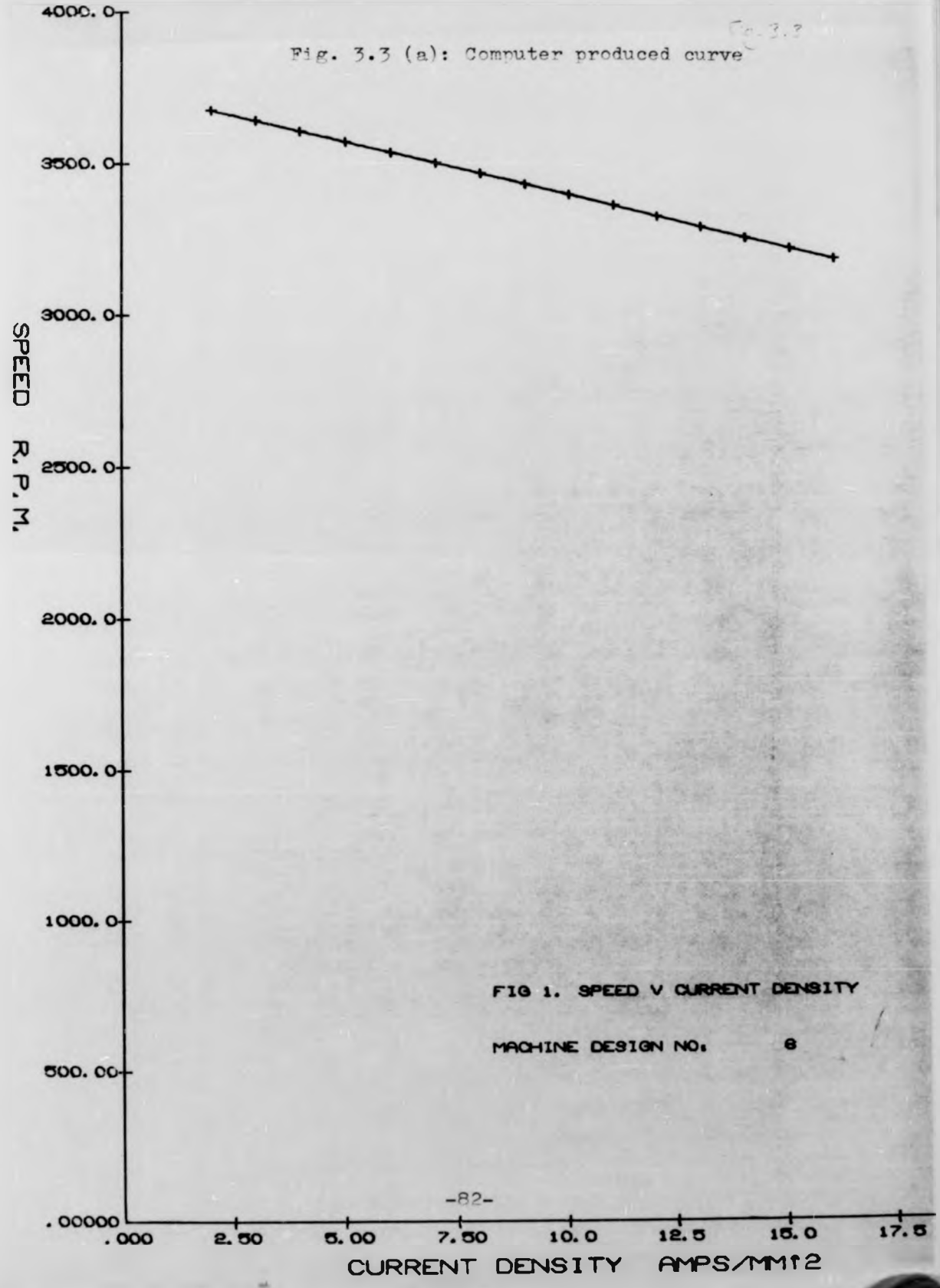

Fig. 3.3 (b): Computer produced curve

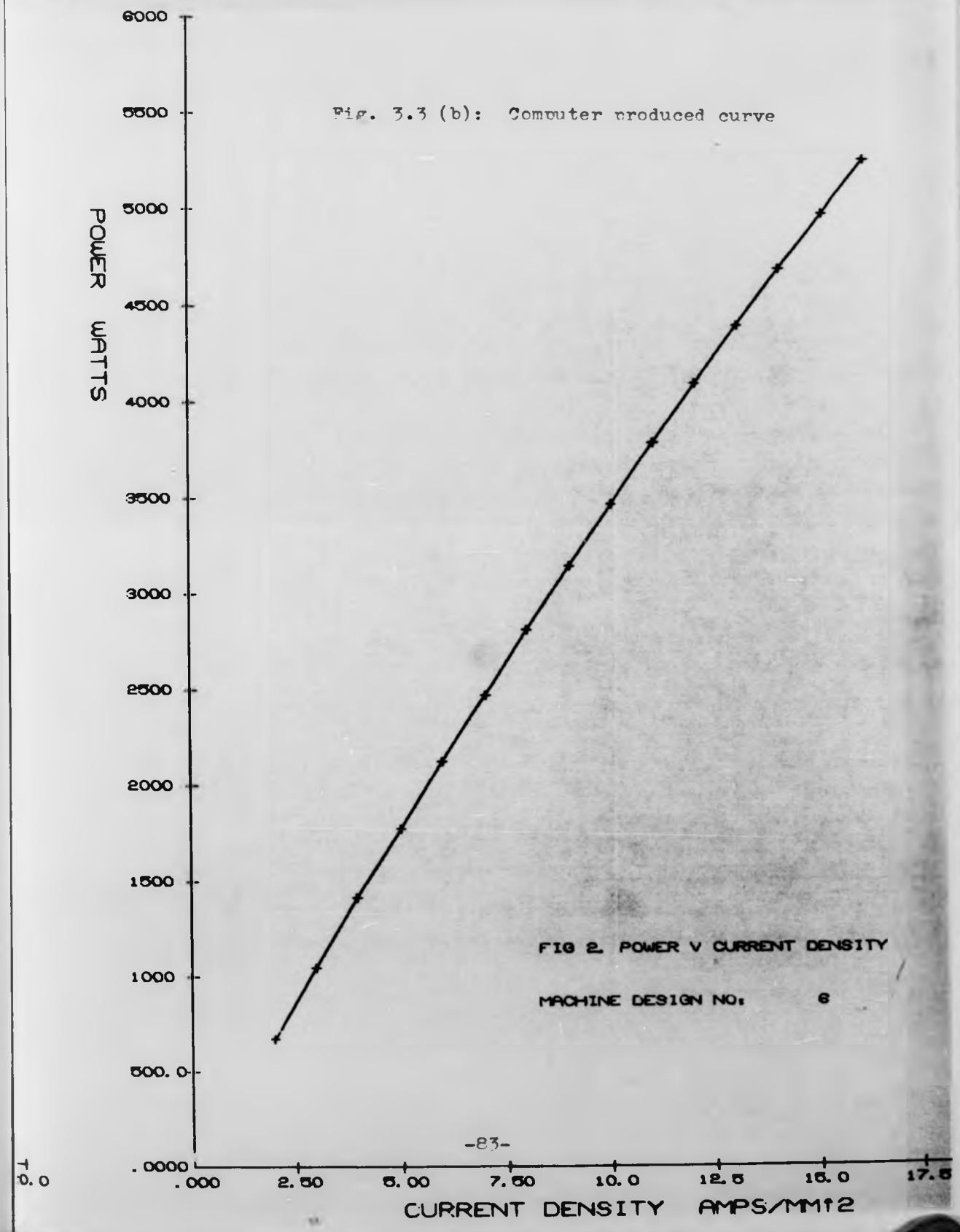

Fig. 3.3 (c): Computer produced curve

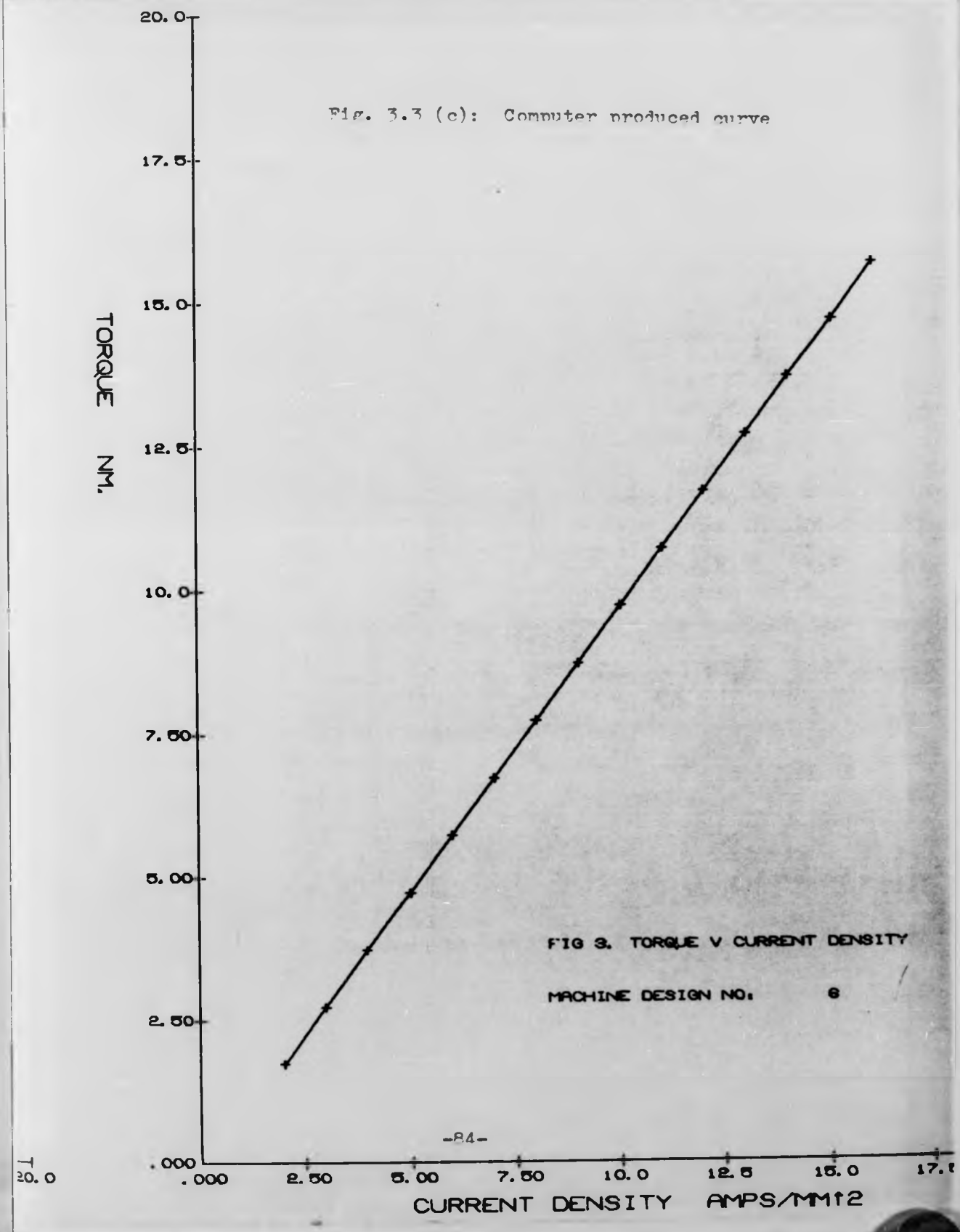

Fig. 3.3 (d): Computer produced curve

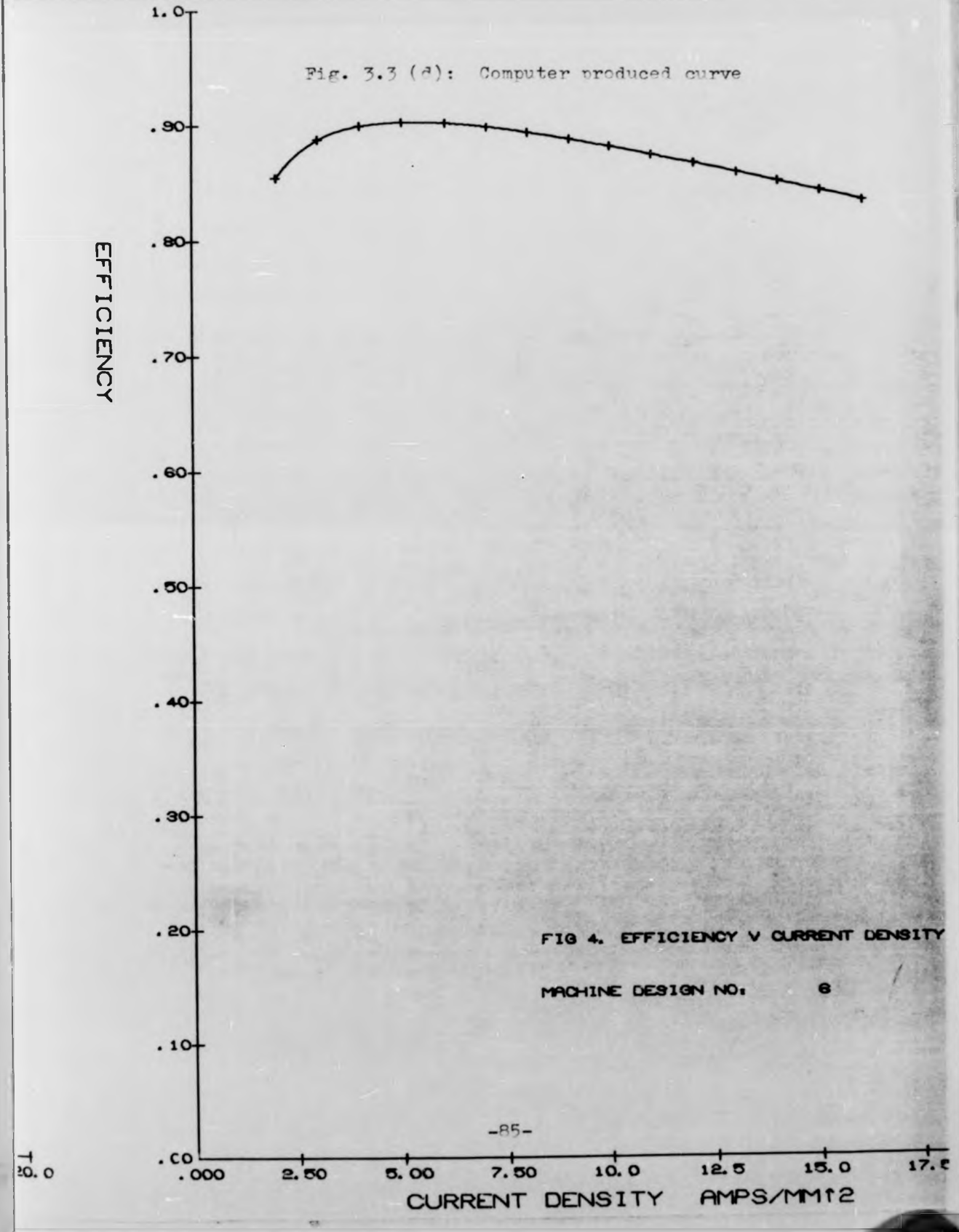

FIG 4. EFFICIENCY V CURRENT DENSITY

MACHINE DESIGN NO: 6

in two separate programs each of which represent one stage of a two-stage design routine.[12] The second stage used an extended and modified version of the early program and the first stage presents alternative designs encompassing a wide variation in parameters such as poles, coils, etc. The only input needed here is the power, voltage and speed required, along with the choice of magnet material. All of the resulting designs will meet the original specification to within a given tolerance. Restrictions may be imposed if necessary and as the program is fully interactive prompts are supplied where appropriate so that the operator need have no working knowledge of computer programming. Selected parameters are varied over a wide range and the results are output as described earlier.

A simplified flow chart of this stage is given in Fig. 3.4 and although the program necessarily contains much mathematical manipulation, the basic relationships may be summarised as follows. With reference to Figure 3.4

$$R_2 = f(n,P,V,B_m)$$

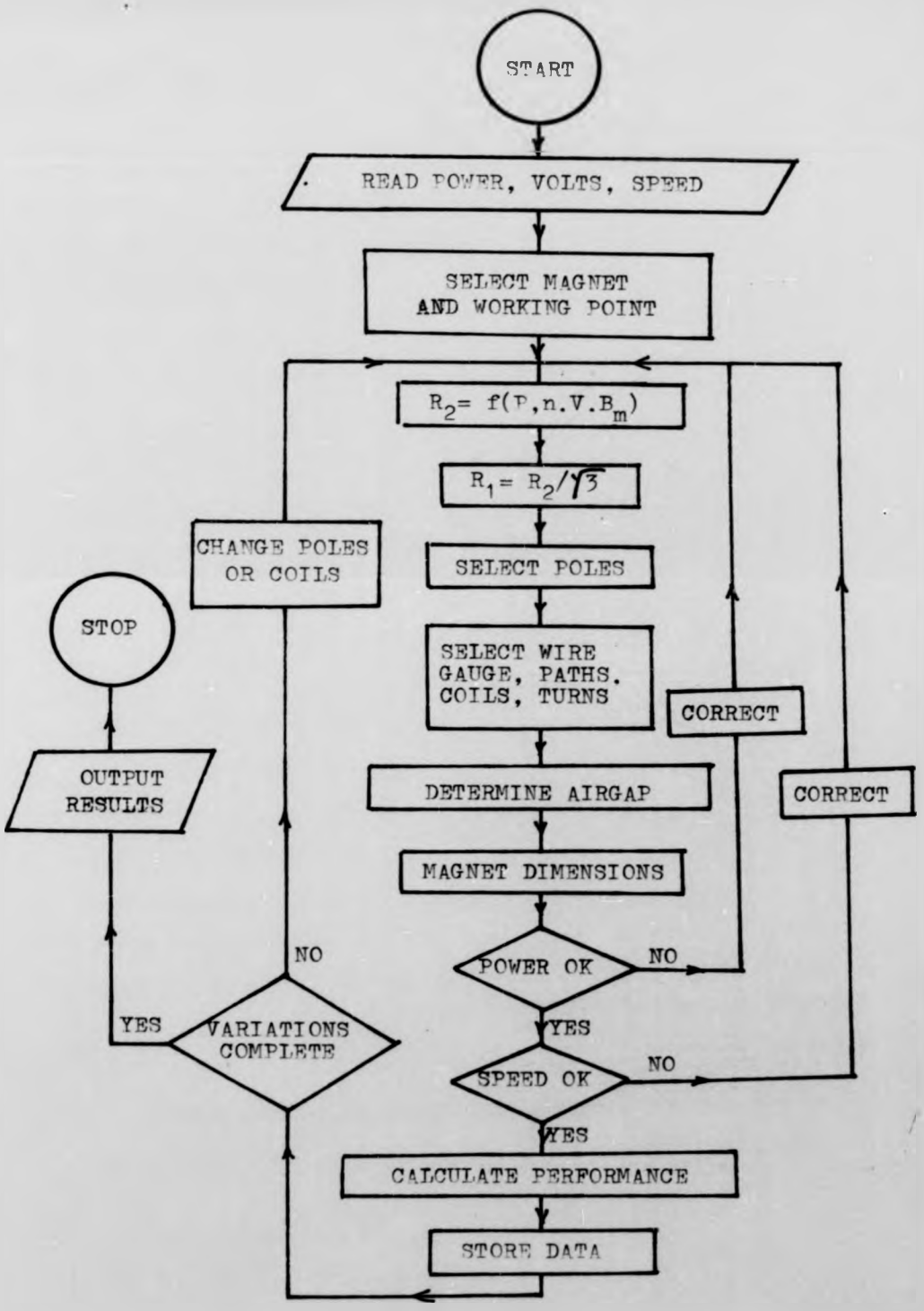

Fig. 3.4 : Flowchart of stage one design

Where R_2 is the outer active radius, n is the rotational speed, P the power output, V the operating voltage and B_m the flux density on the magnet BH curve.

$$R_1 = R_2/\sqrt{3}$$

Where R_1 is the inner active radius. This relation has been found to give maximum power for a given motor diameter (see Chapter 2).

The initial number of poles depends on the value of R_2, while the wire gauge, number of parallel paths, coils and turns per coil are chosen according to the power, voltage and speed. The air gap is determined from the gauge of wire specified with an allowance made for disc thickness and a suitable running clearance. The magnet dimensions may now be calculated from the number of poles, air gap, R_2 and the operating point on the BH curve.

The predicted power and speed are then calculated and compared with the required values.

If agreement is not close enough, a correction factor is applied and the entire procedure repeated. When one particular design has been finalised, the results are stored and new values of poles and/or coils taken. These values override those set initially. After all variations have been allowed for, a complete set of results is output with an indication of the optimum design in terms of efficiency and power density (power per unit weight). Although this summary is extremely condensed, it does represent the interactive nature of the process.

The second stage of the design procedure may be considered even more briefly. Basically data derived from stage one is input, with the option of modification to any parameter. The performance is calculated and the results output as before with the option of graphics. Additional modifications may then be made and the process repeated. A flow chart is given in Figure 3.5. Typical examples of numerical results are shown in Tables 5.1 and 6.1. The design parameters to be input are shown in Table 3.3 which is similar in format to Table 3.1.

UNIVERSITY OF WARWICK

Department of Engineering

DISC-ARMATURE MOTOR- COMPUTER AIDED DESIGN

Project:-

Design Paramters

		1	2	3
1	Machine Design Number			
2	Output Power, Watts			
3	Voltage, volts			
4	Speed, r.p.m.			
5	External Diameter D2, mm			
6	Internal Diameter D1, mm			
7	Number of Poles			
8	Bm, Tesla			
9	Hm, A/m			
10	Airgap, mm			
11	Magnet Density, Kg/m^3			
12	Number of Parallel Paths			
13	Number of coils			
14	Number of Turns/Coil			
15	Gauge of Wire, mm			
16	Current Density, A/mm^2			
	Optional Design Paramters			
17	Leakage Coefficient			
18	Loss Factor			
19	Pole-Arc/Pole-Pitch			
20	Space Factor			
21	Armature Temp. ^oC			
22	Weight of Non-Active Parts, Kg			
23	Mechanical Loss, Watts			
	Actual Power			
	Actual Speed			

Table 3.3 : New C.A.D. input data sheet

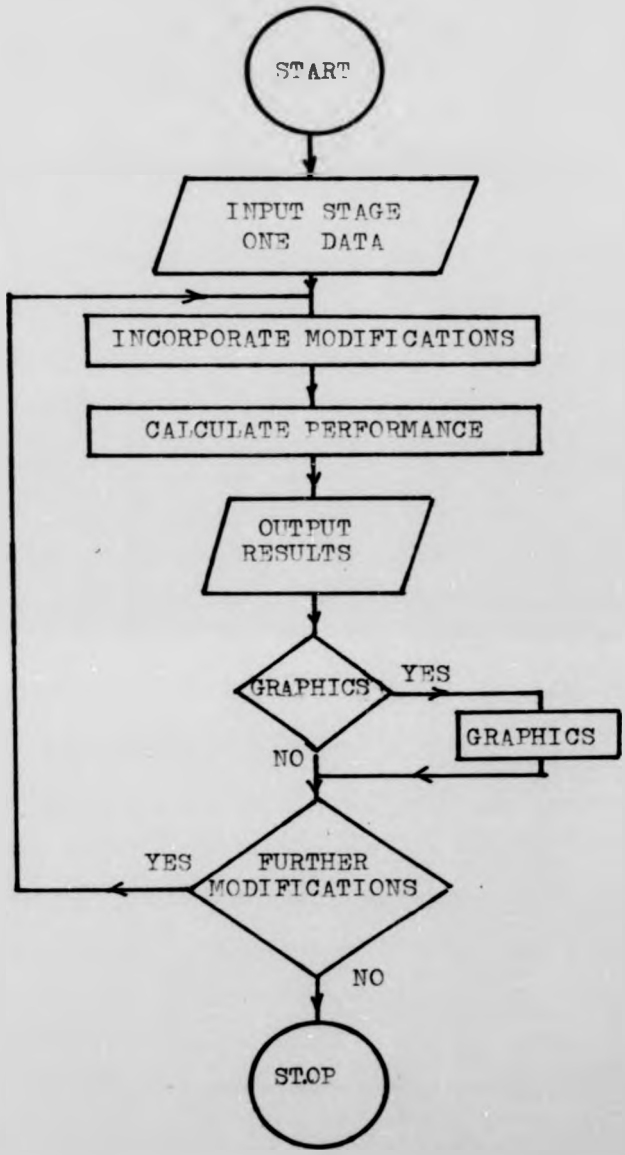

Fig. 3.5 : Flowchart of stage two design

3.4 Optimization of Machine Parameters

The armature winding of an axial-field machine has active lengths of conductors that lie approximately radially, and end-windings connecting these, that lie beyond the active air-gap region. An actual winding is shown in Figure 5.11 prior to encapsulation. The active air-gap is defined to exist from diameter d_1 to d_2 corresponding to the inner and outer diameters bounding the magnets.

One disadvantage of this type of machine is that there must always be some wasted space in the active part of the armature. If the winding is designed to fill as completely as possible the armature at d_1, at all greater diameters, there will be less than a complete fill, whereas the worst utilization of the available volume will be at d_2. The extreme cases are as follows: if $d_1 \ll d_2$, there is very poor utilization of the armature volume; if $d_1 \simeq d_2$, the active conductors have very small radial lengths. A relationship between d_1 and d_2 can be found which maximizes the

output power from the armature, which is:

$$d_2 = \sqrt{3}\, d_1$$

Since the end-windings are part of the circuit between the terminals, these contribute directly to armature resistance and hence I^2R loss may be reduced if these are shortened. The end-windings span approximately one pole pitch connecting opposite ends of a coil as shown in Figs. 3.2 and 3.6. Increasing the number of poles, p, will reduce the pole pitch and the armature resistance. However, if, p, becomes too large, the required number of coils becomes too large, the commutator segments get too narrow, and the performance of the magnetic circuit may be severely degraded.

The stator that corresponds with the windings of Figure 3.2 is shown in Figure 3.6. The arc subtended by each pole is expressed as a ratio of the pole pitch, which is theoretically in the range $0 < \alpha < 1$. For a given α. if p is increased to reduce end-winding resistance, the adjacent edges of neighbouring magnets become closer and the leakage flux between then will increase. The leakage coefficient, IC, which is expressed as the

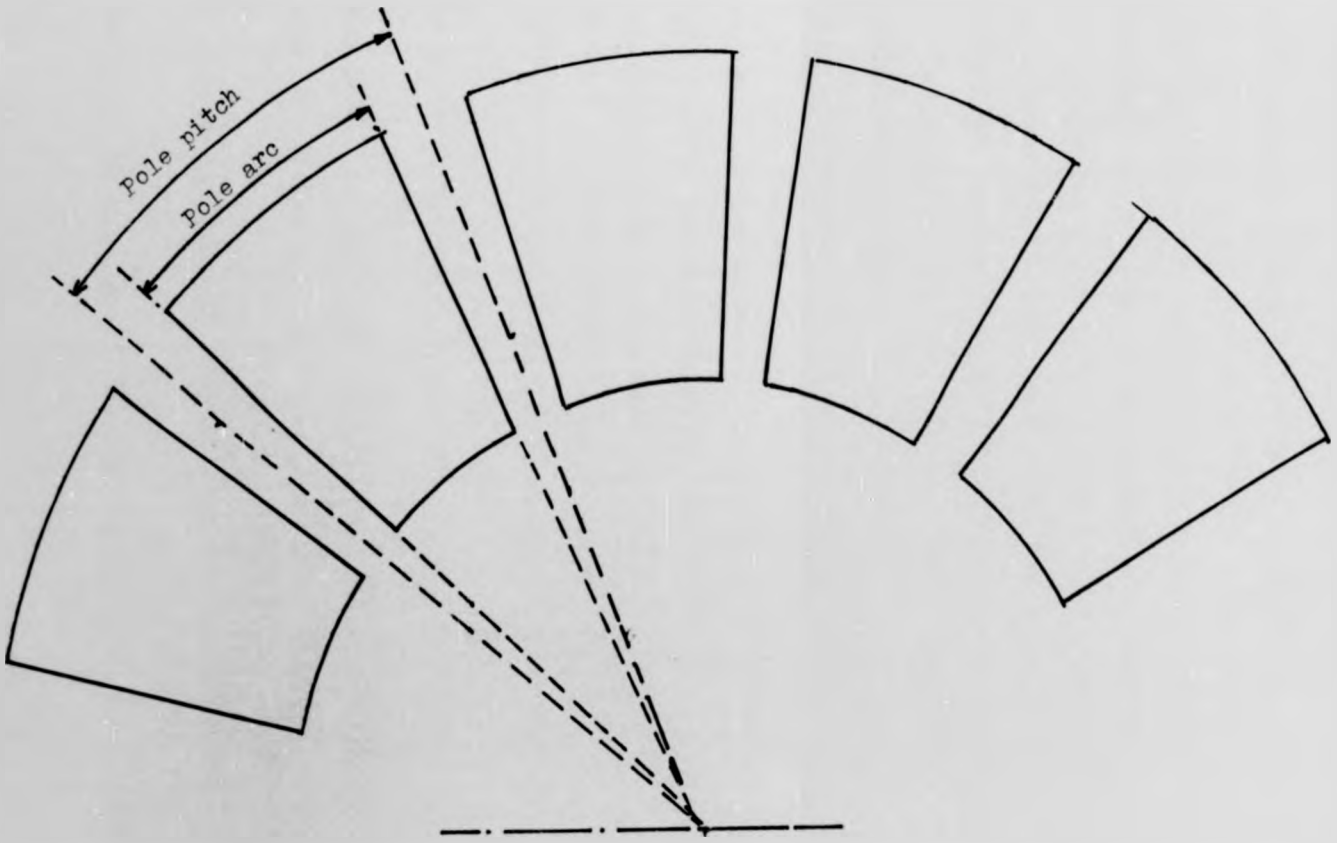

Fig. 3.6 : Stator magnet segments

ratio of magnet flux to useful air-gap flux. must always be greater than unity. Therefore, if p is increased, and we do not wish to enhance the leakage, i.e. LC is to be constant, then α must decrease so that the adjacent pole edges do not become too close. The total magnet area facing the air-gap is consequently reduced, as is the air-gap flux for a given magnet operating condition.

The leakage coefficient LC is difficult to assess. Attempts can be made to estimate leakage permeances, for which methods are outlined in many electrical engineering text books mainly based on Roters.[13] Note that if λ_t is the total permeance, then

$$LC = \frac{\lambda_t}{\lambda_u} \qquad 3.26$$

Where λ_u is the permeance of the useful flux paths. But, the total permeance, λ_t, can be written as

$$\lambda_t = \lambda_u + \lambda_l \qquad 3.27$$

Where λ_l is the (total) leakage permeance, therefore

$$LC = 1 + \frac{\lambda_l}{\lambda_a} \qquad 3.28$$

Formulae to calculate the (total) leakage and the useful permeances have been suggested by many writers. Collections of these are given by Roters[13] (1941) as already mentioned, Edwards in Hadfield[14] (1962), Parker and Studders[19] (1962). The simplest and most necessary procedures are those that give the permeance of the gap itself. For a gap between equal parallel surfaces opposite each other (Figure 3.7).

$$\lambda_g = \mu_o A_g / l_g \qquad 3.29$$

This formula holds whether the gap is circular, square or any other shape including the shape of magnet used in disc armature motor, provided its area is calculated correctly.

The permeance of a gap between inclined surfaces (shown in Figure 3.8) is:

$$\lambda_o = \frac{\mu_o \cdot l_m}{\theta} \log_e \frac{r_2}{r_1} \qquad 3.30$$

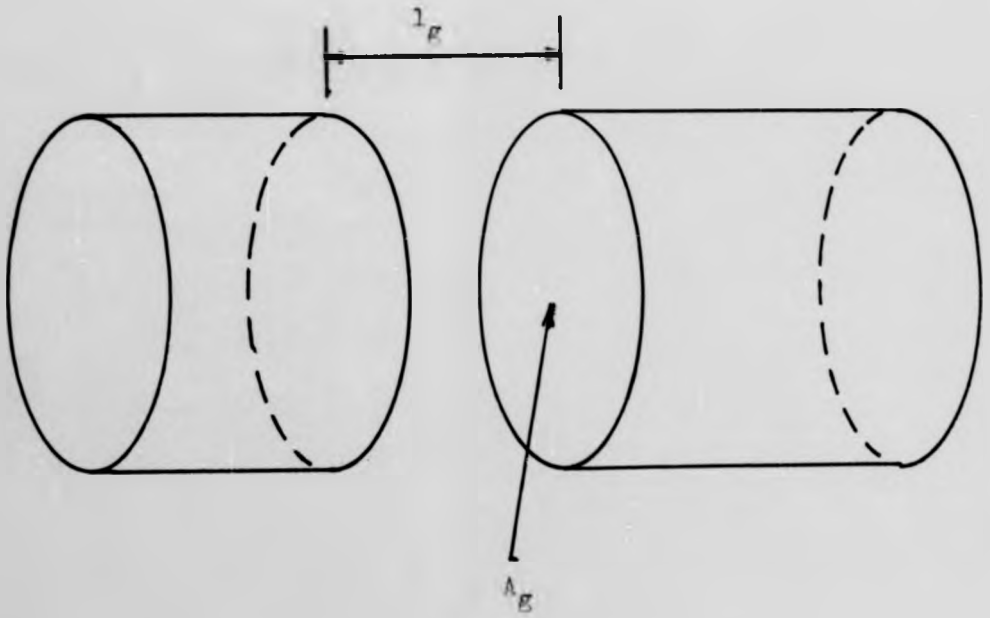

Fig. 3.7 : Gap between equal parallel surfaces

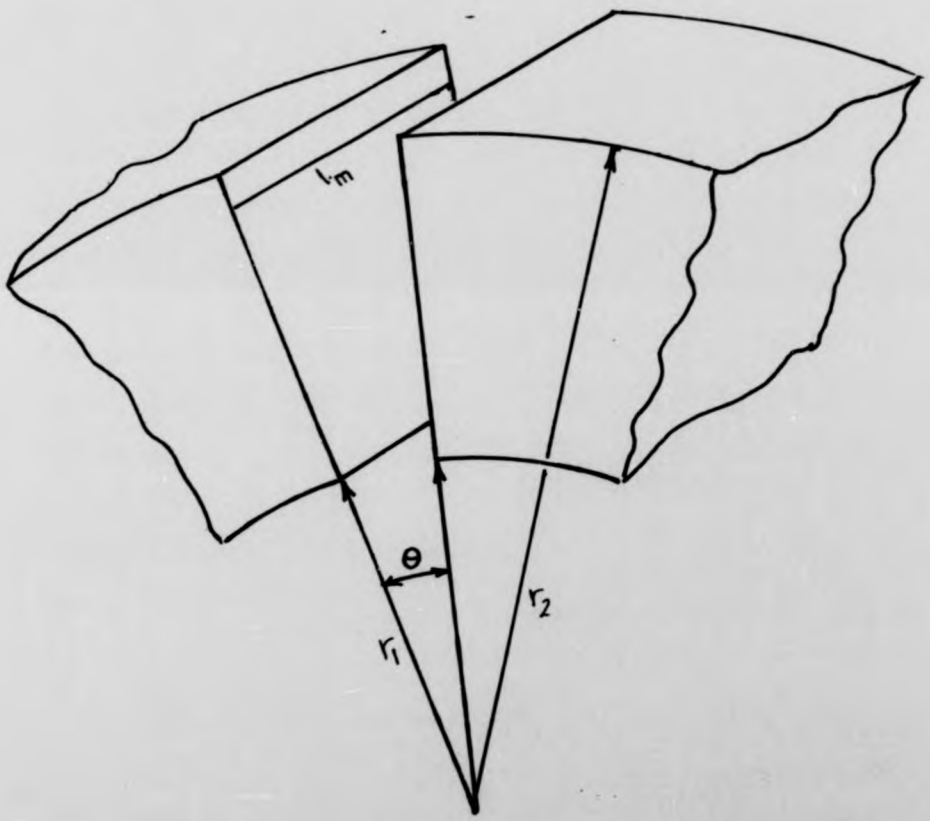

Fig. 3.8 : Gap between inclined surfaces

If a machine's radial and axial dimensions are fixed and a given operating point for the magnets is chosen, then the (total) leakage permeance and the permeance of the useful flux path can be calculated as shown below.

Fig. 3.8 shows that the sides of the magnets are radial and each may be defined from d_1 to d_2 by a unique angular position. Since the pole pitch is $2\pi/p$ and α is the pole arc/pole pitch ratio, the angle between adjacent pole sides is $2\pi(1-\alpha)/p=\beta$ The contributions to the permeance of the inner and outer diameter's surfaces of a magnet is small enough to be neglected. The (total) leakage permeance for both sides of a magnet of length l_m is a good estimate of the actual leakage permeance. Using Equations 3.30. this becomes:

$$\lambda_l = \frac{\mu_o \cdot l_m \cdot p}{2\pi(1-\alpha)} \ln \frac{d_2}{d_i} \qquad 3.31$$

Permeance of the useful flux path, λ_u. is

$$\lambda_u = \frac{\pi_g}{LF} \qquad 3.32$$

Where, λ_g, is the permeance of the air-gap and

the factor LF is a number usually lying between 1.1 and 1.4. It represents permeance reduction due to joints or steel parts that cannot be regarded as having infinite permeability. This is also the same factor which takes account of the magneto-motive force lost in joints or steel parts. Using Equation 3.29 and since:

$$A_m = A_g = \frac{\alpha.\pi(D_2^2 - D_1^2)}{4\ p} \qquad 3.33$$

Equation 3.29 becomes:

$$\lambda_o = \frac{\mu_o.\alpha.\pi}{4p.l_g.LF}(D_2^2 - D_1^2) \qquad 3.34$$

But, it is easily shown that:

$$LC = \frac{B_m\ .\ LF.l_g}{\mu_o.H_m.\ l_m} \qquad 3.35$$

Substituting for l_g from Equation 3.35 into Equation 3.34

$$\lambda_u = \frac{\pi \cdot \alpha \cdot B_m}{4p l_m H_m LC} (D_2^2 - D_1^2) \qquad 3.36$$

Substituting for λ_u and $\lambda_\perp$ from Equations 3.36 and 3.31 into Equation 3.28 and LC becomes:

$$LC = 1 + \frac{4\mu_o \cdot l_m^2 \cdot p^2 \cdot H_m \cdot LC}{\pi^2 \alpha (1 - \alpha) B_m (D_2^2 - D_1^2)} \ln \frac{D_2}{D_1} \qquad 3.37$$

Using Equation 2.29, Equation 3.37 becomes:

$$LC = 1 + \frac{0.334 \mu_o \cdot l_m^2 \cdot H_m \cdot p^2 \cdot LC}{B_m \cdot D_2^2 \cdot \alpha (1 - \alpha)} \qquad 3.38$$

Thus, the equation is also rearranged to bring p to the left-hand side. Thus:

$$p^2 = \frac{B_m \cdot D_2^2}{0.334 \mu_o \cdot l_m^2 \cdot H_m} \cdot \frac{\alpha}{LC} (1 - \alpha) (LC - 1) \qquad 3.39$$

Equation 3.39 shows that if a machine's radial and axial dimensions are fixed and a given operating point for the magnets is chosen, then the pole

number p, the pole arc/pole pitch ratio α, and the leakage coefficient LC are related by:

$$p^2 = K_1 \alpha (1 - \alpha)\ (1 - \frac{1}{LC}) \qquad 3.40$$

Where $K_1 = \dfrac{B_m\ D_o^2}{.334 \mu_o . H_m . l_m^2}$, a constant

This relationship may be visualized if LC is considered to be constant: an increase in α would bring adjacent pole edges closer together, and must be compensated by a reduction in p as prescribed in Equation 3.40 to maintain the same leakage flux. p and α may not be optimized in a machine design for minimum leakage coefficient. Only when these magnetic circuit parameters are related to the armature winding is it possible to optimize them by way of minimizing the I^2R_a power loss as below.

In Section 3.2 we show that the armature resistance:

$$R_a = \frac{2\rho . z}{\pi . G^2 a^2} \times 1.25 \left[(D_2 - D_1) + \frac{\pi}{p} (D_2 + D_1) \right]$$

Equation 3.11 makes a relationship between I, C and a, from which:

$$\frac{a \cdot \pi \cdot G^2}{2} = \frac{2 \times 10^{-6} I}{C} \qquad 3.41$$

Where I is the armature current. Combining Equation 3.11 and 3.18 gives an armature power loss of:

$$I^2 R_a = \frac{C \cdot \rho \cdot I \cdot Z}{2 \times 10^{-6} \times a} 1.25 \left[(D_2 - D_1) + \frac{\pi}{p} (D_2 + D_1) \right] \qquad 3.42$$

Eliminating the variable I from the right-hand side of this equation will allow $I^2 R_a$ to be minimized with respect to machine dimensions only. I is related to the specific electric loading A_c can be shown by:

$$A_c = \frac{I \cdot Z}{a \cdot \pi \cdot D_1} \qquad 3.43$$

But A_c can be shown as:

$$A_c = \frac{P}{15.83 \times 10^{-3} h D_2^3 \pi \cdot B_m} \cdot \frac{LC}{} \qquad 3.44$$

Which is substituted into Equation 3.42 with 3.43 to

give:

$$I^2R_a = \frac{\pi.C.\rho.P.D_1.IC\ 1.25}{31.66 \times 10^{-9}.\alpha.n.D_2^3.B_m}\left[(D_2 - D_1) + \frac{}{p}(D_2 + D_1)\right]$$

3.45

The conductor current density, C, is given a value of 8 A/mm^2 which corresponds to continuous running of the motor at a normal operating temperature of 75^{o}C.

At this temperature ρ has a value of $2 \times 10^{-8}\Omega.m$ by using Equation 2.29 and substituting for C and Equation 3.45 becomes:

$$I^2R_a = K_2 \frac{LC}{\alpha}\left(1 + \frac{11.72}{p}\right) \qquad 3.46$$

Where $K_2 = \frac{4.84\ p}{n.B_m.D_2}$

If one of the three variables p, α, or IC is fixed, then Equation 3.46 may be differentiated after substitution of Equation 3.40, to minimize I^2R_a with respect to one of these quantities. Leakage coefficient IC is determined by the machine parameters, which include p and α. If IC is fixed, the value

that is chosen will express the proportion of leakage flux that will be tolerated in a design. Designs for a given motor specification will be compared using different values for LC. A new constant is now defined as:

$$K_3 = \sqrt{K_1 \left(1 - \frac{1}{LC}\right)} \qquad 3.47$$

Combining Equation 3.46 and 3.47 and 3.40 gives

$$I^2R_a = K_2 \frac{LC}{\alpha} \left[1 + \frac{11.72}{K_3 \left[\alpha(1 - \alpha)\right]^{\frac{1}{2}}}\right] \qquad 3.48$$

The differentiation of which gives minimum I^2R_a when α solves:

$$\frac{1}{\alpha} + \left[\frac{11.72}{K_3}\right] \frac{1.5 - 2\alpha}{\left[\alpha(1 - \alpha)\right]^{1.5}} = 0 \qquad 3.49$$

Similarly, if α is fixed, the constant becomes

$$K_4 = \sqrt{K_1 \alpha(1 - \alpha)} \qquad 3.50$$

Combining Equations 3.46, 3.50 and 3.40 gives:

$$I^2R_a = \frac{LC}{\alpha}\left[K_2 + \frac{11.72\ K_2}{K_4\ (1 - \frac{1}{LC})^{\frac{1}{2}}}\right] \qquad 3.51$$

Differentiation of Equation 3.51 gives minimum I^2R_a when LC solves:

$$1 - \left[\frac{11.72}{K_4}\right]\frac{1.5 - LC}{LC\ (1 - \frac{1}{LC})^{1.5}} = 0 \qquad 3.52$$

It is seen from Equations 3.49 and 3.52 that I^2R_a may be minimized only with constant LC if $0.75 < \alpha < 1$ and with constant α if $1 < LC < 1.5$, although these parameters may take values outside these ranges.

In practice it is found that neither α nor LC change very substantially in a given design specification, and so one of these will be taken as a constant. When either Equation 3.49 or 3.52 is solved, Equation 3.40 is used to find the number of poles.

The usefulness of a computer program is measured by the number of parameters that can be selected for optimum performance. As a result of the development of the afore-mentioned criteria for the selection of all machine parameters has made it beneficial to develop a new design program for the machine. No detailed description of this program is given here, as the program itself is a modified version of the 1981 programs. The principal steps and sequence of calculations are shown by the flow chart in Figure 3.9.

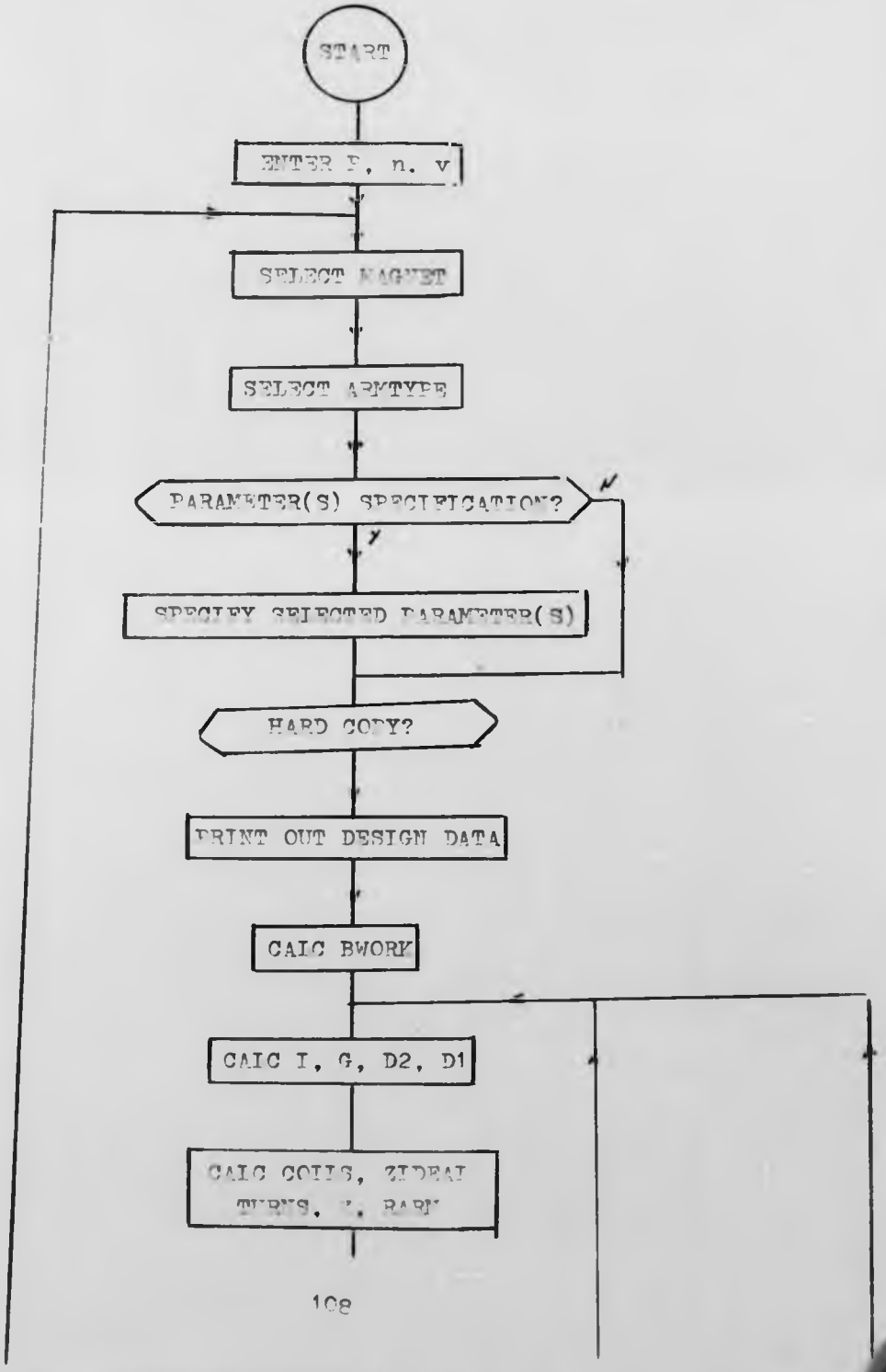
START
ENTER P, n, V
SELECT MAGNET
SELECT ARMTYPE
PARAMETER(S) SPECIFICATION?
N
Y
SPECIFY SELECTED PARAMETER(S)
HARD COPY?
PRINT OUT DESIGN DATA
CALC BWORK
CALC I, G, D2, D1
CALC COILS, ZIDEAL
TURNS, L, RAR'

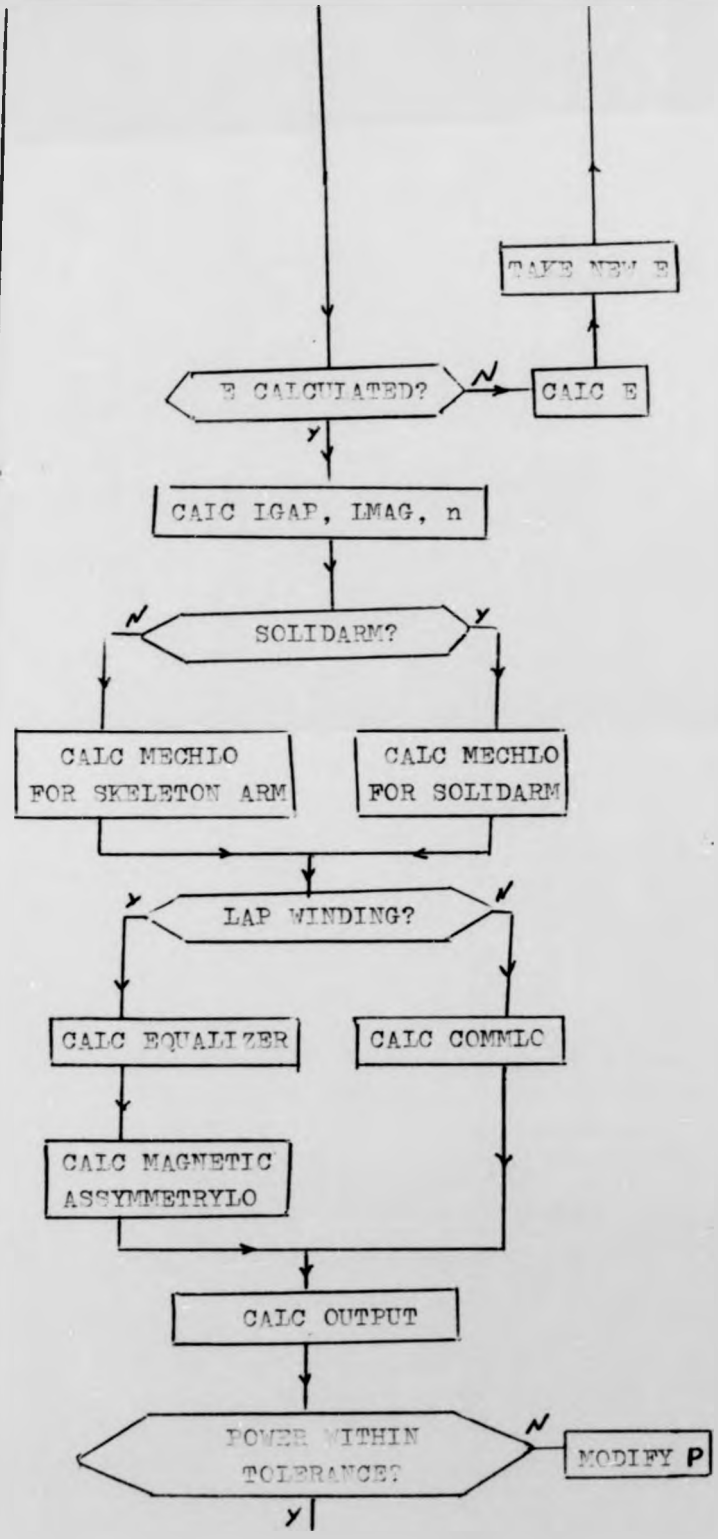
TAKE NEW E
E CALCULATED?
N
CALC E
Y
CALC IGAP, LMAG, n
N
SOLIDARM?
Y
CALC MECHLO FOR SKELETON ARM
CALC MECHLO FOR SOLIDARM
Y
LAP WINDING?
N
CALC EQUALIZER
CALC COMMLC
CALC MAGNETIC ASSYMMETRYLO
CALC OUTPUT
POWER WITHIN TOLERANCE?
N
MODIFY P
Y

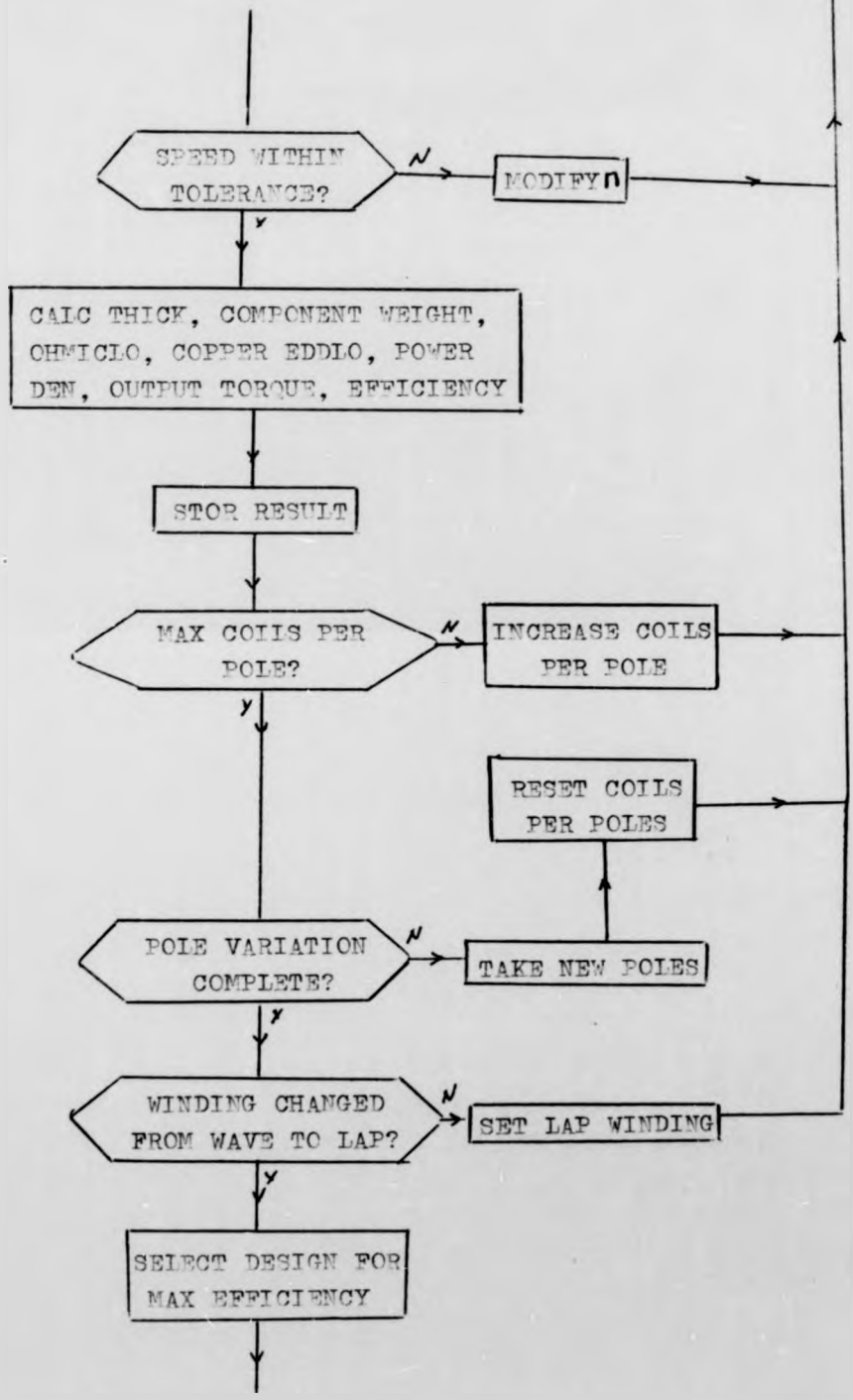
SPEED WITHIN TOLERANCE?
N
MODIFY n
Y
CALC THICK, COMPONENT WEIGHT, OHMICLO, COPPER EDDLO, POWER DEN, OUTPUT TORQUE, EFFICIENCY
STOR RESULT
MAX COILS PER POLE?
N
INCREASE COILS PER POLE
Y
RESET COILS PER POLES
POLE VARIATION COMPLETE?
N
TAKE NEW POLES
Y
WINDING CHANGED FROM WAVE TO LAP?
N
SET LAP WINDING
Y
SELECT DESIGN FOR MAX EFFICIENCY

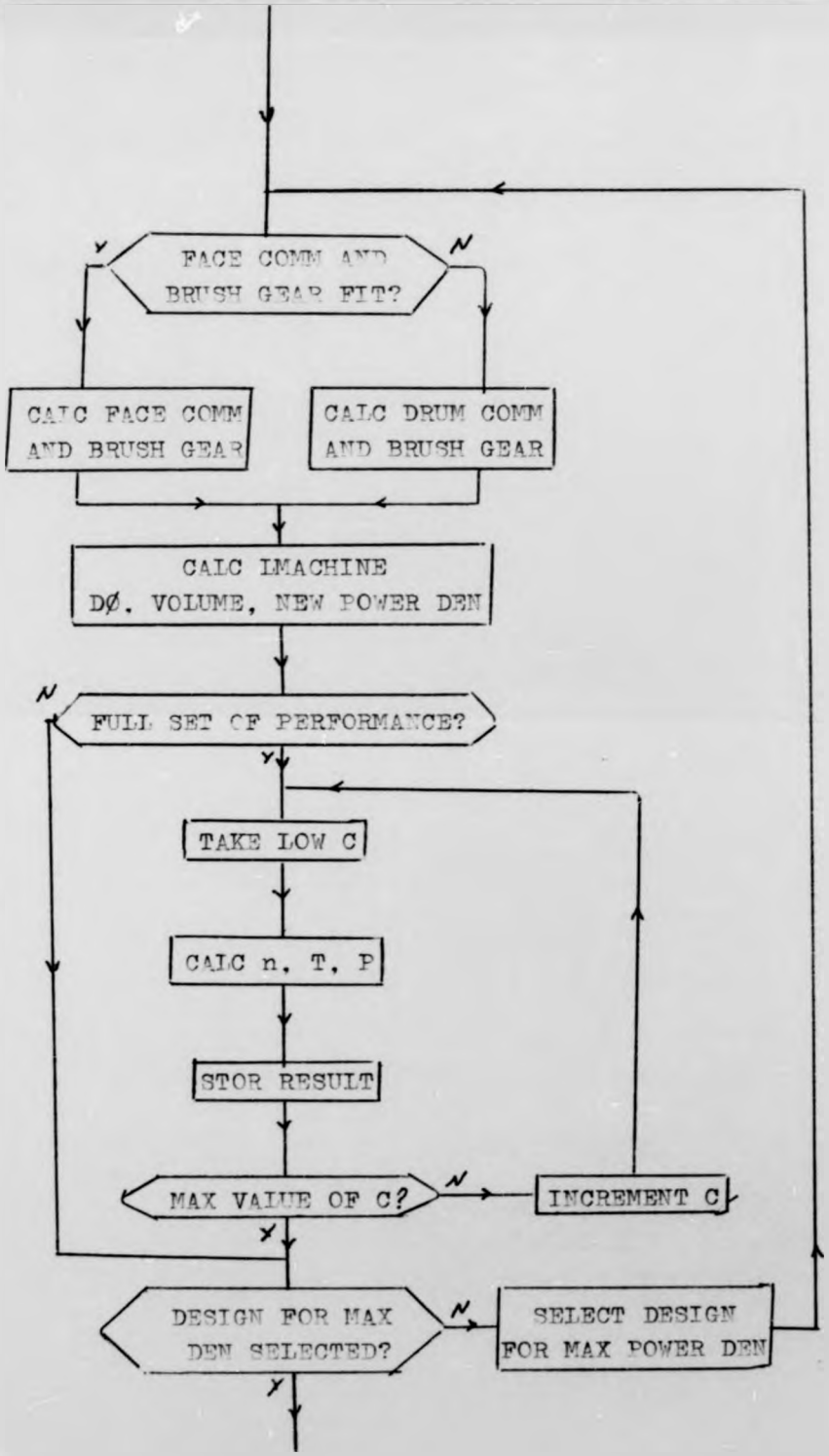
FACE COMM AND BRUSH GEAR FIT?
Y
N
CALC FACE COMM AND BRUSH GEAR
CALC DRUM COMM AND BRUSH GEAR
CALC LMACHINE DØ. VOLUME, NEW POWER DEN
FULL SET OF PERFORMANCE?
N
Y
TAKE LOW C
CALC n, T, P
STOR RESULT
MAX VALUE OF C?
N
INCREMENT C
Y
DESIGN FOR MAX DEN SELECTED?
N
SELECT DESIGN FOR MAX POWER DEN
Y

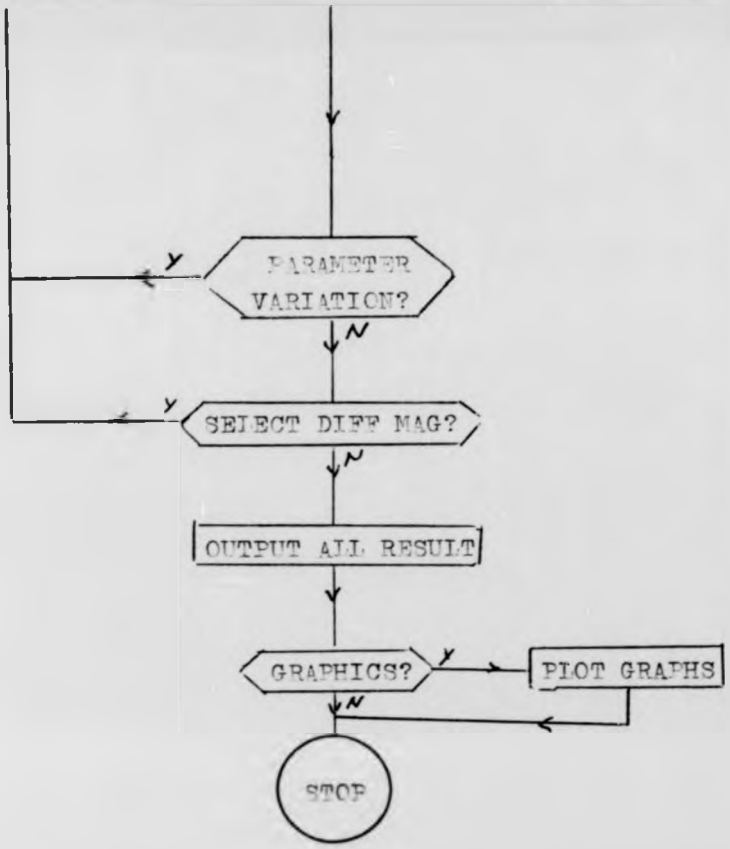
PARAMETER VARIATION?
Y
N
SELECT DIFF MAG?
Y
N
OUTPUT ALL RESULT
GRAPHICS?
Y
PLOT GRAPHS
N
STOP

4.1.1 Magnet Material under Recoil Conditions

So far it has been considered that the magnet is fully magnetized after assembly, the gap is thereafter unchanged, and the magnet is not subjected to demagnetizing influences arising from external causes. If the magnet were to be removed from the assembly and then replaced, a different situation would exist. Figure 4.1 illustrates this. The load-line O1 corresponding to some initial conditions for assembly causes the magnet to work at point 1. If the magnet is removed or "open-circuited", its working point will drop to point 2, which is determined by a new load-line. The slope of this new (or open-circuit) load-line is a function of the length to diameter ratio for cylindrical magnets, as shown in Figure 4.2. For other than circular cross-sections, nearly correct results may be obtained by using the diameter of a circle whose area is equal to the magnet area. When the value of $\underline{B}$ is
$\underline{H}$
known, a line having a negative slope of this

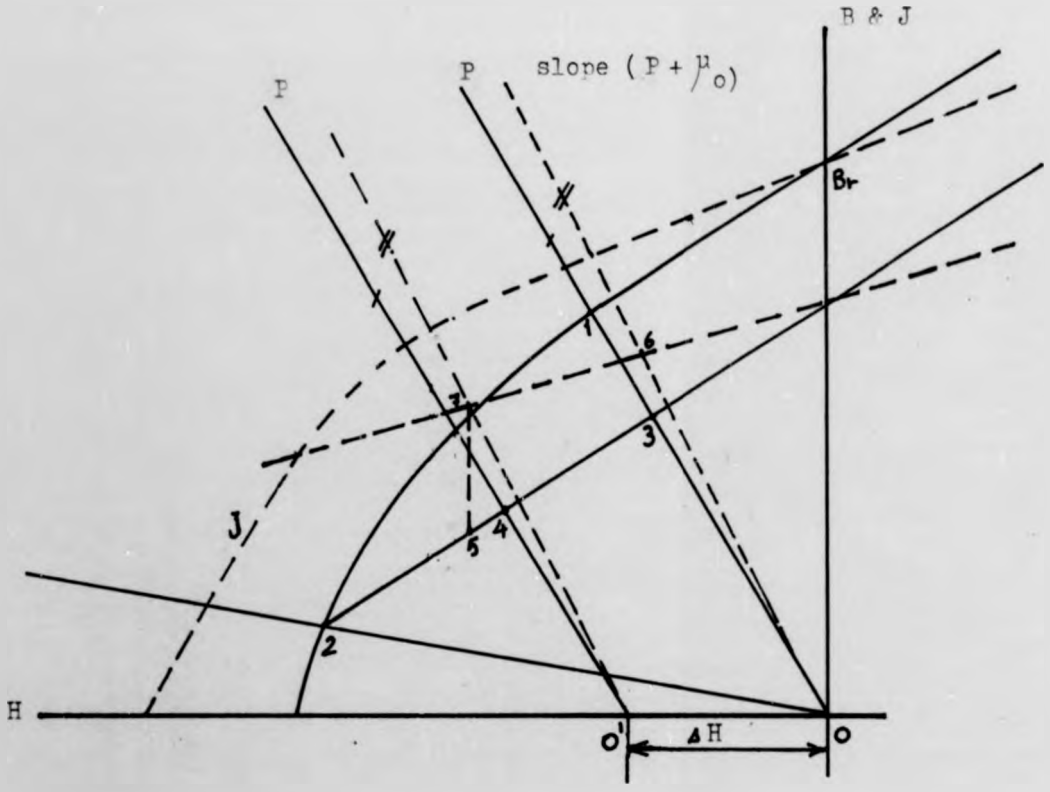

Fig. 4.1 : Estimation of magnet operation from BY characteristic

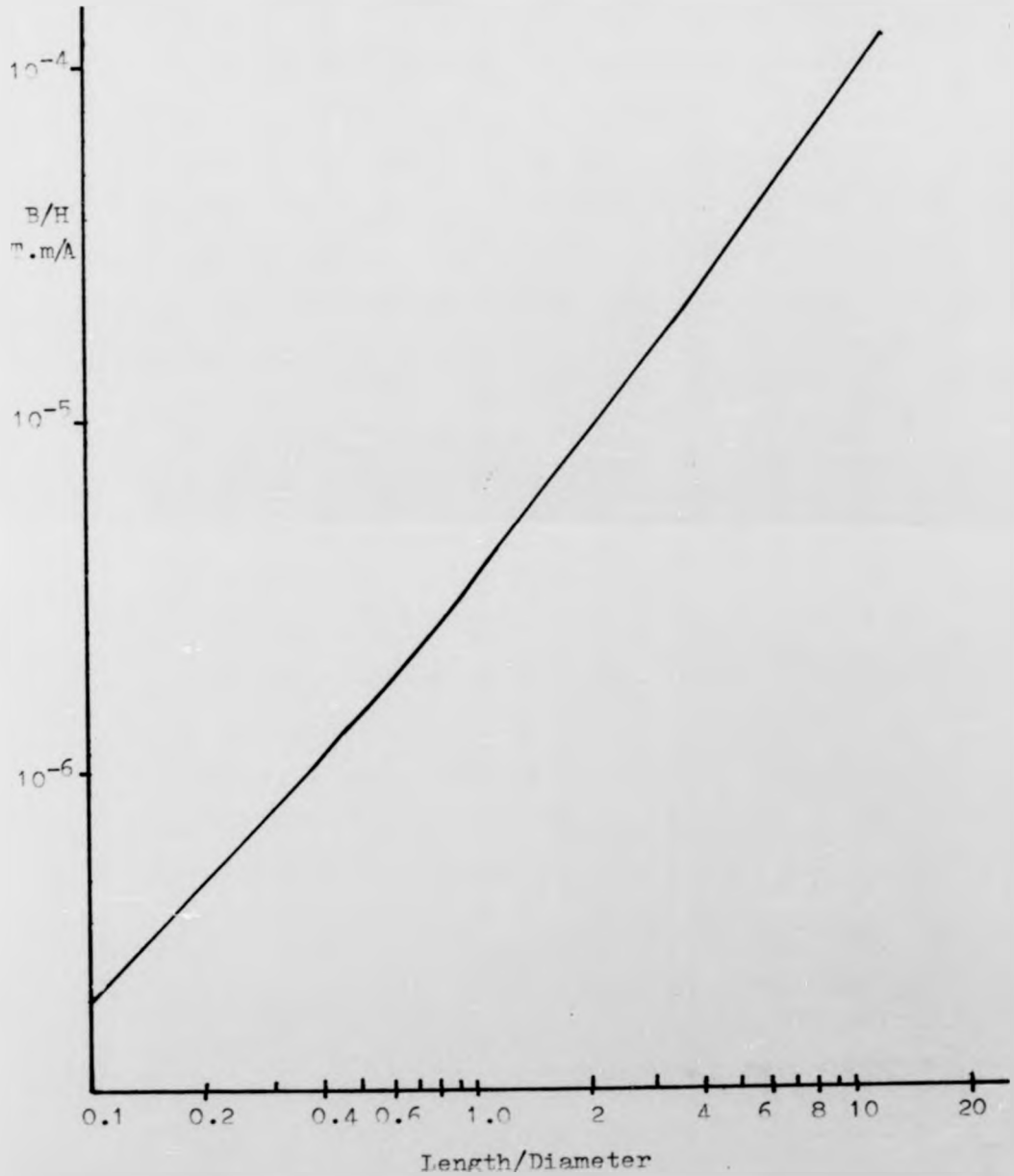

Fig. 4.2 : Open-circuit magnet operation against dimension ratio for cylinders

value is drawn through the origin of the same graph as that on which the demagnetization curve is plotted. The point at which it intersects the curve gives the open-circuit working point of the magnet. If the magnet is now replaced in the assembly, the working point does not necessarily return to point 1. Rather, it moves up along a recoil line within the main demagnetization curve until it intersects the original assembly load-line at point 3, as shown in Figure 4.1. Between the initial point and the B axis, such recoil lines are reversible; in fact, it produces a thin loop of negligible area and it is usual to consider the mean recoil line and its slope. The slope of recoil lines within the second quadrant is almost independent of the value of B from which they originate. This slope, expressed as

$$\mu_o \mu_r = \frac{\Delta B}{\Delta H} \qquad 4.1$$

where μ_r is known as relative recoil permeability and is commonly quoted for permanent

magnet materials.

It can now be seen that a partial loss of flux which varies greatly with the material properties and its working point has been experienced.

In the disc armature motor, such problems will only usually be apparent when assembling a machine. If the magnets are magnetised before assembly, there is always the possibility that on removal from the magnet charger and installation, they will be operating under recoil conditions. Fortunately, the problem is not equally apparent in all materials. This can be illustrated with the aid of Figure 4.3 which details typical room temperature demagnetization curves for materials A and B, exhibiting respectively low and high coercivities. We can observe the demagnetizing effect resulting from the open circuit condition (which is represented by a demagnetizing field ΔH). Both materials are working under ideal conditions for the respective materials, i.e. at a working point above their (BH) max point. After restoring the original condition (i.e.

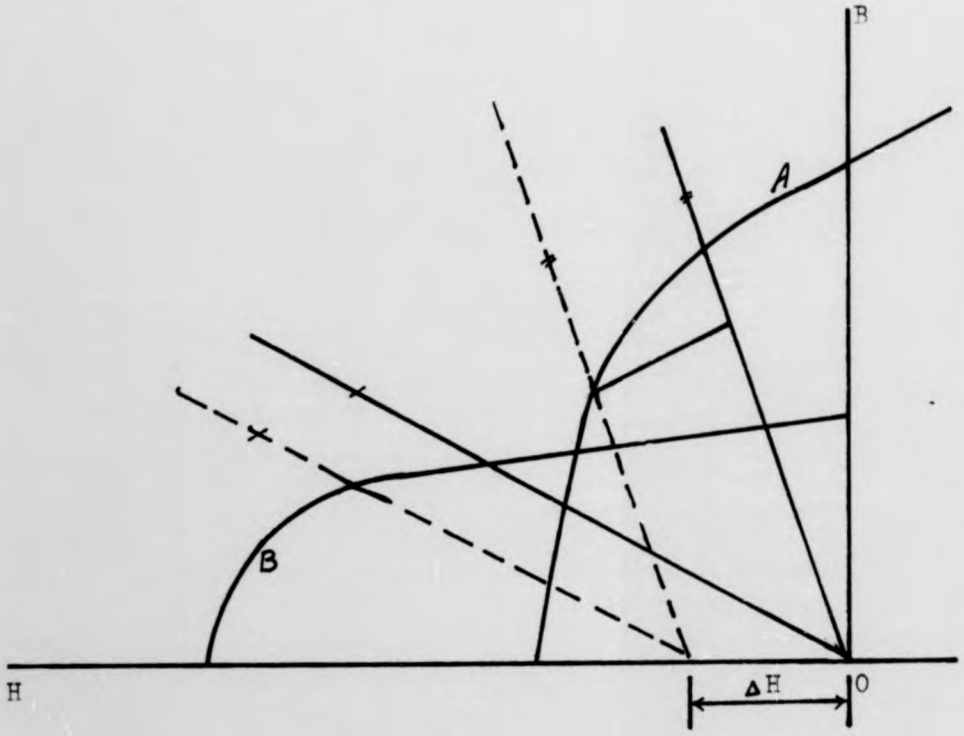

Fig. 4.3 : Recoil operation for materials of low and high coercivity

removal of the demagnetizing field ΔH), material A has, in fact, become partially demagnetized recoiling inside the BH curve with the obvious end result of very poor utilization of the magnet's energy capacity, whereas material B is fully recovered.

In many Ferrite and rare earth magnet assemblies, the loss may be essentially zero because many Ferrite and rare earth grades have demagnetization characteristics that approximate to a straight line. In these cases, the recoil line coincides with the original BH curve for all practical purposes. Therefore it is quite permissible to magnetize them prior to assembly since full magnetization is retained during assembly of the motor.

A further property of Ferrites and Sm Co_5 arising from a combination of high coercivity and low permeability allows the imprinting of poles of opposite polarity in close proximity without progressive self demagnetization. This enables maximisation of the effective

area which is, of course, desirable when one reflects on the relatively low remanance of these materials.

It is the Alnico types that are most susceptible, though, when these are specified, it is not unusual to include, in situ, magnetizing windings within the machine itself (Figure 2.5) so that the magnets may be energised initially after assembly, and also re-energised if ever the motor is dismantled. It has been found that with Alnico magnets used without such magnetizing windings, the working flux density is reduced. To assess whether recoil is likely, it is necessary to consider both the normal demagnetization characteristic and the expected conditions of operation. For example, with some Alnicos operating some way above BH max point, there may exist a small range of operating conditions where recoil operation coincides with the BH curve, i.e. the magnet's open circuit line intersects the BH curve at a point above its "knee".

4.1.2 Estimation of Operating Point of Magnet under Recoil Conditions

Once a permanent magnet electrical machine has been assembled, the only demagnetization effect likely to be experienced are those due to armature reaction.

To facilitate the subsequent discussion on this subject (armature reaction), a method of predicting changes in the flux density of a magnet subjected to external magnetic fields must first be analysed.

The operation of metallic permanent magnets under recoil conditions has been analysed in terms of the BH (normal) characteristic of the magnet material by Walshow[15] and Lynn[16], Desmond and Hanrahan and Toffolo.[17]

The method of analysis used by the above writers will be reviewed very briefly here for the sake of completeness.

Suppose a magnet is working with a load-line of slope P at a point 3 on the B recoil

line (Figure 4.1). Suppose an additional demagnetizing force ΔH is applied by means of a current flowing in a coil. The way to find the new B working point 4 is to draw a line through o' parallel to O1 cutting the B recoil line at 4. 4 is the new value of B.

This is the usual method of estimating the operating point of the magnet when exposed to an external field (3). This analysis, although simplified, has been found to be satisfactory for the study and design of metallic permanent magnets in electrical machines.

The newer anisotropic ceramic ferrite permanent magnets have recently found widespread application and in addition to the physical differences which exist between metal and hard magnets as described by Becker et al[18], the demagnetization characteristics of these two materials is also quite different. It is apparent that the anisotropic ferrite magnets have higher coercivities but lower values of remanence

than the metal magnets. Furthermore, there is a pronounced difference between the JH (intrinsic curve) and BH characteristics of the higher coercivity materials (refer to Figure 4.4), whereas for the lower coercivity materials, the difference is less significant, since

$$B = J + \mu_o H \qquad 4.2$$

Several authors, such as Gould[26], Ireland[20] and Golhardt and Beaudoin[21], have argued that, because of the comparatively large difference between the BH and JH characteristics of the ferrite magnets, the treatment of these magnets under the influence of external fields, differs from the usual approach, and for such magnets the JH characteristic must be employed as shown: a second recoil line, called here the intrinsic recoil line, and related to the recoil line by Equation 4.2 is also shown in Figure 4.1. The slope of the intrinsic recoil line is seen to be $(\mu_{rec} - 1)\,\mu_o$.

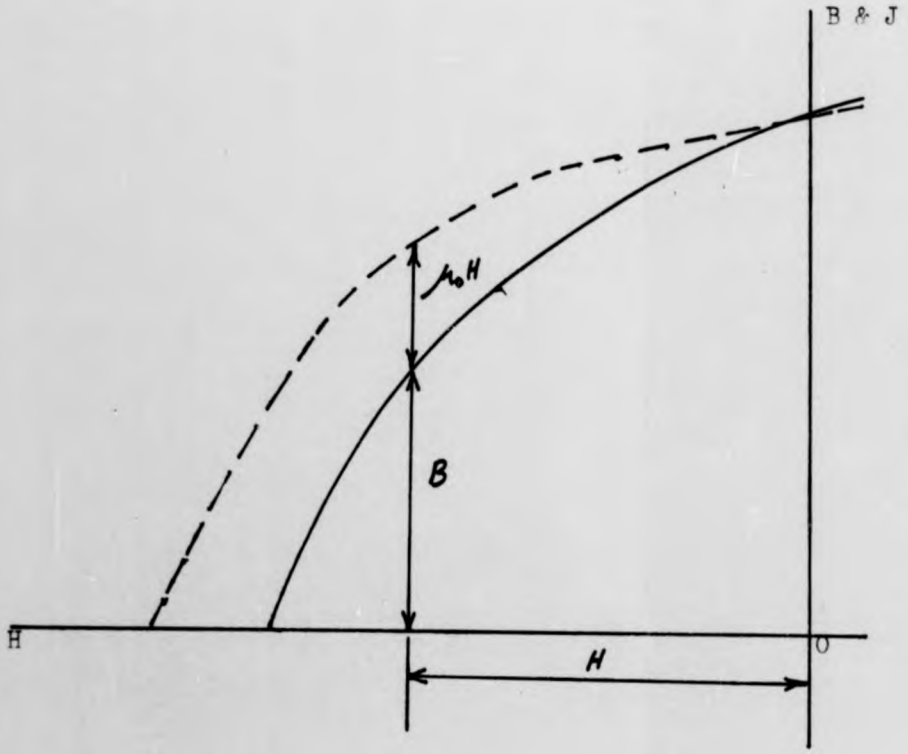

Fig. 4.4 : Typical intrinsic and normal demagnetisation curves

In this method, a line of slope - $(P + \mu_o)$ is displaced by ΔH giving an intercept on the intrinsic recoil line at 7 (Figure 4.1). The corresponding value of flux density on the recoil line, 5, is vertically below 7, and this new operating point differs from that obtained previously, i.e. point 4. Therefore, using this approach, the magnet appears to suffer a greater loss of useful flux density due to the demagnetizing flux than that given by the first method.

Burnett and Overshott[22], have argued that this latter concept is incorrect because the effect of an external demagnetizing field on the JH curve and the intrinsic flux density differs from its effect on the BH curve and flux density. A new method of analysis has been developed which allows the demagnetizing condition of a permanent magnet to be correctly estimated from the JH characteristic of the material. Their method has been shown to be equivalent to the conventional method of analysing permanent magnet systems using the BH characteristic. Therefore, the early method, which has been previously only

employed for metallic magnets, can be equally applied to ferrite permanent magnets and indeed to all permanent magnets irrespective of the properties of the material.

In the opinion of the author, the conventional BH characteristic approach to analysing ferrite (or hard) permanent magnet systems can be justified because the method using the JH curve over-estimates the effect of an externally applied field.

4.2 Armature Reaction

4.2.1 Analysis of Armature Reaction

A primary concern in the design of permanent magnet machines is the interaction of the magnet flux and the m.m.f. produced by the armature current. An analytical derivation of the equations to quantitatively predict the degree to which the permanent magnet is demagnetized by the armature current is presented here.

Consider a conductor in free space and a straight line that originates at $-\infty$ and terminates at $+\infty$ as shown in Figure 4.5 (a)

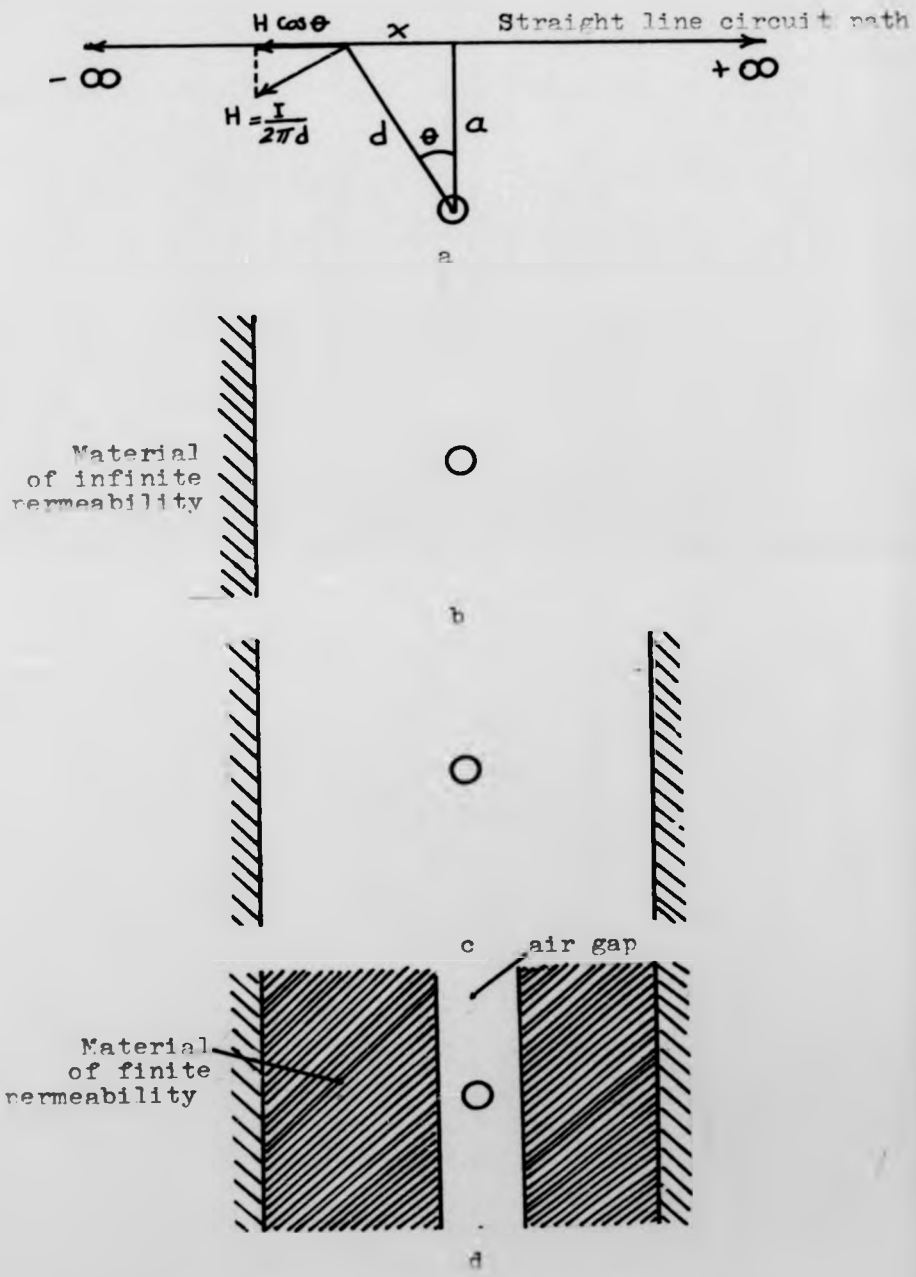

Fig. 4.5 : Magnetomotive force experienced traversing line around an ampere turn source

The general equation of the m.m.f. is:

$$\text{m.m.f.} = \int H \, dl \qquad 4.3$$

Where H has the same direction as dl.
Therefore, the m.m.f. experienced along the line of Figure 4.5(a) is:

$$\text{m.m.f.} = \int_{-\infty}^{+\infty} Hx \, dx \qquad 4.4$$

But, $Hx = H \cos \Theta$ 4.5

And, $H = \frac{I}{2\pi . d}$ 4.6

by substituting from Equation 4.6 into Equation 4.5 and then in Equation 4.4

$$\text{Then m.m.f.} = \int_{-\infty}^{+\infty} \frac{I}{2\pi . d} \cos\Theta \, dx = \frac{I}{2\pi} \int_{-\infty}^{+\infty} \frac{a}{a^2+x^2} \, dx = \frac{I}{2} \qquad 4.7$$

If a material of infinite permeability is placed at a distance from the conductor with the face of the material parallel to the direction of the conductor and perpendicular to the line in Figure 4.5(b) then the total m.m.f. along the line remains unchanged.

However, the entire m.m.f. would be experienced on the part of the line outside the material. If additionally, a second piece of material of infinite permeability is placed across the line so that a free-space region exists along the line between the faces of the two pieces of material, then again the total m.m.f. remains unchanged. However, the entire m.m.f. would be experienced along that part of the line in the free space region. Now, if an additional layer (or layers) of some other material of finite permeability is placed between the faces of the two pieces of material so that only a small air-gap remains to accommodate the conductor, then the total m.m.f. would be distributed between the air-gap and this second material. This latter condition is approximately the equivalent of the axial field machine, provided the flux return ring iron does not become saturated.

Thus, each armature spoke under the pole face contains Z_{spo} conductors, each carrying a current $\frac{I}{a}$, produces a m.m.f. of $Z_{spo} \frac{I}{2a}$

exerted either with, or against, the permanent magnet m.m.f. Figure 4.6 shows a sample section of an armature under the pole face. The total m.m.f. across each section (span between two adjacent spoke centres) is given as follows:

Section No. 1 $+5 \frac{Z_{spo} I_c}{2a}$

Section No. 2 $+3 \frac{Z_{spo} I_c}{2a}$

Section No. 3 $+1 \frac{Z_{spo} I_c}{2a}$

Section No. 4 $-1 \frac{Z_{spo} I_c}{2a}$

Section No. 5 $-3 \frac{Z_{spo} I_c}{2a}$

Section No. 6 $-5 \frac{Z_{spo} I_c}{2a}$

The total m.m.f. across each section is given by the superposition of the m.m.f. contributions from each section and the negative signs indicate that the m.m.f. is in opposition to

the flux direction of the permanent magnet. Thus the net m.m.f. across section No. 5, for example, is derived by noting that five sections act to oppose, and two sections aid, the permanent magnet field giving a net of three in opposition.

The permanent magnet can be partitioned into segments corresponding to the portion of the magnet opposite the sections of the armature between the centres of adjacent spokes, as shown in Figure 4.6. Each segment of the permanent magnet experiences a different m.m.f. due to the armature current.

To illustrate the effect of the armature m.m.f. on any segment of the magnet on the BH curve, the m.m.f. must be expressed in the same magnetic force units.

$$H = \frac{\text{m.m.f.}}{lm + lg} \qquad 4.8$$

Where lm is the magnet length in meters, and H is the magnetic force due to the armature

exerted either with, or against, the permanent magnet m.m.f. Figure 4.6 shows a sample section of an armature under the pole face. The total m.m.f. across each section (span between two adjacent spoke centres) is given as follows:

Section No. 1 $+5 \frac{Z_{spo} I_c}{2a}$

Section No. 2 $+3 \frac{Z_{spo} I_c}{2a}$

Section No. 3 $+1 \frac{Z_{spo} I_c}{2a}$

Section No. 4 $-1 \frac{Z_{spo} I_c}{2a}$

Section No. 5 $-3 \frac{Z_{spo} I_c}{2a}$

Section No. 6 $-5 \frac{Z_{spo} I_c}{2a}$

The total m.m.f. across each section is given by the superposition of the m.m.f. contributions from each section and the negative signs indicate that the m.m.f. is in opposition to

PAGINATION
ERROR

the flux direction of the permanent magnet. Thus the net m.m.f. across section No. 5, for example, is derived by noting that five sections act to oppose, and two sections aid, the permanent magnet field giving a net of three in opposition.

The permanent magnet can be partitioned into segments corresponding to the portion of the magnet opposite the sections of the armature between the centres of adjacent spokes, as shown in Figure 4.6. Each segment of the permanent magnet experiences a different m.m.f. due to the armature current.

To illustrate the effect of the armature m.m.f. on any segment of the magnet on the BH curve, the m.m.f. must be expressed in the same magnetic force units.

$$H = \frac{\text{m.m.f.}}{lm + lg} \qquad 4.8$$

Where lm is the magnet length in meters, and H is the magnetic force due to the armature

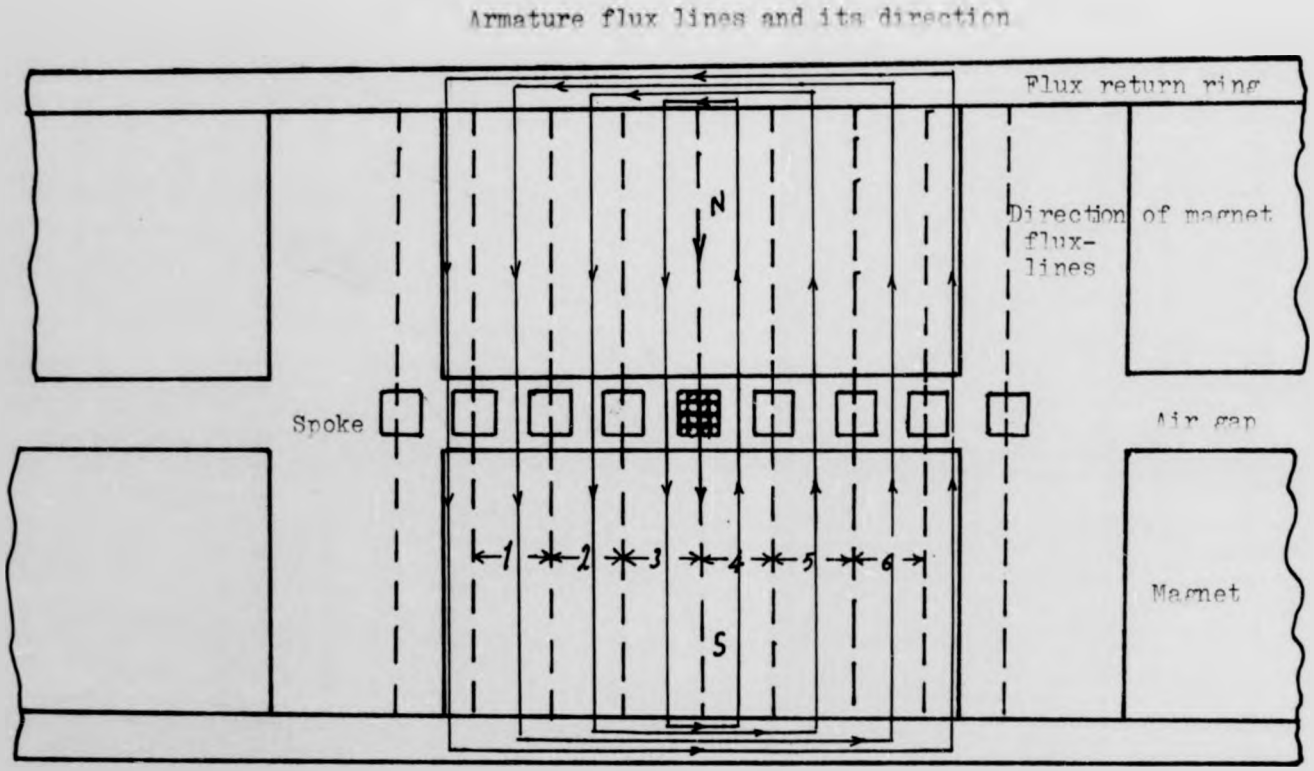

Fig. 4.6 : Sample section of armature under magnet pole face

on a given segment of the magnet.

The m.m.f. may be expressed more specifically in terms of aiding and opposing armature sections, and the maximum amount of force on each section may be arranged to

$$H = (K_o - K_a) \frac{Z_{spo} I}{2a.l_m} \qquad 4.9$$

Where K_o is the number of sections opposed to field flux; K_a, the number of sections aiding field flux; $\frac{Z_{spo}I}{2a}$, the maximum amper turns per section (generally at stall current); and lm, the axial length of a permanent magnet in meters.

The no-load operating point of the magnet is given by the permeance line of slope P. When the armature m.m.f. on a particular segment is negative, then the operating point under this load can be obtained by drawing a line parallel to the no-load permeance line starting from ΔH. The intersection of this line and the BH curve yields the new operating

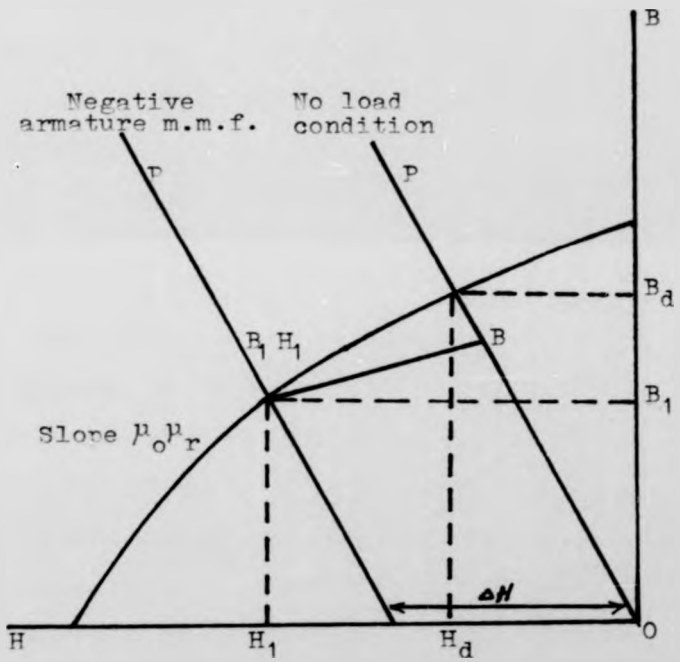

Fig. 4.7 : Magnet segment operating points after application of negative m.m.f.

point for that segment. The process is illustrated in Figure 4.7.

The special case of demagnetization due to the large stall current in the armature can be considered as a condition of a momentary large armature current that decays to zero. The resultant flux densities of the various segments of the magnet when the current returns to zero are the stabilized operating points.

When the magnetic force H is positive, the operating point shifts up along a recoil line, while the current increases to a peak, then shifts down along the recoil line as the current decays and returns to the initial operating point. When the magnetic force H is negative, the operating point shifts down along the demagnetization curve while the current increases to a peak and then shifts up along a recoil line as the current decays to zero. The resultant stabilized operating point is given by the intersection of the recoil line and the no-load permeance line.

As constructed in Figure 4.7 the reduced operating point for H corresponding to the peak stall current is indicated by the intersection of the offset permeance line and the BH curve at values B_1 and H_1. The stabilized operating point can then be computed by

$$B = \left[P/(P + \mu_r \mu_o)\right]\left[B_1 - \mu_r \mu_o H_1\right] \qquad 4.10$$

Where P is the slope of the no-load permeance line and H_1 is read as a negative value in the second quadrant. Thus after the stall current returns to zero, all segments of the magnet subjected to positive magnetic forces stabilize at the initial no-load point and those segments subjected to negative forces stabilize at a flux density as determined above.

When the m.m.f. on a segment is positive, the no-load operating point shifts up along a recoil line (refer to Figure 4.8). The flux density at the new operating point is given by

$$B = B_d + \left[P/(P + \mu_r \mu_o)\right] (\mu_r \mu_o \cdot \Delta H) \qquad 4.11$$

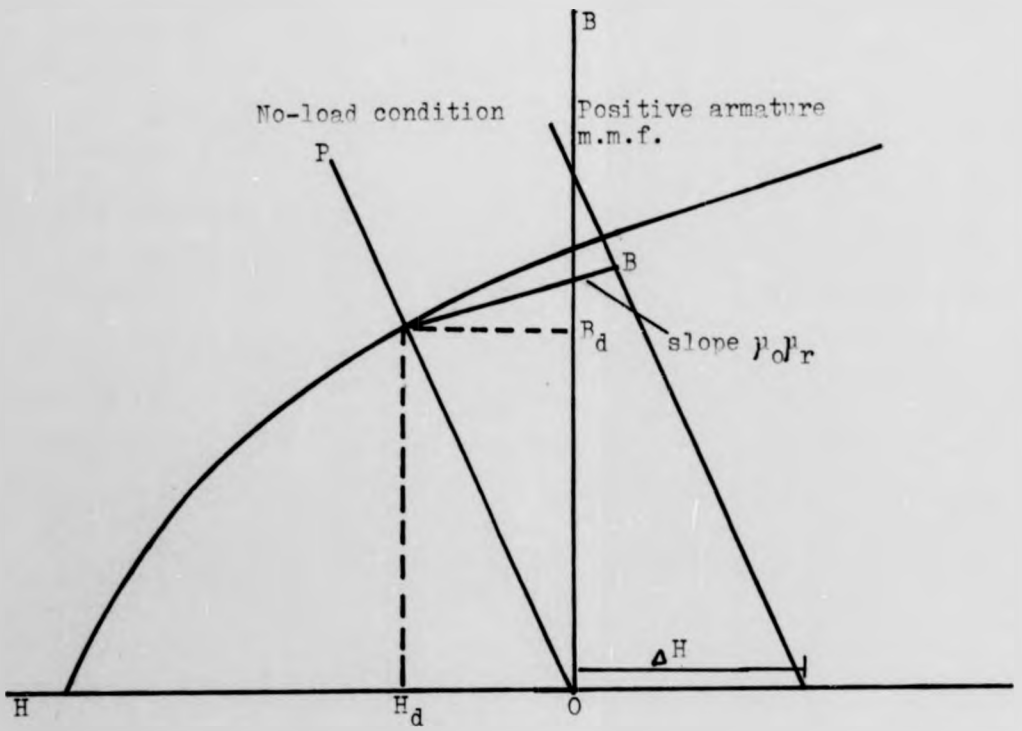

Fig. 4.8 : Magnet segment operating points for application of positive m.m.f.

Where B_d is the flux density at no-load, P is the slope of the no-load permeance line and μ_r is the relative recoil permeability.

The stall current decays to the lower running current rather than zero. In this situation the segments of the magnet that experience negative magnetic forces, stabilize at an operating point described by the intersection of the recoil line and the permeance line originating from ΔH_a, corresponding to the armature running current (refer to Figure 4.9). Thus the stabilized operating point flux density is:

$$B = \left[P/(P + \mu_r \mu)\right]\left[B_1 - (\mu_r \mu)(H_1 - \Delta H_a)\right] \quad 4.12$$

Where P is the no-load permeance; B_1, the flux density at stall current; H_1, the magnetic force at stall current operating point (negative in second quadrant); ΔH_a, the magnetic force due to armature running current (negative); and μ_r, the relative permeability of the magnetic material.

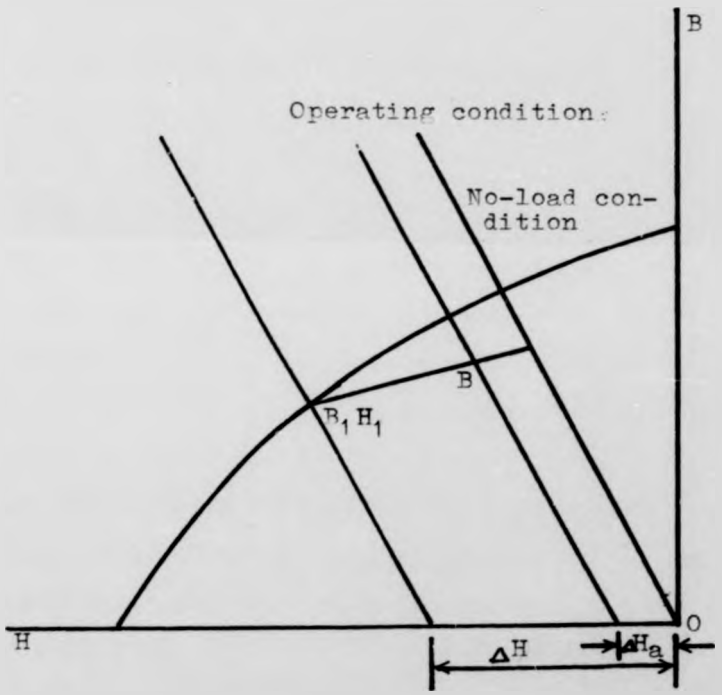

Fig. 4.9 : Magnet segment operating points under load after application of negative m.m.f.

The operating point on the segments experiencing positive magnetic forces is computed in calculating the stall current demagnetization, with H corresponding to the armature running current.

If the armature were always to rotate in the same direction, then the various segments would experience the same magnetic force each time the motor is started. Thus those segments which receive positive forces would have operating points above the initial no-load point. If, however, the armature rotation is reversed, then these segments would experience negative forces. The polarity of all forces would be reversed. The effect of this reversing is to cause the operating point to shift up and down a new recoil line.

The final stabilised line can be determined from tracing the cycle from negative to positive, and back to negative. The initial negative swing takes the operating point down along the demagnetizing curve to the point B_1, H_1 as indicated in Figures 4.7 and 4.10.

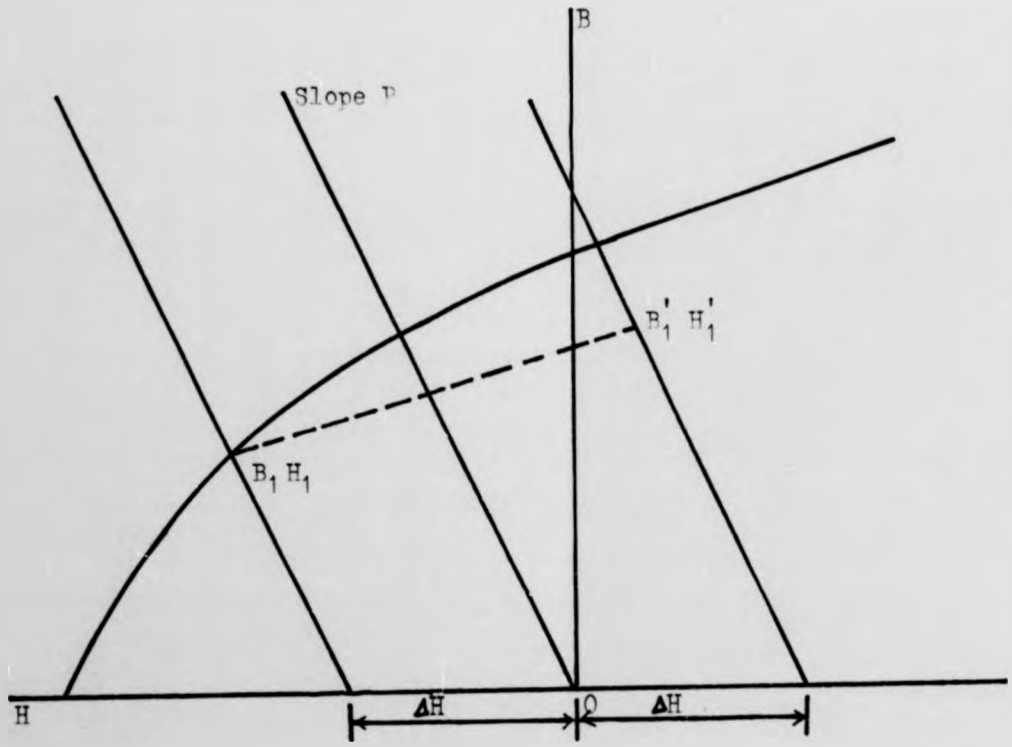

Fig. 4.10 : Magnet segment operating points after reversal

The reversal to positive takes the operating point up along a recoil line to point B_1^1, H_1^1 (Figure 4.10). This point can be computed from the Equation 4.12 which calculates the operating point under load after stall, with H positive. Reversing again to negative takes the operating point down the upper side of the recoil line back to B_1, H_1. This process defines the end points of the recoil line B_1, H_1.

The analytical approach thus far described, deals with a static situation. However, the major consideration is the stall current demagnetization which only occurs at the instant of starting and decays with increasing armature speed. Since the worst case is the initial current surge, and since the duration of this current is immaterial, the static analysis is applicable to the prediction of stall current demagnetization.

In the case of the running current, the armature is rotating at a high speed. The static analysis is not necessarily the best

approach. An alternative approach is to consider the armature surface to be a current sheet such as the outer edge of section No. 5 receives an m.m.f. of $-4\ (\frac{Z_{spo}\ I_c}{2})$ while the centre receives zero, and the outer edge of section No. 1 receives an m.m.f. of $+4\ (\frac{Z_{spo}\ I_c}{2})$.

It is then assumed that the m.m.f. is linear and that the m.m.f. at any point is proportional to the distance away from the centre.

However, it may be just as well to ignore these effects. The recoil line is determined by the stall current. If the running current is considerably smaller than the stall current, the operating points do not shift very far from the stabilized point. Thus the recoil line may be considered linear over this range and there will be no net change in total flux per pole. For every negative change in flux (points on the armature to the right of the centre), there is an equal positive change (the corresponding point to the left of centre).

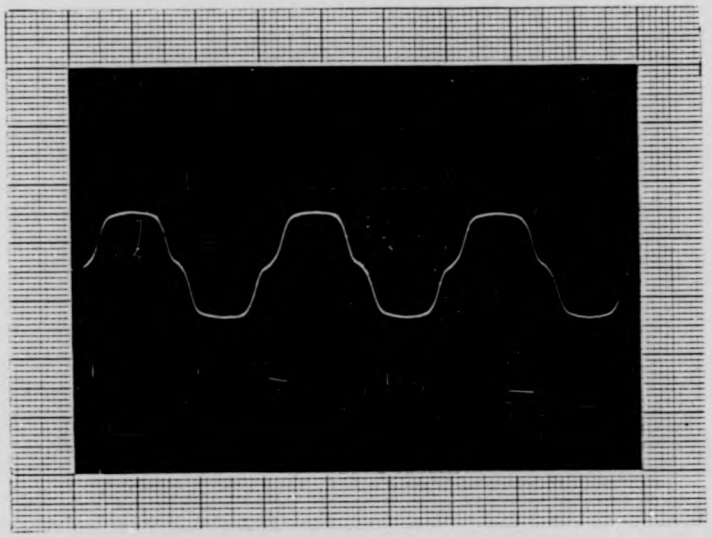

(a)

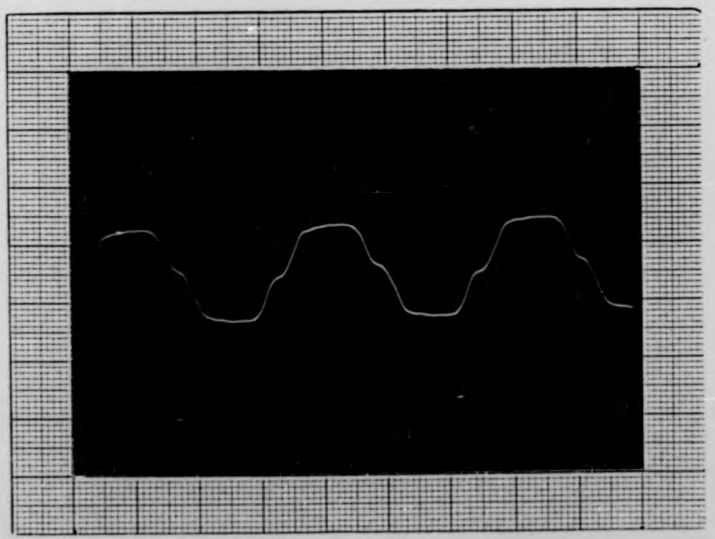

(b)

Fig. 4.11 : The airgap flux distribution:
(a) at no nload (magnet poles flux only)
(b) at full load (flux due armature current - 120A - and magnet poles)

Figure 4.11 (a) and (b) shows the air-gap flux at no-load and full-load respectively for the 10kw disc motor. This is accomplished by fixing a surge coil of one turn of thin cross-section wire on the disc armature and then the coil terminals are taken outside the closed motor through a groove along the steel shaft and are connected to copper slip rings which are fixed on a wooden disc which in turn is fixed to the rotating shaft (as shown in Figure 4.12. The e.m.f. generated in the search coil was picked up by means of two slipping brushes and fed into an oscilloscope, then a photograph of the wave-form was taken by a polaroid camera.

Figure 4.11 (a) shows the no-load flux pattern of the air-gap due to magnet poles only. On the other hand, Figure 4.11 (b) shows the resultant air-gap flux distribution due to magnet poles and armature current and it is obvious that the previous discussion is quite close to the result shown by the photo-graph, in that the armature has the effect of introducing a certain distortion in the air-

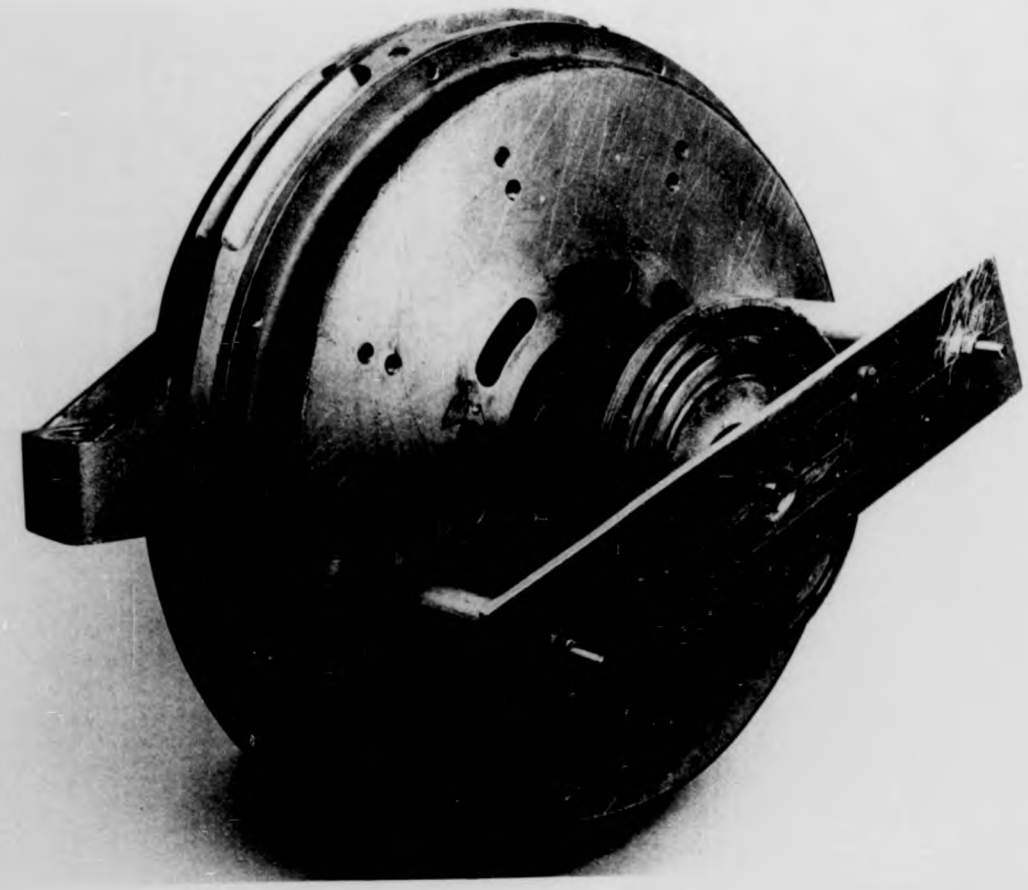

Fig. 4.12 : 10kW disc motor with equipment for measuring airgap flux

gap flux; but at normal load this distortion has a net effect equal to zero.

4.2.2 Armature Reaction Calculation

It is shown in Section 4.2, that when a motor is operating, there is a m.m.f. across each pole face of the stator generated by the armature when passing a total current, I, namely:

$$\text{m.m.f.} = ZI/2pa \qquad 4.13$$

The sense of this m.m.f. is so as to aid the magnetizing force of the stator at the leading pole tips and to oppose the stator magnetization at the trailing tips. (In a generator, this sense is reversed.)

It is also shown that in a motor with salient permanent magnet poles, the effect of the armature reaction at maximum current will lead to unhomogeneous magnetization over the circumferential extent of the magnet with partial demagnetization at the trailing tips

and subsequent operation along a recoil line.

There have been several papers published [23,24] on the demagnetizing effect of armature reaction in D.C. motors using permanent magnet stator. However, these papers do not give a useful method for the assessment of the demagnetization in a given motor with a permanent magnet stator of specified size and properties. However, the work done here has suggested a semi-empirical approach which does give this practical lead.

The average overall effect of armature reaction can be found by measuring, after magnetization, the back e.m.f. at known speed and then repeating this measurement after the passage of a known current through the clamped armature. E_b can be found by driving the motor (at a no-load) or as a generator, and measuring output volts, E, where

$$E = \frac{\phi . Z . p . n}{60\ a} \qquad 4.14$$

Equation 4.14 shows that the change in E/n must be due to a proportional change in ϕ .

This change is due to unhomogeneous demagnetization of the magnet but it has been shown to be both convenient and useful to consider it as representing a similar, average change in the magnet flux density at zero current, B_m.

Suppose a given motor has a permanent magnet stator with properties as in Figure 4.13 The zero-current load-line B_m/H_m is such that when magnetized after assembly the mean magnet flux density is B_{mf} on the demagnetization curve but, after passing a current, I. through the clamped armature. F/n and ϕ have been reduced so that the proportionately reduced mean magnet flux density is B_m on the same load-line. The recoil permeability of the magnet material is such that an external demagnetizing field H_a would have been required to produce a uniform reduction of flux density from B_{mf} to B_m.

The apparent demagnetizing field H_a is equivalent to a demagnetizing m.m.f. on the magnet of $H_a\ l_m$. But this apparent m.m.f.

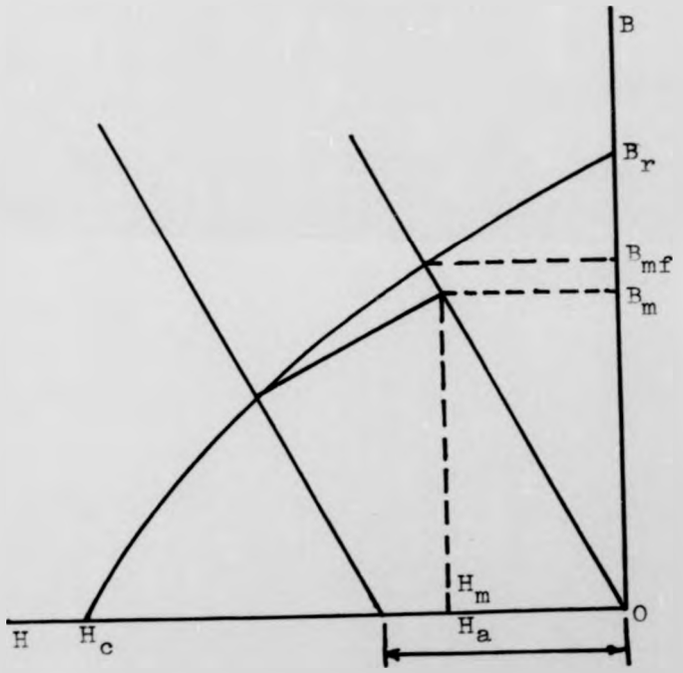

Fig. 4.13 : Magnet segment mean operating point

is the result of an armature m.m.f. as given by Equation 4.13 applied substantially perpendicular to the direction of magnetization.

It has been shown that an almost constant proportionality between armature m.m.f. per pole, F, and the demagnetizing m.m.f. H_a lm would have been required to produce the same mean demagnetization. Consequently, it is suggested that the effect of armature reaction due to a specified maximum armature current, I, is the same as a direct demagnetizing m.m.f. H_a lm superimposed on the magnet field at zero current. The appropriate value is:

$$H_a \text{ lm} = e.F = e(Z\ I/2pa) \qquad 4.15$$

Where Z is the number of armature conductors, I, is the maximum armature current, p, the number of stator poles, a, the number of parallel armature current paths, lm, the magnet length and e, is a constant. With conventional machines the armature reaction can be significant and serious with, e, close to 0.2.[25,26] This value appears to hold independently of motor designs and sizes or

of magnet material or of number of poles. But, the value of, e, may change with abnormally large air-gaps.

In the disc motor, the armature reaction of the air-cored coils has an extremely small effect due to the large air-gap, and e, may have a very low value. Armature reaction demagnetization is thus negligible in machines of this type and such effects have never been experienced in any of the prototypes.

The final effect again depends on the magnet material specified and in traction applications where high coercivity ferrite is almost exclusively used, it would be even less pronounced than with Alnico. However, since the cross m.m.f. of armature reaction is equivalent to a smaller m.m.f. applied directly to the magnet, in a motor using Alnico magnets it should be possible to neutralize the demagnetizing effect by the appropriate direct magnetizing m.m.f. From Equation 4.13 the apparent demagnetizating ampere-turns per pole is e(Σ I/2 pa). Consequently, if each magnet pole is fitted

with a supplementary winding with at least 0.5 e Z/pa turns, which is connected in series with the armature, neutralization should be affected when the armature current passes through them in the correct direction. The resistance of such windings should be low compared with armature plus brush resistance, in fact this is not difficult to achieve. In motors using Alnico magnet, it is already customary to fit a magnetizing winding on each pole and to leave this in place for possible use in servicing operations. There is very little difficulty in arranging that the number of turns and the resistance are appropriate for both magnetizing and neutralisation.

4.3 Permanent Magnet Stability

The designer of a permanent magnet machine is concerned to know under what conditions and for how long the magnet will continue to fulfil the purpose for which it was designed. Any permanent magnet, after being fully magnetized, is likely to perform differently under different

conditions. There is not, however, any one permanent magnet material that is the most stable in all possible circumstances. The material that is best for withstanding high temperatures is not necessarily the best for withstanding low temperatures, or external magnetic fields.

This section summarises the known facts on magnet stability in "normal" environments, that is over a moderate temperature range somewhat above and below atmospheric temperatures (within which the electrical machine is working), and under the influence of moderate values of external magnetic field and mechanical vibration.

The kind of stability required depends on the condition in which the machine is used. For example, unless appropriate precautions are taken in the design, the temperature to which a machine using ferrite permanent magnet may be exposed in transit on a Winter's night in Central Europe or North America, are sufficiently low to cause damage.

Until recent years the permanent magnet manufacturer has dealt with stability queries by reassurances based on the long-term use of magnets in the same or similar applications and the absence of complaints from regular users. Now, however, a body of factual information has been built up from which the magnet designer can (to a certain extent) predict the behaviour of magnets in various specified circumstances.

In the opinion of the author, some claims that the results published about the stability of permanent magnets are sufficient to enable the designer to predict the behaviour of his design accurately, are overstated. Slight changes in shape, size, composition, or treatment, may cause the commercial product today to differ significantly from the particular samples on which the published results were based.

4.3.1 Factors Controlling Stability

A permanent magnet, when magnetized to

saturation and removed from the magnetizer, is in a state of thermodynamic instability in that the reduction of the polarisation, J, from the saturated value to the working value, is a relaxation of domain orientation and a movement of domain boundaries. Any disturbing factor, such as structural change in the material, change of external field, mechanical vibration, increase of temperature, or even the atomic vibration associated with any fixed temperature above absolute zero, will tend to cause further small movements of domain boundaries and a consequent slight reduction of the polarisation and the external flux produced by the magnet. Nevertheless, given a structurally stable material and a small initial reduction of the flux, permanent magnets operated within a limited temperature range, can remain stable for many years to within about 0.01% of their flux value measured at a fixed temperature.

Given structural stability with operation at a fixed temperature, the change of magnetization due to any change of field is not completed instantaneously, but is

followed by small additional changes which are proportional to the logarithm of elapsed time. Hence, from the moment of removal from the magnetizer, a magnet tends to decrease slightly in strength. Such charges are usually described as magnetic viscosity. One method of avoiding such losses is to keep the magnets for several months after magnetizing before testing the machine. This process is known as ageing, or sometimes natural ageing. Artificial means of speeding up this process such as deliberately demagnetizing the magnets slightly by means of a small demagnetizing field or exposing them to a temperature cycle, are often employed. Such stabilization processes are often referred to as ageing.

The most serious, although not the most common, cause of a change in the strength of a magnet, is an alteration in its composition or structure. Such alterations are known as metallurgical changes. Some magnets are in a metastable state, and the metallurgical changes may proceed slowly even at room

temperature, and considerably more quickly at higher temperatures, e.g. highly reactive material such as cobalt/rare earth alloys, may be degraded by oxidation at room temperature, but in most permanent magnet materials, metallurgical changes occur only at considerably higher temperatures. Structural changes occur independently of the state of magnetization and are detected by a change in the demagnetization curve.

When the temperature of a magnet is changed, there is usually a reversible decrease in magnetization with increasing temperature. This change is called reversible, because the magnet returns to its original strength when it returns to room temperature. If a magnet is cooled below room temperature there is, of course, a reversible increase in magnetization.

In addition to the reversible losses, temperature changes cause irreversible flux losses in an otherwise stable material for several reasons. First, there is increased atomic vibration with increase of temperature, giving additional domain relaxation, so that

on decreasing the temperature there is a flux loss. Secondly, there is a change in the shape of the hysteresis loop with temperature, and in particular a reduction in the coercivity. In some materials the coercivity is lower at high temperatures, and in others it is lower at temperatures lower room temperature. Thus in some materials, irreversible losses may result from cooling as well as heating. In both cases, if the demagnetizing curve tested at the extreme temperature, cuts the load line of the magnet at a lower B value, then there will be an irreversible flux loss on returning to room temperature. These losses are irreversible in the sense that they are not restored by returning the magnet to room temperature. Unlike the metallurgical losses, they can be restored by remagnetizing the magnet at room temperature.

Mechanical vibration and shock is comparable with thermal vibration. However, there is no evidence that mechanical effects, other than fracture of the magnet, cause flux losses on a magnet which has had normal

stabilisation by either temperature cycling or an alternating field. Recorded tests by various authors on losses due to shock and vibration have confirmed that this has a very minor effect with modern magnet materials, but special cases may require pre-stabilization by application of the maximum vibration likely in practice.

In an electrical machine, magnets are likely to operate under the temperature changes, field change and mechanical disturbance simultaneously. However, the various causes of instability are not additive, since the identical small change may be initiated by a demagnetizing field, or by a temperature increase, or by a mechanical shock, or by some random thermal fluctuation during a time-lapse. One kind of artificial stabilization, whether thermal cycling or field cycling, will substantially reduce the losses which might otherwise occur due to another cause but will not wholly eliminate them except by excessive flux reduction.

All the causes of flux loss except structural change tend to give higher losses as the magnet working point gets to a steeper part of the demagnetization curve. Consequently, magnets with high coercivity give better stability.

In summary, for a high-stability permanent magnet the following points are desirable:

a) a material structurally stable over the working temperature

b) designed for a working point above the "knee" of the demagnetization curve as measured at any temperature in the working range

c) after magnetization, a heating/cooling cycle somewhat beyond the working temperature range

d) application of an alternating field with peak value greater than any likely stray fields when in use

e) the combined effect of c) and d) should produce a flux loss from the fully magnetized condition of at least 1%; up to 5% is desirable for maximum subsequent stability.

The kind of peak alternating field value necessary for stabilisation is indicated in Table 4.1. There remains the normal reversible temperature coefficient, dependant on material, and, in some cases, on a magnet working point.

4.3.2 Temperature Effects on a Ferrite Magnet

A serious disadvantage of hard ferrite is its high temperature coefficient of magnetization which at $-0.2\%/C^{o}$ is some ten times greater than that for metal magnets. This loss of flux is related to the decreasing B remenance of the material with rising temperature. This loss of flux is reversible for a range of temperatures within which the electrical machine works. However, under certain working conditions, it is important to

TABLE 4.1 Different Permanent Magnet Properties

Material names	Mean reversible temperature coefficient		Peak a.c. field for 5% flux loss
	% per °C	range °C	kA/m
Alcomax, Alnico 5	-0.01 to 0.02	-40 to 200	5
Hycomax, Alnico 8	-0 to 0.02	-40 to 200	20
Columax, Alnico 5-7	-0.02	-40 to 200	4
Columax Hycomax, Alnico 9	-0 to 0.13	-40 to 200	20
Anistropic Ferrite	-0.19	-40 to 200	14
Anistropic Ferrite high H_c	-0.19	-40 to 200	110
Bonded Ferrite	-0.19	-20 to 70	-
Sintered Sm Co_5	-0.04	-40 to 100	320
Bonded Sm Co_5	-0.04	-40 to 50	-

consider the accompanying increase in coercive force of 0.4 - 0.5%/C^{o} rise which effectively results in a shift to the left, the "knee" of the demagnetization curve. Thus, provided the initial working permeance line is above the "knee" of the curve, it will remain so with further increases in temperature and therefore losses will be reversible.

However, when temperature is reduced to sub-zero temperatures, remanance increases while coercivity decreases. The original values of remanance and coercivity are regained when the temperature returns to normal but the flux may or may not return to its original value. This change in flux due to temperature change is shown in Figure 4.14. Two demagnetization curves are given for the same material, one for operating at room temperature and the other for operation at sub-zero temperature. By considering operation of the magnet at two permeance lines P_1 and P_2, the significance of the working point can be described. At permeance line P_1, the magnet operates at point 'A' whilst at room temperature, but when

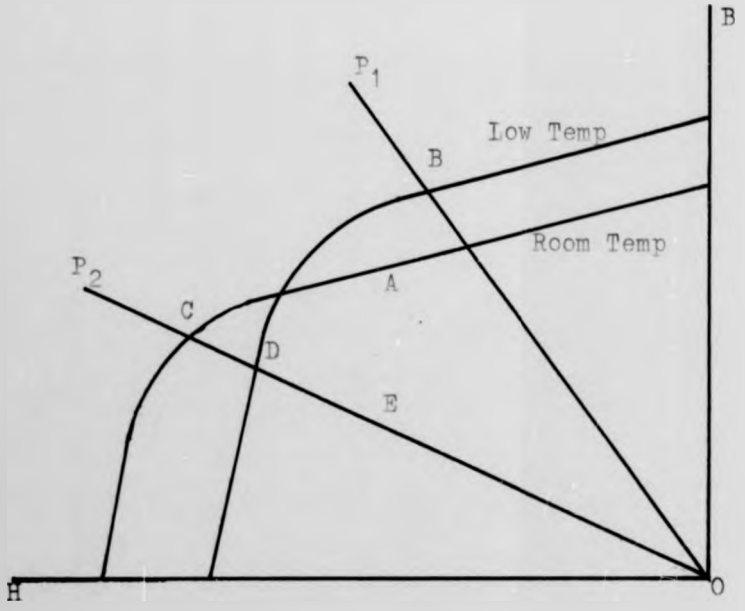

Fig. 4.14 : Change in magnet flux due to temperature change

cooled operates at point 'B' producing a higher flux density. By heating back to room temperature, the flux density returns back to point 'A' and has therefore undergone a reversible change.

By contrast, the magnet working at permeance line P_2 operates at point 'C' whilst at room temperature, but when cooled operates at point 'D'. In this case, there has been a loss of flux density and by heating back to room temperature, the operating point returns to point 'E' which is inside the demagnetization curve, hence the losses are irreversible. It can be realised that irreversible losses due to low temperature exposure may be eliminated by operating the magnet sufficiently high on the demagnetization curve.

Figure 4.15 shows the variation of E (i.e. ϕ), the terminal voltage, with the temperature rise of a 10kW disc machine using Ferrobe III. This is done by running the motor as a generator at different magnet temperatures ranging from room temperature up to 50°C. The magnet was heated by running the

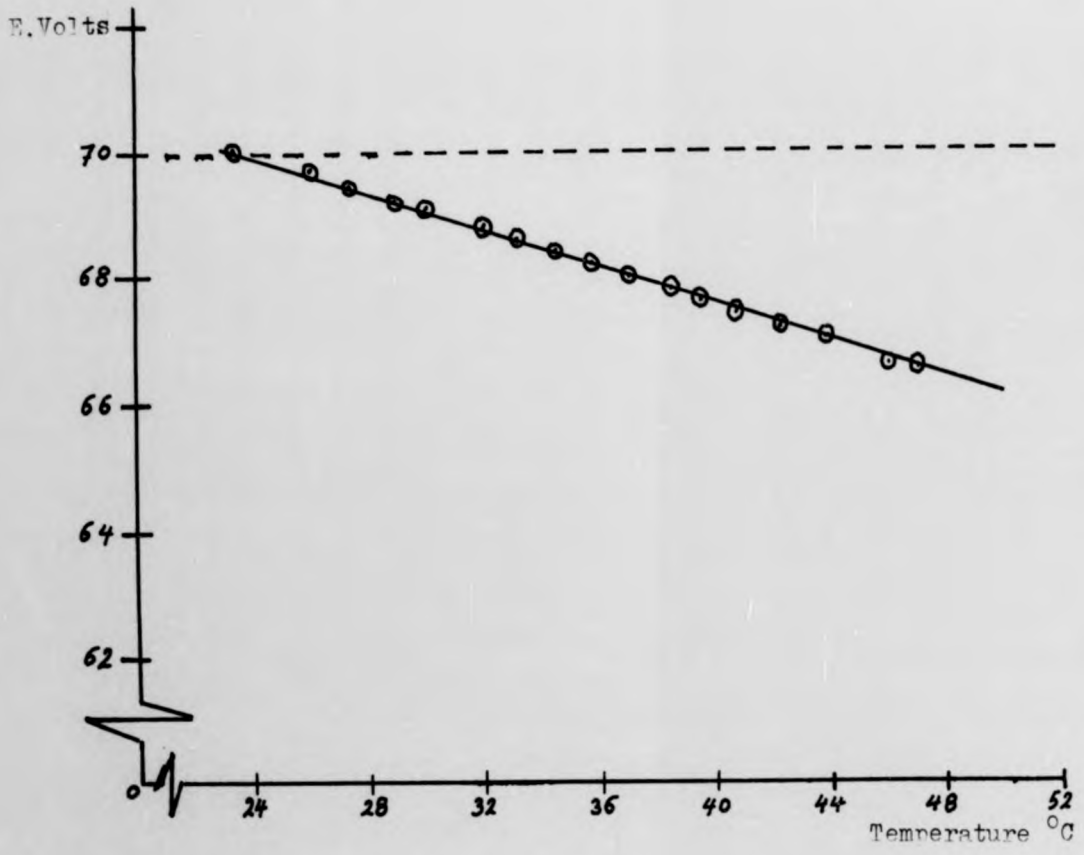

Fig. 4.15 : Open-circuit voltage against magnet temperature at constant speed for 10kW disc machine

motor on load between each reading when running as a generator. All readings were taken at the same speed. As can be seen, the relationship is a line of slope equal to 0.19 which gives the right value to the reversable temperature coefficient of ferrite magnet material.

4.4 Magnet Materials for a Disc Motor

In everyday language, matter is either magnetic or non-magnetic. Magnetic materials are visibly attracted by a magnet of average strength, and non-magnetic materials are not. Actually all materials react in some slight degree to a magnetic field, although a powerful magnet and sensitive equipment is often required to demonstrate this reaction. Such experiments enable apparently non-magnetic materials to be divided into several different classes: diamagnetic, paramagnetic and anti-ferromagnetic materials. Some commercially made permanent magnet materials such as the steel and Alnico alloys are described as ferromagnetic, while others such as barium ferrite are described as ferrimagnetic. The words ferromagnetic and ferrimagnetic describe different types of

ordering that make a material appear in the popular sense magnetic.

In a thesis of this nature, it is often unnecessary to specify to which sub-class a particular magnetic material belongs, and often the word magnetic is used with its every day meaning.

There are three main groups of permanent magnet material in common use today: Alnico. Ferrite and the Rare Earth Cobalt alloys. Magnets made from these materials are generally made anisotropic with the properties in one direction (usually along the length) considerably better than in the other directions. This section contains a brief description and some indication of the physical properties and method of manufacture on each of these types of materials.

The Alnico (Fe-Co-Ni-Al) materials, which cover a wide range of different grades as shown in Figure 4.16 are metallic alloys.

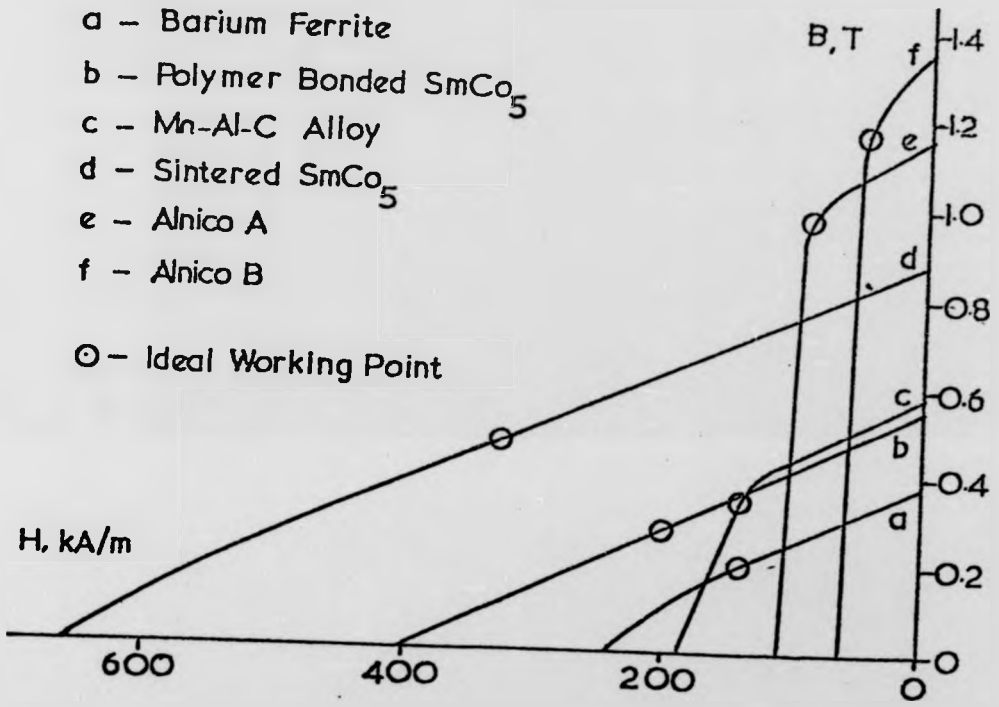

Fig. 4.16 : Demagnetisation curves of different material

Shape anisotropy is the major cause of the properties of the Alnico alloys, in which the metallurgical heat treatment produces a fine structure consisting of needle-shaped magnetic particles in a non-magnetic matrix.

The composition of this alloy is roughly 25% Co, 8% Al, 14% Ni, with the balance iron and it may be produced either by melting or sintering the component metals together. The anisotropy is generated by cooling the magnet from a high temperature in a magnetic field followed by a prolonged tempering treatment. The degree of anisotropy can be improved by casting the alloy into a chilled mould so that columnar crystallization is induced, and then heat treating with the field parallel to the direction of columnar growth. Varying the composition and the heat treatment are common procedures to manufacturers of all different grades - for example, increasing the cobalt content up to 35%, yields a material with a higher coercivity and reduced remanance. such as 'Hycomax' grade.

The fully treated alloys may be crushed, bonded with resin and pressed to give magnets with close dimensional tolerances, but inferior magnetic properties.

With the exception of the bonded material, Alnico alloys are hard and brittle at all stages of normal production, they are the most difficult of all the permanent magnet alloys to machine. They are cast as close as possible to the required size, any necessary holes being formed by the insertion of cores in the mould and, after heat treatment, reduced to the final dimensions by grinding.

A comparatively soft grinding wheel has proved most suitable for this purpose; diamond wheels have not been successful. The alloys tend to chip along the edges during grinding and very small cuts must be taken if this is to be avoided. The alloys may be cut using a high-speed slitting wheel, while another, but expensive, way of cutting (and machining) these alloys is by spark erosion.

Ferrite is a ceramic consisting of mixed oxides and has the general formula MO 5.5 Fe_2 O_3. where for good permanent magnets. M, is either barium or strontium. It is made by firing iron oxide with the oxide (or carbonate) of the barium or strontium. (The resulting materials are a magnetic compound of hexagonal crystal lattice with a single preferred axis of magnetization and a high magnetocrystalline anisotropy.) This is followed by carefully controlled ball milling in water to give a black slurry of controlled ferrite content. The slurry is fed into a mould and pressed to eliminate water and form a compact. This is done while a magnetic field is applied in the desired magnetic axis. The best magnetic properties are attained when field axis and pressing axis coincide. After ejection and slow drying, the compact is fired. The final firing leads to a marked linear shrinkage, but since the ferrite is an assembly of platelets formed of crystal particles, shrinkage is less in the pressing axis and more in the perpendicular axis.

Ferrite is a ceramic consisting of mixed oxides and has the general formula MO 5.5 $Fe_2 O_3$. where for good permanent magnets. M, is either barium or strontium. It is made by firing iron oxide with the oxide (or carbonate) of the barium or strontium. (The resulting materials are a magnetic compound of hexagonal crystal lattice with a single preferred axis of magnetization and a high magnetocrystalline anisotropy.) This is followed by carefully controlled ball milling in water to give a black slurry of controlled ferrite content. The slurry is fed into a mould and pressed to eliminate water and form a compact. This is done while a magnetic field is applied in the desired magnetic axis. The best magnetic properties are attained when field axis and pressing axis coincide. After ejection and slow drying, the compact is fired. The final firing leads to a marked linear shrinkage, but since the ferrite is an assembly of platelets formed of crystal particles, shrinkage is less in the pressing axis and more in the perpendicular axis.

It is difficult, after firing, to achieve a better dimension than $\pm 2\%$. Essential surfaces can be ground and for ferrite magnets bonded diamond wheels give the most economical results. Dies are designed to incorporate any necessary holes at the pressing stage. In the 'green' state, the compact may be cut with care, but after firing they become hard and brittle.

As an alternative to pressing and sintering, the reacted powder may be bonded with rubber or polymers, and either pressed to the required shape to give rigid magnets, or rolled or extruded to give a flexible sheet or strip. A certain degree of anisotropy may be imparted, depending on the amount of work done at the rolling or extruding stage, and on the application of a magnetic field during these processes. Such a sheet or strip can be cut to required sizes with knives. Although rubber-bonded magnets are soft, they will break if an attempt is made to bend them round too small a radius. Plastic-bonded magnets

range from soft to moderately rigid, depending on the plastic used and the degree of loading of magnetic material. All bonded magnets have a comparatively poor resistance to abrasion.

Cobalt and the rare-earth metals form a series of intermetallic compounds, notably RCo_5, where R is one of the rare-earth elements. Present production is based mainly on cobalt-samarium. They owe their permanent magnet properties to the extremely high magneto-crystalline anistropy of their hexagonal crystal structure. This intermetallic compound is formed by melting cobalt and a slight excess of samarium in an inert atmosphere. Crystals of near single-domain size are produced by ball milling, again with stringent precautions against oxidation. A field-aligned compact is pressed, followed by sintering, in an inert atmosphere at a carefully controlled temperature and a controlled cooling to room temperature. Magnetizing requires extremely high effective fields. Frequently, the application of the necessary field may be

difficult in a completed assembly and pre-magnetizing with subsequent assembly may be necessary. The material is brittle and of rather low mechanical strength, and although conventional grinding wheels may be used, diamond slitting wheels are necessary to cut the magnets.

Magents may also be produced by bonding the RCo_5 powder with polymer and pressing in a magnetic field to the required shape.

Alnico-type magnets have superior magnetic characteristics, but its major materials are cobalt and nickel which are very scarce and therefore very expensive, especially cobalt as it is in rather limited supply internationally. Because of this, the demand for ferrite-type magnets (which mainly consist of iron oxide) is recently increasing. However, its magnetic characteristics are inferior to those of an Alnico-type magnet. And the magnetic characteristics of this type of magnet have already been refined close to the theoretical limit. Therefore, the development of a new magnet, which does not rely upon either

cobalt or nickel and still has high magnetic energy, is in demand.

In recent years, a new anisotropic permanent magnet of non-expensive alloy components has been developed in Japan.[27,28] The new magnet is made of manganese, aluminium and carbon which are abundant, instead of cobalt and nickel which are rare and expensive. The Japanese also claim that the new magnet has magnetic energy comparable with the Alnico type magnet which contains much cobalt and nickel, and has advanced mechanical strength and good machinability in that it can be shared and drilled. The anisotropic directional property is produced by a warm-extrusion method which does not need magnetic field during the extrusion process. Although this alloy has an attractive low raw material cost, it is not widely available for commercial applications yet.

In 1983 there was a race between American and Japanese researchers[29] to develop a new type of magnet which could lead to a new generation of permanent magnet motors which, it was claimed, would be more efficient and cheaper than existing motors.

Towards the end of 1983, the Japanese company, Sumitomo Special Metals, claimed to have developed samples of a new magnetic material which can produce fields equal to those of the most powerful existing magnets but which could be produced at a much lower cost. Neodymium iron is claimed to provide superior magnetic properties at a potentially lower cost. At present, there is no independent assessment of the likely impact of these new materials on the design and performance of electrical machines. But experts in the U.S. and Japan believe that motors using this material could replace larger induction motors in most applications requiring more than 150W of power, and that such motors could have applications ranging from kitchen appliances to large industrial drives and that the material could lead to a breakthrough in electric vehicle motors.

Currently, the cheapest magnets are made from Ferrite, but their energy is limited and they can be used economically only in small electric motors. For larger motors, magnets from samarium-cobalt are required.

Researchers claim that a neodymium magnet could yield an energy level as high as samarium-cobalt magnets but at a cost similar to those of ferrite magnets.

In 1984, IG Technologies of Indiana started marketing their own permanent magnetic material products under the label NeIGT (Neodymium-Iron-Boron).[30] Appendix 4 shows some of the properties and characteristics of this material.

Chapter 5 Motor Construction and Performance Testing

5.1 Motor Construction

The motor considered in this section is built to the specification given in Table 5.1. Armatures using both solid and skeleton forms are explained and a comparison made of their construction. Figure 5.1 shows the production chart of the prototype motors which were built in the University. The chart detailed that the stator and the armature construction may be performed concurrently if necessary up to final assembly. Although twin rotor motor, single rotor version and D.C. generator are being produced, the mechanical details of each are identical and the same components, magnets and tools are used in their manufacture (Figure 5.2 to 5.4).

A shaft is made up of mild steel which has a key way on it that locks the armature hub of the rotor onto the shaft. The bearings used for the twin rotor unit, which were obtained from the SKF Company, are capable of running well above 4000 r.p.m. A steel hub such as the one shown in

DISC-ARMATURE MOTOR DESIGN

DESIGN NO: 240

DESIGN SPECIFICATION

OUTPUT: 11500. WATTS
VOLTS: 98. V
SPEED: 0. RPM

DESIGN DATA

OZ: 305. MM
OI: 175. MM
POLES: 8.

MAGNETIC CIRCUIT DATA

BG 0.330 TESLA
HG 33000. A/M
LGMEXT 2.30
LGACT 1.20
PHI .0081 WEBERS
ALPHA .72
LAMDA 63.1 MM
WEIRON 15.26 KG
[illegible]
WGIRON 4.74 KG
GAP 12.00 MM
HARDSY 4700. KG/M**3
BMS 1.60 TESLA

[illegible]

PATHS 8.
CONDS 72.
TURNS 4.
[illegible]
GAUGE 1.63 MM
[illegible]
CURDEN 8.0 A/MM**2
[illegible] AMPS
LOSS 626.58 WATTS
EFF %
TEMP 75. DEGREES
SF .85
RARM 0.035 OHMS
EB 91.31 VOLTS

Table 5.1 : Design paramaters of 10kW disc armature motor

WGTMAP 35.86 KG
TOTWGT 39.23 KG
MECHLO 497. WATTS
SPEED 4100.6 RPM
POWER 11662.3 WATTS
TORQUE 27.16 NM
PWRWGT 297.27 WATTS/KG
EFF .910

PERFORMANCE SPECIFICATIONS

CURRENT DENSITY AMP/MM**2	ARMATURE CURRENT AMPS	SPEED RPM	POWER WATTS	TORQUE NM	EFFICIENCY
1.	16.69	4284.9	1029.4	2.29	.642
2.	33.39	4258.6	2607.2	5.85	.813
3.	50.08	4232.2	4365.3	9.40	.866
4.	66.78	4205.9	5703.9	12.95	.890
5.	83.47	4179.6	7222.9	16.50	.901
6.	100.16	4153.2	8722.3	20.05	.907
7.	116.86	4126.9	10202.1	23.61	.909
8.	133.55	4100.6	11662.3	27.16	.910
9.	150.24	4074.2	13084.9	30.71	.908
10.	166.94	4047.9	14423.9	34.26	.906
11.	183.63	4021.5	15658.4	37.82	.903
12.	200.33	3995.2	17307.2	41.37	.900
13.	217.02	3968.9	18668.3	44.92	.896
14.	233.71	3942.5	20012.1	48.47	.892
15.	250.41	3916.2	21335.2	52.02	.888
16.	267.10	3889.9	22638.7	55.58	.883

Table 5.1 (continued) : Design parameters of 10kW disc armature motor

Fig. 5.1 : Production chart of disc motor

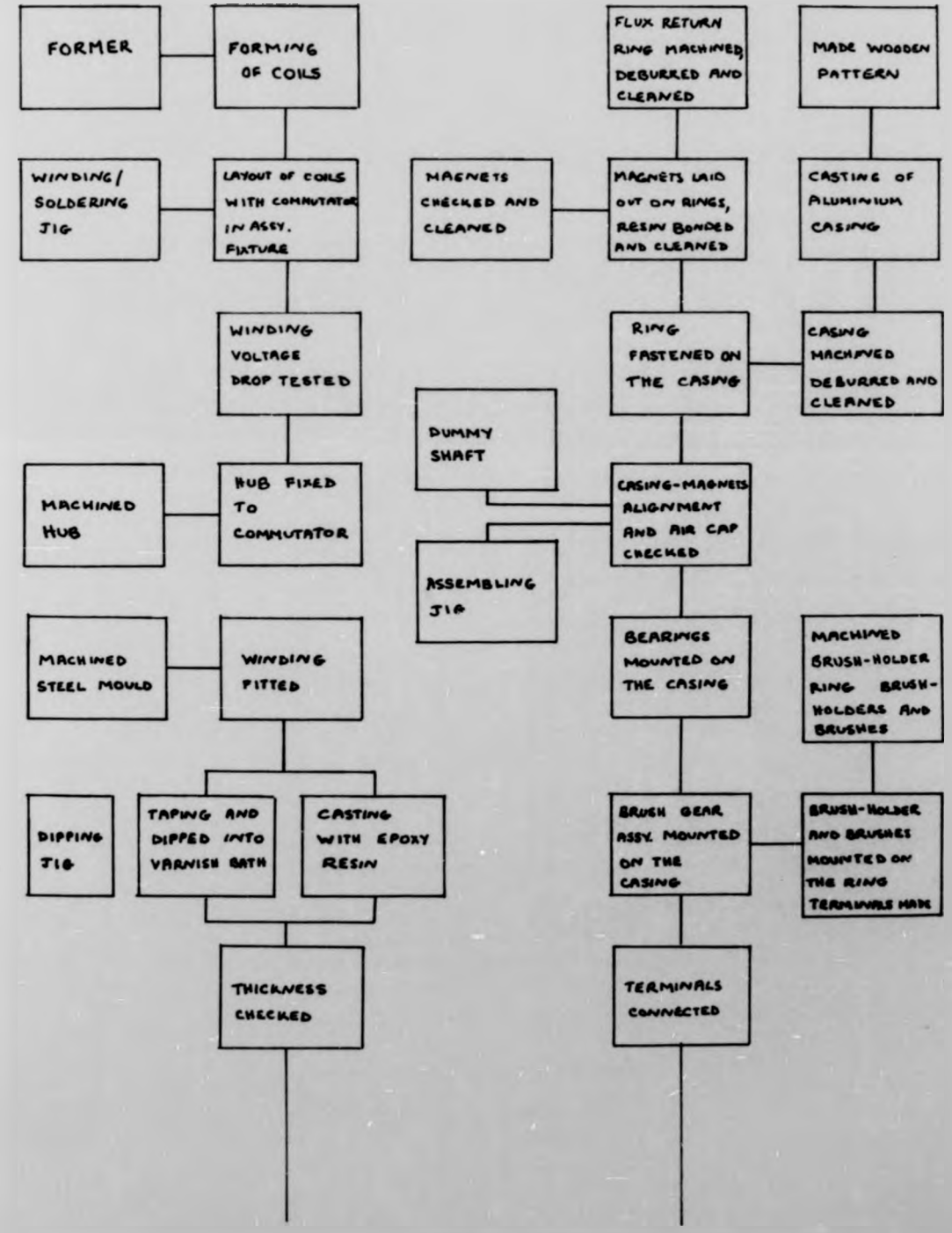

Fig. 5.1 (continued) : Production chart of disc motor

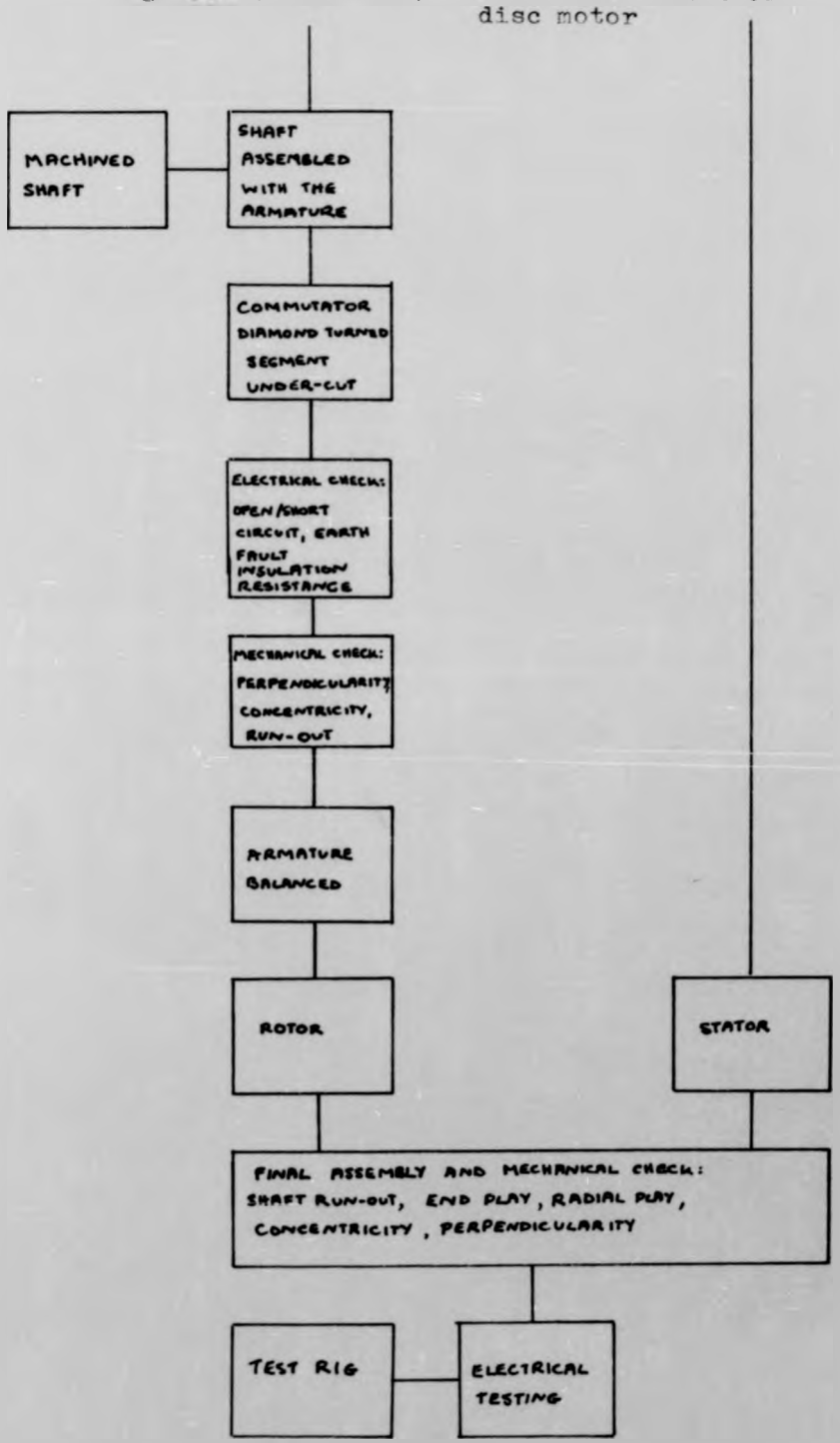

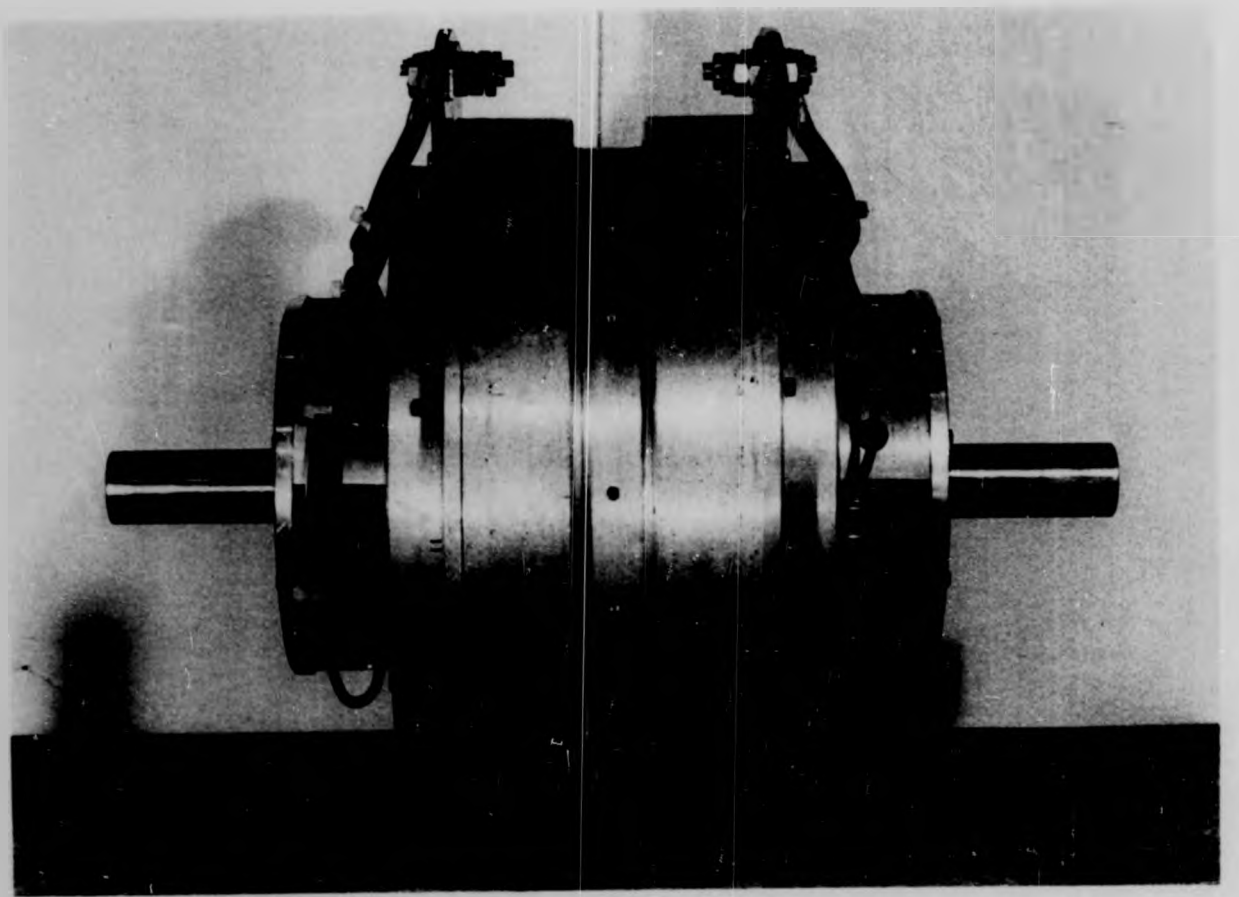

Fig. 5.2 (a) : 20kW twin rotor disc motor

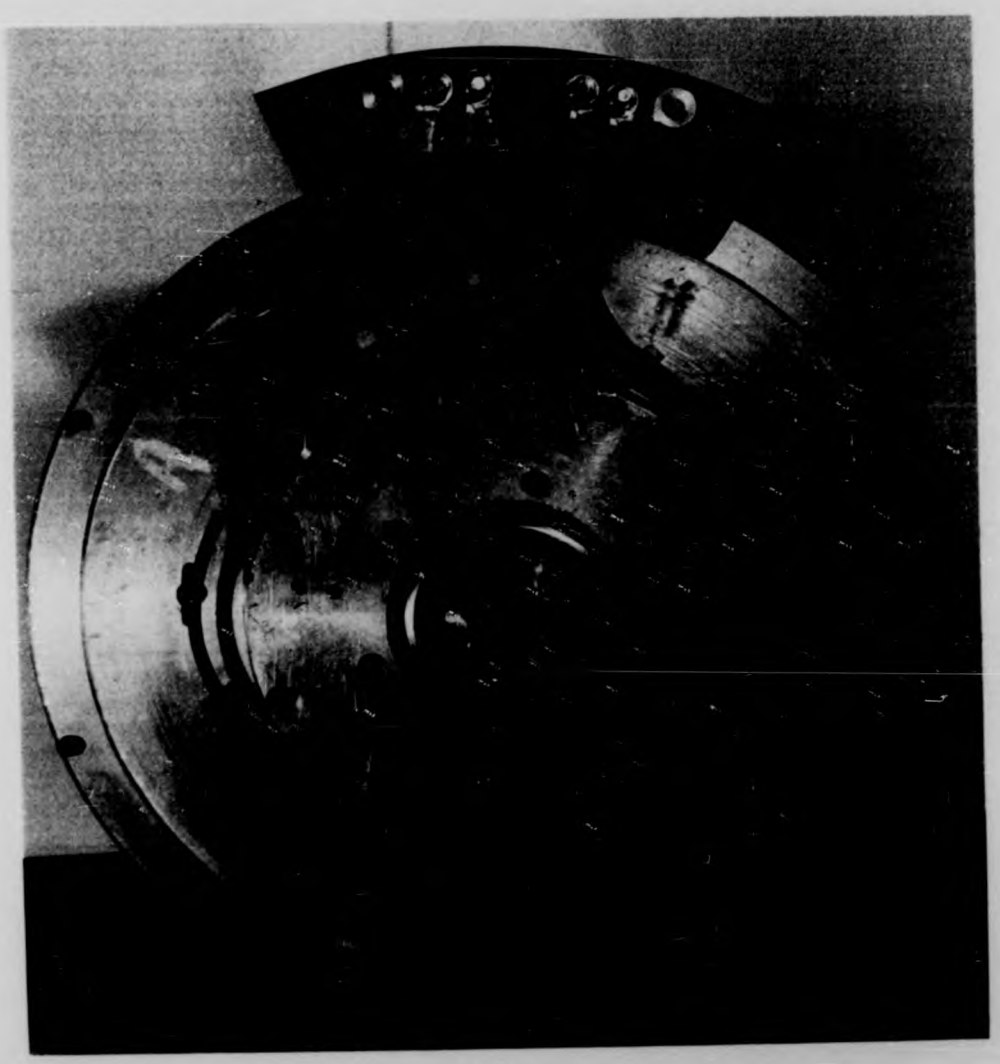

Fig. 5.2 (b) : 20kW twin rotor disc motor
(side view)

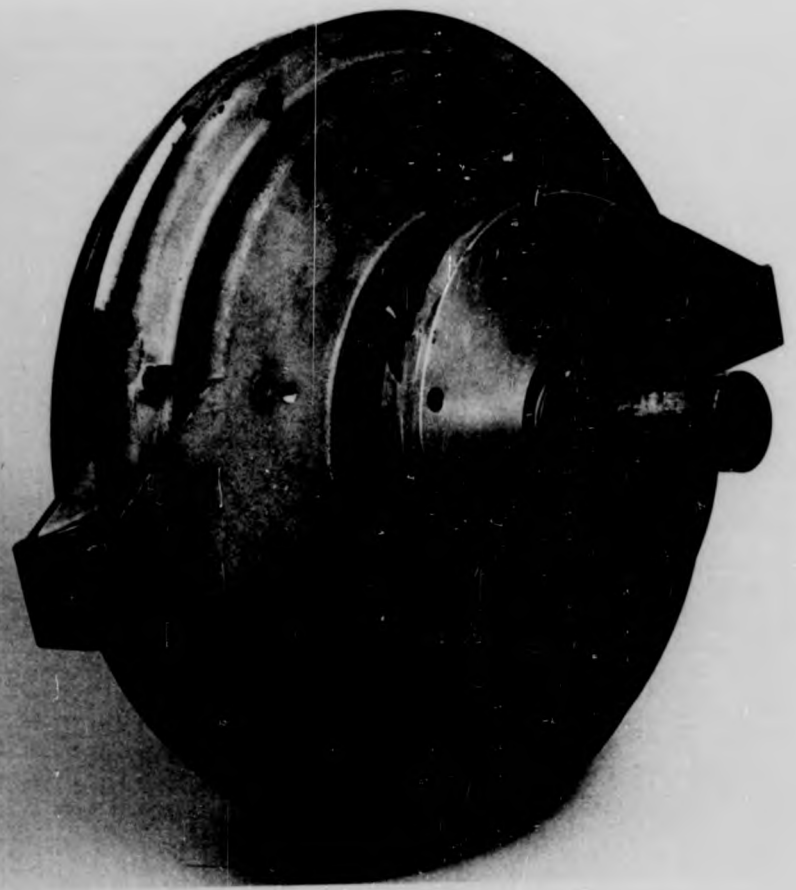

Fig. 5.3 (a) : 10kW single version disc motor (drive end)

Fig. 5.3 (b) : 10kW single version disc armature motor
(non drive end)

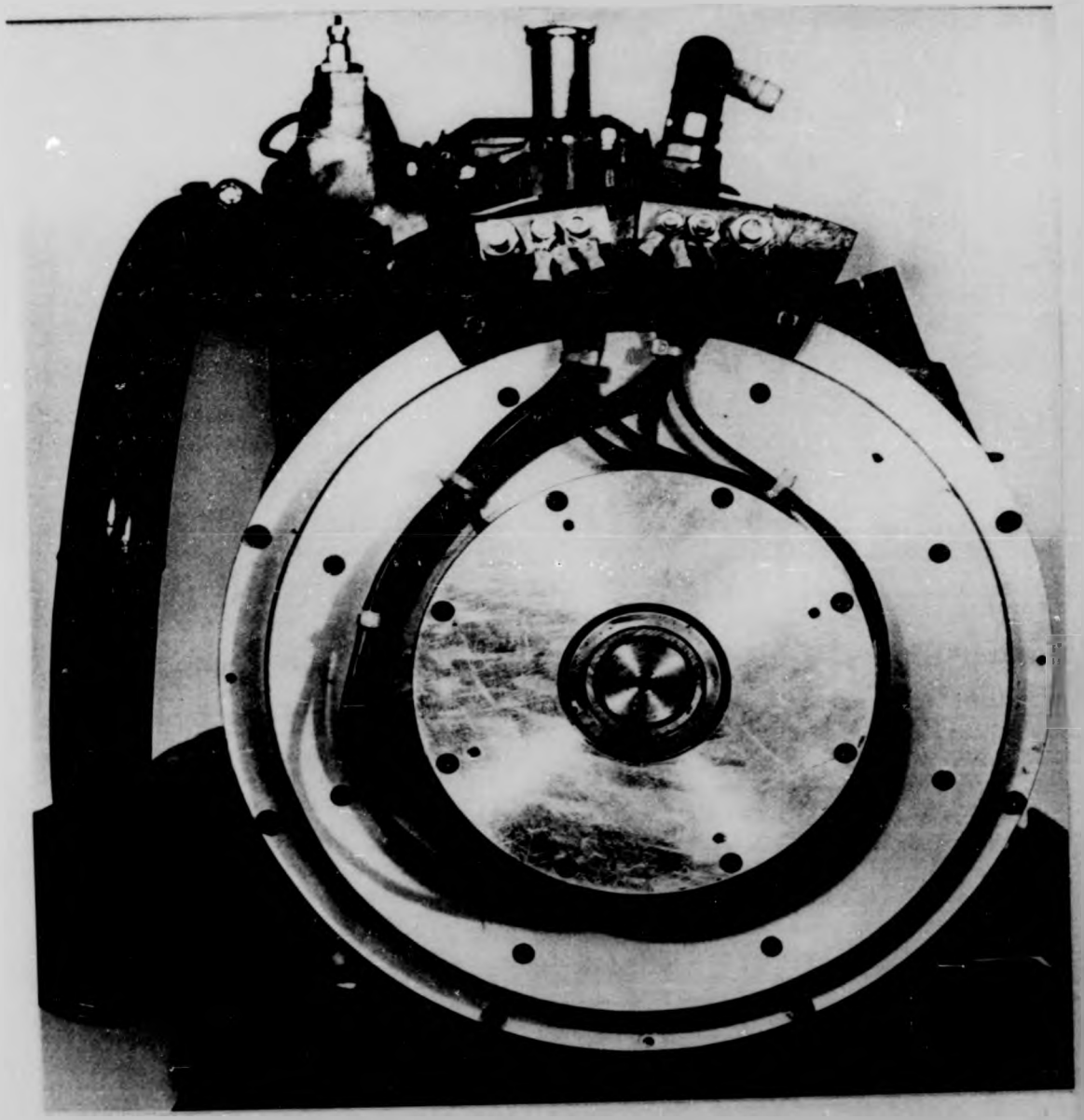

Fig. 5.4 : 8kW disc armature generator

Figure 5.2 is used as an integrated central part of the armature to provide reliable mechanical engagement between rotor and shaft. The four pin keys have the role of keying copper winding to the hub through the plastic matrix surrounding them and the winding.

5.2 Stator

The mechanical details are conventional with extensive use of aluminium alloy. The twin rotors have one central partition, two outer ring casings, two side casings and two end caps. These parts enclose two separate housings each of which accommodate one rotor. The central aluminium partition has an outer circumference of ring form and eight sector-shaped cuts through which eight long (84mm) magnets are tightly fitted. The centre of this partition is designed to form a cylindrical through hole with enough room to house two inner roller bearings. In order to secure full integration between this central bearing housing and the rest of the partition

under abnormal conditions of mechanical service, eight radial ribs, between the inner and outer rings, are introduced in the design.

The side casings are funnel shaped with side toothed protrusions extending beyond the magnet casing dimensions to accommodate the brush gear and commutator. This gives the added facility of allowing the brushes to be removed without dismantling the brush assembly. As is well known, the magnets are not fully effective unless the two sets are in alignment. This was achieved by having slotted holes in the side casings for the fixing screws, thereby allowing the magnets to be self-aligning.

The end caps which house the outer ball bearings also hold the brush gear. The brush holder ring assembly which is shown in Figure 5.6 consists of eight-off sheet brass brush holders mounted on class 'F' epoxy resin glass fibre ring. The ring is made with slotted holes

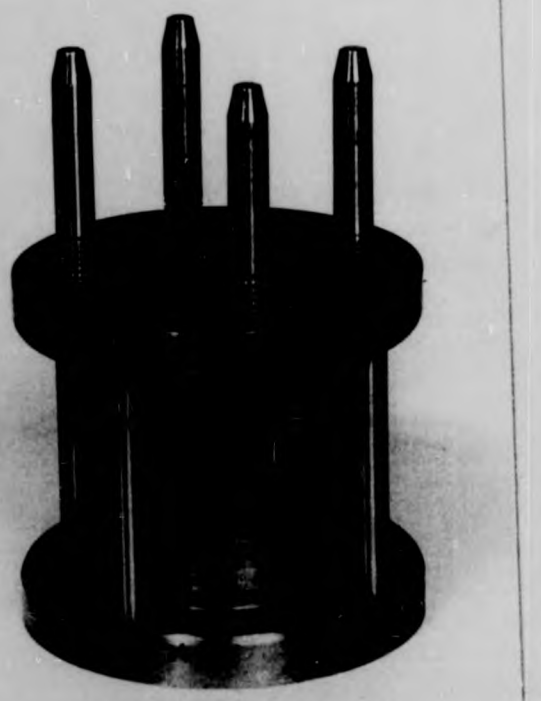

(a)

(b)

Fig. 5.5 : (a) The original steel core of the solid disc armature
(b) The modified steel core for the solid disc armature

for the fixing screws, so it can be slightly rotated about the geometrical neutral axis. By adopting such a design it is possible to perform the required adjustment to locate the electrical neutral axis conveniently; by slightly loosening the fixing screws with an Allen key through the brush removing openings. As in previous prototypes, the advice of a brush manufacturer has been sought regarding brush grade and size for a machine of these dimensions, power and speed. Morganite metal/impregnated brushes of the grade DM4A, are finally specified. Figure 5.7 shows photographs of the stator components of a twin rotor motor.

The early task in constructing any prototype disc armature motor is the specification of the magnets as the small quantities that are generally required often take some time to be produced. Occasionally, the magnet manufacturer will have a standard shape which is close to that designed - in this situation it may be worth re-designing the motor so that this can be used. However, for the 20 k.W. motor and subsequent versions,

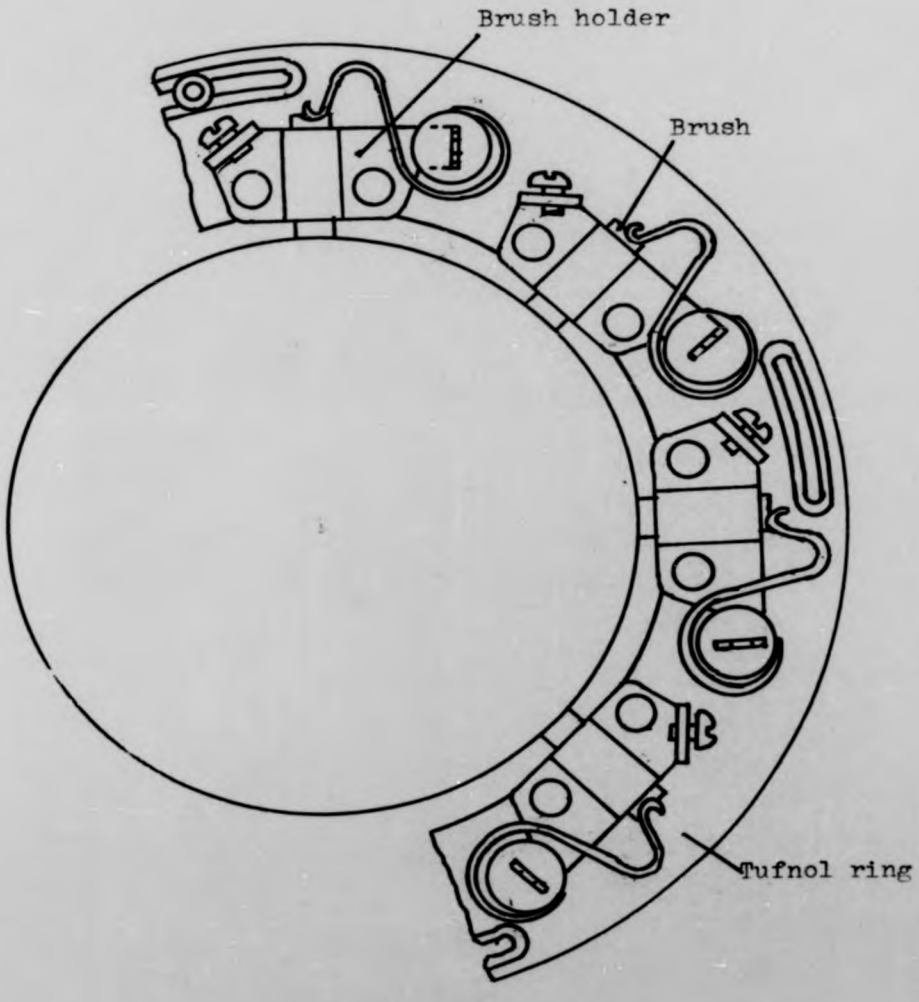

Fig. 5.6 : Brush holder ring assembly

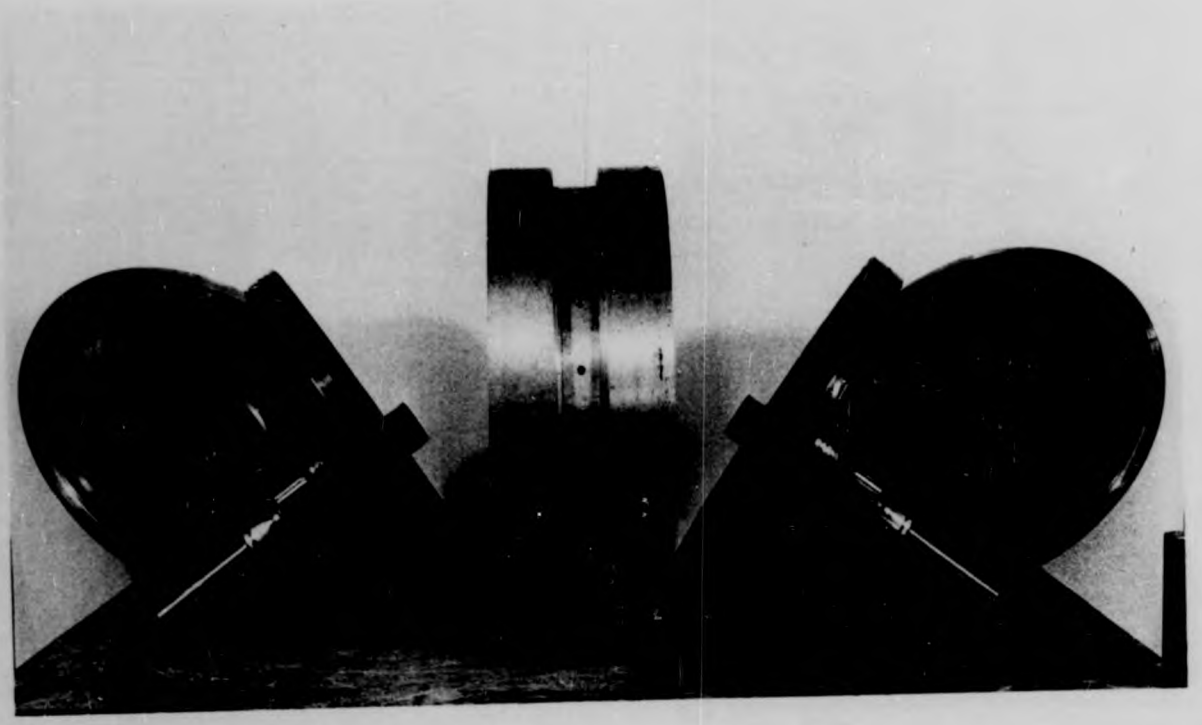

Fig. 5.7 (a) : Components of 20kW twin rotor disc motor

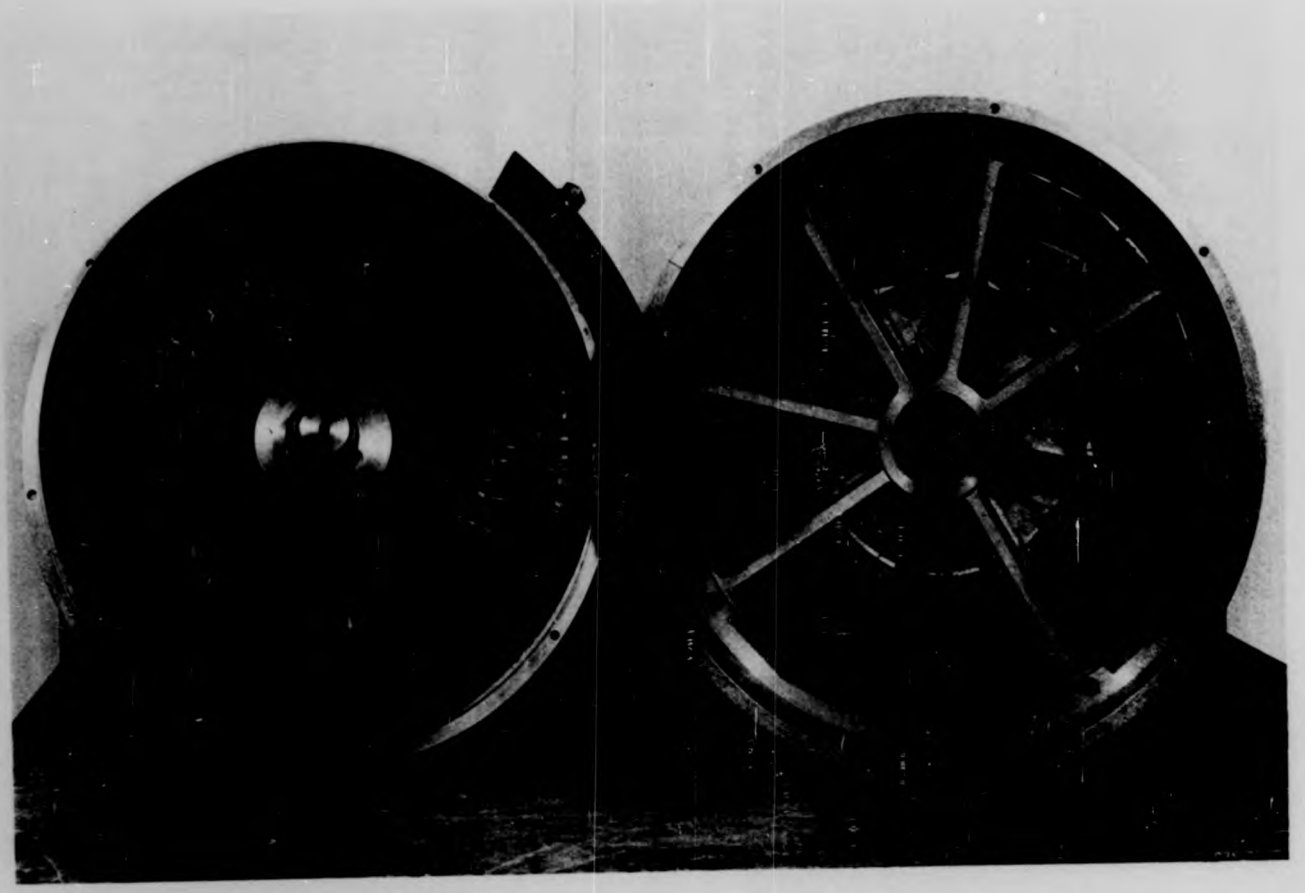

Fig. 5.7 (b) : The central part and the solid armature of the twin rotor disc motor

purpose-made segments of the Feroba III are specified and these are cut close to the desired shape from a magnet slab because the magnet manufacturers cannot produce magnets of a length in excess of 26mm due to manufacturing difficulties. Therefore, to produce magnets of over 26mm, a multilayer construction has to be used.

After delivery, the magnets are checked for the dimensions and tolerances stated in the drawing and physically inspected to ensure that it is free from loose chips and imperfections which would result in chips or particles under normal conditions of service. A chipped edge or surface can be tolerated provided it does not extend to more than 20% of the edge or 10% of the surface and is otherwise in agreement with the drawing.

In general, even with good manufacturing control, some minor mechanical imperfection is unavoidable. The imperfections such as minor cracks, porosity, voids and shrinkage cavities do not constitute reasons for rejection.

Chapter 5

Motor Construction and Performance Testing

Supplied with the magnets are demagnetisation curves of the long and short magnets (Figure 5.8). A comparison of these curves with the standard curve used in the design, indicates that the long magnet has lower characteristics than the short and/or standard magnet due to the larger number of layers used to construct it. It may therefore be assumed that the magnets supplied are not within the specification and that the field will not be as predicted. In order to prove the contrary, it is important to carry out an accurate measurement of the flux on the actual magnetic circuit. For this purpose a magnetic circuit test rig was built (Figure 5.9). The test rig was designed to hold the magnets in the same position as that of the stator and to simulate the original magnetic circuit conditions, a dummy shaft and the necessary flux return rings are used.

A Magnetech MIF-1 Digital Integrating flux meter is used to measure the flux using the search coil technique (Figure 5.9). The digital display gives a direct reading of flux in milli-Weber-turns. The meter operates on the basis that when a coil is moved through a magnetic

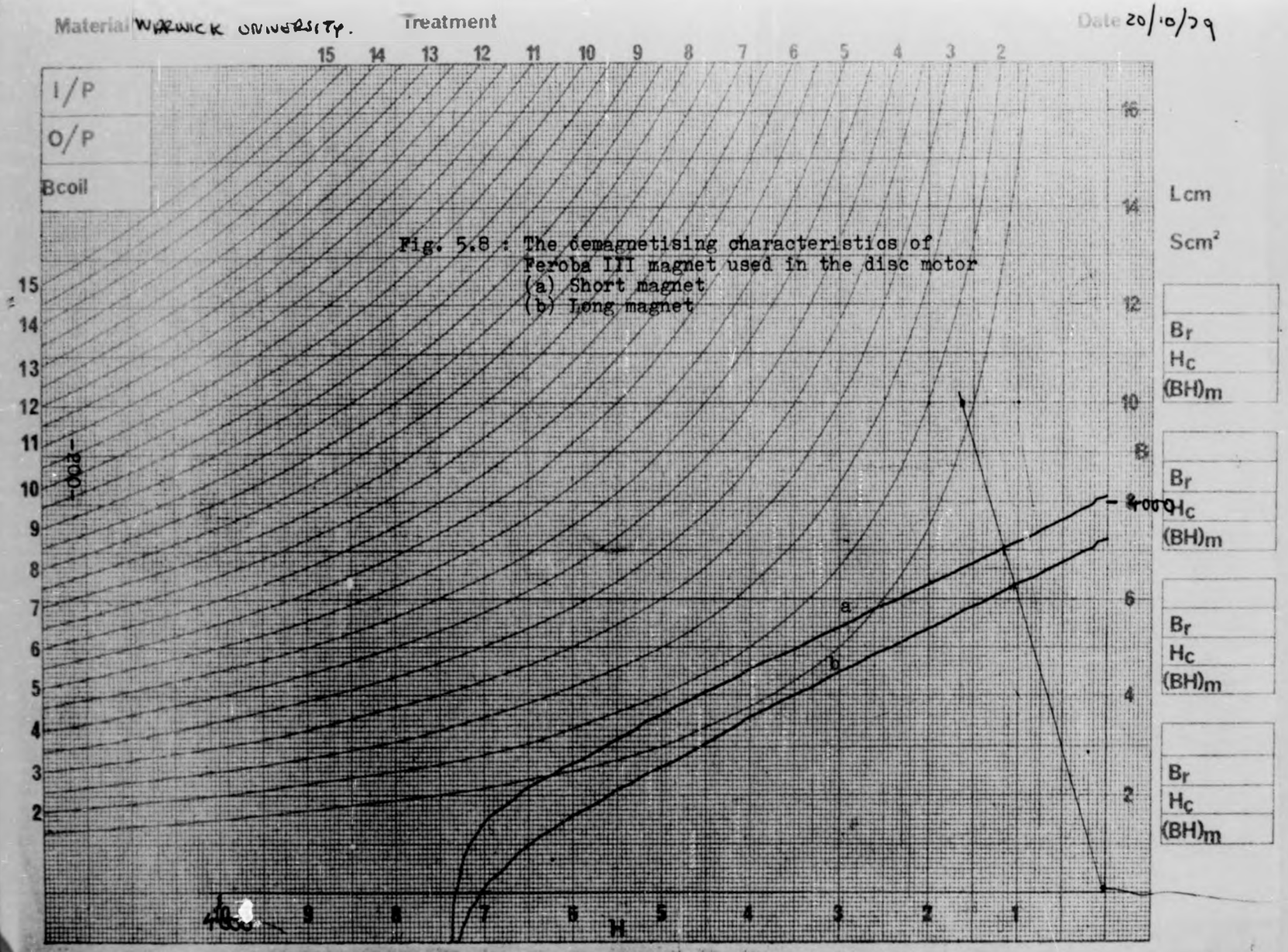

Fig. 5.8 : The demagnetising characteristics of Feroba III magnet used in the disc motor
(a) Short magnet
(b) Long magnet

field gradient, a voltage is induced in the coil. This voltage is proportional to the rate of change of magnetic field and the number of turns on the coil, i.e.: e.m.f. = $- N\frac{d\phi}{dt}$. This e.m.f. is integrated with respect to time, then the total flux change can be measured. The integration is performed using a conventional integrating circuit.

The measurement of the flux of the twin rotor disc armature motor shows that the flux per pole is 1.23 milli-Weber which is higher than the predicted value. This flux improvement is related to the lower loss factor of the magnetic circuit of such construction due to the cancellation of the central flux return rings (two) and their associated reluctance.

The measurement of the flux of the single version disc armature motor shows that the flux is 1.16 milli-Weber which is identical to the predicted value. However, the single version disc armature motor is employing short magnets only, therefore the measured value is as expected.

In fact the measurements were repeated after the motor was subjected to high starting current in order to deduce whether there is a flux reduction due to armature reaction or mechanical vibration. The result showed that there is no such reduction in flux.

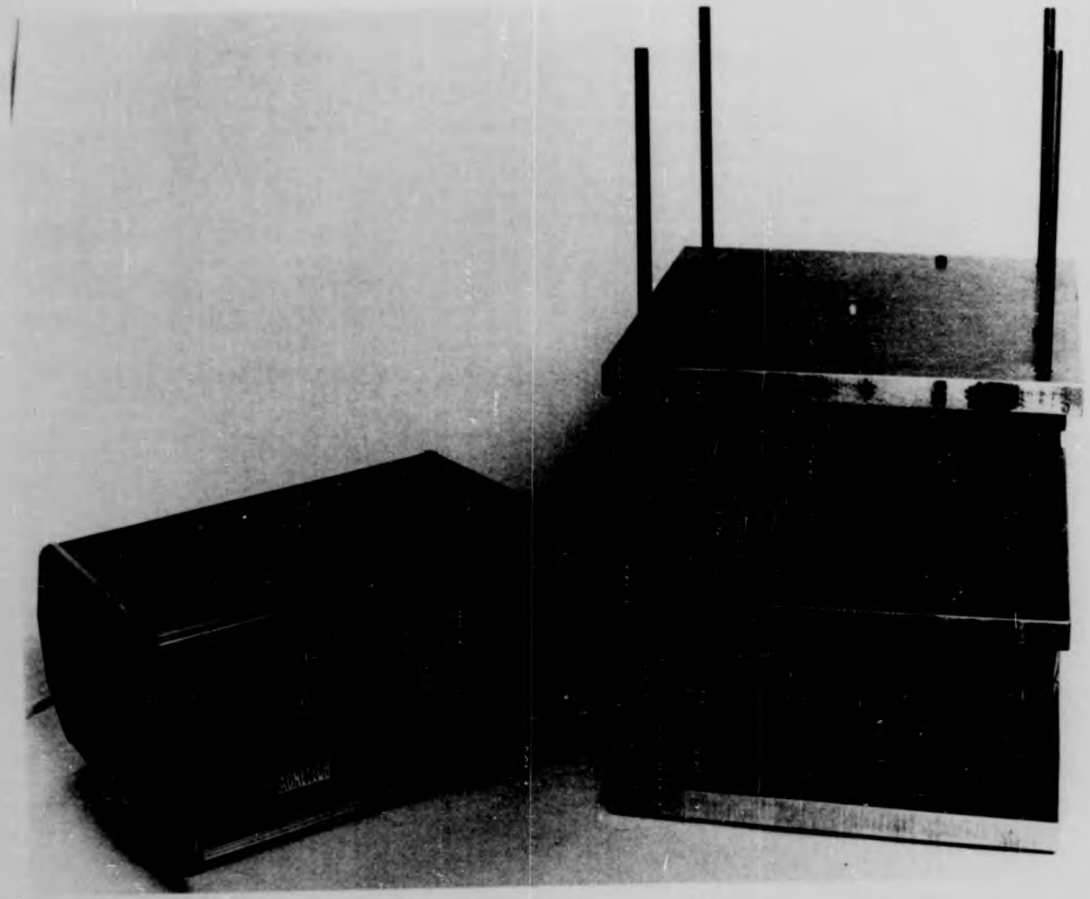

Fig. 5.9 : The magnetic circuit test rig and the flux meter

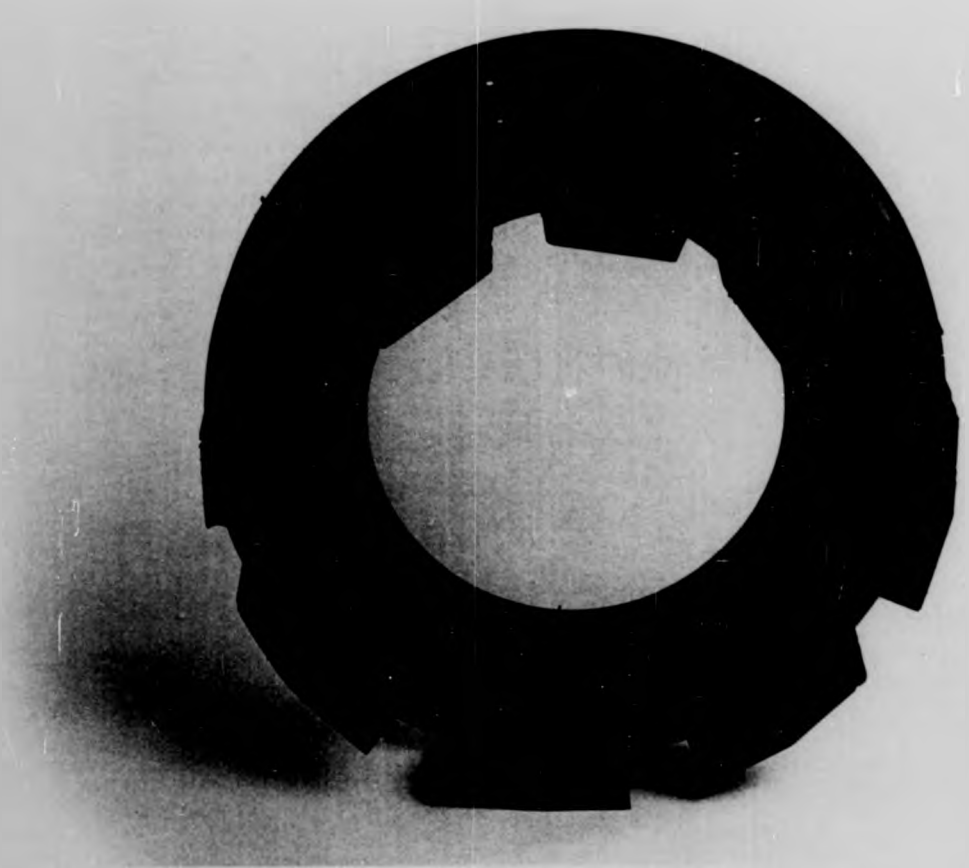

Fig. 5.10 : Magnet poles fixed on the flux return ring

Chapter 5

Motor Construction and Performance Testing

Magnets are joined to flux return rings, as shown in Figure 5.10, by the use of modern adhesives. The adhesive used is Loctite 317 with Loctite NF activator which provides a quick curing process. The surfaces to be joined must be ground flat, in order that the gap is kept to a minimum. To obtain bonding of high strength, both surfaces which are to be bonded together are cleaned with methylated spirits.

5.3 Armature

5.3.1 The Main Winding

The armature consists of two double layer coreless windings. These two windings are positioned back-to-back and the end windings of each face in opposite directions towards either set of magnets, wrapping over above and below the magnets. Each single double layer winding is constructed from pre-formed wire-wound coils which are individually formed by

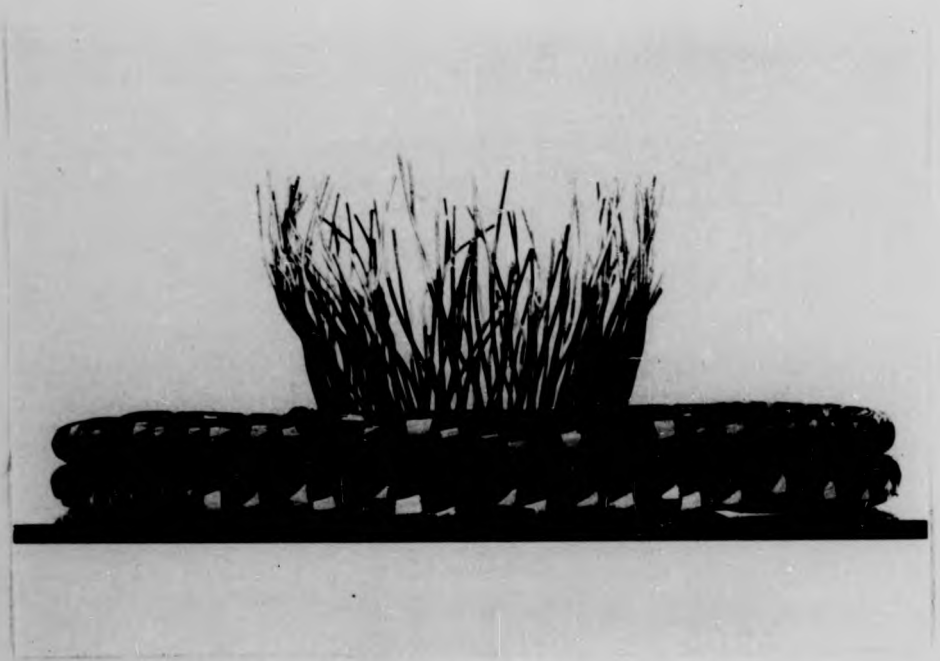

Fig. 5.11 (a) : Armature winding

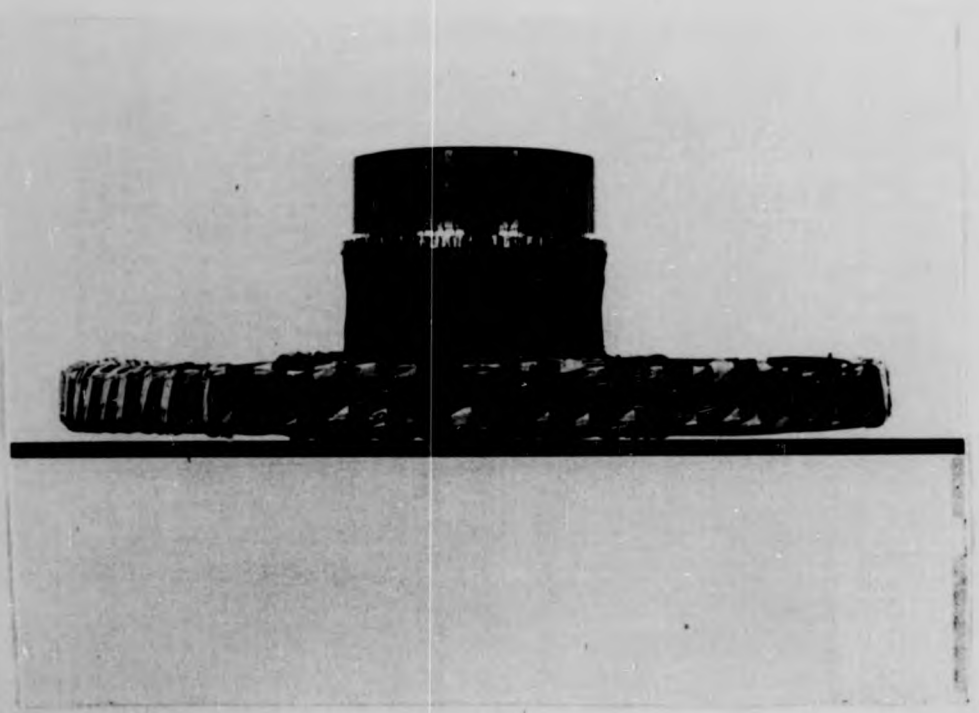

Fig. 5.11 (b) : Armature winding connected to the commutator

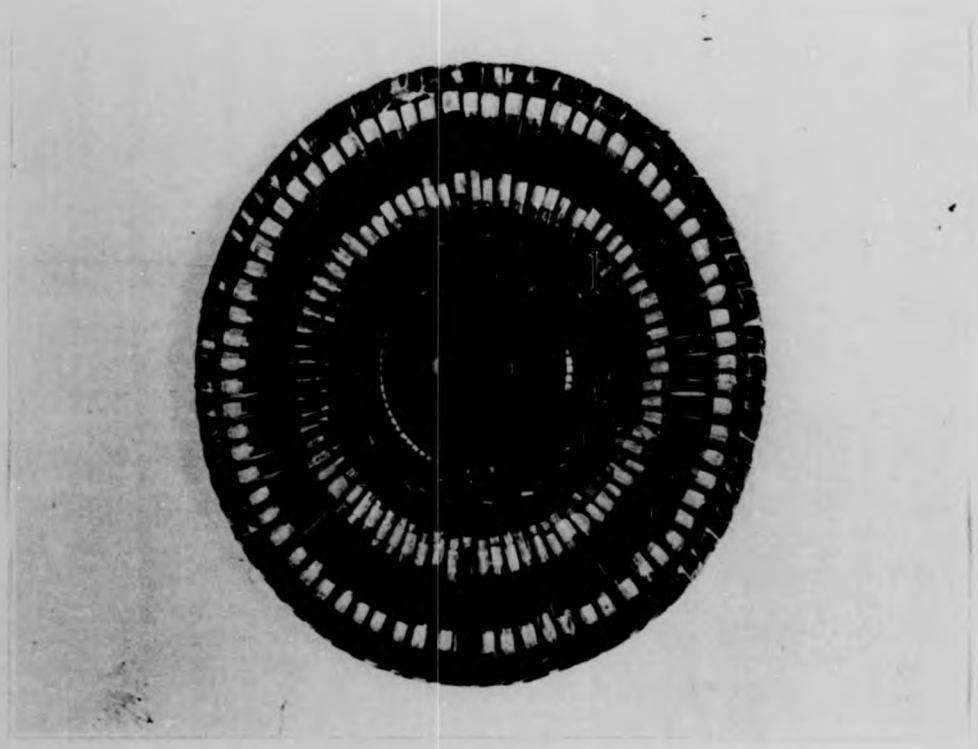

Fig. 5.11 (c) : Top view of the armature

winding enamelled copper wires on a specially made-up former. Then the coils are assembled on a winding jig and bonded to each other by strings with the side of each coil directly underlying the side of another coil and the complete winding is therefore disc shaped.

This assembly is made possible by bending the ends of the coils up, so that they no longer lie in the plane of the disc. One side of each coil is longer than the other, by an amount that makes it possible for the end windings to nest closely together in an annular array with the ends of each coil fitting between the ends of an adjacent coil. Because of the unconventional nature of the armature, prototypes are constructed in the above described arrangement completely by hand.

Once the individual coils are assembled as the winding shown in Figure 5.11 , they are soldered to the commutator which is a production item. For the soldering operation,

a wooden jig is used to hold the winding against the commutator in its correct position above the winding. Each single coil of one double layer is connected in series to the corresponding back coil of the other double layer and the other end of the coil is then connected to adjacent commutator segments. Therefore, the final winding is a simple lap winding of four layers and eight turns per coil. Then the strings are replaced with a special tape which can withstand high temperatures. Finally, the whole armature is pressed gently and put in an electric oven at 120°C for approximately one hour to remove the stress introduced into the coil when being formed and to cure the tape.

5.3.2 Equalizer Connections

A simple lap winding has as many parallel paths as poles, and each parallel path is made up of coil sides which lie under two adjacent poles. If the flux under all poles is equal, the e.m.f. induced in all parallel paths will

be equal. But in practice, it is possible that the e.m.f. induced in various parallel paths may not be equal owing to the following reasons:

i) there may be a difference in the values of reluctance of magnetic paths of corresponding parts of the flux return ring.

ii) the length of air gap may not be the same under all the poles owing to some defects in machinery or in assembling.

iii) the poles may have different strengths owing to defects in manufacturing.

iv) the coils may have inaccurate positions resulting in unsymmetrical winding about a pole-pair owing to some error in armature assembling.

The unequal values of e.m.f.s generated in different paths gives rise to resultant e.m.f.s which act across the armature windings. These e.m.f.s acting across the local armature circuit produce large circulating currents as

the armature resistance is very small. These currents flowing through the brushes, result in considerable inequality of brush arm currents, giving rise to I^2R losses in the winding on no-load, and adding to the losses on full-load both in the winding and brushes. They also introduce commutation difficulties, causing over-heating and sparking. In order to rid the brushes of these circulating currents, equalizer connections are used. These equalizer connections or equalizers are low resistance copper conductors which connect those points in the winding which, under ideal conditions, have no difference of potential between them. If there are differences of potential between such points, as is normally the case, equalization of potential will result from the flow of current through these low resistance conductors which bypass the current. This bypassing of circulating currents relieves the brushes of excessive loading to which some of them would otherwise be subjected. Figure 5.12 shows part of a 72 segment, 8 pole machine. The

points indicated by P_1, P_2, P_3, each of which occupy identical positions with respect to poles of like polarity, may be connected in the manner indicated at the bottom of the diagram. It is clear that the points which are to be connected together must be two pole pitches apart. The connections were taken from corresponding commutator segments (segments to which coils two pole pitches apart are connected). The equalizer connections are in the form of rings in which case they are known as equalizer rings.

The perfect arrangement is to equalize the potential of all the coils but it is not possible in practice as the number of connections becomes very large. It is usual to have 5 to 20 rings, each having as many coils connected to them as the number of pairs of poles.

The distance between coils of the same potential

$$Y_{eq} = \frac{\text{Total number of coils}}{\text{pair of poles}} = \frac{C_c}{p/2} = \frac{2C_c}{p} \text{ coils} \qquad 5.1$$

Y_{eq} is the equipotential pitch and is expressed in terms of coils and C_c is the number of coils.

Total number of tappings = number of rings x pairs of poles.

$$\text{Total number of tappings} = m \times \frac{p}{2} = \frac{mp}{2} \qquad 5.2$$

Where m equals the number of equalizer rings. Distance between adjacent tappings is equal to the total number of coils divided by the total number of taps.

Which is

$$Y_{ph} = \frac{C_c}{m \times \frac{p}{2}} = \frac{2C_c}{mp} \text{ coils} \qquad 5.3$$

Y_{ph} is the phase pitch and is expressed in terms of coils.

In order that equalizers may be used, the armature winding must be symmetrical This requires that the number of commutator

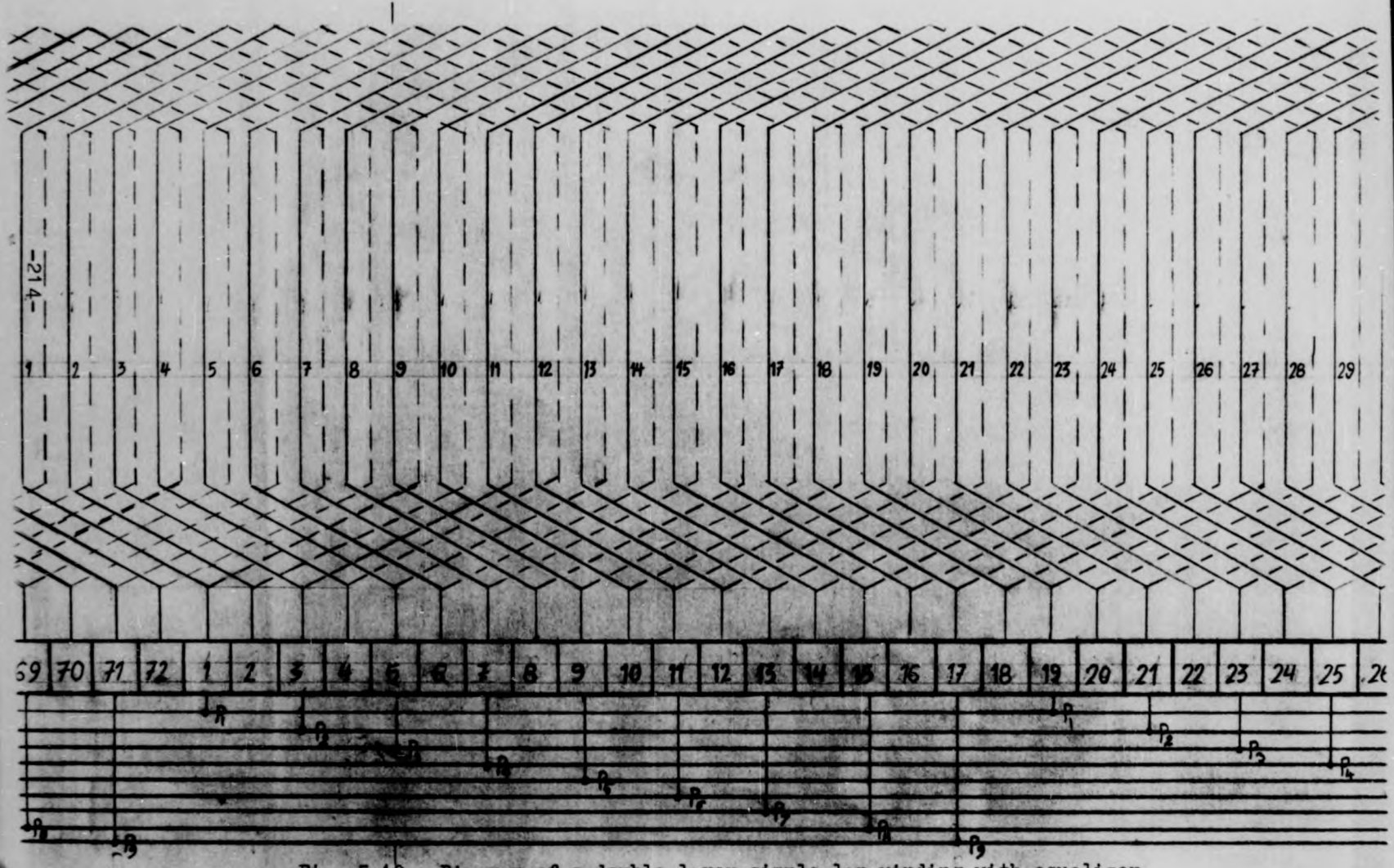

Fig. 5.12 : Diagram of a double layer simple lap winding with equalizer connections

segments is a multiple of pair of poles.

It is to be noted here that there are no circulating currents in a simple wave winding even if the magnetic circuits under different poles are not uniform, as in this winding the coil sides form a parallel path and are distributed over all the poles and hence all the parallel paths are affected equally by the asymmetry in the magnetic circuit. Thus there is no necessity to provide equalizer connections for a simple wave winding.

5.3.3 The Resin

After the whole armature winding has been formed, it is necessary to provide it with mechanical strength and rigidity. One way of achieving this is to encapsulate the armature in epoxy resin.

Since there is only a small clearance between rotor and stator over a considerable

radial distance, it is important that the encapsulated armature disc has extremely good dimensional stability which is maintained even under extreme operating conditions.

The solution to the problem of tailoring epoxy resin to meet specific requirements is a difficult task. The approach must begin with a basic understanding of the conditions under which the resin will be used.

The factor that dictates the choice of a particular epoxy formulation is initially the operating temperature of the armature and material selection is mainly determined by its ability to withstand thermal shock and thermal cycling without deterioration to their initial mechanical strength. To fulfil these criteria often means that the resins must have good adhesion which make it particularly suitable for moulding around metal inserts even in thin sections. In this case, material of low viscosity is required, i.e. a thin resin must be used to

prevent the occurrence of voids and to allow the winding to be thoroughly coated. A long pot life is desirable to prevent material wastage and allow ease of manufacture.

Another essential requirement of epoxy resin used in the encapsulation of armature winding is the low shrinkage factor to minimise stress during the cure period so that the resin will not crack or separate from components. For this reason, a resin with a low curing temperature is often preferable. In addition, the thermal expansion coefficient of the resin must be matched to that of the armature component as closely as possible to prevent the resin parting from the copper material of the winding during the cure and post-cure periods. Only epoxy resins capable of class F service, and providing mechanical support over this range of operating temperatures, must be employed.

The inherent heat generation associated

with armature operation mode imposes the use of epoxy resin of a relatively high thermal conductivity in order to dissipate such heat and reduce the danger of excessive temperature rise which may damage the winding insulation and/or degrade the physical and mechanical properties of the disc.

In addition to choosing an appropriate epoxy system, each resin may be altered by the use of inorganic fillers. These improve the mechanical properties of a resin by reducing the quantity of organic material and hence the amount of shrinkage during cure. They also impart better thermal properties to the resins.

5.3.4 Mould

Having chosen the proper epoxy resin system and the right filler, a steel mould for the armature is designed and manufactured, the general arrangement of which is shown in Figure 5.13.

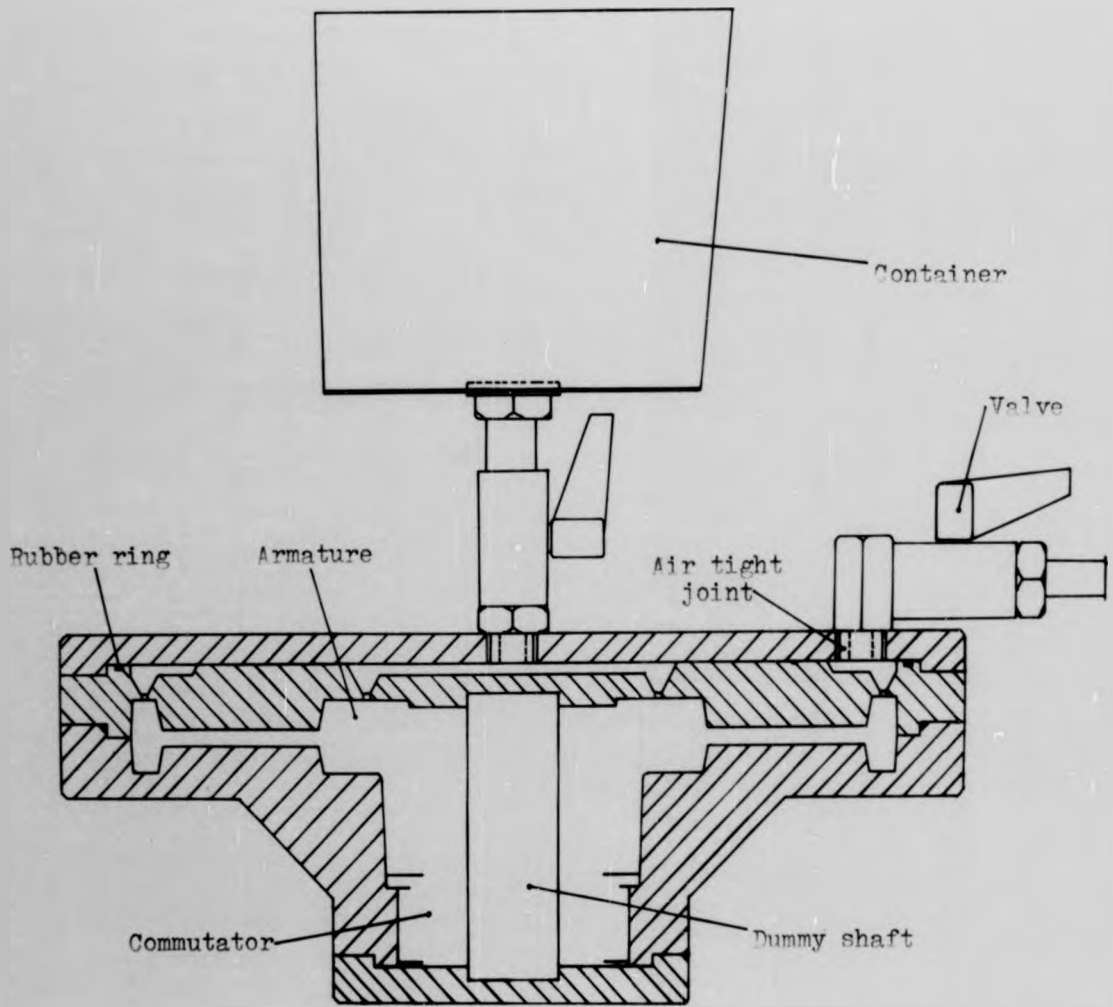

Fig. 5.13 : General assembly of the mould

Chapter 5

Motor Construction and Performance Testing

The mould was constructed of five parts to ensure there was no undue strain on the armature during disassembly. These can be identified in Figure 5.14 which shows the mould partially dismantled. To ease the removal of the armature from the mould, all long edges that lie in the axial direction are offset slightly from this axis. A suitable taper of 3^{o} was chosen, which was large enough to be of some assistance to this, and also small enough not to interfere with the machine's designed dimensions.

The armature hub and commutator which fits onto the motor shaft is positioned in the lower half of the mould and fixed in position by a dummy shaft which is itself located in the top half and in the base plate of the mould.

The epoxy resin is injected through the central hole in the filling plate. It then passes through twelve inner holes in the top mould and is then pushed out through twelve outer holes.

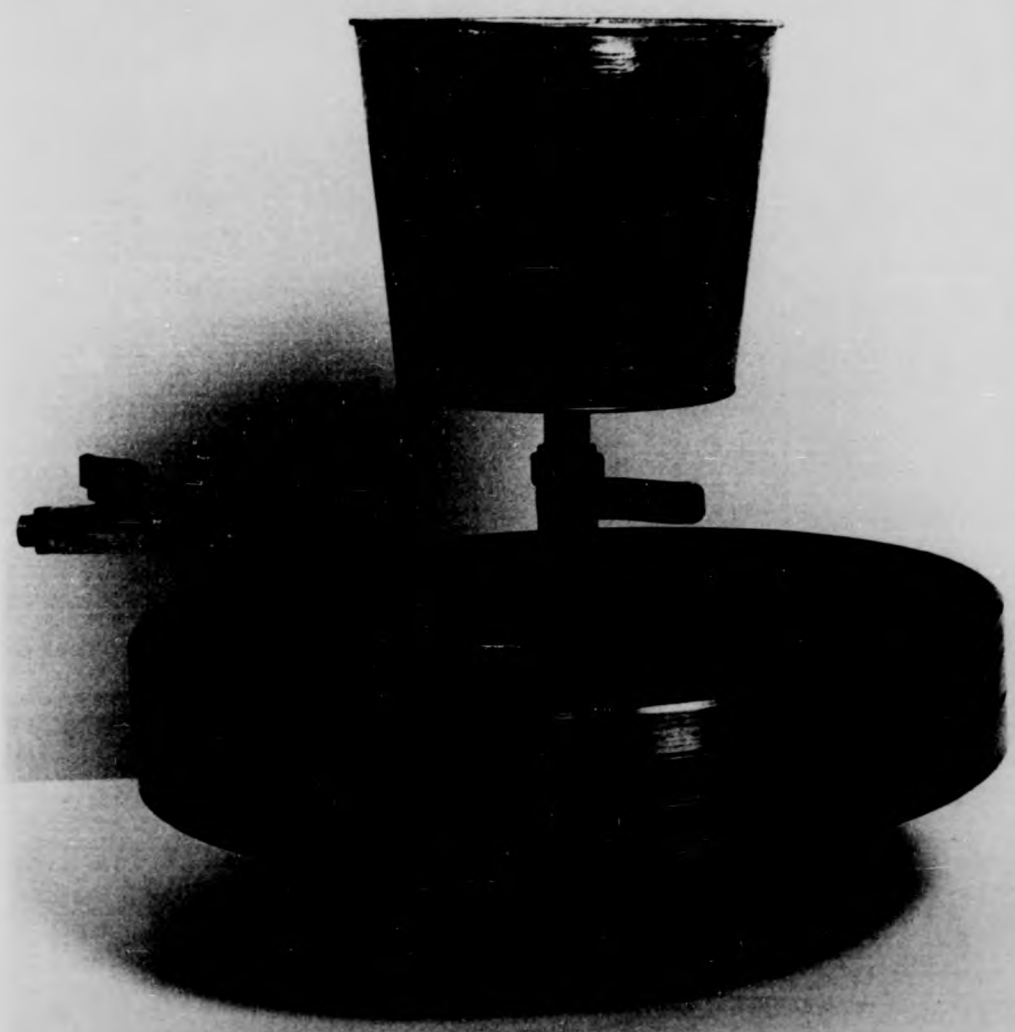

Fig. 5.14 (a) : The steel mould

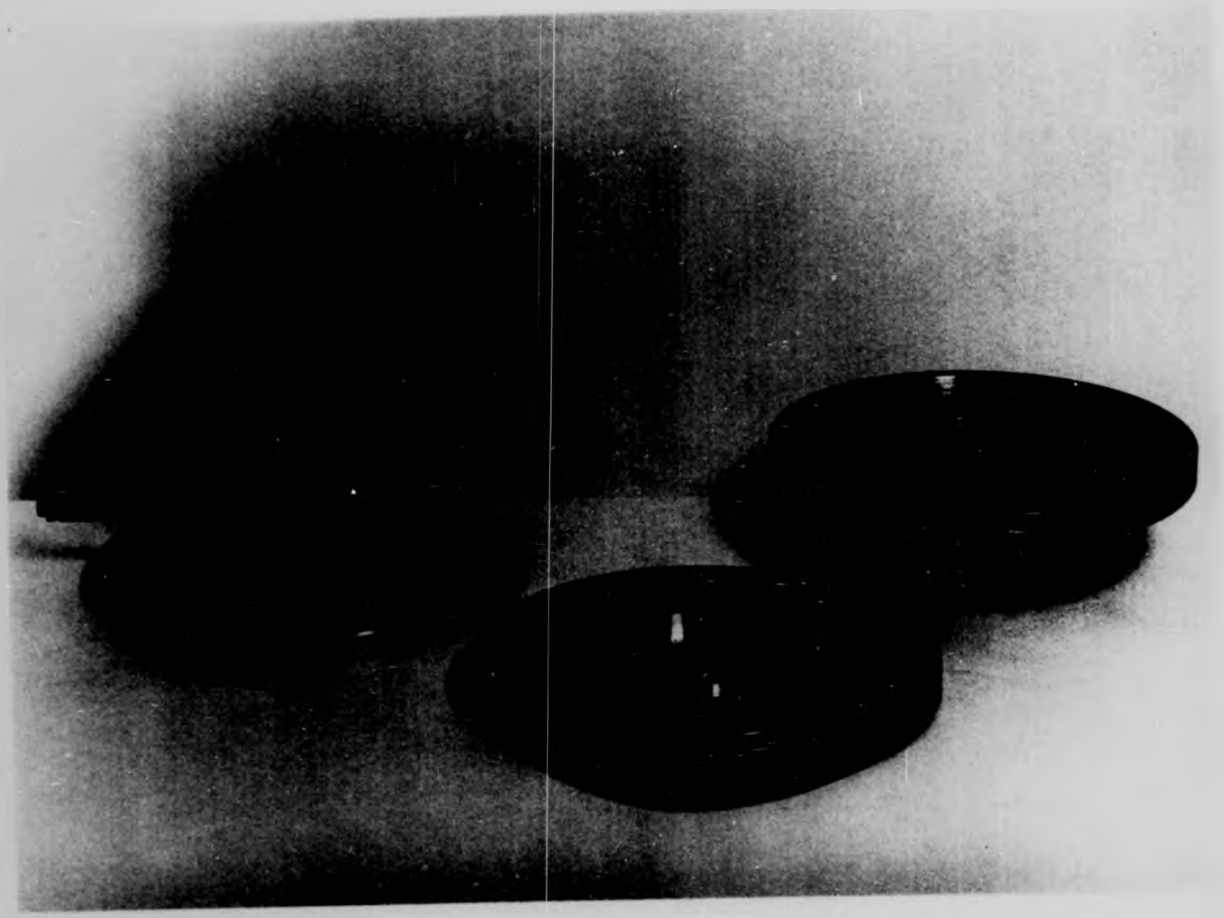

Fig. 5.14 (b) : Components of the steel mould

To commence the disassembly, five threaded holes were introduced through the periphery of the filling plate and the top half. The holes of the two parts are positioned alternately so that the filling plate can be jacked away first and then the top half removed. The base plate and the dummy shaft are removed as well. The armature is then released by pressing the commutator gently.

The final step before encapsulation is to fit the armature gently inside the mould and tighten it up. This is to ensure that the armature thickness is at the specified value and to check that the armature coils are in the right position. After approximately ten hours, the mould is disassembled and the armature is checked again. If the thickness of the armature and the position of the coils are correct, then it is ready to be encapsulated.

5.3.5 Encapsulation

A releasing agent is applied to all interior surfaces before moulding to ease

the armature extraction, and the join between the base plate and the flanged base is sealed with silicone rubber (in fact this is applied to all subsequent joins between mould parts whenever they exist). Then the armature is loaded into the mould and the encapsulation process is carried out after pre-heating the armature, mould and resin to approximately 60°C. Sufficient resin constituents are prepared and these de-aired and mixed as required. During this time, the mould is vacuumed and the pressure is reduced to 5mbar. At this stage, the prepared epoxy resin is poured into the chamber, valves are opened to allow resin to be drawn into the mould, and the vacuum valve is closed. When the resin has ceased to flow into the mould, the chamber, the valves and the pipework are disconnected and removed from the mould. All the equipment is then cleaned by a suitable cleaning agent (acetone or cellulose thinners) before the compound has hardened. Then the mould is left in an oven at 100°C for at least 10 hours. Subsequently, the mould is removed from the oven and allowed to cool for at

least one hour. Finally the mould is opened and the encapsulated armature is removed from the mould. It is then necessary to check the armature thickness again, to make sure that it does not exceed the required value. Once this has been done, the commutator segments are undercut, the armature is balanced and it is then ready for installation in the motor (Fig. 5.15).

Although the encapsulation process just described is a slow and time-consuming procedure, it is very suitable for prototype work. Techniques are available today to perform such operations to produce smaller armatures much more quickly, and on a commercially viable basis. The armature was encapsulated by Robnorganic Systems Ltd. and the moulding material used is an epoxy resin type PX237C (the specification is detailed in Table 5.2) which was supplied by the same company.

Later sections discuss the problems of the

Fig. 5.15 : Solid disc armature

Manufacturers of—
Electronic Component Coatings · Formulated Silicones and Epoxy Resins · Encapsulation of Electrical and Electronic Components · Robnor Twin Packs for Epoxy, Polyurethane, Polyester Resins and Silicone Rubbers

Robnorganic SYSTEMS LIMITED

Directors: Peter Kerley G C N Snelgrove M D Hampleman

Registered in England No 664718

Table 5.2: ROBNOR EPOXY CASTING RESIN PX 237C

This resin system is a warm curing casting system formulated for the encapsulation of electrical components. It possesses particularly good resistance to thermal cycling and to thermal shock.

It can be supplied in any of the standard range of colours or its natural colour which is a light cream.

Mixing

If in twinpack form, mixing is carried out as described in the twinpack literature. If in bulk, the resin and hardener are mixed in the ratio 17:2.

The usable life of PX 237C when mixed is as follows :-

12 hours at 20°C
4 hours at 40°C
2 hours at 60°C

Curing

Cure the system for at least :-

24 hours at 60°C
10 hours at 80°C
4 hours at 100°C
2 hours at 120°C

Properties

Initial Viscosity	50-60 poises
Specific Gravity	1.56
Resistance to Heat (continuous)	120°C
Thermal Conductivity	7×10^{-4} cal/cm °C
Electric Strength	110-120 kV/cm
Volume Resistivity	$> 15 \log_{10}$ ohm cm
Coefficient of Expansion	$4.5\text{-}5.0 \times 10^{-5}$ in/in linear/°C
Deflection Temperature	130°C improved by extended post cure.
Elasticity	270-330 kg/mm^2 (unfilled)

NOTES

Cleaning equipment

All equipment must be cleaned before the compound has hardened. Acetone or cellulose thinners are suitable cleaning agents.

plastic used to encapsulate the armature winding which eventually led to adopting a skeleton armature structure. In order to produce such an armature, a modified core of Tufnol material was designed (see Figure 5.33 (a)). This has slotted holes around the wide flanged end (non-commutator side) to fix the main winding to it by special tape.

The processes for building skeleton armatures are the same as for the encapsulation process up to the stage of making the armature ready for encapsulation. From this point, the procedure of this alternative method diverges from the encapsulation method. The armature is wrapped with heat-curing glass-fibre tapes and dipped into a polyurethane varnish (p. varnish) bath for several minutes. Then it is taken out and drained until the p. varnish spreads out on to the armature coils. Then the armature is loaded into the mould. Finally, the mould is put into an electric oven at 150°C for approximately seven and a half hours. Then the same procedure is carried out as when finishing off

Fig. 5.16 (a) Skeleton armature (commutator side)

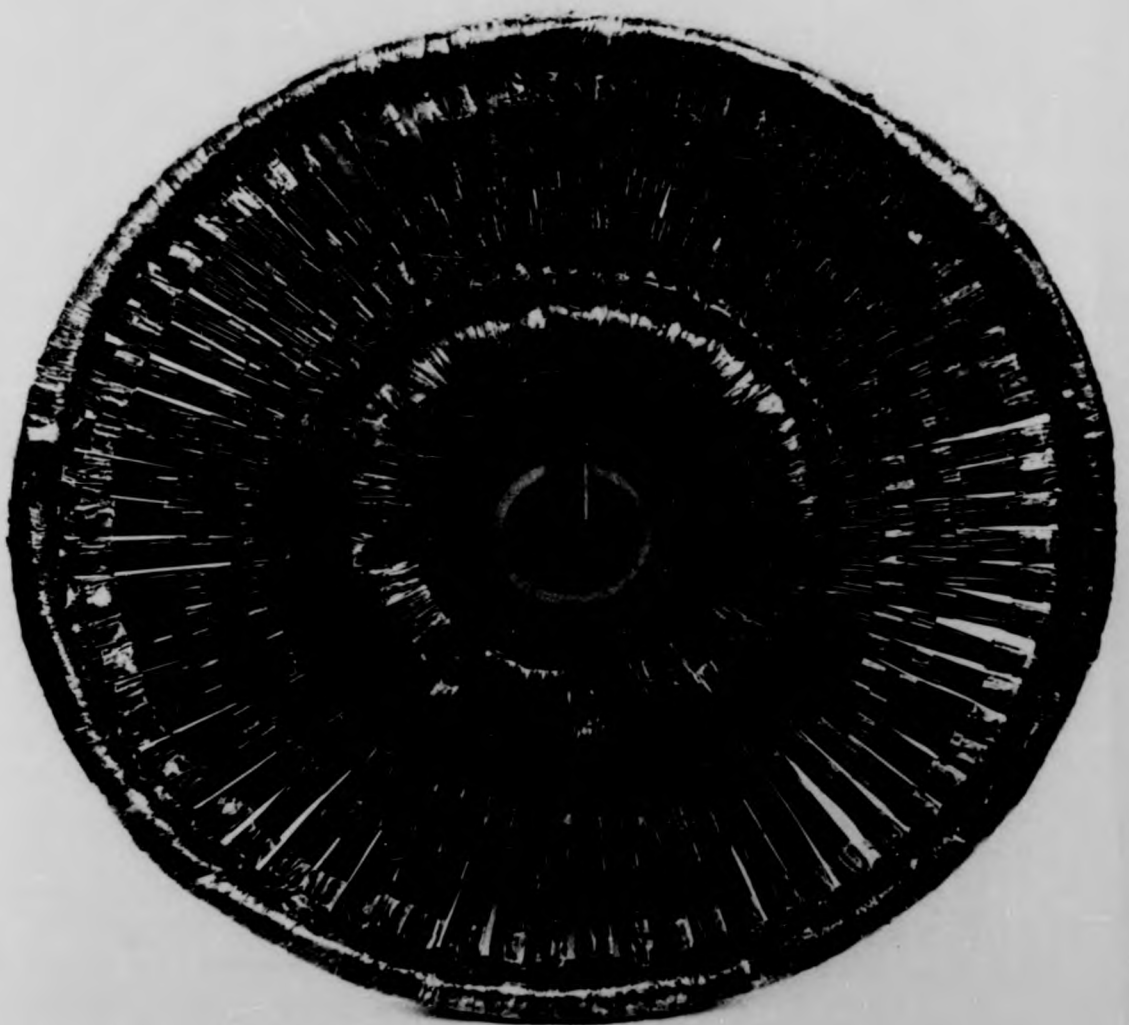

Fig. 5.16 (b) : Skeleton armature (non commutator side

the encapsulation process for the armature. A typical armature, which has been cast by dipping it into a p. varnish bath is shown in Figure 5.16.

The method mentioned above is very simple and straightforward. Also it offers some attractive advantages since p. varnish is applied only to the surface of the armature coils, heat dissipation becomes less of a problem. As there is no pre-preparation or mixing for the material used in this method and the amount of it is all that is required as the aim of this method is only to provide rigidity for the armature windings, so this method has the advantage that the armature will have less weight than if the method described in Section 5.3.5 had been used. Consequently the cost of material is reduced, there is less waste, and this method requires less supervision.

5.4 Test Rig and Instrumentation

The diagrammatical layout of the test rig is shown in Figure 5.17. A Ward Leonard

A. Torquemeter
B. Tachometer
C. Induction motor
D. D.C. machine
E. Loading generator
F. Disc motor
G. Variable transformer
H. Rectifier

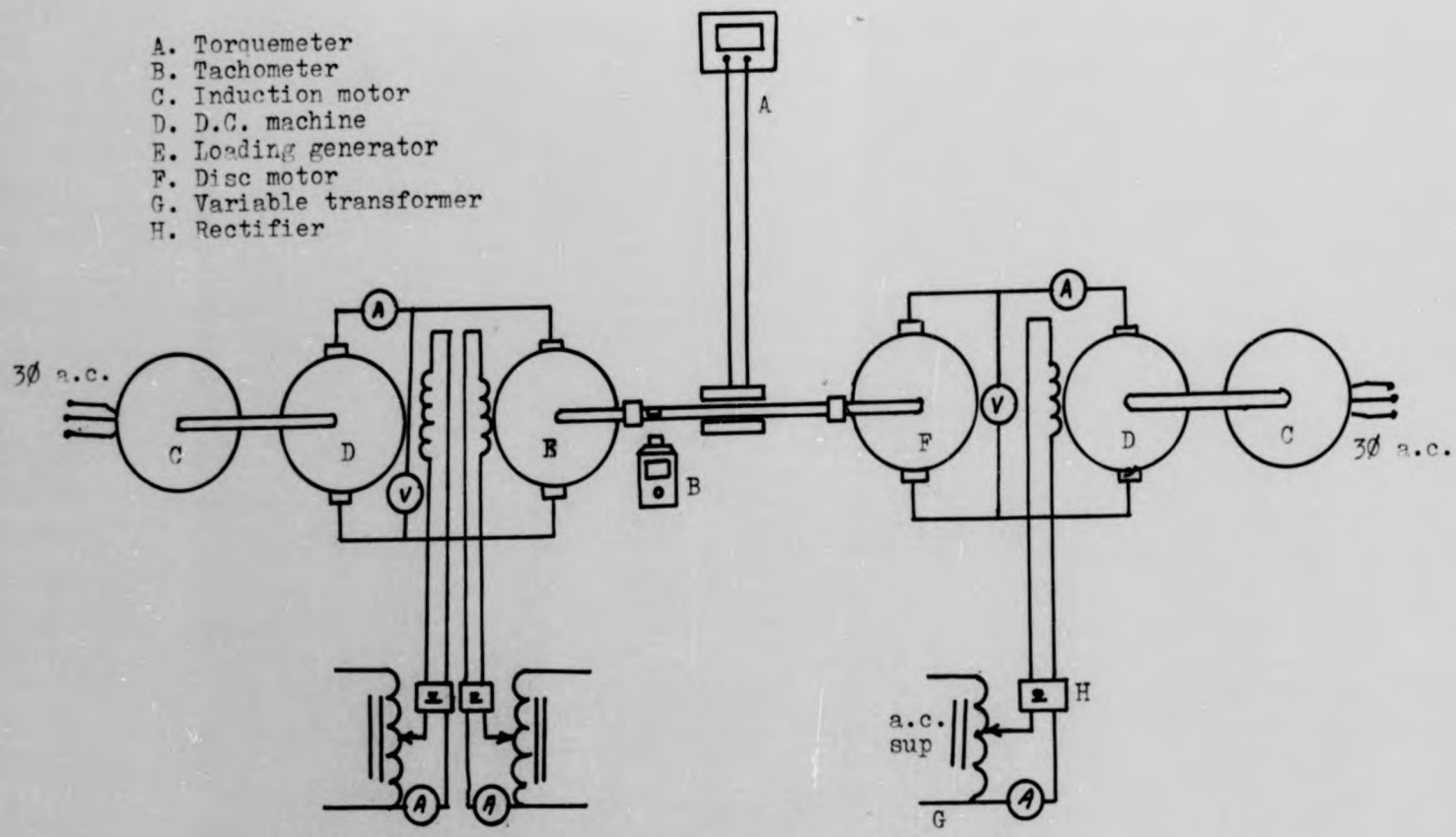

Fig. 5.17 : Diagrammatical layout of the test rig (Ward Leonard system)

Fig. 5.18 : D.C. machine-induction machine set (used to feed power to the mains)

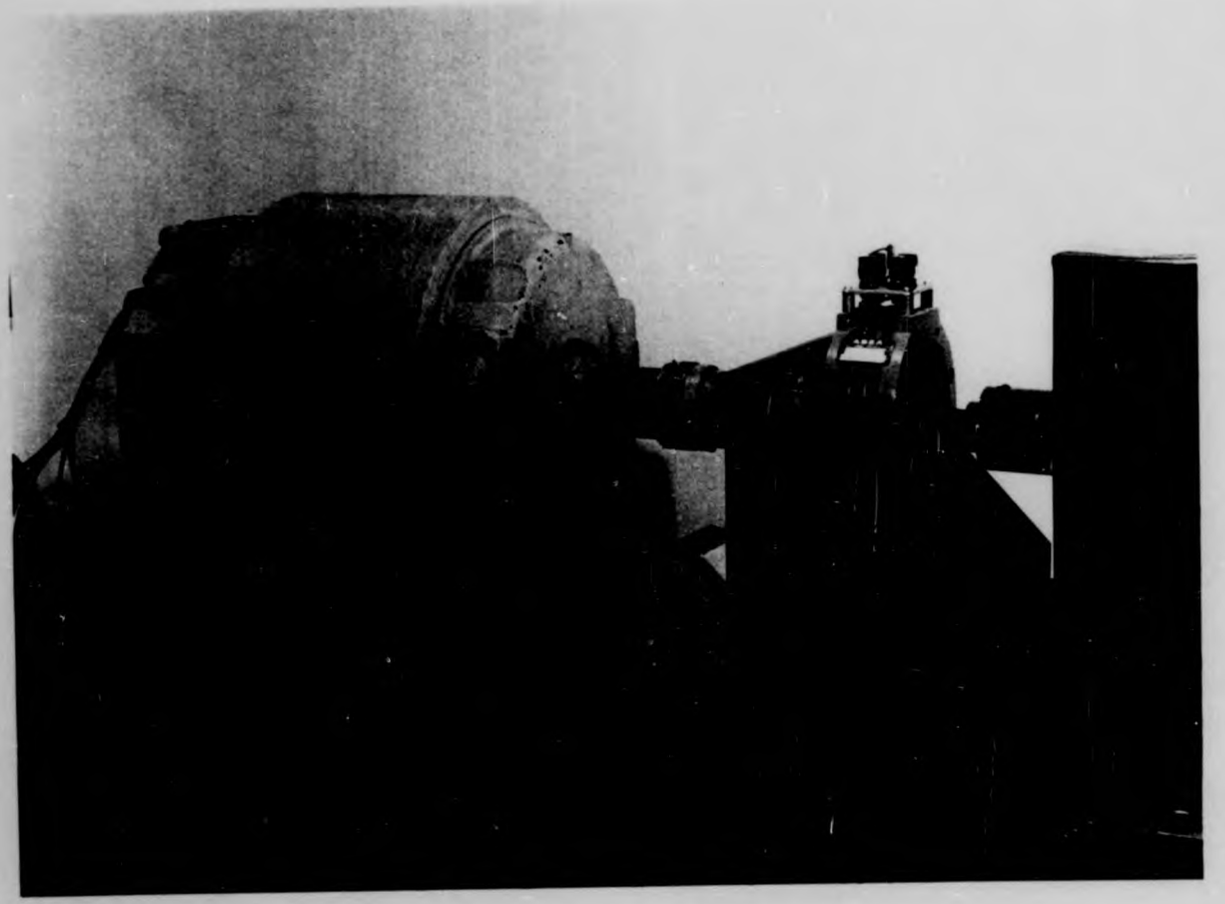

Fig. 5.19 : Load machine (D.C.) and torductor ring

system was used to carry out the load test of the machine. It is known that in this system an induction machine and a D.C. machine set are mechanically connected, as shown in Figure 5.18, and another D.C. machine (Figure 5.19) is coupled mechanically to the test machine. These two sets are electrically connected. Having variable field excitation of the two D.C. machines enables the load of the test machine to be controlled as well as allowing the test machine to run as a motor or generator. As far as the disc machine is concerned, all tests which are given in this Chapter were obtained when the machine was running as a motor. Power for the disc armature motor is derived from a separately excited D.C. machine which is coupled to an induction motor (Figure 5.20).

Output torque from the motor is measured using an ASEA 'Torductor' (type 5693 - 719/A) which enables accurate measurement of torque to be made (Figure 5.14). Its operation depends on the fact that in a

Fig. 5.20 : D.C. generator-induction motor set used to supply power to test machine

shaft subjected to torsional stress, changes occur in the permeability of the shaft. This unit consists of one central set of excited coils and two identical pick-off coils connected in opposition. Each ring has four pole windings distributed around a central shaft in a similar fashion to a stator of a radial machine. The central shaft, which is used to connect the experimental machine to the load, acts as the rotor and consequently as a magnetic return path. When there is no torsional stress on the shaft, the flux linking both pick-off coils is identical and the voltages induced in these coils cancel each other out. When the shaft is put under stress, the field is distorted and the two induced e.m.f.s are no longer equal, giving a resultant output in proportion to applied stress. The output was recorded by using a digital multimeter. This measuring torque-meter does not require direct contact to the rotating shaft, therefore it provides an ideal method for shaft torque measurement. The torque unit was calibrated against applied weights as shown in Figure 5.21.

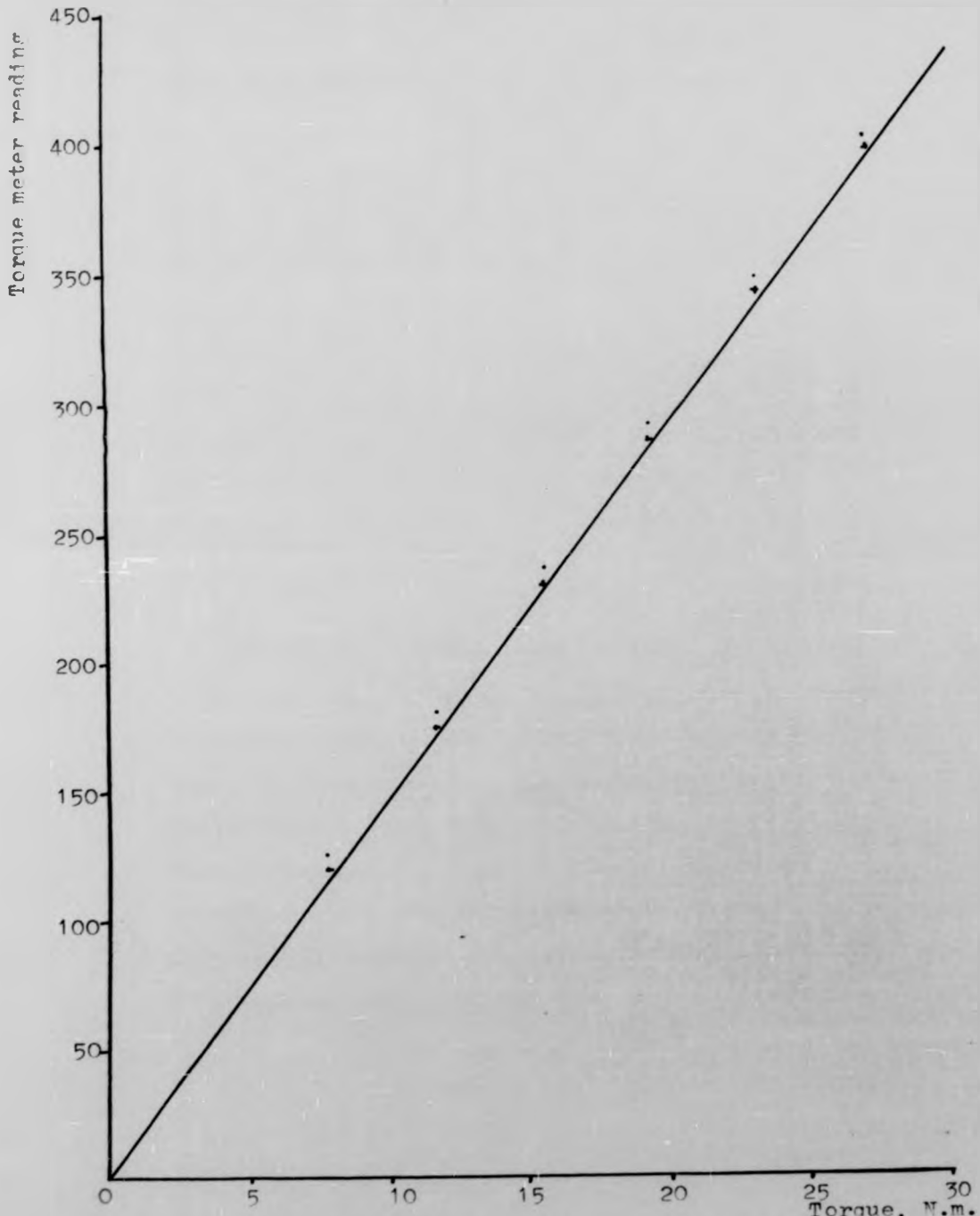

Fig. 5.21 : Calibration curve for the Torque Meter

Chapter 5

Motor Construction and Performance Testing

One press button digital hand tachometer, which is shown in Figure 5.22, was used to measure the output shaft speed of the disc machine. The instrument works on the principle of counting the number of revolutions of the shaft by detecting light reflected by a reflective marker fixed on the shaft. The meter is fitted with automatic range selection of an accuracy ± 1 digit for the range between 1000 - 10000 RPM.

A number of thermocouple sensors of nickel and chromium wire were inserted at different spots on the magnet poles, motor case and bearing case, to measure the temperature of the stator parts. A 2751-K series digital thermometer with a 12-channel switch was used. The instrument has an accuracy of $\pm 0.2\%$ of the reading and temperature range is 0 to 450^{o}C.

A Wall heat-spy digital infra-red thermometer model DHS-8E was used to measure

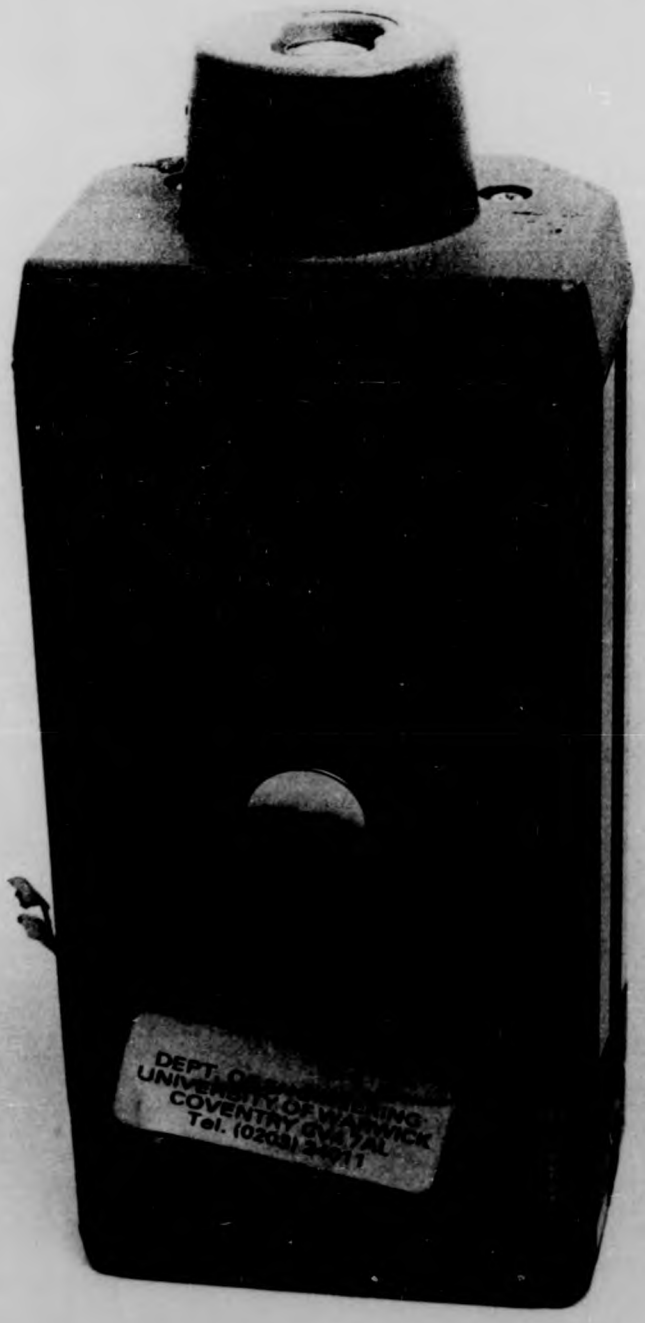

Fig. 5.22 : Hand tachometer

the temperature of moving armature (see Figure 5.23). The heat-spy instrument measures temperature by detecting the infra-red energy emitted from the measured source. The amount of energy emitted is proportional to the body temperature. Heat-spy collects this energy by means of fixed focus optics onto a sensitive detector and reads out directly in degrees Centigrade. It is fast because it collects the infra-red energy at the speed of light, and the detector has a very low mass. The time constant is 0.1 second, about 10 times faster than conventional contact methods. Measurements are displayed in less than one second. The display is a LED digital readout with a range of 0 to 500°C. When the above temperature is exceeded, the readout will blink, indicating overrange. The meter up-dates at the rate of 5 times per second. The detector responds to temperature change (98%) in 0.4 seconds. The meter utilizes an internal light spot projector which illuminates the target area

Fig. 5.23 : Heat spy infrared thermometer

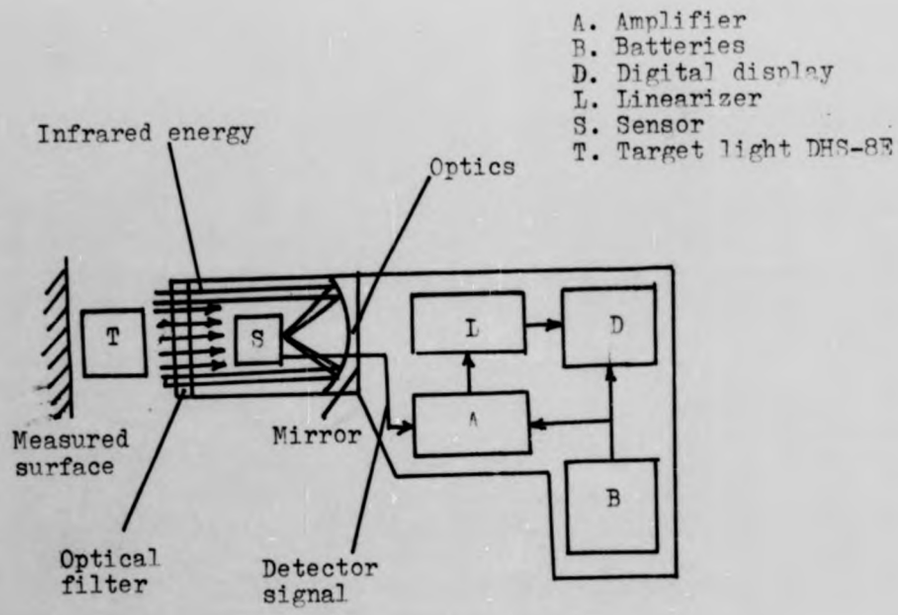

Fig. 5.24 : Heat spy thermometer block diagram

being measured. The DHS-8 measures a target size of 5mm at 25mm (see Figure 5.24). Therefore, the heat-spy surface thermometer is a practical, rugged and ideal instrument for measurements of temperature in rotating machinery.

5.5 Tests and Results

Prior to carrying out load tests, the brushes were first set to the optimum position. A series of preliminary tests were then carried out followed by the following main tests (all the results which are included in this Section are obtained from testing a single rotor version using a skeleton armature).

a) No Load Tests

These tests were carried out with the rotor output coupling disconnected. Input power and speed were measured for a range of supply voltages. Tests were repeated with spaces between magnet poles filled with wooden wedges to form a complete ring

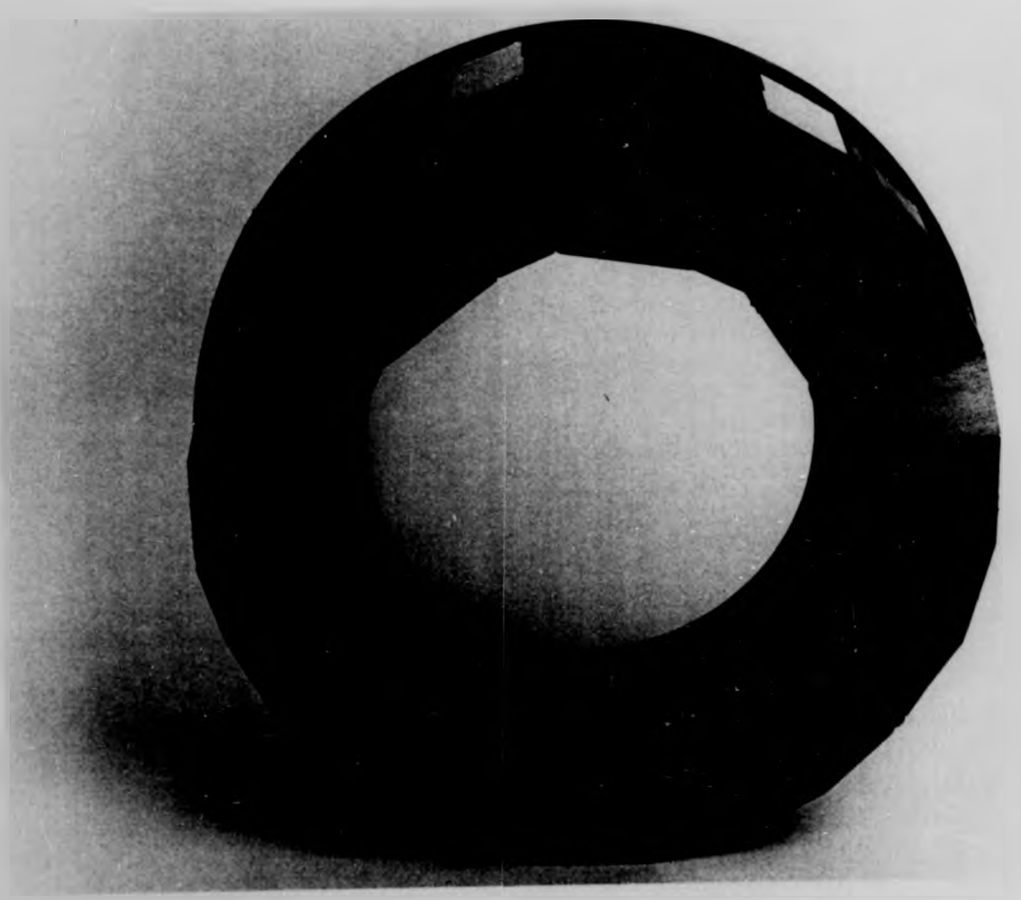

Fig. 5.25 : Stator magnets with wooden wedges between pole

(see Figure 5.25). The results are shown in Figure 5.26 which include the early no load test of solid armature discs, for comparison purposes.

In the first running light test of the single rotor version using solid armature (96V, 4200 rev/min), the motor was found to be drawing excessively high currents, and high temperatures were observed on the shaft. Initially the current was 8A and in later tests currents of 10A and 12A were observed. After consulting the bearing company, all the bearing seals were removed. This reduced the current to 5.8A which is close to the design value. No such problems were encountered when the twin-rotor machine was tested, because the bearings specified were of a different make, type and size (see Section 5.1). In tests carried out on early twin and single rotor motors, the temperature rise on the casing had not levelled out, even when the motor was running light. It was evident that a form of natural or forced cooling must be introduced.

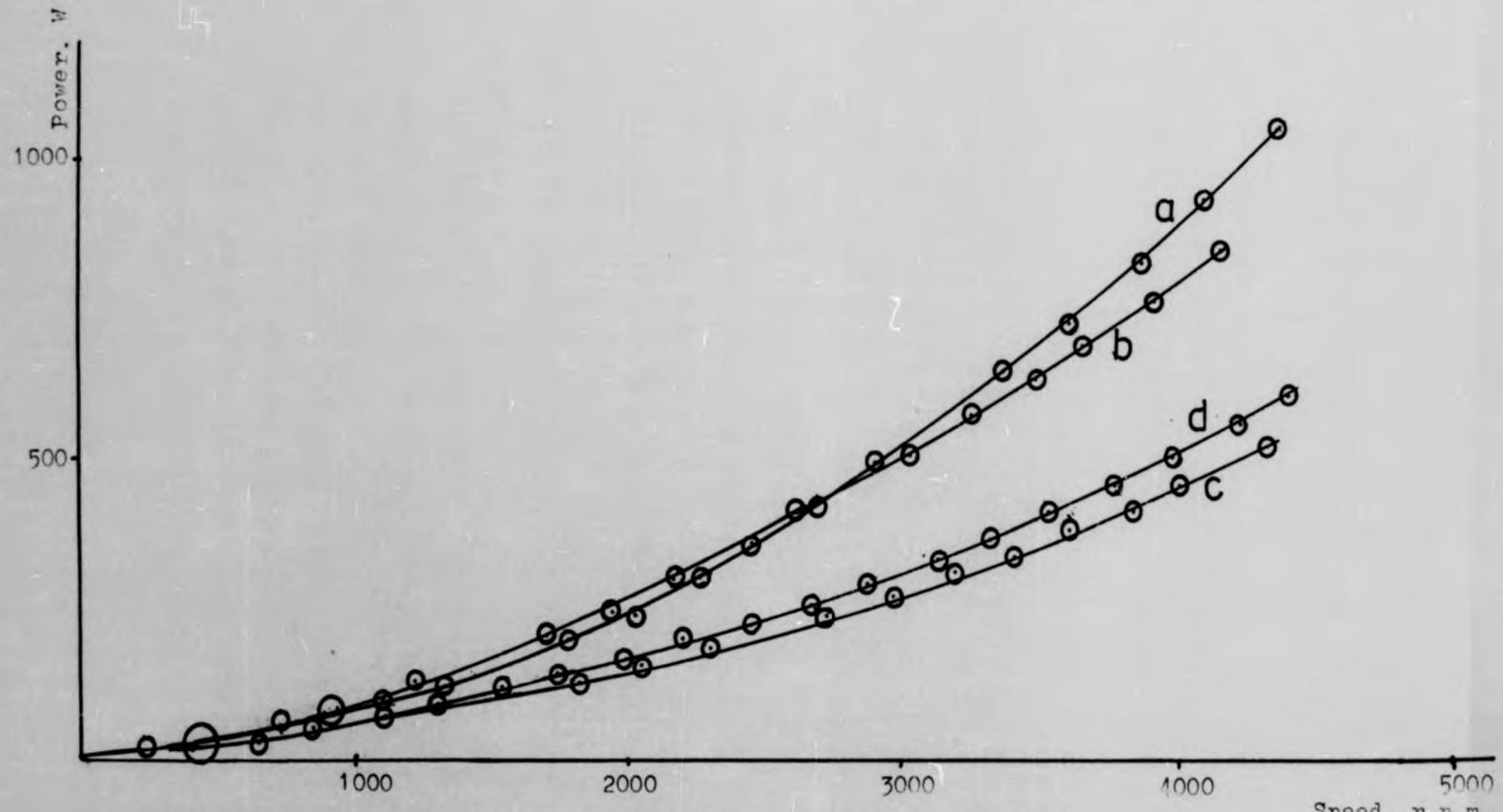

Fig. 5.26 : No load test

(a) Skeleton armature
(b) Skeleton armature with wooden wedges between magnet poles
(c) Solid disc armature (enclosed motor)
(d) Solid disc armature (ventilated motor)

As a first measure, it was suggested that ventilation holes, which may be pluggable for comparison purposes, be drilled in the periphery of the casing. Therefore, in the final version, apertures have been appropriately dispositioned in the motor frame to allow natural ventilation. The disc shaped structure of the motor allows effective self-ventilation and a good flow of air through the motor was observed. As an example, steady-state temperatures were recorded after running light for two hours as follows: armature 38°C; commutator 40°C; magnet 35°C; frame 35°C; ambient 18°C.

b) Load Tests

During the preliminary tests it was found that the motor speed for any set voltage and motor load was extremely sensitive to temperature. To obtain consistent performance data therefore, all load tests were carried out with the motor at high temperature, where temperature changes were small over the

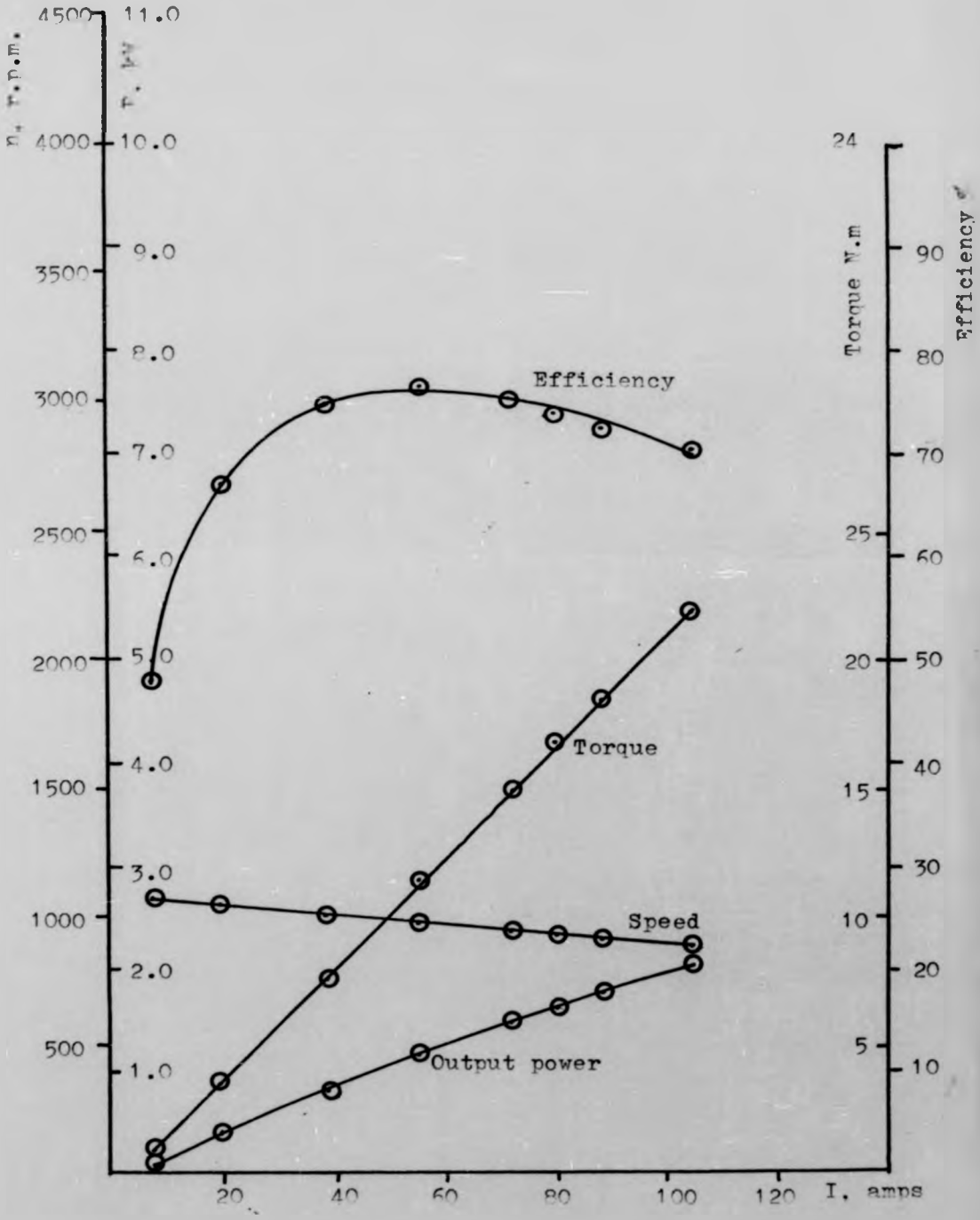

Fig. 5.27 : Performance curves of 10kW motor at 24V

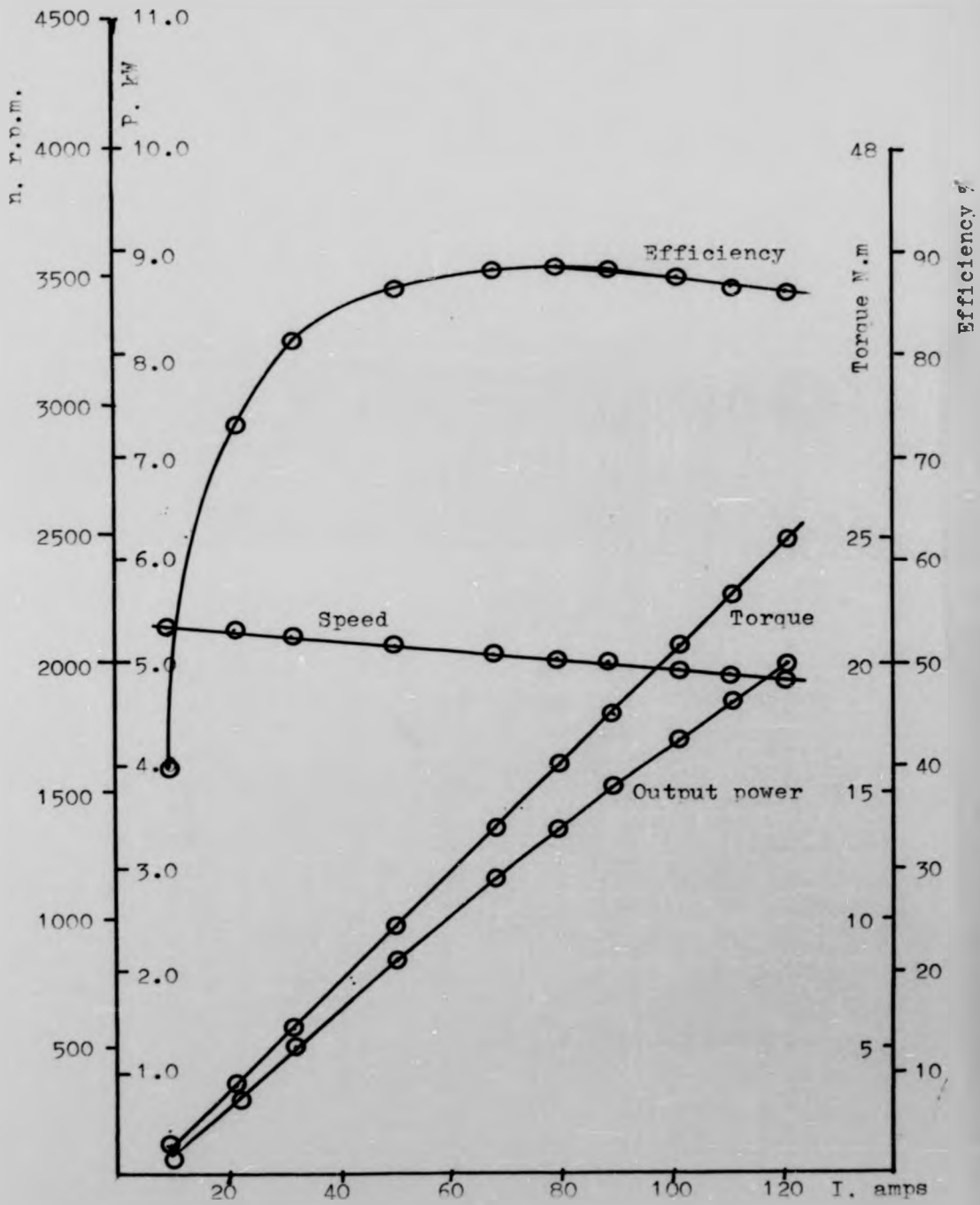

Fig. 5.28 : Performance curves of 10kW motor at 48V

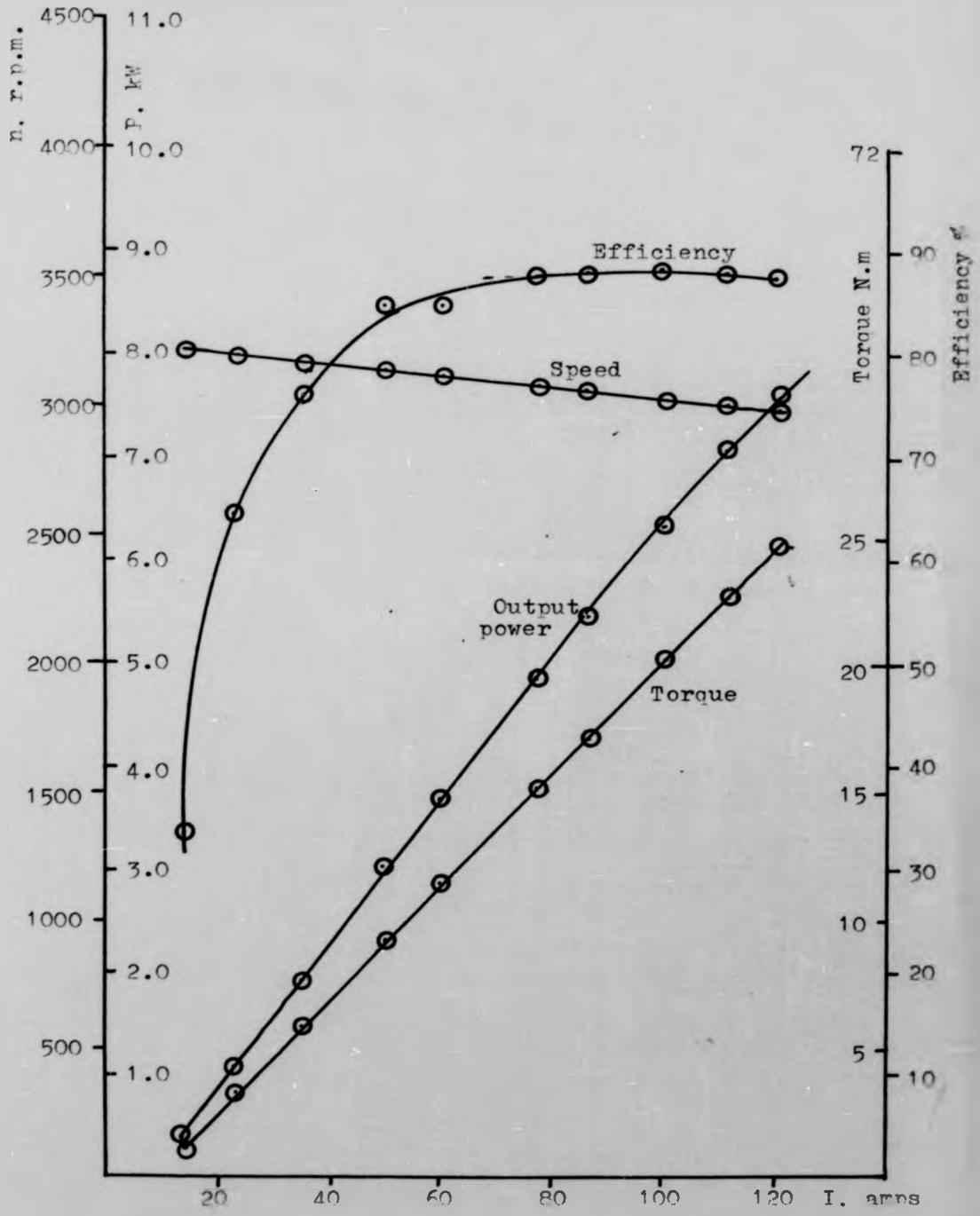

Fig. 5.29 : Performance curves of 10kW motor at 72V

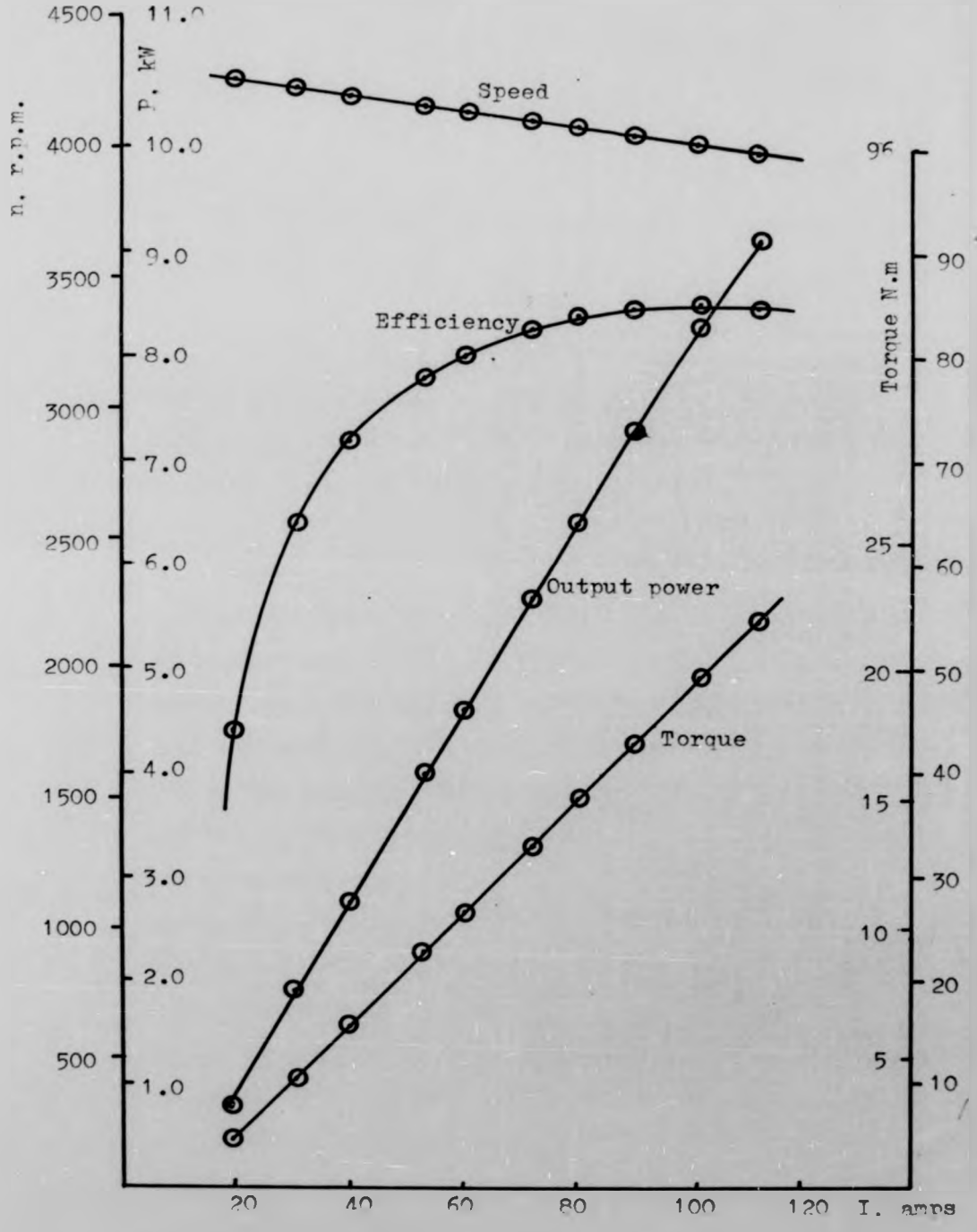

Fig. 5.30 : Performance curves of 10kW motor at 96V

period of each test. Performance data at 24, 48, 72 and 96 volts are given in Figures 5.27 to 5.30.

Load test results from (1) twin rotor motor, (2) single rotor version of enclosed design and (3) single rotor version of ventilated design shown in Appendix III.

Noting that (a) all these motors use a solid armature of steel hubs of four keying pins structure which have high magnetic stray losses (as explained later); (b) the lack of ventilation in motor (1) and (2) which led to the high temperature of operation; (c) the type of bearings in motors (2) and (3) have abnormally high losses; (d) the low flux per pole and high armature resistance (due to a manufacturing fault in the magnets and armature) in motor (3). Taking account of all the above facts, the characteristics of all these motors which were measured at different voltages are broadly in accordance with the expected performance (Figure 5.31).

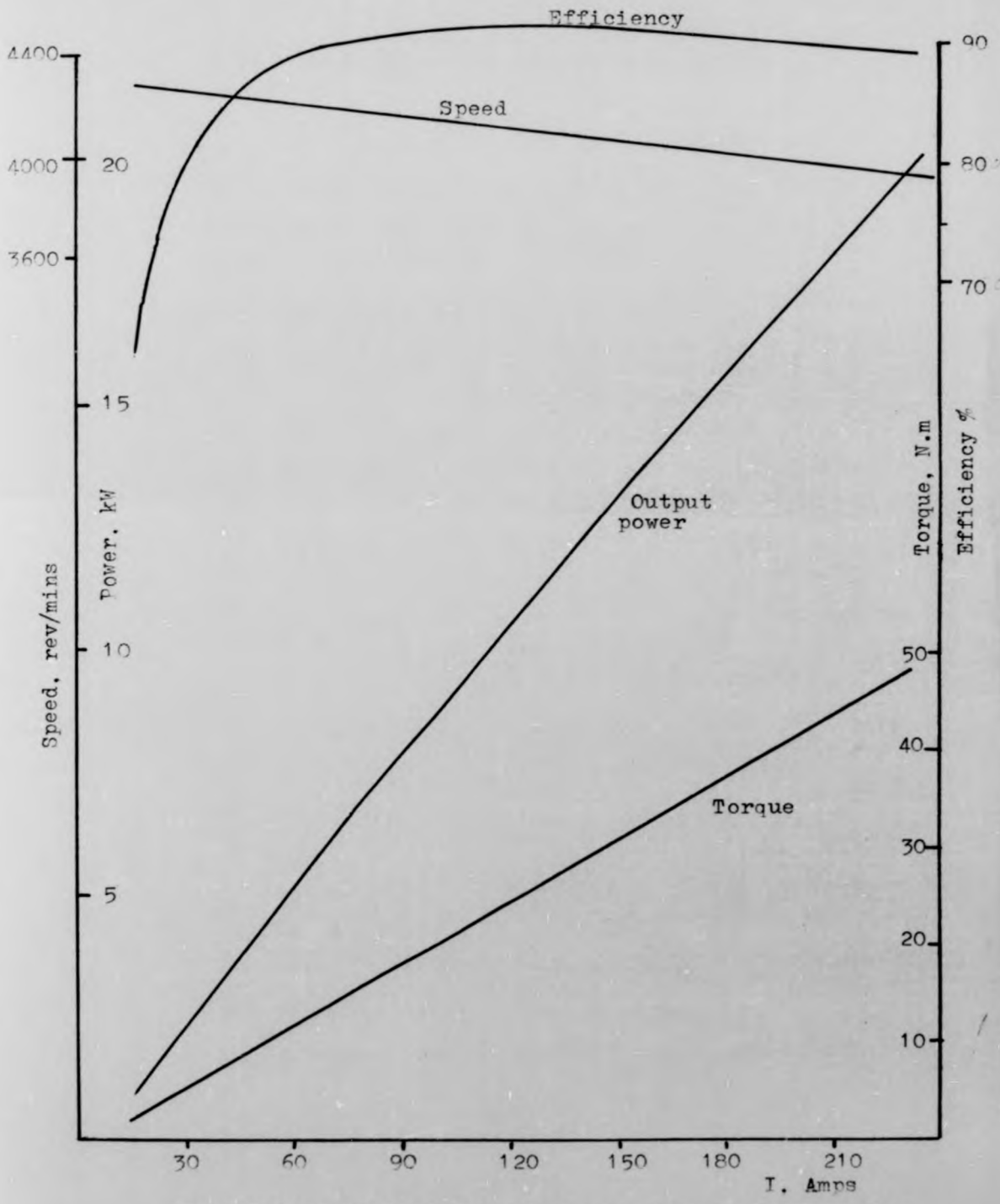

Fig. 5.31 : Predicted performance curves of 10kW motor

But of all solid armatures, none withstood a heat run test. The failure sequence appeared to start from the core of the disc causing major cracking at a radius somewhat less than d_1 in the area of the four keying pins. The excessive heat caused severe swelling of the encapsulant around the hub. The swelling in this area led to the disc running on the magnets at the inner magnet diameter, causing short circuits, and subsequent over-heating of the failed coils and breaking up of the outer rim. A redesign of the disc core in order to reduce the amount and thickness of encapsulation and reduce the drastic variation in the amount of encapsulant around the core and key pins, was necessary. A new core as the one shown in Figure 5.5 (b) was produced. In addition to redesigning the hub, the main winding was wrapped in fibre-glass tape which is cured by heat treatment to reinforce the encapsulation as shown in Figure 5.32. The reinforced winding was

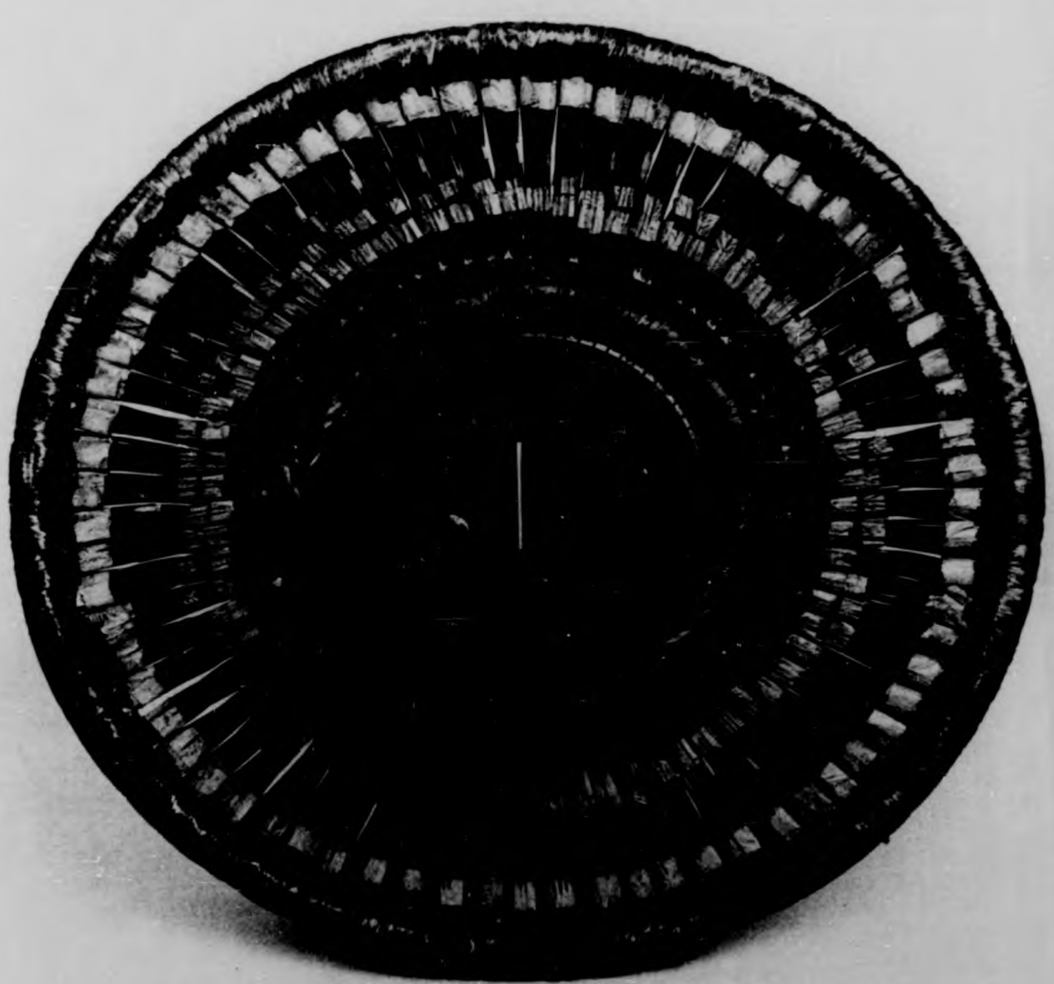

Fig. 5.32 (a) : Reinforced armature winding (commutator side)

Fig. 5.32 (b) : Reinforced armature winding
(steel core side)

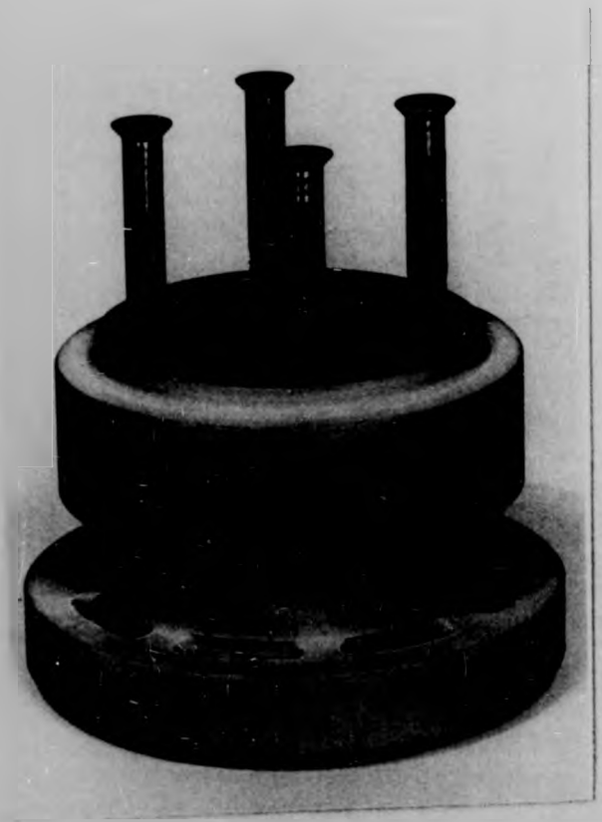

(a)

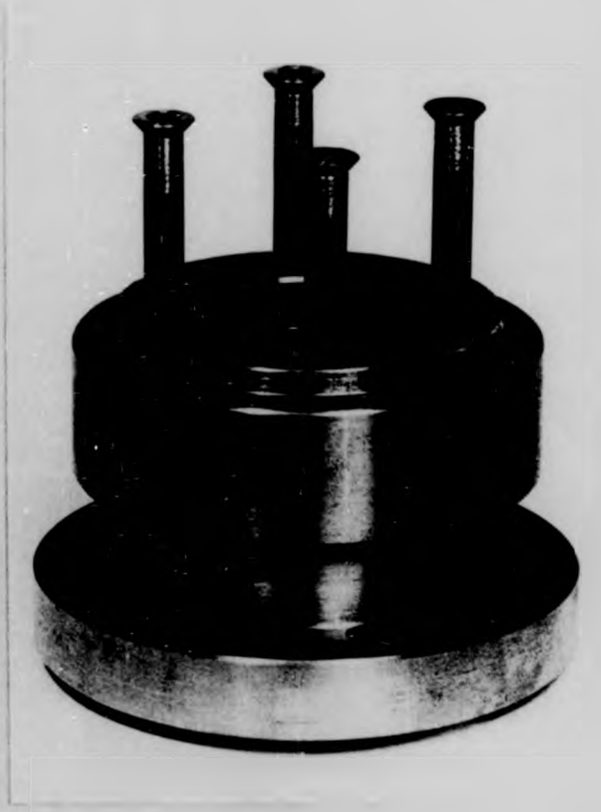

(b)

Fig. 5.33 Skeleton armature cores
(a) Tufnol core (b) Steel core

physically sound. As a result, a decision was taken to produce a skeleton armature without any plastic moulding using a steel core, as shown in Figure 5.33(b). All the modifications mentioned above still do not include any vital alteration to reduce the origin of the heating. To achieve such a goal it is essential first to locate the reason for the heating and its source. After a preliminary investigation, it was realised that the heat was associated with load, therefore it was classified as load dependent losses accordingly. Analysis led to the idea that the armature current has a field pattern which concentrates the main electro-magnetic field through the central core and axle, which has the effect of developing eddy current through them. Forced air cooling might help, but the real problem was to reduce the origin of the heating.

A reconstruction of the core and axle in a non-magnetic material was a prime solution to reduce the origin of the heating. A core of Tufnol material, as shown in

Figure 5.28(a) was designed and employed in the final skeleton armature version. After testing it has been found that this was necessary; as a matter of fact no working conditions have been found in which a core temperature rise could occur.

Under hot conditions, the machine was working without injurious sparking and without injury to the surface of the commutator, or to the brushes at any point in the characteristics between maximum service speed and maximum rated current.

Unfortunately over-load test was not possible because the loading machine was not capable of developing the required over-load. Usually, under such test, the machine should be capable of sustaining a 300% increase of torque over rated output for a minimum period of 5 minutes.

The machine passed over-speed test. At this test, the machine stood for 2 minutes at a speed equal to 1.2 times the maximum service speed. This was done under rated current

(hot conditions).

c) Heat Run Test

The test was carried out at 96 volts and constant input current of 88A from cold. The stator temperatures were measured by means of thermocouples positioned at the following locations: on the outside of the motor casing. adjacent to the outer race of the non-drive end bearing and on the side of one of the permanent magnet pole pieces.

The armature temperatures were read by a heat-spy meter from a ventilation hole. Therefore the readings are the temperature of the outer periphery of the armature which is not the hottest point of the armature. But the modest temperature recorded on the armature periphery gives the impression that the inner armature periphery. which is the hottest point in the armature. is heated either within or even below the permissible temperature rise. Figure 5.34 shows the change in the armature temperature against time which demonstrates a low heating time constant.

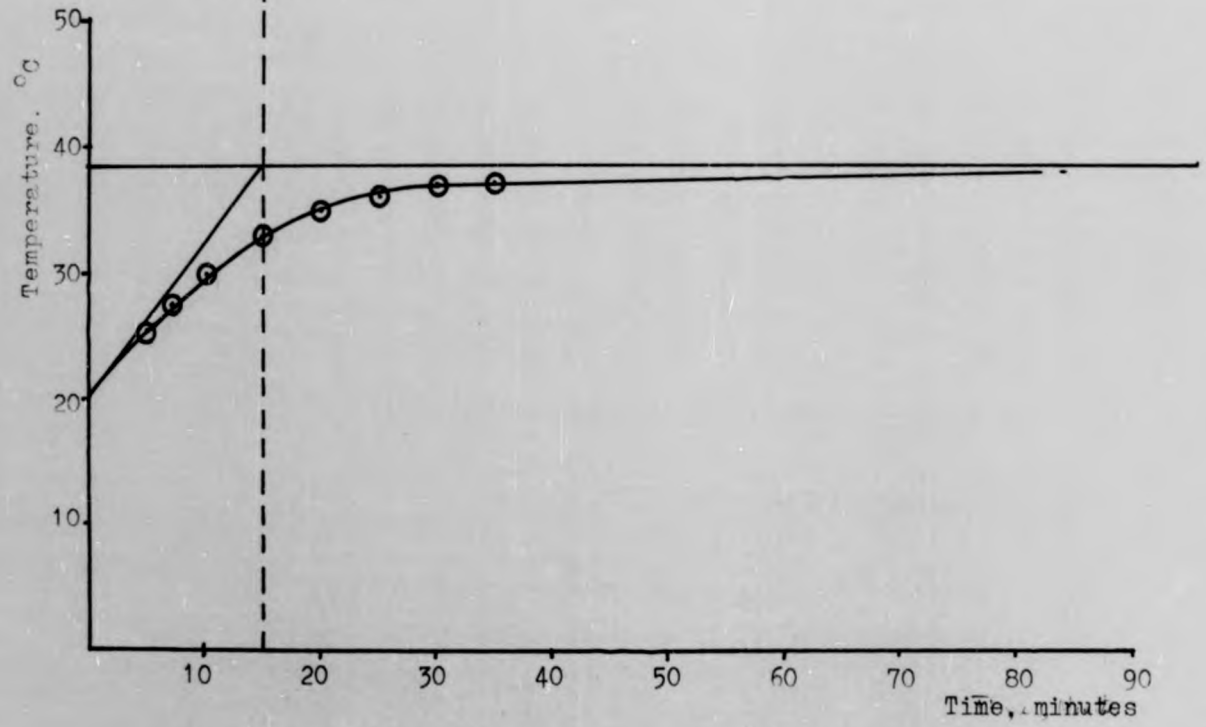

Fig. 5.34 : Temperature rise/time curve of skeleton armature

5.6 Losses

A disc machine, like any other DC machine, has losses which appear as heat and must be dissipated from the machine because of the limitations set on the working temperature of the insulation. In general, losses may be roughly classified as load dependent like I^2R, or speed dependent, like friction and windage losses. In the next Section we are going to explain an element of loss which is significantly more pronounced in a disc armature motor than a conventional machine and this is the high eddy current loss of the copper conductor. This loss is high due to the absence of iron in armature. As a matter of fact, in the conventional structure, the iron teeth work as flux paths by-passing the winding. No attempt to investigate such losses have been made previously. This is either because most previous prototype motors were small and it is difficult to assemble such losses in them, or prototypes of comparative size to 10kW were not run successfully so as to

be investigated thoroughly.

5.6.1 Eddy Current Loss

Suppose that a metal slab is traversed by flux (Figure 5.35(a)) - if B is increasing, there is induced in the metal an e.m.f. which sets up a current round the path indicated by the curving arrow. Such currents are known as eddy currents. They are a source of loss wherever conducting material is placed in a changing field.

31

It is possible to calculate the eddy current in a metal sheet under variable flux conditions, provided that we can make the following assumptions:

(a) The flux varies sinusoidally.

(b) The width of the metal sheet is very great compared with its thickness.

(c) The effect of the eddy currents, in modifying the distribution of magnetic flux, may be neglected.

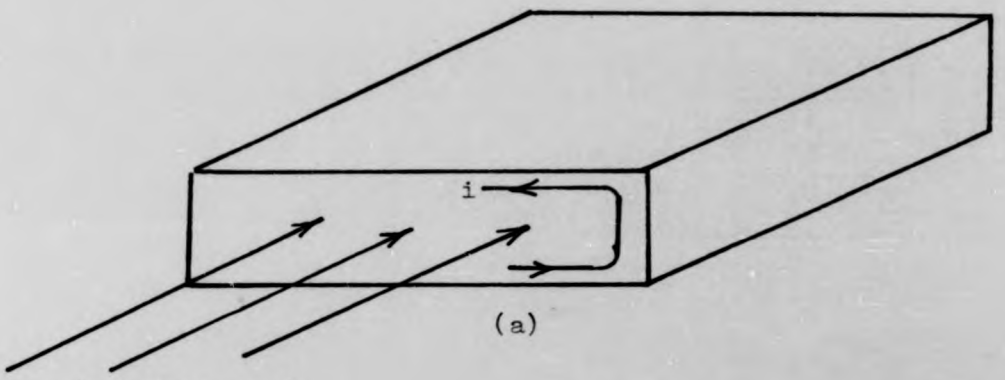

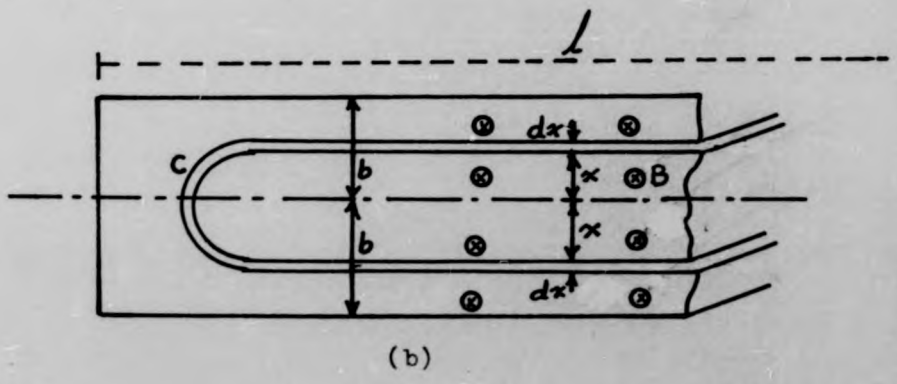

Fig. 5.35 : (a) Eddy current induction in a metal slab
(b) Eddy current calculation

Consider a metal sheet of width b, length l, and resistivity ρ, carrying a uniform flux density of peak value B_{max} and frequency f (Figure 5.35(b)). The direction of the flux is perpendicular to the plane of the diagram; the induced currents will be in the direction shown. We shall calculate the e.m.f. induced in a circuit which consists of two layers, each of thickness dx, situated at distances x on either side of the mid-plane of the sheet and joined by curved portions C near the edges of the metal conductor.

The flux traversing the space between the layers is given at any instant by:

$$\emptyset = 2(l.x.B_{max} \cos wt) \qquad 5.4$$

since B is sinusoidal. The irregularity at the ends is here neglected. The induced e.m.f. in the circuit formed by the layers is $\frac{d\emptyset}{dt}$, or:

$$\text{e.m.f.} = 2(l.x.w.B_{max} \sin wt) \qquad 5.5$$

The resistance of the circuit, again neglecting the effect of the ends, is $2\rho l/dx$ per unit depth (measured in the direction of B); therefore the eddy current loss in the two layers is given by

$$dWe = \frac{(2(l.x.w.B_{max} \sin wt))^2}{2\rho l} dx \qquad 5.6$$

and the factor $\sin^2 wt$ has a mean value of $\frac{1}{2}$. The mean rate of loss in the whole conductor is therefore

$$We = \frac{1}{2}\int_0^b \frac{(2(l.x.w.B_{max}))^2}{2\,l\,\rho} dx \qquad 5.7$$

$$= \frac{l.b^3.B_{max}^2\, w^2}{3\rho} \quad \text{per unit depth in the direction of B} \qquad 5.8$$

More conveniently, we write the loss formula as

$$We = \frac{b^2\, B_{max}^2 w^2}{3\rho} \quad \text{per unit volume} \qquad 5.9$$

We notice that if the width 2b. is divided into N laminations of thickness, 2b/N, the loss changes from $l.b^2.B_{max}^2.w^2/3\rho$ to:

$$l.N.x.\frac{(b/N)^3\ B_{max}^2\ w^2}{3\rho} \qquad 5.10$$

In other words, the loss in the pile of N laminations is $1/N^2$ of the loss in the unlaminated metal sheet. If we consider other shapes than flat sheets, or if we relax some of the conditions under which this calculation has been made, we shall expect to find changes of detail in the formula 5.9, but the general effect of each factor upon the loss will not change.

We shall calculate We in two simple cases. First, for a conductor of rectangular cross section, of dimensions a x b, with a uniform field B applied at right angles to the sides of length b (Figure 5.36(a)). It is beyond our power to take account of the changes in the field which the eddy currents themselves produce;

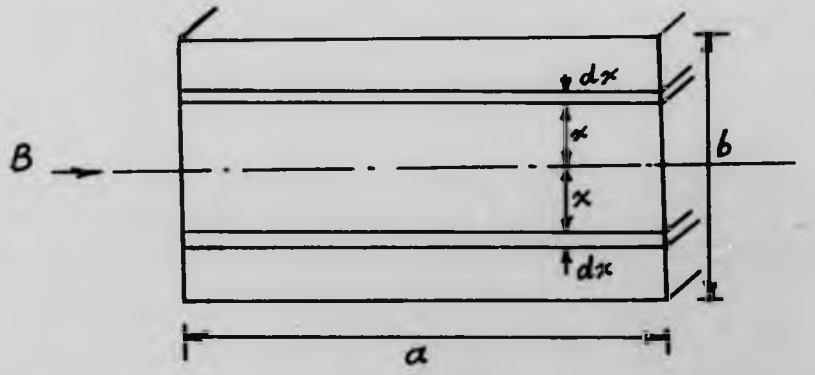

(a)

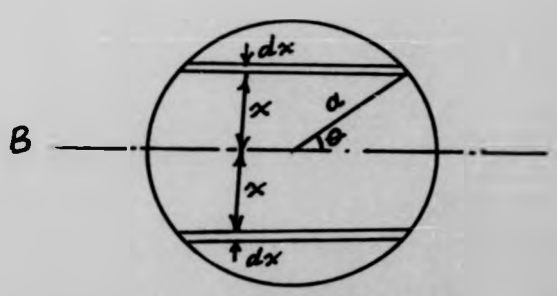

(b)

Fig. 5.36 : Calculation of eddy current in:
(a) Rectangular conductor
(b) Circular conductor

we must be content to assume that the flux density is B at each point. Consider, then, the induced current in two layers of thickness dx, at distance x on either side of the mid-plane. The induced e.m.f. in this circuit is - 2jw.x.B per unit length, and the resistance is $2\rho / a.dx$ per unit length; therefore the loss is given by:

$$dWe = (2 \times B\ w)^2 \left(\frac{a.dx}{2\rho}\right) \text{ per unit length,} \qquad 5.11$$

and the whole loss in the conductor is:

$$We = \frac{2.B^2.w^2.a}{\rho} \int_0^{b/2} x^2\, dx \qquad 5.12$$

$$= \frac{a.b^3.B^2.w^2}{12\rho} \text{ watts per meter} \qquad 5.13$$

The argument is exactly the same as that used in finding the eddy current loss for metal sheet; it is here given rather more briefly. The conductor has been assumed to be so long that the irregularities

occurring at its ends can be neglected.

We shall now carry out the same calculation for a conductor which has a circular cross-section of radius (Fig.5.36(b)). Considering again the induced current in two layers at distances x from the mid-plane. we find, as before. that the induced e.m.f. is -2j.w.x.B per unit length. The breadth of the strip, however, now depends upon x, being equal to $2\sqrt{(a^2 - x^2)}$; so that the resistance of the circuit formed by the two layers is $\rho / \sqrt{(a^2 - x^2)}\ dx$ per unit length. The loss in the two layers is therefore:

$$dWe = (2.x.Rw)^2 \left[\frac{\sqrt{(a^2 - x^2)}\ dx}{\rho}\right] \qquad 5.14$$

It is convenient to write this in terms of the angle θ indicated in Figure 5.36(b). We find that:

$$x = a.\sin\theta\ ,\ dx = a.\cos\theta\ d\theta, \sqrt{(a^2 - x^2)} = a.\cos\theta;$$

Therefore:

$$dWe = \frac{(2a^2.B.w)^2}{\rho} \sin^2\theta \cos^2\theta \, d\theta \qquad 5.15$$

and the whole loss is:

$$We = \frac{(2a^2.B.w)^2}{\rho} \int_0^{\pi/2} \sin^2\theta \cos^2\theta \, d\theta \qquad 5.16$$

The method of evaluating the integral will be found in any standard work on the calculus; its value is $\frac{\pi}{16}$. We therefore obtain:

$$We = \frac{\pi}{4} \frac{a^4.B^2.w^2}{\rho} \text{ watts per meter} \qquad 5.17$$

The axial fields across the air-gap has different values of flux. It has a magnitude of approximately B_g at the magnet surface and decreases approximately linearly to B_{ave} at the mid-plane of the air-gap (Figure 5.37). If a conductor is placed in the air-gap, the part of the conductor on the righthand side stays at a higher flux density than that of

the lefthand side. Thus a higher e.m.f. is produced in the righthand side of the conductor. Therefore, a potential difference is created between the right and the left portion of a conductor which causes circulating currents. These circulating currents give rise to losses.

Let B_{diff} be the difference between the flux densities on the left and righthand side of the conductor. This B_{diff} has a magnitude of approximately $B_{max\ diff}$ at the righthand side of the conductor and decreases approximately linearly to zero at the lefthand side of the conductor.

The loss due to this field difference is given by:[32]

$$We = \frac{1}{3} \frac{\pi B^2_{max\ diff}\ a^4\ w^2}{4\ \rho} \qquad 5.18$$

Where $B_{max\ diff} = \frac{4\ B_g\ (1 - \alpha)a}{lg}$ and the $\frac{1}{3}$ factor arises from the linear variation of flux. 5.19

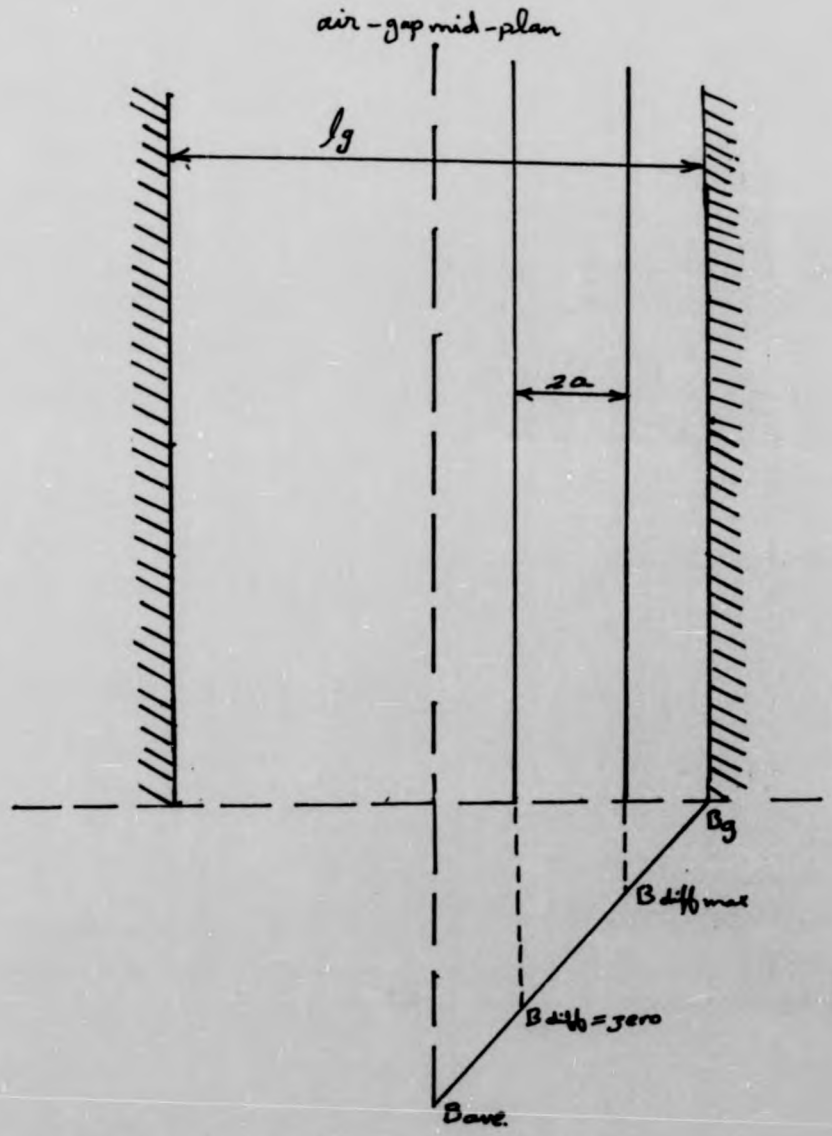

Fig. 5.37 : Conductor in air gap

In practice, typical values of B_g, , a and lg result in the loss due to the main field being greater than that due to the field difference. Therefore, for the sake of simplicity, the latter is neglected.

The production of excessive eddy currents can be avoided by properly subdividing the conductor. These subdivisions are insulated from each other and thus the eddy currents of one cannot travel to the other. Let the conductor of a radius be divided into N strand. The radius of each strand will be $\frac{a}{\sqrt{N}}$. then the total loss changes to:

$$N \frac{\pi}{4} \frac{\left(\frac{a}{\sqrt{N}}\right)^4 B^2 W^2}{\rho} \qquad 5.20$$

In other words, the loss in the conductor of N is $\frac{1}{N}$ of the loss in the solid conductor.

Now the relationships derived above are valid only when the subdivisions are not connected in parallel in such a manner as to

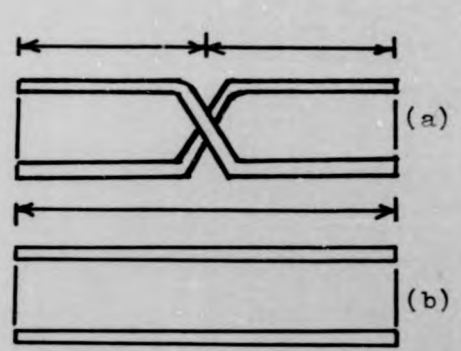

Fig. 5.38 : Armature conductors in stranded form
(a) Twisted
(b) Parallel

permit a path for eddy currents. A parallel connection between the subdivisions is necessary and therefore the subdivided conductors should be connected in parallel only when a complete balance between the subdivisions has been secured. This may be obtained by twisting or transposing the conductors. For example, let us consider a conductor subdivided into two parts. If the two subdivisions are placed in the air-gap as shown in Figure 5.38(b), they link with different values of flux. Therefore such an arrangement does not give any benefit because the two subdivisions have unequal e.m.f.s induced in them and since they are connected, parallel eddy currents flow in the local circuit formed by them (subdivisions).

Now consider the crossed conductor arrangement of Figure 5.38(a). Here the two parallel circuits are identical and therefore have equal e.m.f.s indicated in them. This arrangement, known as transposition, eliminates eddy circulating currents from one subdivision to another.

Armature conductors have their layers twisted so that every subdivision occupies all possible layer positions for the same length of conductor. This gives symmetrical lengths for every subdivision and thus equalizes the eddy e.m.f.s in all the subdivisions. Therefore, the layers can be connected in parallel without producing eddy circulating currents. In long conductors the twisting may be carried out three to four times.

5.6.2 Losses Separation

All previous calculations based on the load tests show that the calculated sum of the known electrical and mechanical losses in the motor is less than the difference between measured input and output power. Therefore it was felt that further research into the existence of eddy current paths was necessary. Such a task was possible only by evaluating the known components of losses quantitatively, one by one, and the difference between the total power losses and such known components

have to be analysed in order to relate it to its source of origin, so they are no longer unknown.

In order to obtain the different elements of losses, the experimental machine was driven by the load machine which was running, in this case as a motor. The input current and voltage to the load machine were recorded using standard meters. The experimental machine was disconnected from the power supply and then driven as follows:

(1) light (Fig. 42A)(the open circuit voltage was recorded over a range of speeds (Fig. 41))
(2) as (1) with no brushes (Fig. 42A)
(3) as (1) but the magnets were replaced by dummy (wooden) poles (Fig. 5.39). This is to simulate the initial conditions for the windage losses (Fig. 42A)
(4) as (3) with no brushes (Fig. 5.42B)
(5) as (2) but the armature (Fig. 5.40) has no equalizer (5.42B)
(6) with the shaft only (no armature)(Fig. 5.42C)
(7) as (6) with no magnet poles (Fig. 5.42C)

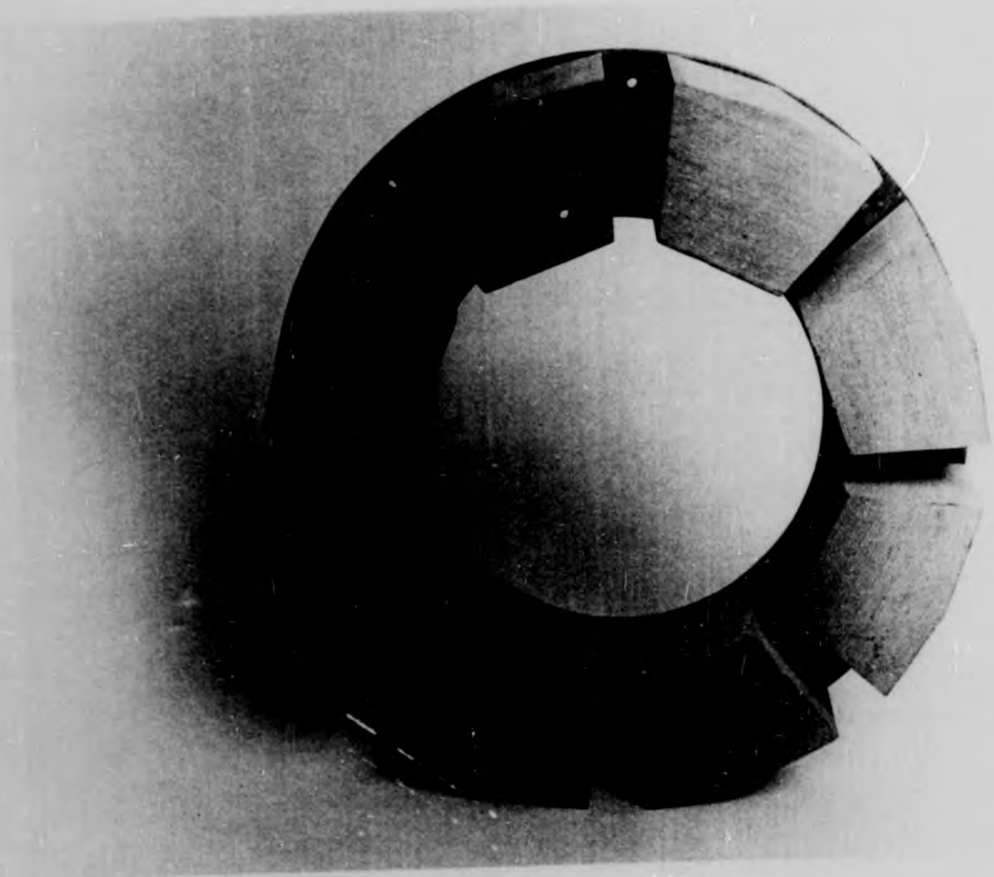

Fig. 5.30 - Dummy poles (wooden)

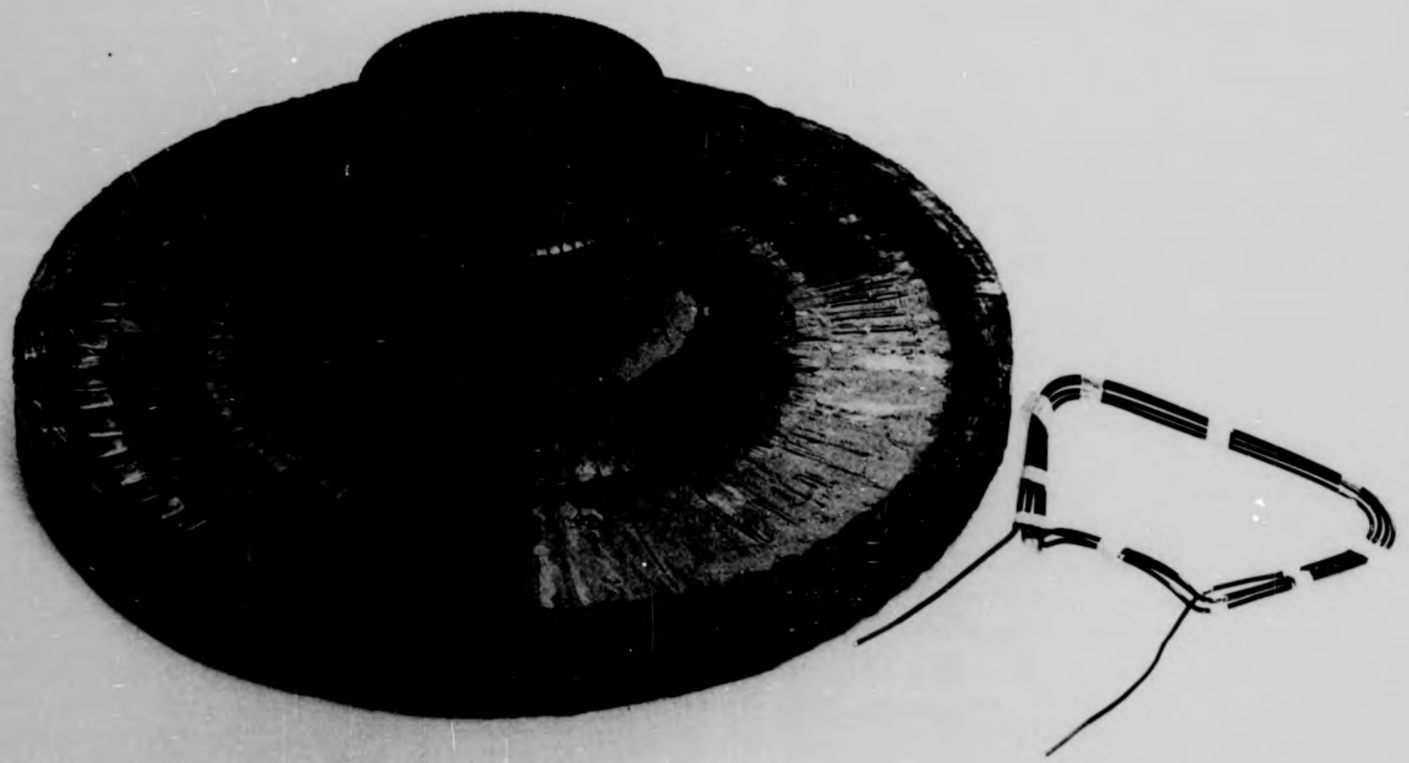

Fig. 5.40 : Skeleton armature with no equalizer connections

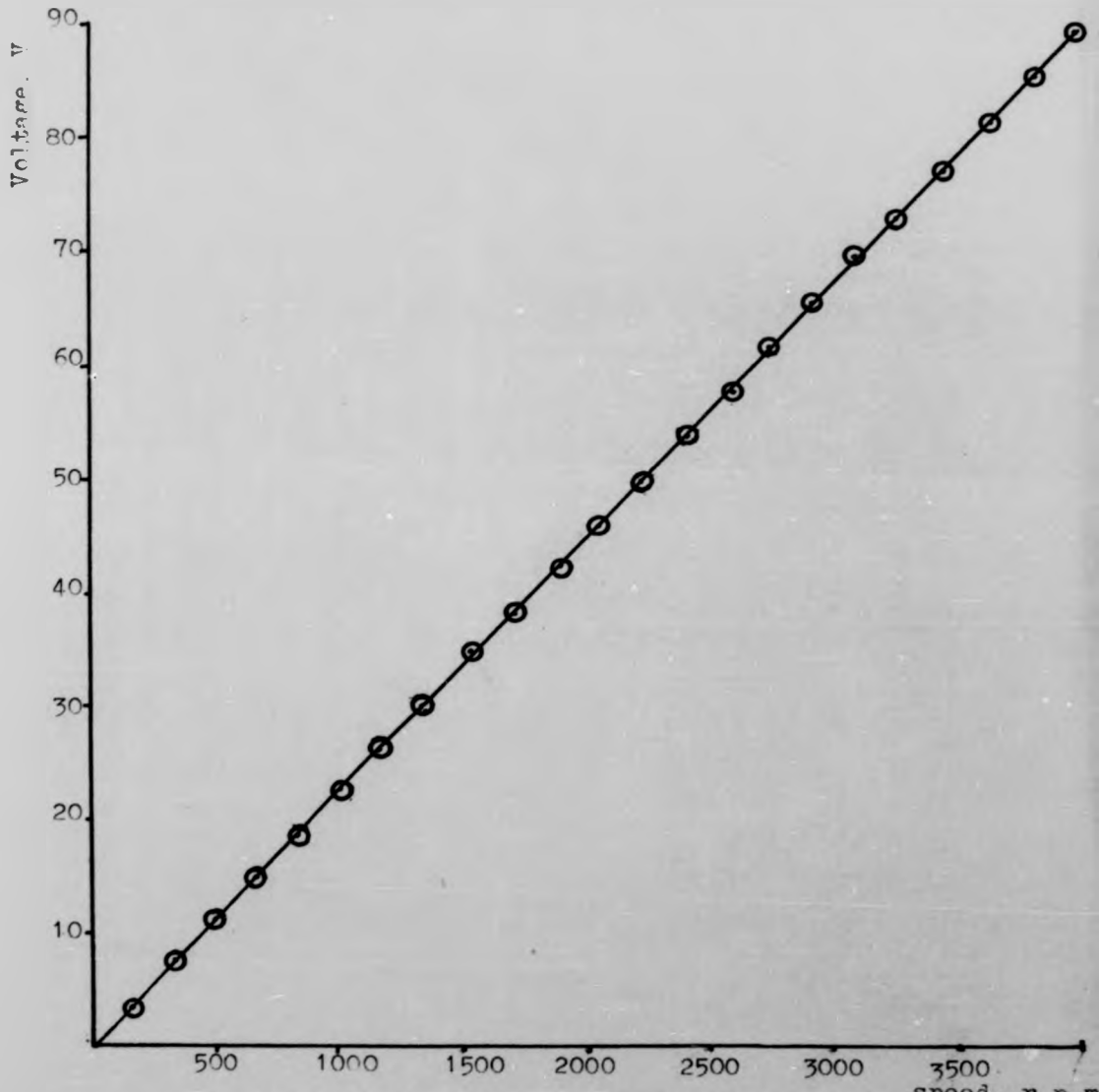

Fig. 5.41 : Open circuit voltage/speed curve of 10kW disc machine run as a generator

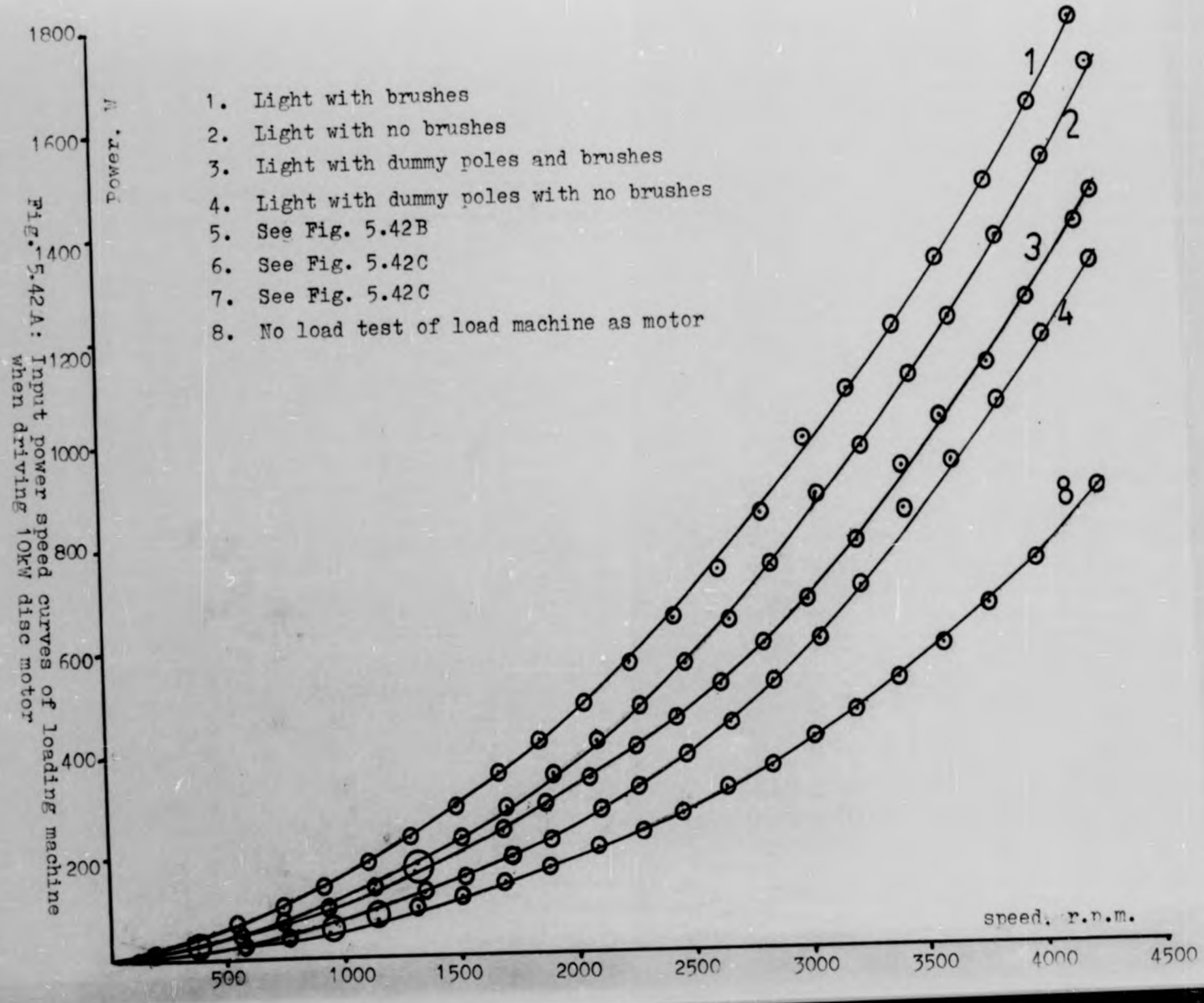

Fig. 5.42A: Input power speed curves of loading machine when driving 10kW disc motor

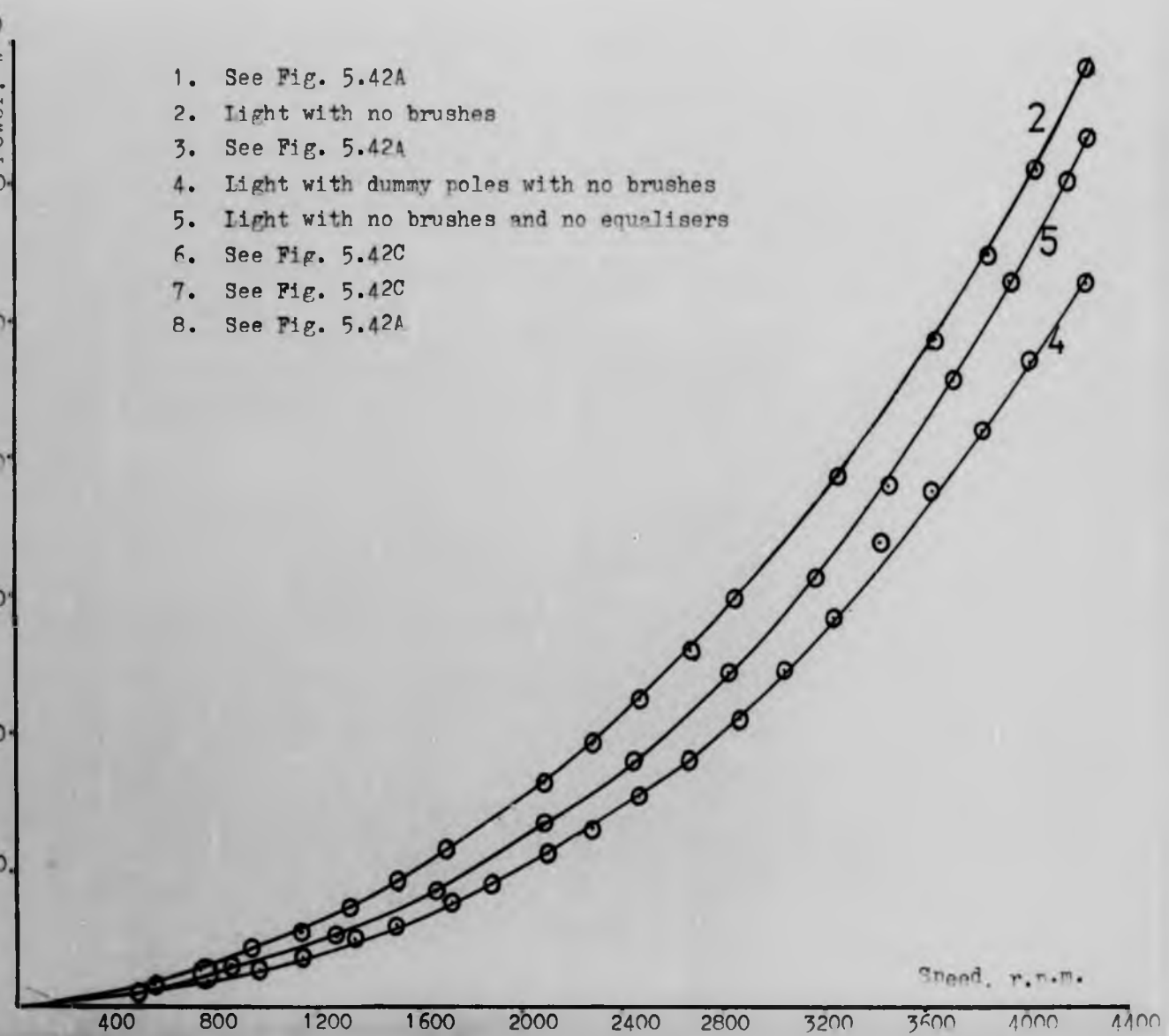

Fig. 5.42B: Input power speed curves of loading machine when driving 10kW disc motor

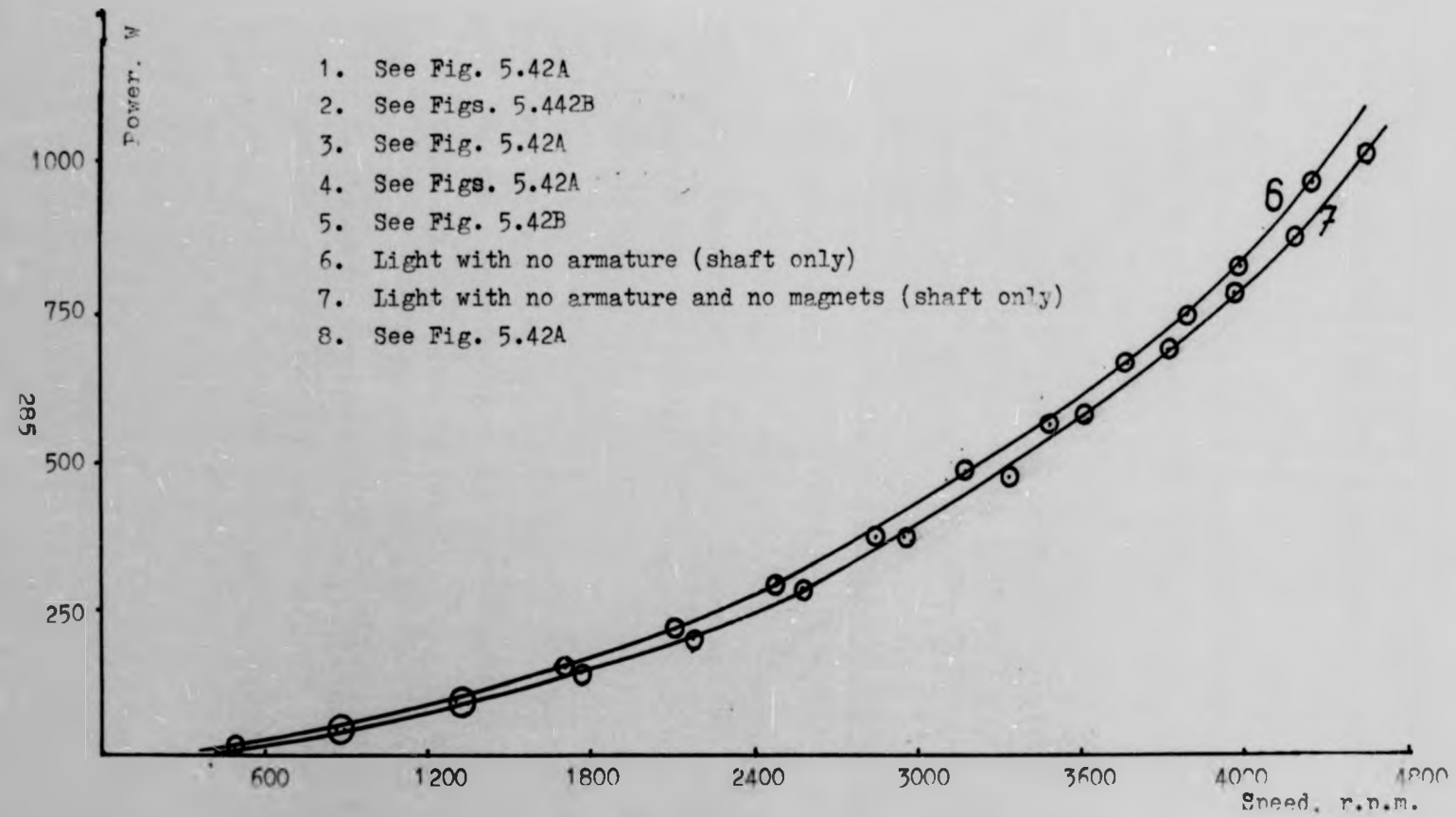

Fig. 5.42C: Input power speed curves of loading machine when driving 10kW disc motor

After that the load machine (driving motor) is run light and its armature resistance was measured while hot. The tests were enough to separate most of the loss elements.

(A) the difference between (1) and (2) represents the brush friction losses and the brush share of losses of inaccurate coil positions.

(B) the difference between (3) and (4) represents the brush friction losses only.

(C) the difference between (4) and no load test of loading machine (as motor) represents the windage and bearing friction losses.

(D) the difference between (6) and (7) represents the losses due to the sum of the magnetic leakage flux of the permanent magnet poles through the rotating shaft.

(E) the difference between (5) and (4) represents the losses due to eddy currents in the copper winding plus the losses due to (D).

(F) the difference between (E) and (D) represents the losses due to eddy currents in

the armature winding only.

(G) the difference between (2) and (5) represents the losses due to the equalizers.

The results of the no-load test with the spaces between permanent magnet poles filled with wedges shows that (C) losses can be minimized by using a full ring construction instead of the current toothed construction of the magnetic pole rings. The wedges may be made of a cheap plastic or aluminium, however, any light non-magnetic material will serve the purpose.

As mentioned in Section (D) losses can be reduced or eliminated by reconstructing the shaft in a non-magnetic material such as EN 58 J non-magnetic stainless steel.

As explained in (F), losses can be reduced by using multiples of elementary thin wires connected in parallel instead of a single solid wire used in current armatures. The

machine finished winding will improve the physical construction over the hand-finished winding used in the current prototype machines and this, in turn, will minimise the (G) losses. These latter losses may be further reduced by better control on magnet-flux return ring joints, magnet lengths and air-gap lengths adjacent to each magnet pole in order to get balanced flux per pole. In addition, the unhomogeneous reluctance of the different parts of the steel ring which may lead to unhomogeneous air-gap flux, can be relaxed by thickening the ring slightly by a small amount.

For the same matter, magnet poles belonging to the same batch are used to assemble each set of magnet rings. This is necessary in order to minimise the effect of different magnet characteristics resulting from different magnet batches.

Chapter 6 The Converted Hybrid Vehicle

The objectives of this chapter are to investigate and evaluate the technical performance of the twin armature disc motor and its associated traction system in the existing Nova hybrid vehicle. Prior to the investigation of the Nova hybrid car, there follows a brief description of electric and hybrid vehicle systems with relevant theoretical background and energy considerations. This background material is presented as an aid to understanding and evaluating the system used in the Nova hybrid car as compared to other electric and hybrid vehicle systems.

6.1 Description of Electric and Hybrid Vehicle Systems

6.1.1 Electric Vehicles

Electric vehicles are powered by an electric motor drawing current from rechargeable storage batteries, fuel cells or other portable sources of electrical current.

Thus, electric vehicles, in general, are powered by batteries and are driven by electric

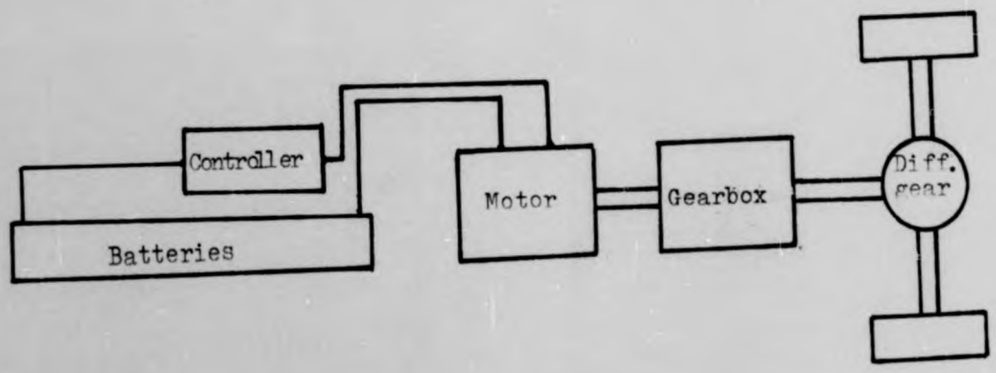

Fig. 6.1 : Drive system of the electric car

motors. Their propulsion systems normally consist of a battery, motor speed controller, motor, an interface between the motor and wheels (a transmission and/or differential), other appropriate controls, and a battery charger. A schematic diagram of the drive system for such an electric vehicle is shown in Figure 6.1. The battery charger may or may not be located aboard the vehicle.

6.1.2 Hybrid Vehicles

Hybrid vehicles are propelled by a combination of an electric motor and an internal combustion engine. Although other types of hybrid vehicles have been built (such as heat engine-flywheel systems), this thesis is limited to a discussion of hybrid vehicles using a heat engine and a battery.

6.1.2.1 Types of Hybrid Vehicle

All heat engine-battery hybrid vehicles may be grouped into two general classes, series and parallel. In the series system (Figure 6.2) all of the net power output

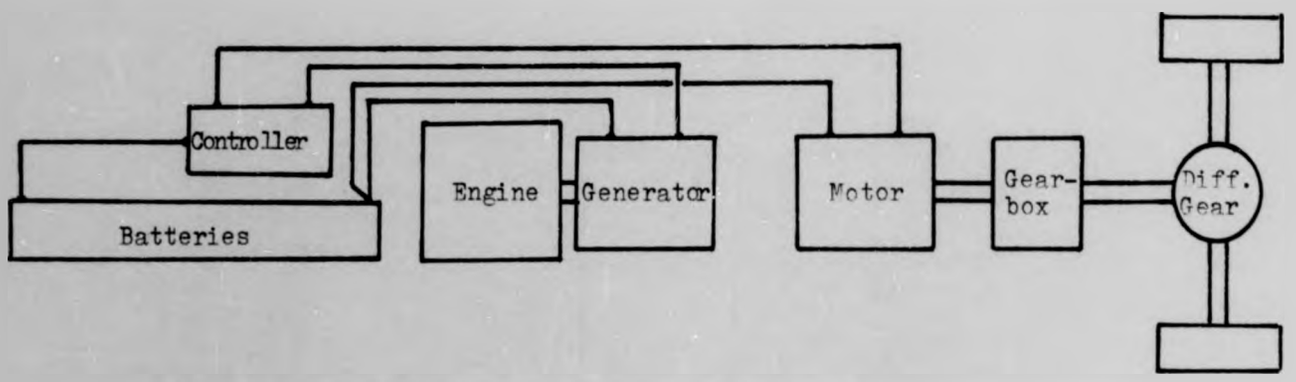

Fig. 6.2 : Drive system of the series hybrid car

of the heat engine is converted into electric power by a DC generator or by an alternator-rectifier. The electric power is reconverted to mechanical power by an electric motor connected to the drive wheels, either directly or through a gear reduction system. Vehicle speed is controlled as in an electric vehicle. Whenever the power requirement of the vehicle is greater than the power supplied by the engine-generator set, the additional power needed is drawn from the batteries. When the engine-generator set power output is greater than the vehicle's requirements, the excess power is used to charge the batteries. The engine may operate essentially at constant speed and load for optimum fuel economy. The motor can also be driven by the wheels to provide regenerative braking.

In the parallel system, only the power required to charge the batteries is converted to electric power. The majority of the engine power is delivered through a mechanical transmission directly to the wheels. A typical example of a parallel hybrid drive system is shown in Figure 6.3. In this example, the heat engine is mounted on the

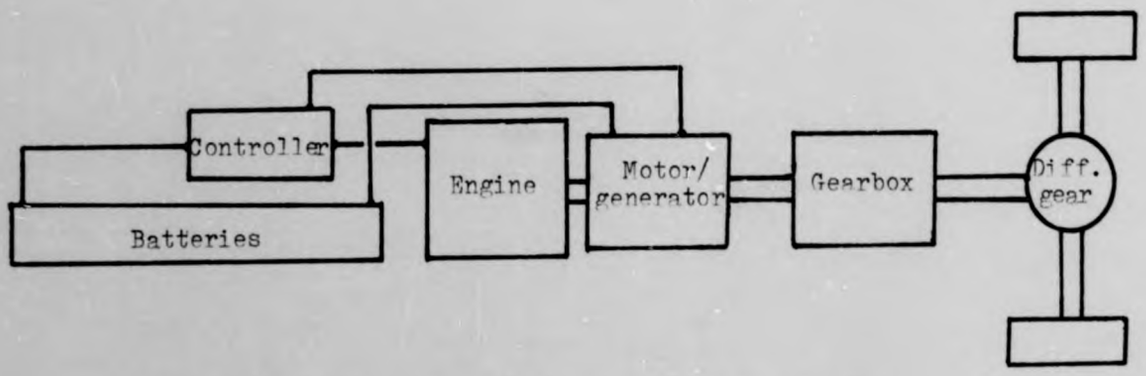

Fig. 6.3 : Drive system of the parallel hybrid car

same shaft as the electric motor. In some hybrids, a clutch is provided to disconnect the heat engine from the drive system, while in others, the heat engine is connected directly to the transmission so that the motor and engine are in parallel. In all cases, the motor torque and engine torque are additive so that the motor is smaller than required in a series system. When the vehicle drive power requirements exceed the engine capacity, the extra power is provided by the battery through the electric motor. In most parallel systems, the motor also serves as a generator for charging the batteries. The motor, as a generator, is not always driven by the heat engine, but it also can be driven by the wheels to provide regenerative or electrical braking.

6.1.2.2 Operating Modes

The mission prescribes the operating mode of a hybrid vehicle and therefore, to a large extent, the overall design of the vehicle. If the vehicle is driven primarily in the city, for short distances, it may operate as an

all-electric vehicle with the batteries being recharged externally. For longer trips, a mode that primarily uses the heat engine may be employed. All the operating modes may be grouped into two general classes which are described next.

The simplest mode involves continuous operation of the heat engine at, or near, maximum power and efficiency. The heat engine provides the power needed for cruising at high speed. The additional power required for acceleration is supplied by the electric motor. Any excess power available from the heat engine is used to charge the batteries. Usually the system is designed to operate so that the batteries are not depleted.

The other mode of operation is the on-off mode. Here the heat engine operates only when the vehicle is running at high speed or when the battery is depleted. The battery powered electric motor provides the vehicle power at lower speeds and augments the heat engine during acceleration. Battery depletion may occur in many on-off operating modes so the range can be limited by battery

capacity. Petroleum fuel consumption can be lowered with this operating mode as more of the propulsion energy is provided from electricity, as recharge is from an extra (non petroleum) electric source. The all-electric operation at low speeds also helps to reduce emmissions.

6.1.2.3 Hybrid Vehicle Components

With the exception of a heat engine (alone or with a generator or alternator), a hybrid vehicle uses the same types of components as an all-electric vehicle. The electric-mechanical drive in a series hybrid vehicle is identical to the drive in an all-electric vehicle. The heat engine-generator (or heat engine-alternator) and its control are usually added as a completely separate unit. The electric drive in a parallel hybrid vehicle also can be the same as an all-electric vehicle. The transmission, however, must accept power inputs from both the heat engine and the electric motor, and the control system must control two power sources in parallel. Therefore a parallel hybrid drive system requires variable-speed transmission to

match the heat engine to the load requirements of the vehicle (i.e. conventional automatic transmissions, conventional manual 3- and 4-speed transmission, etc).

In general, the transmissions are adaptable to hybrid vehicles with modifications for the second input drive. Transmissions designed specifically for a parallel hybrid system are not available.

Control of the electric motor for either a series or parallel hybrid drive train is the same as that for an electric vehicle drive motor. The overall control system of a parallel hybrid vehicle is even more complex than that of an electric vehicle or series hybrid. However, they all have the same principles, except that in the paralled hybrid vehicle, the motor power and power for battery charging must be controlled simultaneously.

6.1.2.4 Heat Engines for Hybrid Vehicles

The operation of a heat engine for a hybrid vehicle differs from a conventional

engine in that the hybrid heat engine does not have to change speed rapidly and it runs for longer times at high power. The ideal hybrid heat engine should be as lightweight and durable as possible. The optimum capacity of engine is slightly above the average power required to drive the vehicle; the battery system provides the additional power necessary for acceleration, overtaking and hill climbing. The hybrid vehicle can provide substantial gains in fuel economy because the engine is sized for cruise requirements and is operated at near peak efficiency.

Conventional vehicle engines are not ideal for the conditions just given. They are designed to give long life at an average power level of 20 percent of their maximum power capability, which is below peak efficiency.

Emission control can be simplified in the hybrid engine operated at constant power level. The on-off mode of operation, on the other hand, can use emission control techniques that have been developed to meet emission standards for the conventional car.

6.2 Road Power, Range and Energy Considerations

For any vehicle, power required at road wheels for cruising at a steady speed on a level road is given by:

$$P_w = F_1 v + F_2 v \qquad 6.1$$

Where v is vehicle speed in m/sec. F_1 and F_2 are the tyre rolling resistance and aerodynamic drag respectively in N. But:

$$F_1 = C_1 M_v \qquad 6.2$$

and:

$$F_2 = C_2 v^2 \qquad 6.3$$

Where C_1 is tyre friction coefficient in N/kG and C_2 is the aerodynamic drag as shown by the following equation:

$$C_2 = 0.5 \rho C_D A \qquad 6.4$$

Where ρ is the atmospheric density in kg/m^3.

C_D aerodynamic drag coefficient (dimensionless), A is the vehicle frontal area in m^2 and M_v is the vehicle mass in kg.

Therefore, substituting from Equations 6.2 and 6.3 in Equation 6.1 leads to the following equation:

$$P_w = v(C_1 M_v + C_2 v^2) \qquad 6.5$$

Equation 6.5 shows that road power is the power used to overcome tyre rolling resistance and aerodynamic drag, i.e. the power needed to actually propel the vehicle, and this should be as large as possible in comparison with the other components of power. This means that most of the input power is transferred to the road wheels of the vehicle and is not being dissipated in the drive components.

The electric vehicle range at constant speed and level road is given by:[37]

$$R = 3.6\, v \left[\frac{C\, M_B\, \eta_D}{v(C_1 M_v + C_2 v^2)}\right]^{-\frac{1}{b}} \qquad 6.6$$

Where C is the specific battery energy density for 1-hour discharge in Wh/kg, M_B battery mass in kG, η_C is the drive system efficiency which includes the transmission, motor and controller efficiency, 3.6 is a conversion factor and b coefficient relating average battery specific power to discharge time which has a representative value of - 0713; therefore, $\frac{1}{b} = 1.4$.

Equation 6.6 may then be written as:

$$R = 3.6v \left[\frac{C\ M_B\ \eta_D}{v\ (C_1\ M_v + C_2\ v^2)} \right]^{1.4} \qquad 6.7$$

The energy consumption at constant speed is equivalent to the power required at the wheels to drive the vehicle at speed V, divided by the vehicle's overall efficiency from the wall plug to the wheels. Therefore, the energy consumption (kWh/km) at constant speed may be expressed as:

$$\text{Energy consumption} = \frac{1}{3600} \left(\frac{P_w}{\eta_B\ \eta_C\ \eta_D} \right) \qquad 6.8$$

Where P_w is the power required at the road wheels. η_B is the battery efficiency and η_C the charger efficiency.

Substituting P_w from Equation 6.1 Equation 6.8 becomes:

$$\text{Energy consumption} = \frac{1}{3600}\left[\frac{v\,(C_1 M_v + C_2 v^2)}{\eta_B\,\eta_C\,\eta_D}\right] \qquad 6.9$$

Where $\frac{1}{3600}$ is a conversion factor.

Equation 6.7 may be used to calculate the range of an electric vehicle (or the hybrid vehicle in all electric mode), when cruising on a level road under battery power alone.

Equation 6.5 and 6.9 may be used to calculate the engine output of a hybrid vehicle for cruising on level road with battery floating.

$$\text{Engine output (kW)} = \frac{P_w}{\eta_D\,\eta_G} \qquad 6.10$$

Where η_G is the generator efficiency.

6.3 The Sports Car, the Dragonfly Nova

Having built a viable twin-armature DC disc motor, and in order to establish its feasibility as a traction motor, it became clear that the next stage would be to re-build a practical road vehicle. Like many of the earlier conversion projects, the new vehicle is based on a conventional mass produced car. In this case a Nova sports car was chosen.

The Nova car itself is supplied in kit form only, using a strong fibreglass body mounted on the well-proven Volkswagon Beetle floor pan and chassis as shown in Figure 6.4 [33,34] It is usually powered by a Porsche or Autocavan 2.2 litre engine.

The Dragonfly Nova shown in Figure 6.5 uses the basic kit with the necessary modifications for conversion to a hybrid. Special rear stub axles have been assembled for the converted Nova, allowing mechanically independent driving from two individual running shafts. The vehicle is fitted with front disc brakes and sports suspension

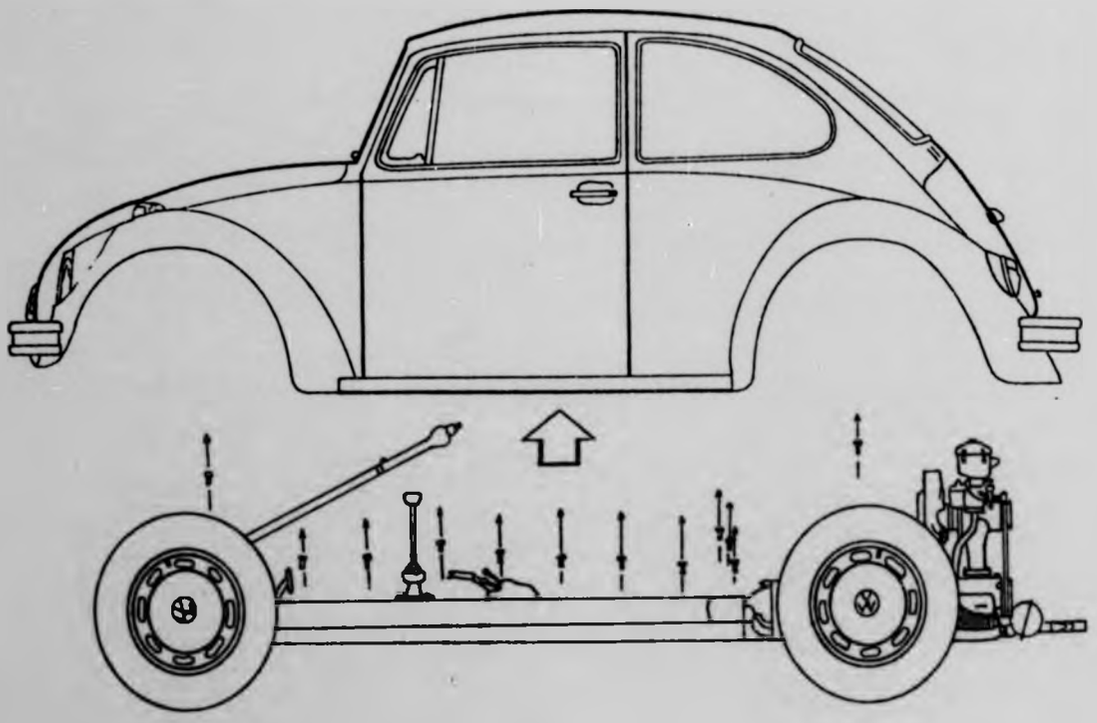

Fig. 6.4 (a) : Volkswagon Beetle floor pan and chassis

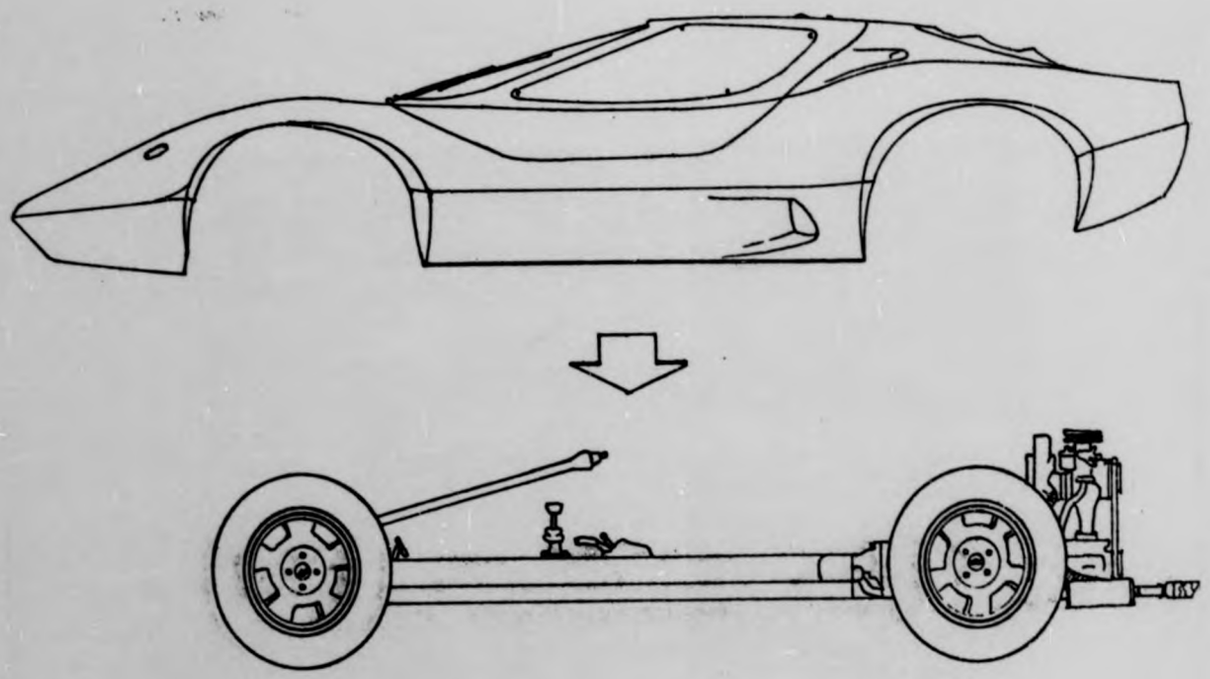

Fig. 6.4 (b) : Nova fibreglass body

Fig. 6.5 : The Dragonfly Nova

units. The weight distribution is improved to achieve a front-rear loading of 40% - 60% respectively, and the centre of gravity is lowered by about five inches as shown in Figure 6.6. The twin-armature disc motor fitted in the Dragonfly Nova is rated at 96V, 20kW, 4000r.p.m. and weighs 60 kg (see Chapter 5). The motor has two mechanically independent output shafts. Each shaft drives a rear wheel through a 4:1 reduction-gear using a toothed-belt (as shown in Figure 6.7) thereby eliminating the need for a mechanical differential gear. Significant savings in weight and cost result from adopting the twin-armature arrangement rather than two separate motors. The vehicle is supplied with eight Tungston type 369 12V 13 plate starting, lighting and ignition batteries. Each has a capacity of 68Ah at the 20-hour rate and weighs a total of 110kg. A schematic diagram of the vehicle drive is shown in Figure 6.8.

The most significant aspect of this converted Dragonfly Nova, is that it carries an

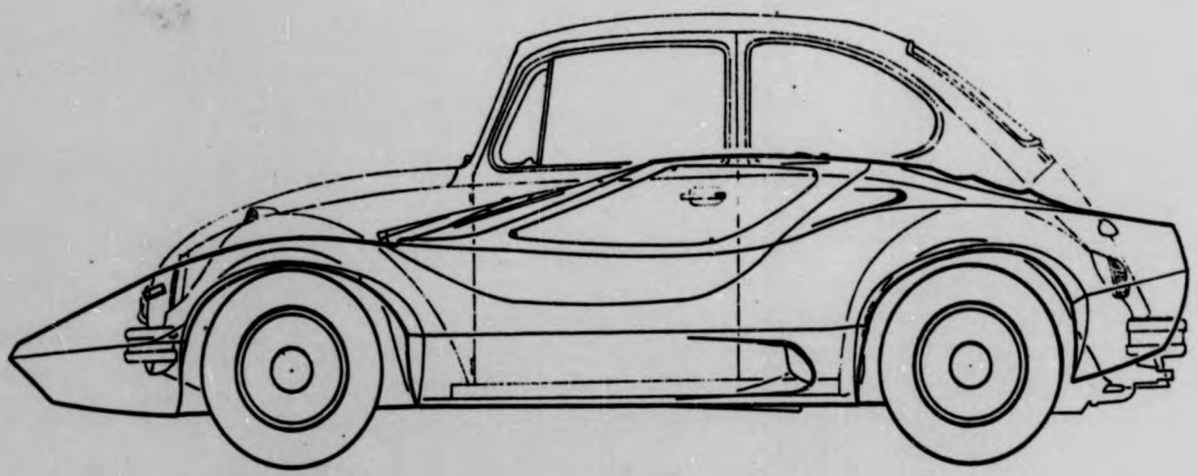

Fig. 6.6 : Weight distribution and centre of gravity improvement

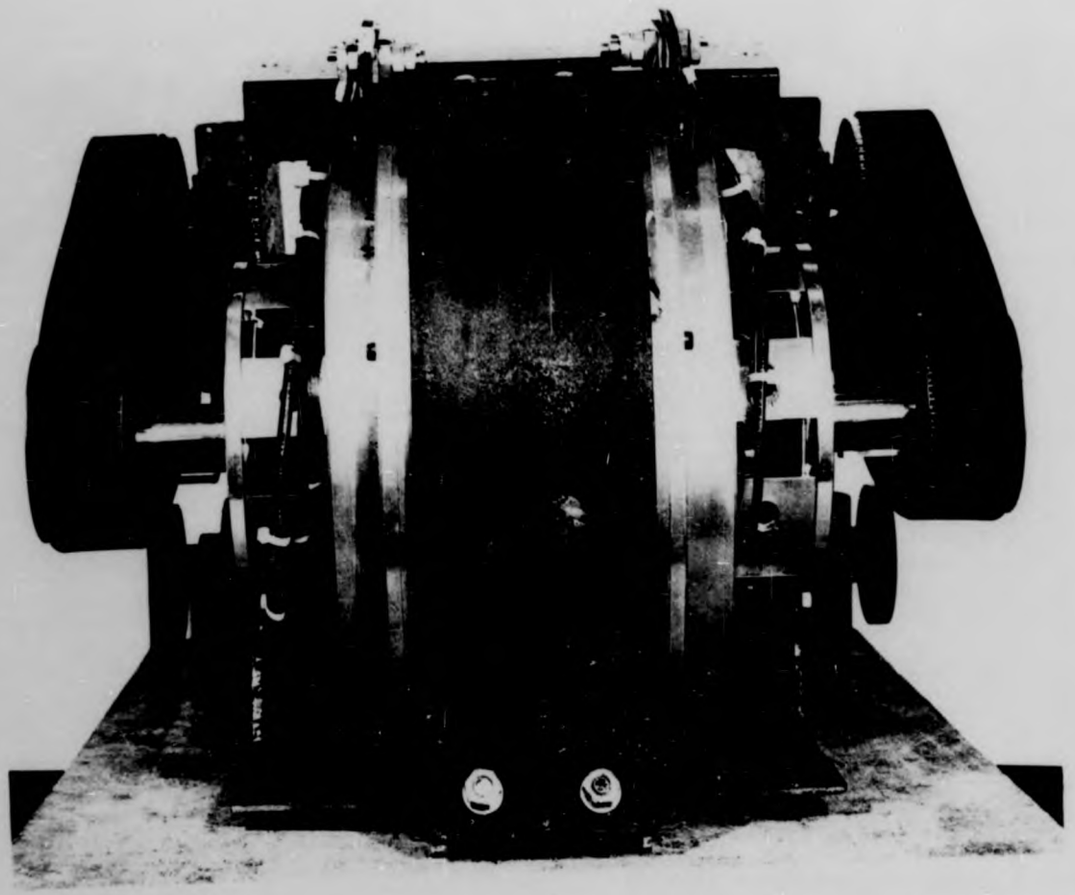

Fig. 6.7 (a) : The twin rotor disc motor and its associated belt reduction gears (front view)

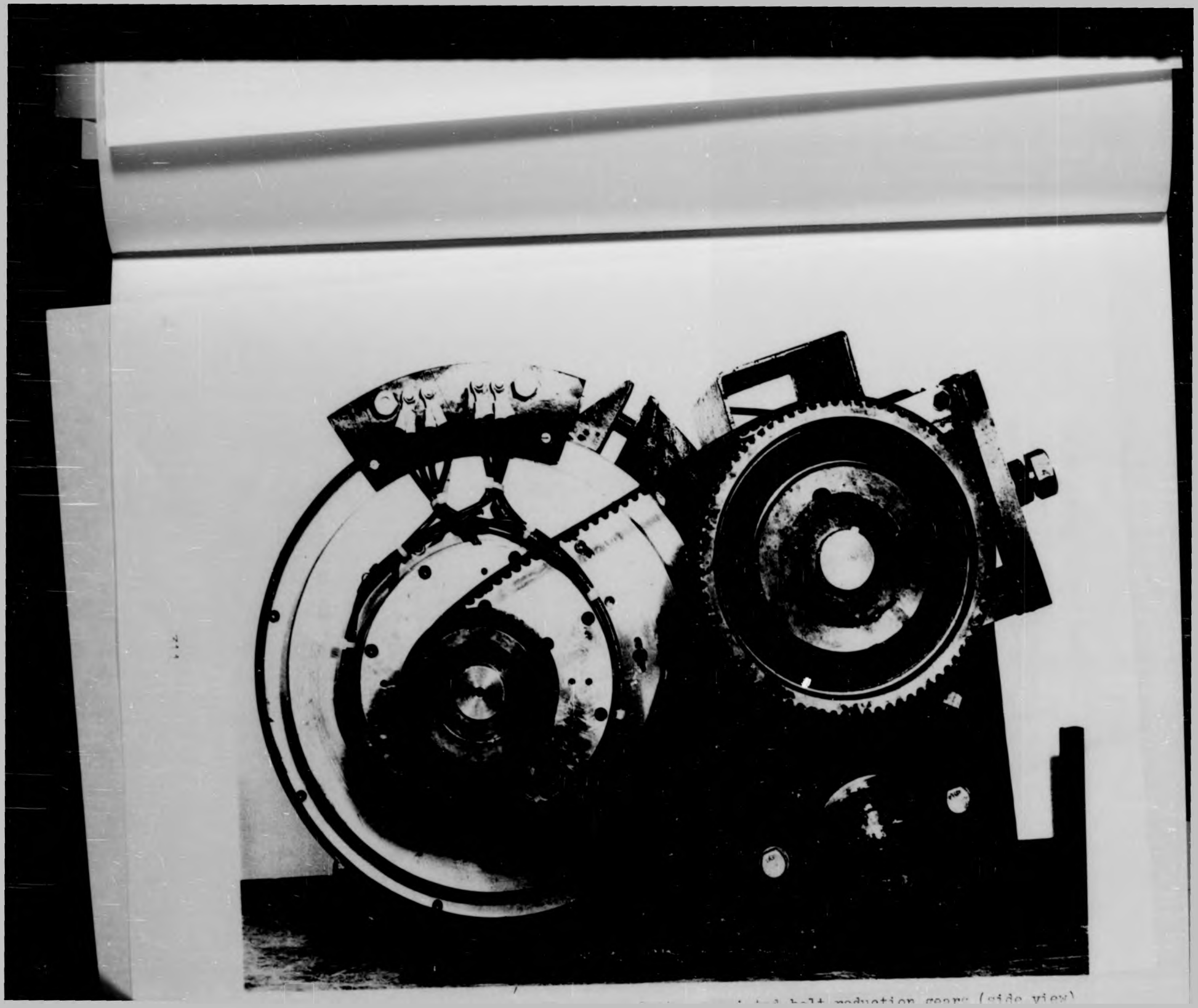

...belt reduction gears (side view)

engine-generator set to provide mean running power while the batteries are limited to providing short duration peak power. The batteries also act as a store for regenerated power or surplus generated power. This modifies the purely electric car concept to that of a series hybrid. It has been found both experimentally and through computer simulation, that the exhaust emissions and energy efficiency of a series hybrid vehicle, using a diesel engine and lead-acid storage batteries, are much better than had been previously expected. The primary reason for this seems to be the capability, with the series hybrid arrangement, of maintaining the engine operation at a very favourable brake specific fuel consumption level. With either the conventional mechanical drive system or the parallel hybrid arrangement, it is extremely difficult to obtain a constant speed and load.

The lead acid battery is at a 250:1 energy to weight disadvantage against petrol. The fuel cell has considerable potential in

Fig. 6.7 (b) : The twin rotor disc motor and its associated belt reduction gears (side view)

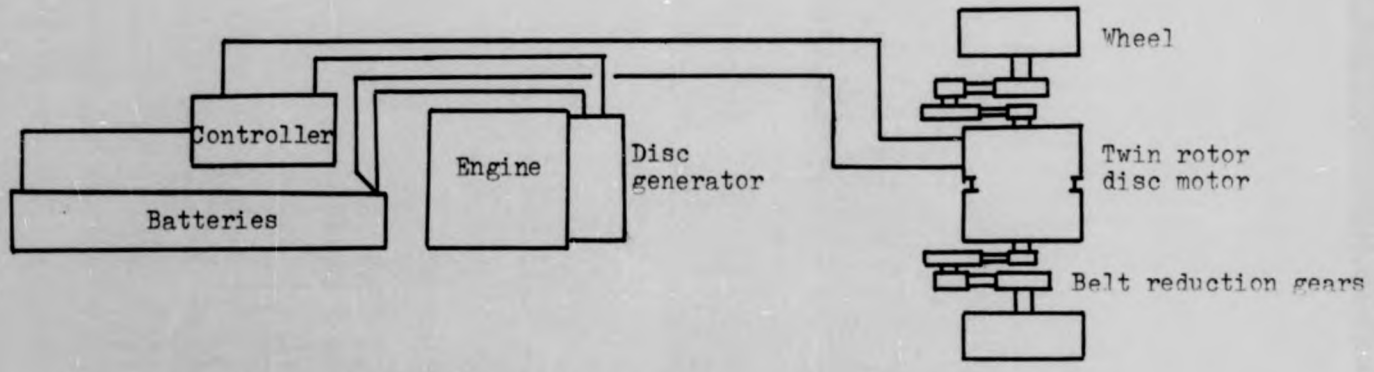

Fig. 6.8 : Drive system of the Dragonfly-Nova hybrid car

an electric vehicle application. The great fascination of the fuel cell, is that it converts chemical energy into electrical energy with relatively high efficiency. Until this is commercially and technically viable, the alternative is to use a mechanical engine-generator set to generate the electricity. Unfortunately such an engine would be noisy and have the usual disadvantages of a mechanical system. On the other hand, there are several advantages. A major one is that such an engine generator set, suitably matched to a vehicle's average power with its fuel, would have a 12:1 range advantage over the equivalent weight of batteries.

The most suitable series hybrid application is in frequent stop/start driving such as city driving or the duty cycle of delivery vehicles. For this application, it is possible to envisage small engine units of only 250cc. The Dragonfly Novas presented the worst case application since these cars are intended for long distance running at reasonably high average speeds. After a considerable study

of available engines, it was decided to use a Petter AC2 Twin Cylinder diesel unit. This 608cc engine has a continuous maximum output of 8.2kW at 3000 r.p.m. and a one-hour rating of 9.0kW at this speed. The engine capacity is calculated by Equation 6.10. This would be directly coupled to a disc generator of almost identical design to the drive motor and which could be used to start the diesel engine from the 96V battery pack. The windings had to be altered for the lower rated speed (see Table 6.1). The combined engine generator unit (Figure 6.9) weighs 120kg, of which the diesel engine weighs 79kg.

The power circuit in Figure 6.10 is simple, with the added advantage of allowing regenerative power. Besides using the infinitely variable rotating drum controller, it is possible to switch to series or parallel motor drive. This enables selection of town or country driving respectively.

The control circuit in Figure 6.11 is very basic and to design a more sophisticated system, which could optimise the

DISC-ARMATURE MOTOF DESIGN

DESIGN NO: 242

DESIGN SPECIFICATION

OUTPUT: 8000. WATTS
VOLTS: 140. V
SPEED: 3000. RPM

DESIGN DATA

D2: 305. MM
D1: 176. MM
POLES: 8.

MAGNETIC CIRCUIT DATA

BW 0.330 TESLA
HM 35000. A/M
LCOEFF 1.30
LEAGI 1.20
PHI .001160 WEBERS
ALPHA .75
LMAG 63.2 MM
WGTMAG 14.28 KG
THICK 6.69 MM
WGTFRR 4.04 KG
GAP 12.00 MM
MAGDSY 4700. KG/M**3
BWS 1.80 TESLA

ELECTRIC CIRCUIT DATA

PATHS 4.
COILS 11.
TURNS 8.
Z 2136.
GAUGE 1.60 MM
WGTWIN 4.02 KG
CRTDSY 8.0 A/MM**2
AMNCRT 64.34 AMPS
LOSS 702.55 WATTS
LAY 4
TEMP 75. DEGREES
SF .85
RARM 0.146 OHMS
ER 129.08 VOLTS

Table 6.1 : Design parameter of 8kW disc generator

OUTPUT DATA -316-

WGTNAP 15.53 KG
TOTWGT 38.76 KG
MECHLO 245. WATTS
SPEED 2939.3 FPM
POWER 8034.2 WATTS
TORQUE 26.10 NM
PWRWGT 207.26 WATTS/KG
EFF .892

PERFORMANCE SPECIFICATIONS

CURRENT DENSITY AMP/MM**2	ARMATURE CURRENT AMPS	SPEED RPM	POWER WATTS	TORQUE NM	EFFICIENCY
1.	8.04	3126.9	810.8	2.48	.720
2.	16.08	3100.1	1859.6	5.85	.844
3.	24.13	3073.3	2969.6	9.23	.879
4.	32.17	3046.5	4020.2	12.60	.893
5.	40.21	3019.7	5052.1	15.98	.897
6.	48.25	2992.9	6065.1	19.35	.898
7.	56.30	2966.1	7059.1	22.73	.896
8.	64.34	2939.3	8034.2	26.10	.892
9.	72.38	2912.4	8990.3	29.48	.887
10.	80.42	2885.6	9927.5	32.85	.882
11.	88.47	2858.8	10845.7	36.23	.876
12.	96.51	2832.0	11745.0	39.60	.869
13.	104.55	2805.2	12625.3	42.98	.863
14.	112.59	2778.4	13486.7	46.35	.856
15.	120.64	2751.6	14329.1	49.73	.848
16.	128.68	2724.8	15152.6	53.10	.841

Table 6.1 (continued) : Design parameter of 8kW disc motor

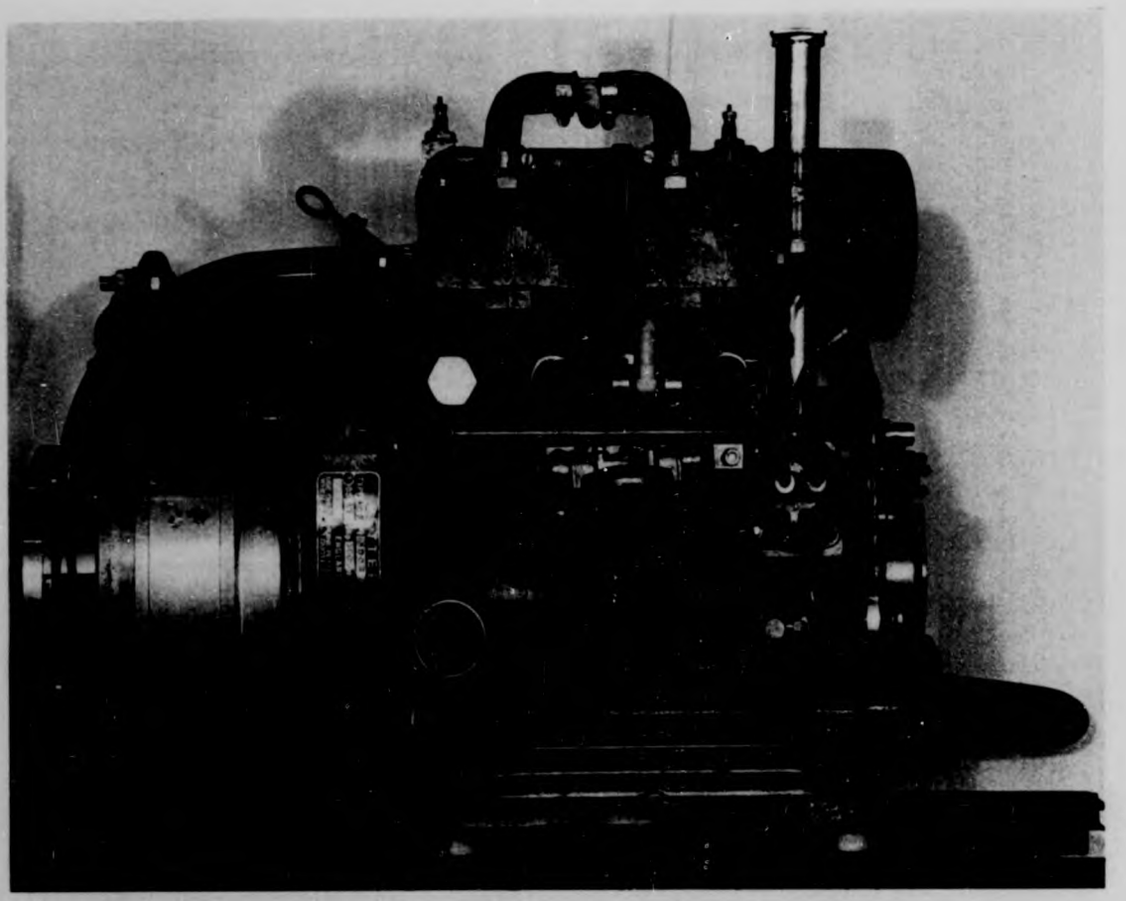

Fig. 6.9 : Diesel engine - disc generator

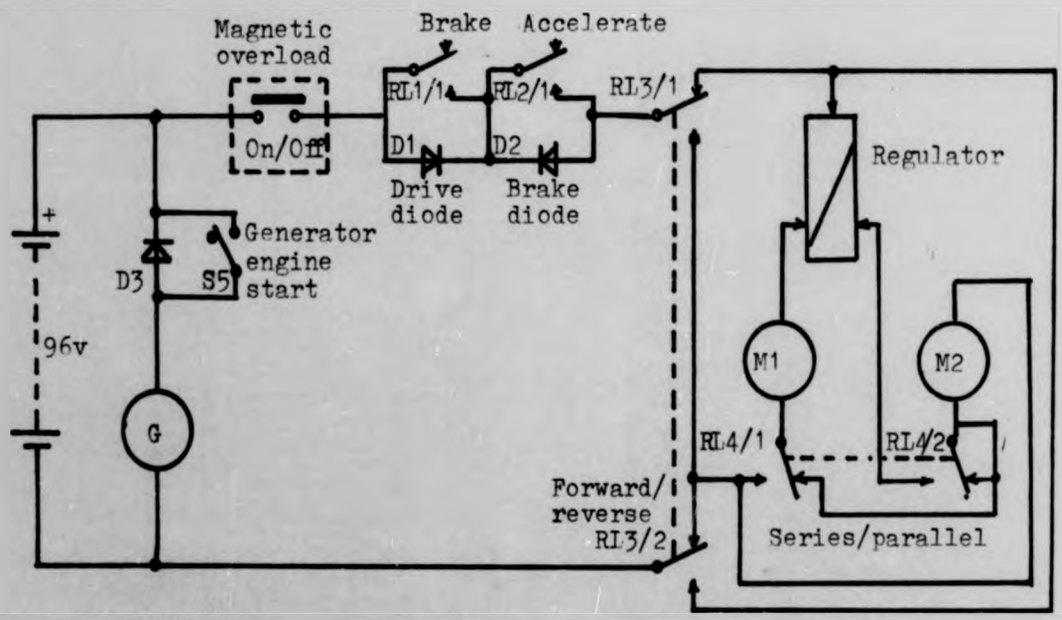

Fig. 6.10 : Power circuit - Nova car

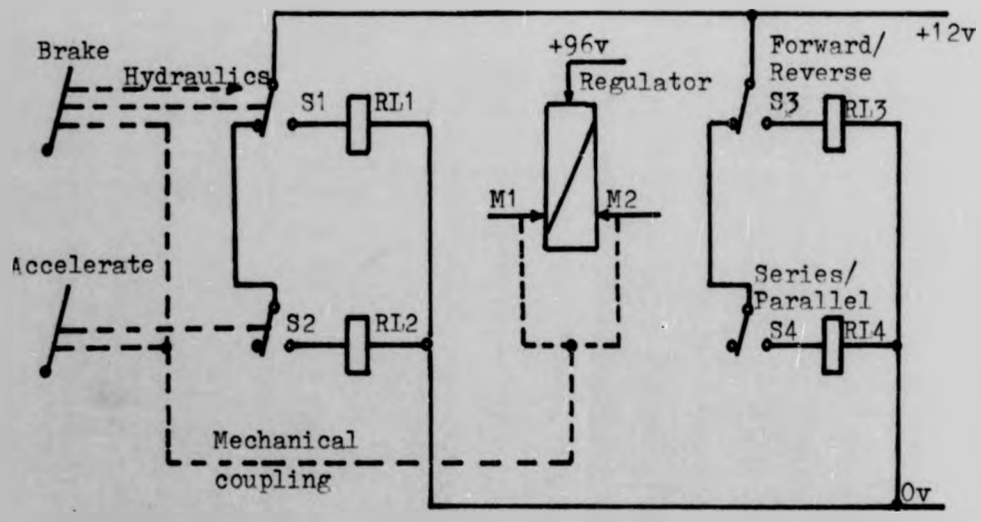

Fig. 6.11 : Control circuit - Nova car

loading of the engine, generator, batteries and motor, would require extensive testing until further data is obtained.

The instrumentation uses up-to-date digital circuitry such as a battery charge/discharge integrator. This provides the driver with a bar indicator display showing not only the battery state, but the continuous power charge/discharge difference by which to regulate his driving speed. It can also be used to indicate the levels at which the engine can be stopped or started in light, urban driving conditions.

The predicted performance of the Dragonfly Nova with regard to energy economy is calculated as follows. Allowing for generator losses, Table 6.2 shows that the resulting 7.5kW output would be sufficient to allow an average vehicle speed of 50 m.p.h. with zero battery discharge and a calculated fuel consumption of 76 m.p.g. Figure 6.12 shows the required power at road wheel against the speed of the Dragonfly hybrid. The curve is

TABLE 6.2

Power requirements for the Nova Car when cruising on level road under engine power alone, i.e. with battery floating

Assumptions:

1. $C_1 = 0.13$
2. $C_2 = 0.39$
3. Gearbox efficiency = 95%
4. Motor efficiency = 90%
5. Generator efficiency = 90%
6. Controller efficiency = 100%

	Cruise speed		
	40 mile/h	45 mile/h	50 mile/h
	64 km/h	72 km/h	80 km/h
Road wheel power (kW)	4.0	5.1	6.5
Motor output (kW)	4.2	5.4	6.8
Generator output (kW)	4.7	6.0	7.6
Engine output (kW)	5.2	6.6	8.5

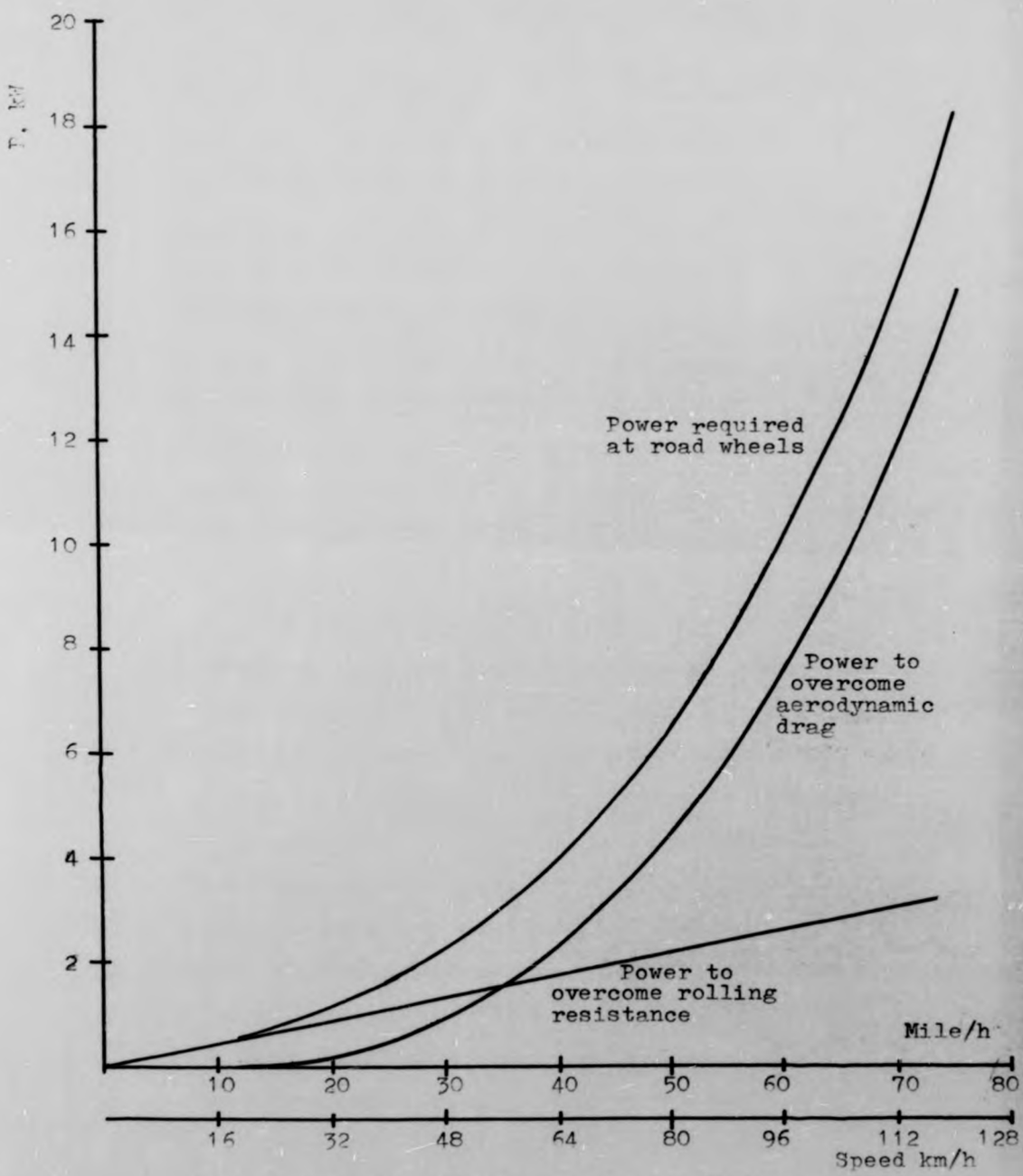

Fig. 6.12 : Required power at road wheel against speed of Dragonfly-Nova hybrid car

6.12

obtained using Equation 6.5 taking into consideration assumptions made in Table 6.2 A speed of 60 m.p.h. could be maintained continuously for about 51 miles with no increase in fuel consumption, but the batteries would be discharged. Urban driving at an average speed of 30 m.p.h. would demand light loading of the engine causing a decrease of efficiency. Nevertheless, fuel consumption could be improved by stop-start cycling of the diesel engine.

Thus the converted Dragonfly Nova seems attractive because it has the potential of reducing petroleum consumption and emissions below that of conventional vehicles with reasonable acceleration and cruising speeds. It also provides the driver with the option of running on its batteries only. In this mode, the Nova has a calculated range of about 20 miles at an average speed of 50 m.p.h. This enables it to be used as a commuter vehicle, which can charge its batteries overnight from mains power. The diesel engine is not directly coupled and can be removed easily for servicing, while the car is still

useable. Although not all garages are geared to deal with small diesel engines, the one installed is expected to give 2000 hours use before its first major service.

Much is talked about the problems of recharging battery-powered electric vehicles. Various ideas for a network of re-charging or exchange stations for batteries have been muted, such as coin-in-the-slot/token parking meters which could supply plug-in power, etc. All this demands an enormous capital outlay over a period of many years, and until this exists the purely battery-powered car is at a severe disadvantage against IC engined cars which already benefit from a world-wide servicing and fuelling network. A hybrid car, like the Nova, which is substantially diesel-electric rather than purely battery-electric, would benefit immediately from the existing infrastructure.

6.4 The Electric Bed Test

In order to investige the viability of the twin-armature disc motor and the feasibility of the drive system used in the Nova hybrid car, a new vehicle test rig was built. The

mechanical rolling test bed available in the Department had several shortcomings which the new vehicle test rig was able to overcome.

During testing, the mechanical rolling test bed provided an unstable load for the vehicle. This resulted from the continuously varying frictional losses between the vehicle tyres and the load (rollers) due to the rise in temperature of the rolling components. The increase in temperature limited the time for which a vehicle could be tested under a constant set of test conditions.

The rolling test bed is not suitable for testing different vehicles, unless its flywheel is changed to match different inertia. In addition, the power output of a vehicle being tested on the rolling test bed could not easily be measured.

All these problems were eliminated in the new test rig, enabling the performance of

electric and hybrid vehicles to be considered and investigated at constant speeds. The new test facility enabled testing of different vehicles without any mechanical changes to the test equipment. It was possible to simulate an upward or downward gradient and reproduce exact sets of test conditions to obtain enough data for any statistical analysis. The new test rig system has the facility of feeding the vehicle output energy into the mains rather than wasting it as heat. This advanced facility provided by the new system is based on the concept of replacing the mechanical (rolling resistance)load by a more accurately measureable electrical load. This is accomplished by replacing the vehicle driving wheels by an electric machine which is used to provide the vehicle load. Figure 6.14 shows the two machines mounted on a steel structure base which is bolted to the floor of the vehicle laboratory. The load machine has the facility to move forward and backward on slotted rails to allow different spans for different vehicles. A propeller shaft (shown

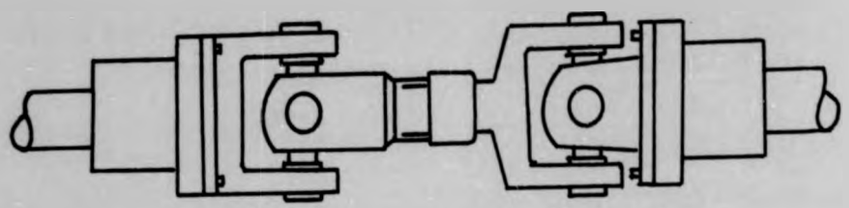

Fig. 6.13 : Propeller shaft

in Figure 6.13 is used to couple the vehicle to the load machine. This has joints to allow for mis-alignment and a telescopic extension for fine adjustments for a tight fitting connection. Special couplings are attached to each end of the propeller shaft to connect the shaft to the vehicle and load machine, as shown in Figure

The diagrammatical layout of the test rig is shown if Figure 6.14. This Figure also shows that the electrical output power of the load machine feeds a third DC machine which, in turn, drives an induction machine above a synchronous speed so that it acts as a generator feeding the vehicle output power into the three phase mains. Some vehicle loading systems use a solid state controller to feed the vehicle output into the mains, rather than use an extra DC machine and induction machine set. The advantage of using the extra machine is that the load current can be controlled by controlling the field current of this additional machine rather than the full armature current of the load machine. This system allows the

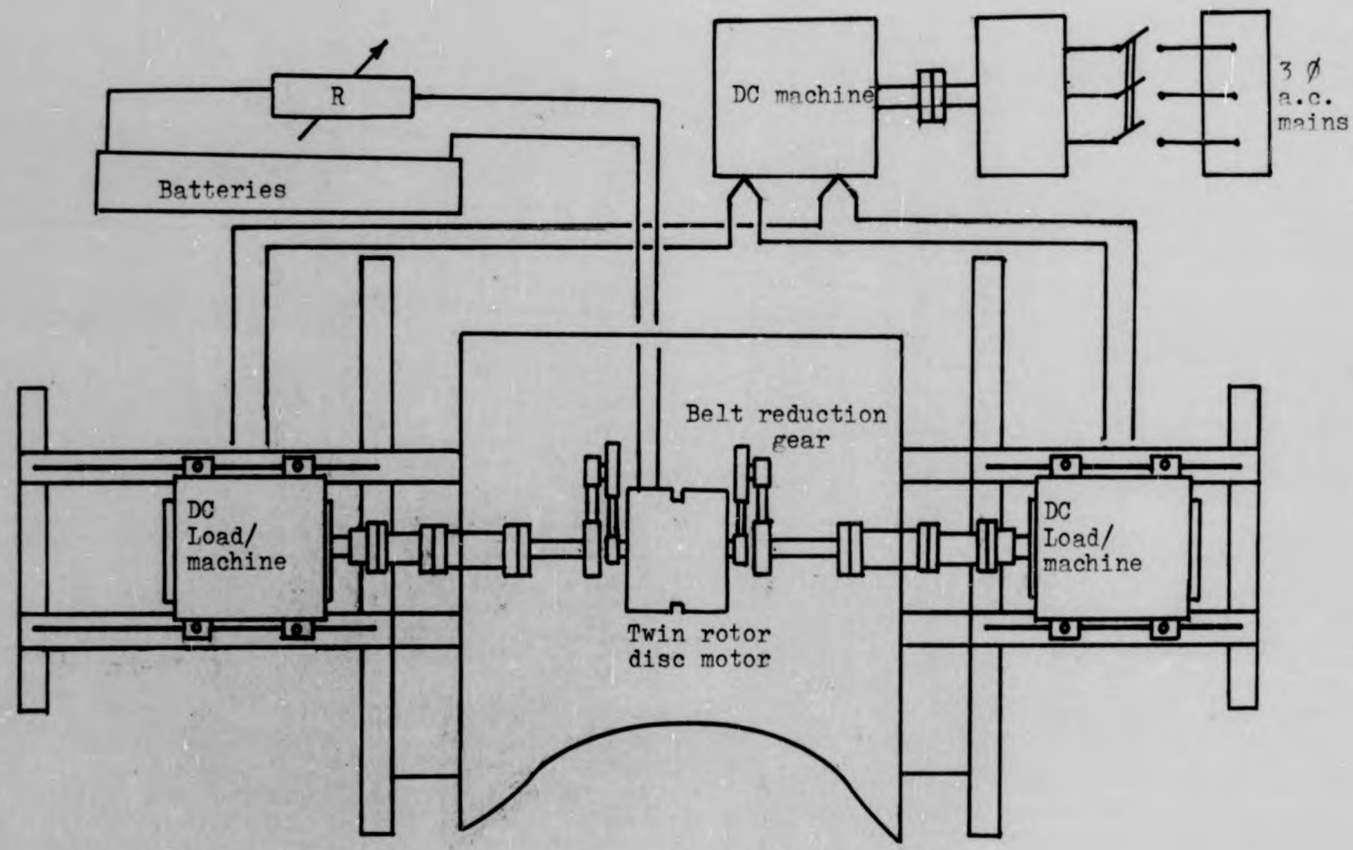

Fig. 6.14 : Diagramatical layout of the test rig

TABLE 6.3

Ratings of the electrical machines used for vehicle test rig.

The induction motor was manufactured by Newman Industries Ltd. The machine mechanically coupled to the induction motor was manufactured by Brush Electrical Machines Ltd. The two machines connected to the vehicle under test were manufactured by British Thompson Houston Co Ltd.

	Induction motor	Brush d.c. machine	B.T.H. d.c. machine
Volts	415 ± 6%	220	220
Amps	147	40	30.2
Power	7.5kW (10 H.P.)	7.5kW	5.6kW
Speed	1430 r.p.m.	1500 r.p.m.	900 r.p.m.
Winding	Delta	Shunt	Compound
Rating	Continuous	Continuous	Continuous
Field time constant			0.486
Armature time constant			0.416
Frequency	50Hz		
Phase	3		

direction of power flow to be reversed (regenerative action). The specifications of the machines used in the test rig are given in Table 6.3. In effect, a vehicle load is changed by controlling the field currents of the three DC machines.

6.4.1 Measuring Equipment

In order to assess how the various vehicle components perform under test operating conditions, instrumentation must be installed which can be used to record the relevant values of voltage, current, torque and speed associated with these components. The instrumentation used on the electric test bed allows the following parameters to be measured: battery voltage and current, motor voltage and current, load machine's input torque and speed. The battery voltage and motor voltage are measured directly by voltmeters. Battery and motor currents are measured by the use of two high-current shunts in the electric circuit. Measurement of the voltages developed across these, allows the current to be determined and the voltages

themselves are measured by a battery-powered mean-sensing digital voltmeter.

In any electro-mechanical system, it is important to determine the mechanical power at some point in the drive chain and this is accomplished on the electric test bed by indirect measurement of the torque transmitted along the load machine shafts.

In this case, only one torductor was available. The need to measure the input torque of both load machines is demonstrated by the results presented here. The availability of another torductor was financially unattractive, so direct torque measurement on the test bed was not possible. Therefore, some other means of finding input torque to the load machines was necessary.

An indirect method of measuring input torque to the load machine was employed in which the torque is deduced from the load machine output current, speed and field current. This method provides reliable

readings without recalibration since the machine's parameters do not change with time. The test machines were connected in the Ward Leonard arrangement shown in Figure 6.15 In order to measure the torque of the machine being tested, a ring torductor was used (see Chapter 5). Both load machines were tested when 'motoring' and 'generating'.

The torque of a DC machine is given by $T = K I_f I$. This equation is valid in the non-saturation region of the machine operation and torque is constant for a given field and armature current up to the machine's rated speed. However, the load machines were anticipated to be in use at over rated speed where the above relationship would not hold. Readings of torque were obtained for armature currents increasing in 5A steps up to 100-percent overload and at speeds increasing in 100 r.p.m. steps up to 60-percent over rated speed. These readings were obtained for field currents in 0.1A steps up to the maximum field current. A complete set of readings could not be obtained but the necessary areas of generator operation were covered and were

1. d.c. Load machine 1
2. d.c. Load machine 2
3. d.c. Machine
4. Induction motor
5. Variable transformer
6. Speed counter
7. Magnetic pick-up
8. Torquemeter
9. Coupling
10. 60 Tooth gear
11. Load resistance
12. Torque transducer

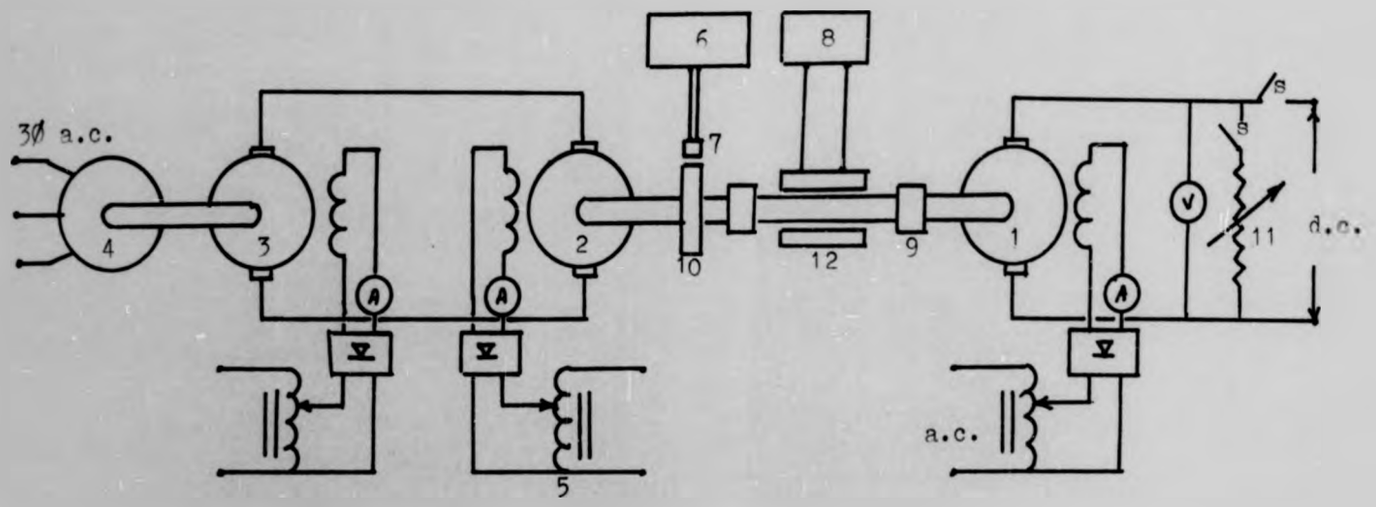

Fig. 6.15 : Ward Leonard arrangement

found to be sufficient for the work reported here.

The input torque to the machines when generating was calculated by measuring field current, armature current and speed (as mentioned earlier). The nearest measured values of these quantities were looked up and then the input torque calculated by interpolation. A low resistance (0.5Ω)was used for field current measurement. For measuring armature current, high current shunt was used. Voltages developed across these are measured by digital voltmeters.

The load machine's speed is measured by means of a special toothed wheel fitted on the machine's shaft. A magnetic transducer is placed next to the wheel which is used to generate a series of pulses, the frequency of which is proportional to the rotational speed of the shafts. This is fed into a digital counter to obtain the shaft speed in r.p.m.

The instrumentation described above is sufficient for an accurate analysis of the

vehicle's performance. With proposed testing conditions established, experimental testing may be carried out to collect the data necessary for such an analysis.

6.5 Dragonfly Nova Car Test

After the first prototype twin-armature disc motor was completed, the motor was successfully tested up to full speed, running light, at the University. By this time, the company (sponsor) was very concerned by the delays and was anxious to install the twin-armature disc motor into the Dragonfly Nova sports car as quickly as possible to display it to potential customers and to exhibit it at Electrex (1980). Reluctantly, it was therefore decided to release the motor to the company without undertaking a full test programme on it at the University. It was expected that after the exhibition, the Dragonfly Nova car would be returned to the University with the twin-armature disc motor installed, for testing on the electric test rig which had been originally developed for the purpose, and that the twin-armature disc motor

would eventually become available for comprehensive bench testing.

After that, the vehicle was only made available to the University for two weeks. Thus the only possible tests were to investigate the twin-armature disc motor. To save time, the motor was left in its actual place in the car with the belt reduction gear on. In order to set up the test, the car was driven on to the electric test rig and the wheels removed. Then the wheel hubs were connected to the load machine, as shown in Figure 6.14.

Two sets of load tests were carried out, one with the armatures in series and one with them in parallel. The output torque of the disc motor could not be measured directly because the transmission system did not allow any room to fit transducers to the motor shafts. Hence the motor output had to be calculated. The results of the tests described here are given in Tables A1.1 to A1.4 for parallel and series tests respectively. A description of the method of calculation of motor, trans-

mission and vehicle efficiency are given in Appendix 1. The armature voltage for these tests was varied in multiples of 12V by arranging the batteries in series and parallel groups of the appropriate voltage using a carbon pile to adjust the voltage to the value required.

It should be noted that the vehicle controller was not available. So simplify the calculation of input torque, the field excitation current of the load machines was left at constant value (0.7A) for all the tests. The load was changed by varying the field current of the third DC machine which was coupled to the induction machine.

When the two identical armatures are connected in series, and applying Equation 2.21 where the armatures have the same current and the permanent magnets provide a constant flux, the two independent output torques of the twin-armature disc motor would be equal. The total applied voltage would be equally divided between the two armatures and they would run at the same speed. Inspection of the results shows that the armature voltages, speeds and

output torques were not equal. This results from the fact that the transmission losses on one side were higher than the transmission losses on the other side. It is believed that this was caused by the belt tension not being properly adjusted when the unit was being installed in the vehicle. Since this effect considerably increases the losses, care must be taken to make sure that the tension is correct on installation. The belt tension criteria must be taken in order that the vehicle losses are minimised. Indeed both armatures supply the same output torque, but one sees a higher load. The rotation speed of the armature with the greater load, starts decreasing. This alters the voltage distribution on the armature terminals and the rotation speed of the other armature starts increasing. Hence, for the series tests, as the load current is increased, the speeds and voltages of the armatures diverge, as do the torques supplied to the load machines. This gives another important reason for ensuring that the transmission is properly adjusted. When the armatures are connected in parallel, the

machines run at the same speed despite this difference in load.

When the vehicle corners, with the armatures in parallel, the standard voltage equation of a DC machine becomes:

$$V = E.m.f_a + I_a R = E.m.f_b + I_b R_b \qquad 6.11$$

Where the e.m.f. of a DC machine is given by:

$$E.m.f. = K\phi n = K.I_f.n \qquad 6.12$$

I_f in Equation 6.12 is constant, then during cornering, as n falls, e.m.f. will fall for a constant applied voltage. Hence I will increase. This will increase torque ($T = K.I_f.I$) which will tend to increase wheel speed. The reverse is happening to the other wheel so the vehicle will resist the turning force. While the motors are intrinsically safe when connected in parallel, care must be taken whilst they are connected in series, to make sure the armatures share the applied voltage equally.

Figures 6.16 to 6.18 show the twin armature disc motor, transmission and overall vehicle efficiency versus armature current for armature B at voltages of 24, 48 and 96V. Unfortunately the curves do not show these efficiencies at the rated load of this armature. This is due to the limited capability current for high power reading. However, the curves demonstrate that the twin-armature disc motor has high efficiency at low load. Its high efficiency over a wide speed range is demonstrated by these tests as well. The values of efficiency plotted in Figure 6.16 are not necessarily the optimum for a particular speed but are the highest efficiencies encountered in these tests.

In addition to load tests, a heat run test at 90V was carried out on one armature. After 15 minutes of running at 70A, testing had to stop when the armature failed. On inspecting the motor, magnets were found to be adrift from their mountings and there was severe mechanical damage to the disc, causing it to be scarred. It was not possible to see from the damage whether the magnets had

a. 96V
b. 48V
c. 24V

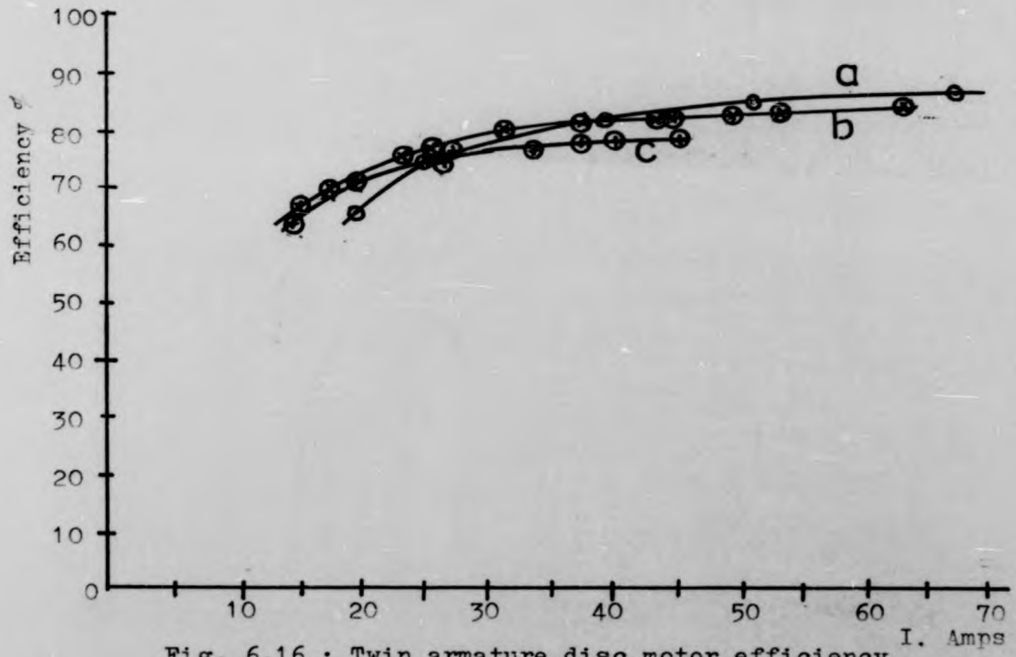

Fig. 6.16 : Twin armature disc motor efficiency versus armature current (armature B)

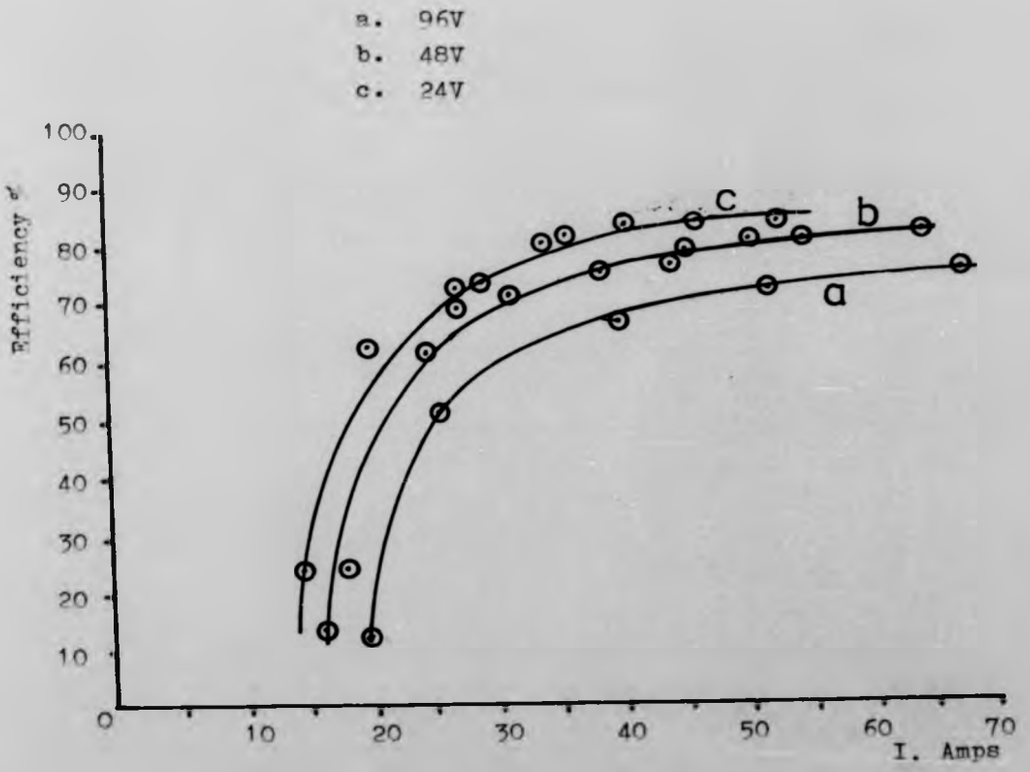

Fig. 6.17 : Transmission efficiency versus armature current

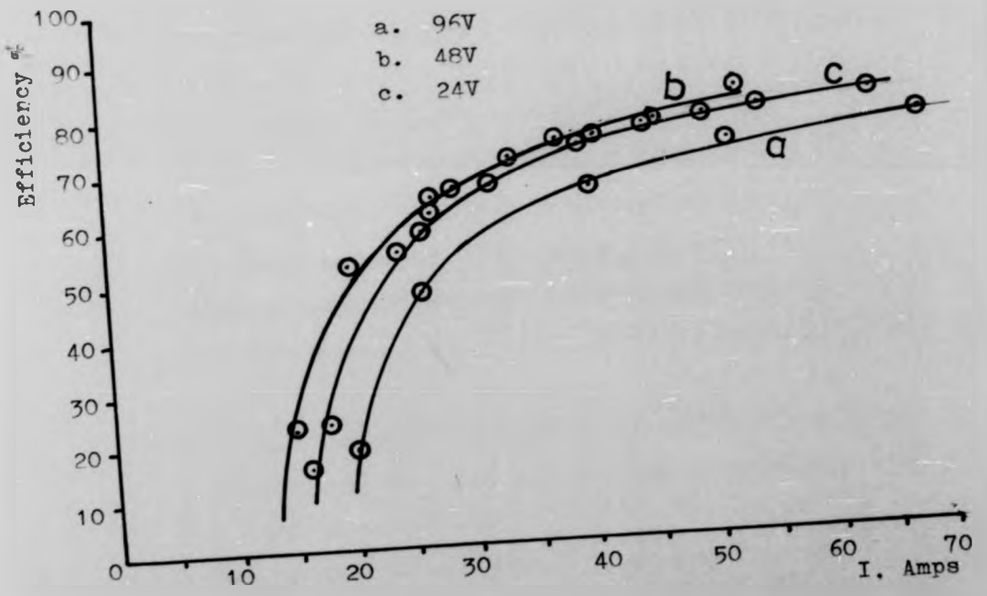

Fig. 6.18 : Overall vehicle efficiency versus armature current

come adrift first or whether the disc had failed first causing the magnets to become dislodged.

6.6 Transmission Considerations

Prior to comparing the efficiency of the transmission system used in the Dragonfly sports car, to the efficiency of the usual transmission system used in petrol powered vehicles, there is a brief description of these systems. This background material is presented as an aid to understanding the evaluations and comparisons of the results reported here.

The Dragonfly car transmission consists of two identical reduction gear systems which fit into the output shafts of the twin-armature motor. Each gear system has a reduction ratio of 4:1 derived through double 2:1 reduction stages, using toothed belts and cogwheels as shown in Figure 6.7. This in turn drives rear stub axles which are suitable for running from two independent driving shafts. On the other hand, the conventional transmission

consists of a change-speed gearbox to which the motor/engine is coupled through the clutch, a propeller shaft, a differential unit and twin rear half-shafts with associated universal joints and bearings.

For comparison purposes, it will be assumed that all losses between the motor output shaft and the road wheels may be accounted for by transmission inefficiency. In order to satisfy these objectives, information was required on conventional transmissions. To this end, data obtained from a 3rd year undergraduate project was used. The project involved testing the transmission system of a converted vehicle (the Reliant Robin) which uses a DC series motor and transmission system consisting of the same components as in the standard IC engined version of the vehicle. Measurements were taken while the transmission was being driven by the DC series motor and loaded by a band brake on the rear wheels. A theoretical approach was also applied which showed very close agreement with the results obtained by experiments. A full description of this 3rd year project with the techniques used is given in Reference 35.

The efficiency is determined for various values of output speed at constant output torque, and various values of output torque at constant output speed.

Comparing the results for the Robin and Nova, Figure 6.19 shows that the transmission chosen for the Dragonfly Nova increases its efficiency compared to the Reliant Robin car. The efficiency plotted for the Reliant Robin car is the transmission system in fourth gear which represents the most efficient conditions for this system. The losses of the belt drive transmission system in the Dragonfly Nova were larger than expected. The transmission originally suggested to the Dragonfly Nova car builders, Lee Dickens Ltd., was a chain driven transmission unit manufactured by Renold Ltd. Units similar to the one suggested are used in IC engines to transfer power from the crank shaft to a parallel axis in the gearbox. They are used particularly in front wheel drive vehicles where their compactness is an additional advantage. The measured efficiency of a Renold chain drive transmission is between 98.4 and 98.9 percent.[36]

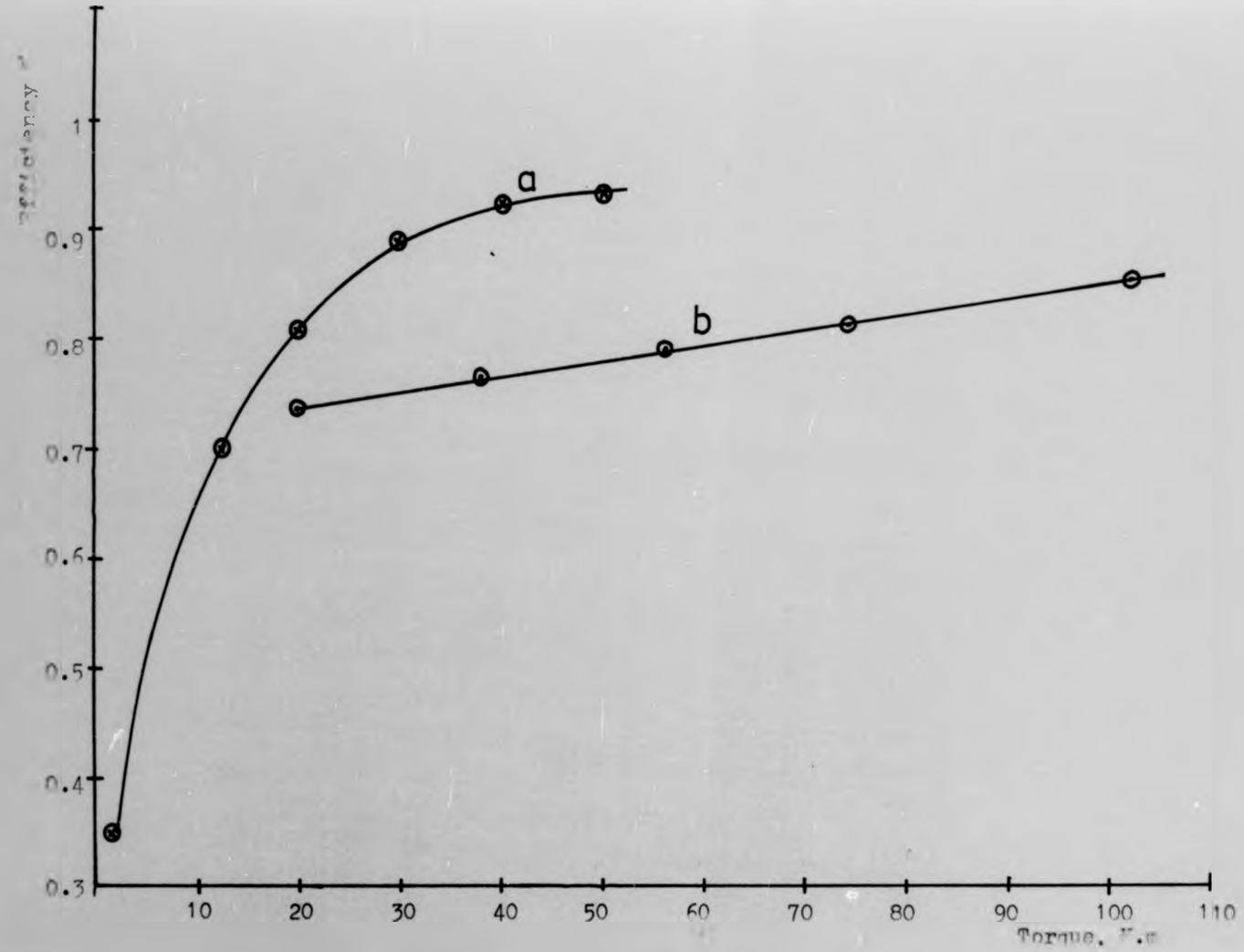

Fig. 6.19 (a) : Efficiency versus output torque
(a) Dragonfly-Nova hybrid car
(b) Reliant Robin

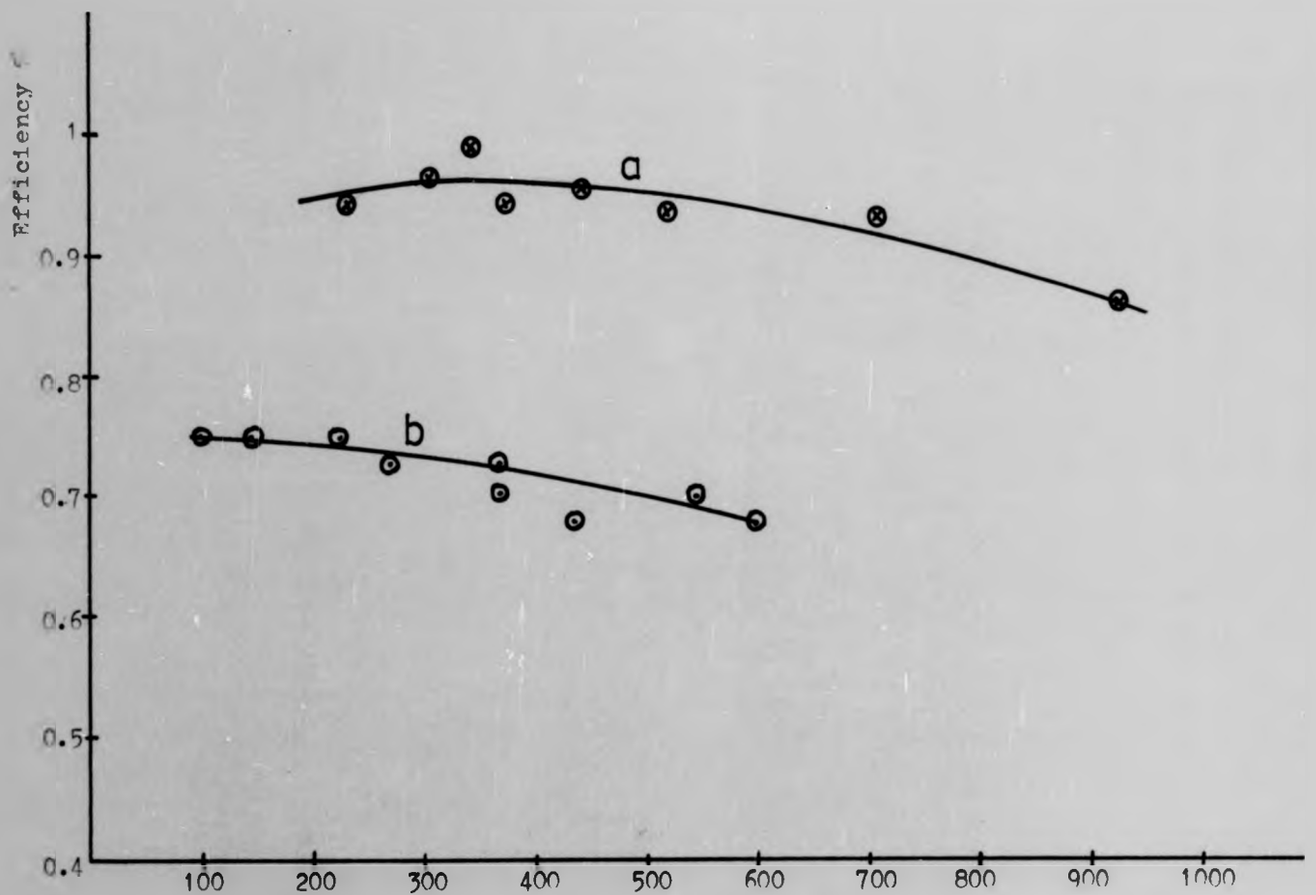

Fig. 6.19 (b) : Efficiency versus output speed
(a) Dragonfly-Nova hybrid car
(b) Reliant Robin

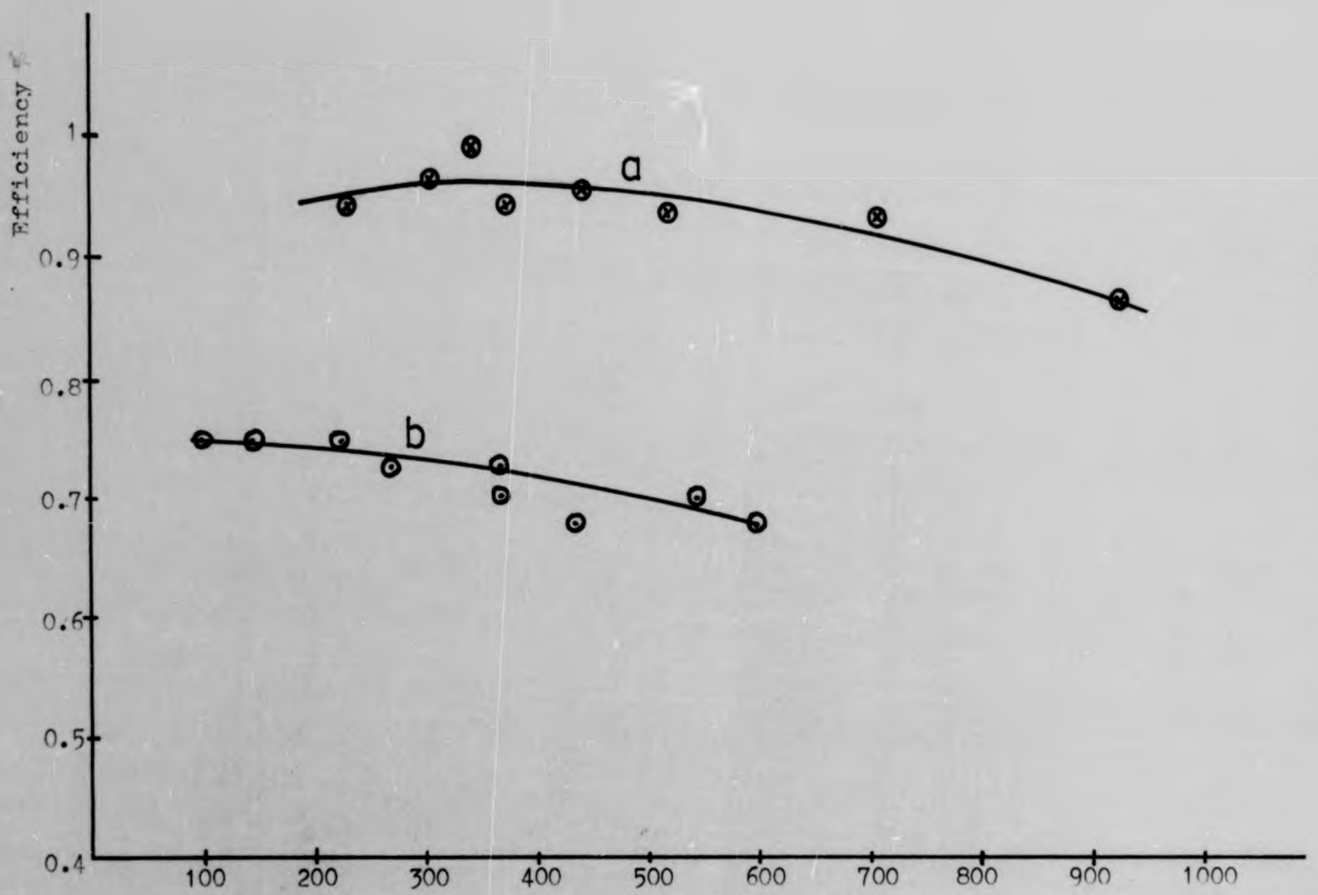

Fig. 6.19 (b) : Efficiency versus output speed
(a) Dragonfly-Nova hybrid car
(b) Reliant Robin

PAGINATION
ERROR

A transmission such as this would greatly increase the performance of the Dragonfly Nova Car.

Chapter 7 Conclusion

The axial-field motor described in this thesis is one that has been developed for a few years, with special theories derived to it. But these theories either go no deeper than is necessary for enabling their readers to perform their professional calculations or probe more deeply but in a mathematical approach beyond the need of engineering.

Chapter 2 attempts to explain in simple terms how a permanent-magnet axial field D.C. machine behaves. Many principles are explained by way of illustrations, or using solutions requiring no mathematical method beyond the engineering level. Mathematical ideas of a more advanced kind, such as line and surface integrals have been necessary; but they have been carefully explained when the need arises

and perhaps the reader will see the utility of these ideas more clearly when they are closely linked with physical facts. In a few places the theory has been carried beyond the needs of engineering; conceivably the author may have been beguiled along one or two fascinating byways, but in general these explorations are needed for completing the picture. Certainly this is true of the theory of field produced by the magnet in a gap, without which several elementary concepts, such as electromagnetic induction by flux cutting, cannot be properly accounted for.

The key to being able to fully design a disc armature motor, or any other kind of d.c. machine, by computer, is to be able to calculate the field distribution from the magnetic circuit parameters. It has been

found that the leakage coefficient, LC; the pole number, p; and the pole arc/pole pitch ratio, α are related by Equation (3.40).

Optimisation of air gap flux density cannot, however, be used as a design criterion. The same three parameters may be related to the armature heating loss though, as shown in Equation (3.48).

Using these two equations, p is eliminated and LC fixed so that I^2R can be minimised with α. By making the leakage coefficient, LC, constant in a design, we are really only expressing what value we would tolerate - a very low value results from a low α or p, either of which move adjacent magnet edges further apart. With LC fixed, α must be between 0.75 and 1.0 to

minimise I^2R: or if α were constant, LC must be between 1.0 and 1.5. Both of these ranges are what machine designers would normally expect to use.

In this way the angular parameters of the motor are found, and with the familiar ratio between the outer and inner active diameters of $\sqrt{3}$ for maximum armature power, all the critical dimensions are deduced.

In addition, algorithms have been written that design a realistic armature winding, selecting a practical combination of coil number, turns, conductor size and connection, that also ensures minimum I^2R power loss. A complete Table of permanent magnet data is searched, and the material is selected on the basis of whether optimum overall efficiency or power density is desired.

A complete motor specification is generated by the computer program on the basis of input data comprising desired power, speed and voltage. The designer specifies also the criteria to be used, and may select any other magnet material or winding connection if he wishes. The real benefit of having the program is the ability to compare a large number of designs with only one parameter varying.

A primary concern in the design of permanent-magnet field motors, is the interaction of the field flux and the flux produced by the armature current. An analytical model has been established to quantitatively predict the degree to which the permanent magnet field is demagnetized by the armature current. As an aid to analysis, the pole face opposite each

armature spoke is treated as a separate section. The maximum amount of magnetizing or demagnetizing force is determined for each section from Equation (4.9). The maximum demagnetizing force per section is then used to determine the stabilized flux densities per section, which in turn are used to determine the stabilized flux per pole for the machine. The effects of armature reversal can be included in the stabilization prediction.

The analytical model was compared with a static test model, and it was determined that the predictions were accurate. Employment of this method of field flux analysis with optimization of armature parameters provides the designer with competent design trade-offs prior to committing expensive tooling operations.

The modest temperatures which were attained on test obtained on a single-disc, self-ventilated "skeleton" version of the machine, led to the conclusion that it might be possible to achieve a further increase in efficiency by reducing the air-flow and hence the resulting windage losses.

A wide range of magnetic material is suitable for use in the motors, ranging from sintered ferrite to rare earth-cobalt. Given that the airgap of the disc motor is quite large because it embraces the thickness of the armature disc as well as the necessary running clearance on either side, magnetic material of high coercivity is needed, especially in traction applications in which high torque (and high armature current) can result in high demagnetizing fields. The ferrites exhibit high coercivity and owing to

their low cost are well suited to the application in spite of their low remanence. The use of high remanence magnets enables motors of slightly higher efficiency to be designed, but, owing to the relatively low coercivity of these materials the amount of magnetic material is large when an airgap of considerable span is needed. Designs have shown that if the selection of magnetic material is based on obtaining maximum power density for the machine, then samarium cobalt should be specified, whereas to achieve the highest flux density in the airgap alnico should be selected. The main drawback of both samarium and alnico materials is that their costs are prohibitively high for many commercial applications. In contrast, the cost of ferrite materials is low enough to make it viable in spite of its low remanence and energy density.

For economic use of Magentic material it is general practice to work the material near to the point on the demagnetization curve which gives (BH) max, but in the case of ferrites it is beneficial in terms of overall cost-effectiveness to work the material at higher values of flux density owing to the low cost and low density of the material. In this way acceptable airgap flux densities were achieved without incurring excessive weight and cost penalties. However, since the flux density is still low in comparison with electro-magnetically excited machines, a high copper content in the armature must be specified to compensate. For this reason ferrite magnets have been listed in the specification of the disc armature motor because the cost saving they represent is more significant than the small loss of efficiency of the motor.

To illustrate the results which can be achieved from application of the above concepts and design philosophies a 96V, 10kW, 4000 rev/min motor is described. In fact a twin-armature version rated at 20kW has been developed for the driver of an experimental hybrid sports car. This machine comprises a common magnetic circuit which houses two disc armatures, each armature independently driving an output shaft which transmits power to a road wheel through belt-reduction gearing, thereby eliminating the need for a mechanical differential gear. Significant savings in weight and cost result from adopting the twin-rotor arrangement rather than two individual motors and furthermore the absence of the differential gearbox cancels the associated mechanical losses and weight which has a positive effect on the overall efficiency and

weight of the hybrid vehicle. The twin armature motor offers a simple and reliable traction system which needs less service and maintenance which, in turn, reduces the running cost.

In addition to the twin armature disc motor, the vehicle is fitted with an on-board engine-generator set to provide the average power requirement while the batteries are specified to provide excess power. The d.c. generator is identical mechanically to the single disc armature motor and the same components are used in its manufacture. The only significant difference is the design of the armature winding which is tailored to match the engine and battery characteristics. Owing to the short axial length of the disc generator it was mounted on the engine as an

overhung load thereby obviating the need for an elaborate bedplate and coupling arrangement.

A vehicle test rig has been described and the necessary instrumentation for testing the performance of the twin armature disc motor in the Nova hybrid vehicle. Test results on the motor show that the machine achieves high efficiency over a wide range of operating conditions and should show good energy economy in electric vehicle applications.

8: References

1. Beagley, T.J., 'Energy and Transport'. Conference of the Association of District Councils Passenger Transport Operators. October 1979.

2. Ali, M.R.N., and Corbett, A.E., 'Design and Performance of 10kW Disc Motor for Electric Vehicle Drives' Drive Electric. 82 Conference. Amsterdam, October 1982.

3. Ali, M.R.N., Anscomb, C., Corbett, A.E. and Roerig, C.S. 'Disc Armature Traction Motors' Drive Electric 80 Conference, October 1980.

4. Ali, M.R.N., Corbett, A.E. 'Design and Performance of a 10kW D.C. Disc Motor with Ferrite Magnets' International Conference on Electrical Machines, Budapest, Hungary, September 1982.

5. Ali, M.R.N., Corbett, A.E., Özpolat, M.A. Roerig, C.S. 'Design and Performance of Disc Armature D.C. Motors for Traction Applications' Fifteenth Universities Power Engineering Conference, University of Leicester, March 1980.

6. Pal, S.K. and Stratton, J.D. 'Performance Limitation in Moving Coil and Conventional Designs of D.C. Permanent Magnet Motors' Second International Conference on Small and Special Electrical Machines, September 1981.

7. 'D.C. Motors, Speed Controls, Servo Systems' Electro-Craft Corp. Book Pergamon Press, 1977.

8. Malcolm McCaig 'Permanent Magnets in Theory and Practice', Book Pentech Press 1977

9. Campbell, P., 'Principles of a Permanent Magnet Axial-Field D.C. Machine' Proc. IEE. Vol. 121, No. 12, December 1974.

10. Nicol, K., 'Elementary Programming and ALGOL' Pub. McGraw-Hill.

11. Turner, A.M., 'Computer Aided Design of D.C. Disc Armature Motors' undergraduate thesis, University of Warwick, 1970.

12. Boerig, C.S., 'The Disc Armature Traction Motor' Ph.D. Thesis, University of Warwick 1981.

13. Roters, H.C., 'Electromagnetic Devices' Book Wiley, 1941.

14. Hadfield, D., 'Permanent Magnets' Book Iliffe, 1962.

15. Walshow, M.H. and Lynn, J.W., 1961, Proc. IEE, 516-527.

16. Desmond, D.J., 1945, JIEE, 92, Pt. II, 229.

17. Hanrahan, D.J. and Toffolo, D.S., 1957 Trans. AIEE, 76, Pt. III, 1098-1103 and 82, 68-74.

18. Becker, J.J., Lubonsky, F.E. and Martin, D.I., 1968, Trans. IEEE, 4, No. 2, 84-99.

19. Parker, R.J. and Studders, R.J.'Permanent Magnets and their Applications' Wisley, 1962, New York.

20. Ireland, J.R., 1968 'Ceramic Permanent Magnet Motors'. Book, McGraw-Hill.

21. Gollhardt, J.E. and Beaudoin, L.W., 1970 Interm. Electron, 20-23.

22. Burnett, J. and Overshott, K.J., 'Analysis of the Dynamic Operation of Permanent Magnets'. 2nd Conference of Advances in Magnetic Materials and their Applications, London, England, IEE, 1976, 158-161.

23. Cornell, A.W., and Parker, R.J., IEEE Trans. Magnetics, MAG-6, 266 (1970).

24. Edson, A.P., and Peters, D.T., IEEE Trans. Magnetics, MAG.7, 511 (1971) (Digest).

25. Gould, J.E., 'Some Aspects of Permanent Magnet D.C. Motors", IEEE Trans. Magnetics, Vol. MAG-6, No. 2, June 1970.

26. Gould, J.E., 'Permanent Magnets in D.C. Motors' Cobalt and Cobalt, 55, 1972.

27. Kubo, T., Ohtani, T., Fojina, S., and Kato, T., 'Anisotropic Mn-Al-C Alloy Permanent Magnets can be Machined and Mass Produced'. JEE, July 1977.

28. Ohtani, T. et al, 'Magnetic Properties of Mn-Al-C Permanent Magnet Alloys' IEEE Trans. magnetics. September 1977.

29. Welowski, J., 'Race is on for Super Magnet Electric Motors' Electrical Review Vol. 213 No. 12, October 1983.

30. IG Technologies, Inc., Indiana, U.S.A.

31. Carter, G.W., 'Electromagnetic Field in its Engineering Aspects' Book, Longmans, 1967.

32. Spooner, E., 'Fully Slotless Turbogenerators Proc. IEE, Vol. 120, No. 12, December 1973.

33. Lee, G.A. and Corbett A.E., 'Development of a Hybrid Electric Vehicle using High Efficiency Disc Motors' Electric Vehicle Development Group, Third International Conference U.K. November 1979.

34. Watson, J. and Lee, G.A. 'Traffic Compatible Hybrid Electric Vehicles - an Outline of Development Work with Vans and Buses'.

35. Bosworth, J., 'Transmissions for Electric Vehicles' undergraduate thesis, University of Warwick, 1978.

36. Moxon, J.C., 'Roller Chain Transmission Drive for Electric Vehicle' Report 359, Renold Limited, June 1979.

37. Brennan, J. and Fox, H., 'Performance Standards for Near-Term Electric Vehicles' Rep. No. IM-2069, General Research Corporation, 1976.

Appendix 1 Results of Tests on Nova Vehicle

The disc motor has two armatures A and B and they drive load machines 1 and 2 respectively, via a 4:1 reduction belt transmission. To calculate the torque output of the transmission, the input of the load machines, the load machine speed and armature current were measured. The field current of the load machines having been left at 0.7 A for every test. The voltage and current for each armature of the disc motor was measured and this gave sufficient data for all the calculations of efficiency. The measured quantities are given in Tables A1 and A2 and the calculated quantities in Tables A3 and A4. A typical calculation of the various efficiencies is given below to show how Tables A3 and A 4 were produced.

Consider armature B when in series with A with the armature current I_b, 40.6 A and a terminal voltage V_b 24.5 V. The load current of 2 is 18.4 A and the machine speed is 234 r.p.m. From the calibration readings at 0.7 A four values of torque are required.

For I_2 = 20 A

Torque T_2 = 24.0 x 1.335 = 32.0 Nm at both 200 and 300 r.p.m.

For I_2 = 15 A

Torque T_{tb}= 19.7 x 1.335 = 26.3 Nm at both 200 and 300 r.p.m.

1.335 is the calibration figure that converts the torductor reading to Nm and T_{tb} is torque input to load machine 2 (or transmission associated with armature B output torque).

Interpolation is only required between the two currents at which calibration readings were taken since for these particular readings the speed does not affect the torque. Using linear interpolation.

$$TAN\emptyset = \frac{(T_{tb} - T_{tb}15)}{(18.4 - 15.0)}$$

but $TAN\emptyset = \frac{T_{tb}20 - T_{tb}15)}{20 - 15}$ hence $T_{tb}\frac{(32 - 26.3)}{5.0}x3.4+26.3$

hence transmission output torque = 30.2 Nm

Transmission output power (Po_{tb}) = load machine input power (Pi_2) = $T_{tb} \cdot w_2$

Therefore $Po_t = \frac{T_{tb} \cdot n_2 \cdot}{30.0}$

Hence $Po_{tb} = \frac{30.2 \times 234.0 \times}{30.0} = 740$ W

Input power to the armature B, $Pi_b = I_b \cdot V_b$ = $40.6 \times 24.5 = 995$ W.

The overall efficiency is then $\frac{740}{995} = 74.4\%$

The armature resistance at the working temperature of the motor is 0.035 . The total brush voltage drop is assumed to be a constant 1.5 V independent of the load current. Hence electrical power losses of the motor are:

$We_b = I_b^2 \cdot R_b + I_b \times 1.5$

$= 40.6 \times .035 + 40.6 \times 1.5 = 119$ W

The running light losses of the motor, the mechanical losses, were measured for both armatures and are shown in Figure A1.1. A least squares technique was used to fit a second order equation to the losses versus speed they are. for armature A:

Losses $= -0.949 + 0.0655 \times n_a + 1.94 \times 10^{-5} \times n_a^2$

for armature B

Losses $= -6.22 + 0.0893 \times n_b + 1.43 \times 10^{-5} \times n_b^2$

where n_a and n_b are speed of armature A and B in r.p.m. respectively,

$n_a = n_1$ GR

$n_a = n_2 \cdot GR$; GR is gear ratio = 4:1. n_1 and n_2 speed of load machine 1 and 2.

Solving for armature B gives mechanical losses, respectively in r.p.m.

$Wm_b = -6.22 + 83.5 + 12.5 = 89.8$ W

Assuming all other electrical losses to be negligable.

Total motor losses, $W_b = Wm_b + We_b$

$= 89.8 + 119.0 = 209$ W

Hence motor output power $Po_b = Pi_b - W_b = 995.0 = 786$ W

Motor efficiency is therefore $\frac{Po_b}{Pi_b} = \frac{786}{995} = 79.0\%$

Transmission efficiency is then given by

$\frac{Pi_2}{Po_b} = \frac{74}{786} = 94.1\%$

Transmission losses $(W_{tb}) = Po_b - Pt_2 = 46$ W.

TABLE A1.1

Results of test on twin armature disc motor with the armatures connected in series.

T	V_B	V_a	I_1	n_1	V_b	I_2	n_2
26.2	24	12.0	8.9	100	12.0	9.6	106
25.0	24	12.0	8.3	102	12.0	8.9	106
20.7	24	12.0	5.9	106	12.0	6.3	110
15.2	24	12.0	2.7	108	12.0	3.0	110
10.2	24	12.0	0.2	114	12.0	0.5	120
44.6	36	17.2	20.0	152	18.8	22.5	170
37.0	36	17.8	15.1	158	18.2	16.5	170
30.4	36	17.6	10.9	162	18.4	11.7	170
23.0	36	17.8	6.4	168	18.2	6.7	172
15.2	36	17.9	2.5	174	18.1	2.5	178
11.0	36	18.0	0.2	174	18.0	0.1	174
53.0	48	23.0	26.6	208	25.0	29.5	234
40.6	48	23.5	17.2	220	24.5	18.4	234
33.8	48	23.7	12.4	225	24.3	13.3	236
27.4	48	23.8	8.7	229	24.2	9.1	238
20.2	48	23.8	4.6	233	24.2	4.7	240
14.8	48	23.9	1.6	238	24.1	1.4	242
57.0	60	27.4	28.9	246	32.6	33.5	304
44.2	60	28.8	19.0	264	31.2	21.0	292
34.8	60	29.5	12.4	274	30.5	13.5	290
25.0	60	29.8	6.5	282	30.2	6.9	292
20.6	60	29.8	3.9	288	30.2	4.3	294
60.2	72	32.8	31.3	298	39.2	36.2	374
51.2	72	34.2	23.9	316	37.8	26.9	360
43.4	72	35.0	18.1	328	37.0	19.6	354
34.8	72	35.2	12.2	336	36.8	13.2	358
25.6	72	35.8	6.5	344	36.2	7.0	358
21.0	72	35.8	4.1	350	36.2	4.4	358
61.4	84	38.5	32.7	358	45.5	38.2	442
53.0	84	40.0	24.8	378	44.0	28.1	426
45.2	84	41.0	19.0	388	43.0	21.0	420
36.0	84	41.3	12.6	396	42.7	13.9	420
27.2	84	41.5	7.2	404	42.5	8.0	424
19.0	84	41.9	2.8	412	42.1	3.2	426
64.2	96	43.0	34.7	408	53.0	41.7	518
53.6	96	46.0	24.8	442	50.0	27.6	492
44.0	96	47.0	17.3	454	49.0	19.0	488
31.8	96	47.8	10.0	464	48.2	11.0	486
24.0	96	47.8	5.3	474	48.2	5.7	490
18.0	96	47.8	2.2	480	48.2	2.4	492

Symbols explained on next page.

TABLE A1.2

Results from tests or twin armature disc motor with the armatures connected in parallel.

V_B	I_a	I_1	n_1	I_b	I_2	n_2
24	50.4	23.7	220	45.8	23.3	222
24	42.8	18.0	220	38.0	17.0	220
24	32.8	11.8	220	29.2	11.0	222
24	30.4	9.9	222	26.8	9.1	224
24	23.6	5.9	226	20.4	5.2	226
36	61.4	33.5	344	56.0	32.7	346
36	54.2	27.5	346	50.0	26.7	344
36	43.2	17.9	346	38.8	17.3	344
36	29.0	8.9	344	26.0	7.8	346
36	22.2	4.8	350	19.2	3.7	350
48	56.0	27.3	458	50.4	25.9	460
48	50.8	22.8	566	44.8	21.0	468
48	43.6	17.4	462	38.0	15.4	460
48	30.8	9.2	472	26.0	7.4	472
48	19.8	2.8	478	16.0	1.1	478
72	72.4	47.8	694	66.4	46.8	694
72	67.6	38.5	706	61.4	37.2	706
72	56.8	26.2	708	51.0	24.7	708
72	44.6	16.9	710	39.6	15.4	714
72	31.0	8.5	726	26.6	6.4	728
72	24.4	4.6	732	20.2	2.8	730
96	76.6	49.1	920	68.4	47.4	924
96	58.8	24.8	946	51.8	23.1	946
96	46.8	16.7	960	40.2	13.8	968
96	33.4	8.5	976	26.2	5.3	968
96	26.8	4.6	980	19.6	1.5	990

I = Total disc armature motor current (A)
V_B = Total disc armature motor voltage (V)
V_a = Armature voltage of A (V)
V_b = Armature voltage of B (V)
I_a = Armature current of A (A)
I_b = Armature current of B (A)
I_1 = Armature current in load machine 1 (A)
I_2 = Armature current in load machine 2 (A)
n_1 = Speed of load machine 1 (r.p.m.)
n_2 = Speed of load machine 2 (r.p.m.)

TABLE A1.3

Performance of motor A calculated from the data given in Tables A1.1 and A1.2.

Armatures in series

T_{ta}	Pi_1	Pi_a	n_{ta}	W_{sa}	W_{ma}	We_a	W_a	Po_a	n_a	W_{ta}	n_{ta}
V = 24 V											
16.8	176	314	56.0	138	28.4	63.3	91.7	222	70.8	46.3	79.3
15.9	170	300	56.7	130	29.0	59.4	88.4	212	70.5	41.6	80.2
12.1	134	248	54.0	114	30.3	46.1	76.4	172	69.2	37.6	77.9
5.8	65.6	182	36.0	116	31.0	30.9	61.9	120	66.0	54.1	54.6
0.5	5.4	122	4.4	117	33.0	18.9	51.9	70.5	57.6	65.1	7.6
V = 36 V											
32.7	520	767	67.8	247	46.0	137	183	584	76.1	64.5	89.0
25.6	424	658	64.4	234	48.2	103	152	506	76.9	82.4	83.8
19.9	338	535	63.2	197	49.6	77.9	128	407	76.1	69.5	83.0
13.0	229	409	56.0	180	51.8	53.0	105	304	74.3	75.2	75.3
5.4	95.0	272	34.9	177	54.0	30.9	84.9	187	68.8	92.1	50.8
0.5	8.2	198	4.1	190	54.0	22.6	76.6	121	61.3	113	6.8
V = 48 V											
40.3	878	1219	72.0	341	67.0	178	245	974	79.9	96.0	90.1
29.0	668	954	70.0	286	71.7	119	191	763	80.0	95.3	87.5
22.1	521	801	65.0	280	73.7	90.7	164	637	79.5	116	81.8
16.5	396	652	60.7	256	75.3	67.4	143	509	78.0	113	77.8
10.0	244	481	50.7	237	76.9	44.6	122	359	74.6	116	68.0
3.5	87.0	353	24.6	266	79.0	29.9	109	244	69.1	157	35.6
V = 60 V											
41.7	1073	1562	68.7	489	82.3	199	281	1281	82.0	208	83.8
31.5	871	1273	68.4	402	89.9	135	225	1048	82.3	177	83.1
22.2	637	1026	62.1	389	94.1	94.6	189	837	81.6	200	76.1
13.2	390	745	52.3	355	97.6	59.4	157	588	78.9	198	66.3
8.4	253	614	41.2	361	100	45.8	148	466	75.9	215	54.3
V = 72 V											
44.8	1398	1975	70.8	577	105	217	322	1653	83.7	255	84.6
37.4	1238	1751	70.7	513	113	169	282	1469	84.9	231	84.6
30.3	1041	1519	68.5	478	118	131	249	1270	83.6	229	79.5
21.0	771	1225	62.9	454	122	90.7	213	1012	82.6	241	76.2
13.2	476	917	51.9	441	126	61.3	187	730	79.6	254	65.2
8.9	326	751	43.4	425	129	46.9	176	576	76.6	249	56.6
V = 84 V											
45.7	1715	2363	72.6	648	133	224	357	2006	84.5	327	85.5
38.9	1540	2120	72.6	580	142	178	320	1800	84.9	260	85.6
31.5	1280	1853	69.1	573	147	139	286	1567	84.6	287	81.7
22.4	930	1486	62.6	556	152	99.4	251	1235	83.1	305	75.3
14.4	609	1123	54.0	519	156	66.7	223	905	80.2	296	67.3
6.1	263	796	33.0	533	160	41.1	201	595	74.8	332	44.2

(continued)

TABLE A1.3 (continued)

T_{ta}	Pi_1	Pi_a	n_{ta}	W_{sa}	Wm_a	We_a	W_a	Po_a	n_a	W_{ta}	n_{ta}
Vt = 96 V											
46.8	2000	2761	72.4	761	158	241	399	2362	85.5	362	84.7
38.9	1801	2466	73.0	665	176	181	357	2109	85.5	308	85.4
29.3	1393	2068	67.4	675	182	134	316	1752	84.7	350	79.5
18.0	918	1520	60.4	602	187	83.1	270	1250	82.2	332	73.4
11.6	576	1147	50.2	571	193	56.1	249	898	78.3	322	64.1
3.7	186	860	21.6	674	196	38.3	234	626	72.8	440	29.7
Armatures in parallel											
Vt = 24 V											
37.2	857	1209	70.9	352	71.7	165	237	972	80.4	115	88.1
30.1	693	1027	67.5	334	71.7	128	200	827	80.5	134	83.8
21.2	488	787	62.0	299	71.7	86.9	159	628	79.8	140	77.7
18.6	432	729	59.3	297	72.5	78.0	151	578	79.3	146	74.7
12.2	289	566	51.1	277	74.1	54.9	129	437	77.2	148	66.1
Vt = 36 V											
46.3	1668	2210	75.5	542	126	224	350	1860	84.2	192	89.7
41.3	1496	1951	76.7	455	127	184	311	1640	84.1	144	91.2
30.0	1087	1555	69.9	468	127	130	257	1298	83.5	211	83.4
17.0	612	1044	58.6	432	126	72.9	199	845	80.9	233	72.4
10.5	385	799	48.2	414	129	50.6	180	619	77.5	234	62.2
Vt = 48 V											
41.2	1976	2688	73.5	712	184	194	378	2314	85.9	334	85.5
35.2	1767	2438	72.5	671	189	167	356	2082	85.4	315	85.4
29.4	1442	2092	68.0	670	186	132	318	1774	84.8	352	80.2
17.7	875	1478	59.2	603	192	79.4	271	1207	81.7	332	72.5
6.2	310	950	32.6	640	195	43.4	238	712	75.0	402	43.5
Vt = 72 V											
51.5	3743	5123	71.8	1471	330	292	622	4591	88.1	849	81.5
48.8	3605	4867	74.1	1262	339	261	600	4269	87.7	662	84.5
40.1	2976	4090	72.8	1114	340	198	538	3552	86.9	576	83.8
29.3	2178	3226	67.5	1048	342	137	479	2747	85.2	569	72.3
17.2	1308	2232	58.6	924	353	80.1	433	1799	80.6	491	72.7
8.0	613	1757	34.9	1144	357	57.4	414	1343	76.4	730	45.6
Vt = 96 V											
51.5	4960	7296	68.0	2336	503	316	819	6477	88.8	1517	76.6
39.4	3903	5645	69.1	1742	524	209	733	4912	87.0	1009	79.5
29.3	2946	4493	65.6	1547	537	147	684	3809	84.8	863	77.3
17.6	1799	3206	56.1	1407	550	89.1	639	2567	80.1	768	70.1
11.3	1160	2573	45.1	1413	554	65.3	619	1954	75.9	794	59.4

T_{ta} = Torque input to load machine 1 (Nm)(motor output = Ta/4)
Pi_1 = Power input to load machine 1 (W)
Pi_a = Power input to disc motor from batteries (W)
n_{sa} = Efficiency of system A from batteries to load (%)
W_{sa} = System A losses between battery and load (W)
Wm_a = Mechanical losses of armature A (W)
We_a = Electrical losses of armature A (W)
W_a = Total losses of armature A (W)
Po_a = Power output of armature A (W)
n_a = Efficiency of armature A (%)
Wt_a = Losses in transmission A (%)
nt_a = Efficiency of transmission A (%)

TABLE A1.4

Performance of motor B calculated from data given in Tables A1.1 and A1.2

Armatures in series

T_{ta}	Pi_1	Pi_a	η_{ta}	W_{se}	Wm_a	We_a	W_a	Po_a	η_a	W_{ta}	η_{ta}
Vt = 24 V											
17.5	194	314	61.8	120	34.2	63.3	97.5	217	68.9	22.5	89.4
16.4	182	300	60.7	118	34.2	59.4	93.6	206	68.8	24.4	88.3
12.7	141	248	56.9	107	35.8	46.1	81.9	166	67.0	25.1	84.0
6.5	75.0	182	41.2	107	35.8	30.9	66.7	115	63.4	40.3	65.2
1.1	14.0	122	11.5	108	39.9	18.9	58.8	63.2	51.8	49.2	22.2
Vt = 36 V											
34.8	620	839	73.9	219	61.1	137	198	641	76.4	21.0	96.7
28.0	499	673	74.2	174	61.1	103	164	509	75.6	10.0	98.0
20.8	370	559	66.2	189	61.1	77.9	139	420	75.1	50.0	88.1
13.3	240	418	57.4	178	62.0	53.0	115	303	72.5	63.0	79.2
5.4	101	275	36.7	174	64.6	30.9	95.5	180	65.3	78.5	56.1
0.2	3.6	198	1.8	194	62.8	22.6	85.4	113	56.7	109	3.1
Vt = 48 V											
43.8	1073	1325	81.0	252	89.8	178	186	1139	86.0	66.0	94.2
30.2	740	995	74.4	255	89.8	119	209	786	79.0	46.0	94.1
23.5	581	821	70.8	240	91.7	90.7	182	639	77.8	58.0	90.9
16.7	416	663	62.7	247	91.7	67.4	159	504	76.1	88.0	82.5
10.2	256	489	52.4	233	92.6	44.6	137	352	72.0	96.0	72.7
3.1	79.0	356	22.2	277	93.6	29.9	124	232	65.2	153	34.1
Vt = 60 V											
46.5	1480	1858	79.7	370	123	199	322	1536	82.7	48.0	96.4
33.2	1015	1379	73.6	364	118	135	253	1126	81.7	111	90.1
24.4	741	1061	69.8	320	117	94.6	212	849	80.0	108	87.3
13.6	416	755	55.1	339	118	59.4	177	578	76.6	162	72.0
9.4	289	622	46.5	333	119	45.8	165	457	73.5	168	63.2
Vt = 76 V											
48.2	1888	2360	79.3	492	159	217	376	2004	84.2	116	94.2
40.1	1512	1935	78.1	423	152	169	321	1614	83.4	102	93.7
32.0	1186	1606	73.8	420	149	131	280	1326	82.6	140	89.4
23.3	874	1281	68.2	407	151	90.7	242	1039	81.1	165	84.1
13.8	517	927	55.8	410	151	61.3	212	715	77.1	198	72.3
9.6	360	760	47.4	400	151	46.9	198	562	74.0	202	64.1
Vt = 84 V											
49.2	2277	2794	81.5	517	196	224	420	2374	85.0	97.0	95.4
41.6	1856	2332	79.6	476	187	178	365	1967	84.3	111	94.4
33.2	1460	1944	75.1	484	184	139	323	1621	83.4	161	90.1
24.5	1078	1537	70.1	459	184	99.4	283	1254	81.6	176	86.0
15.2	675	1156	58.4	481	186	66.7	253	903	78.1	228	74.8
7.0	312	800	39.0	488	187	41.1	228	572	71.5	260	54.5

(continued)

TABLE A1.4 (continued)

T_{ta}	Ti_1	Pi_a	n_{ta}	W_{sa}	Wr_a	We_a	W_a	Po_a	n_a	V_{ta}	n_{ta}
Vt = 96 V											
50.2	2723	3403	80.0	680	240	241	481	2922	85.9	199	93.5
41.1	2112	2680	78.8	568	225	181	406	2274	84.6	162	92.7
30.9	1579	2156	73.2	577	222	134	356	1800	83.5	221	87.7
19.8	1008	1533	65.8	525	221	83.1	304	1229	80.2	221	82.0
12.1	621	1157	53.7	536	223	56.1	279	878	75.9	257	70.7
4.0	206	868	23.7	662	225	38.3	263	605	69.7	399	34.1
Armatures in parallel											
Vt = 24 V											
35.7	830	1099	75.5	269	84.3	142	226	873	79.4	43.0	95.1
28.6	659	912	72.3	253	83.4	108	191	721	79.1	62.0	91.4
19.7	458	701	65.3	243	84.3	73.6	158	543	77.5	85.0	84.3
16.7	392	643	61.0	251	85.2	65.3	151	492	76.5	100	79.7
11.1	263	490	53.7	227	86.2	45.2	131	359	73.3	96.0	73.3
Vt = 36 V											
45.7	1656	2016	82.1	360	145	194	339	1677	83.2	21.0	98.8
39.9	1437	1800	79.8	363	144	163	307	1493	82.9	56.0	96.3
28.9	1041	1397	74.5	356	144	110	254	1143	81.8	102	91.1
14.9	540	936	57.7	396	145	62.7	208	728	77.8	188	72.2
8.1	297	691	43.0	394	147	41.7	189	502	72.6	205	59.1
Vt = 48 V											
39.0	1879	2419	77.7	540	206	165	371	2048	84.7	169	91.8
33.2	1627	2150	75.7	523	211	137	348	1802	83.4	175	90.3
26.8	1291	1824	70.8	533	206	108	314	1510	82.8	219	85.5
14.5	717	1248	57.5	531	213	62.7	276	972	77.9	255	73.8
2.4	120	768	15.6	648	217	33.0	250	518	67.4	398	23.2
Vt = 72 V											
51.4	3735	4781	78.1	1046	352	254	606	4175	87.3	440	89.5
48.2	3563	4421	80.6	858	360	224	584	3837	86.8	274	92.9
37.4	2773	3672	75.5	899	361	168	529	3143	85.6	370	88.2
26.5	1981	2851	69.5	870	365	114	479	2372	83.2	391	83.5
13.1	999	1915	51.7	916	374	64.7	439	1476	77.1	477	67.7
6.2	474	1454	32.6	980	376	44.5	421	1030	70.8	559	46.0
Vt = 96 V											
51.4	4974	6566	75.8	1592	519	266	785	5781	88.4	807	86.0
35.9	3556	4973	71.5	1417	536	172	708	4265	85.8	709	83.4
24.3	2463	3859	63.8	1396	553	117	670	3189	82.6	726	77.2
11.6	1179	2515	46.9	1336	553	63.3	616	1899	75.5	720	62.1
3.4	353	1882	18.8	1529	571	42.8	614	1268	67.4	915	27.8

Symbols are as for Table A1.3 with subscripts changed for the disc motor from (a) to (b).

Appendix II

Results of tests on single version 10kW Disc Motor (enclosed)

The results shown in this Appendix are the raw results as taken down from tests on the disc motor. In addition to load tests. there are limited heat run tests. It also contains results of a blocked rotor test.

3.10.80 FRIDAY (1)

START UP 15.05

LOAD TEST 80 VOLTS AND 96

TIME	VOLTS	AMPS	SPEED	TM	TORQUE	PIN	POUT	%	TEMP
15.15	72	73.5	3000	2.45	12.67	5292	3981	75	27.2
15.30	72	76.0	3100	2.1	10.86	5400	3526	65	30.0
SHUT DOWN TO CHECK TM ZERO O.K.									
START UP 15.35									
15.37	80	90	3462	2.75	14.22	7200	5156 3626	72	43.0
15.40	93.2 92.4	110	4000	3.35	17.32	10252	7256	71	46.0
15.42	96	114	4134	3.36	17.37	10944	7521	69	49.0
15.45	96	115	4162	3.3	17.06	11049 10944	7437	66	53.0
15.50	96	117.5	4211	3.18	16.44	11280	7251	64	60.6
					POINT = 0				
LOAD TEST 48 VOLTS									
16.03	48	47	2226	1.3	6.72	2256	1427	63	61.3
04	48	57.5	2196	1.68	8.69	2760	1999	72	61.6
06	48	64.0	2186	1.9	9.82	3072	2248	73	62.3
	"	70.0	2167	2.12	10.96	3360	2487	74	62.7
08	"	81.0	2144	2.6	12.93	3888	2903	75	62.9
	"	87.5	2129 2136	2.7	13.96	4200	3113	74	63.5
11	"	100.0	2098	3.16	16.34	4800	3591	75	64.3
	"	111.0	1980	3.5	18.1	5326	3659	69	64.5
LOAD TEST 72 VOLTS									
16.15	72	83.4	3215	2.45	12.67	6012	4266	71	66.0
17	"	94	3164	2.82	14.58	6768	4831	71	66.7
	"	102	3146	3.05	15.77	7344	5196	71	67.2
	"	118	3130	3.56	18.41	8496	6035	71	68.2

SHUT DOWN TM ZERO -0.05

LOAD TEST 24 VOLTS.

TIME	VOLTS	AMPS	SPEED	TM	TORQUE	PIN	POOT	?	TEMP
							216.8		
6.25	24	17.5	1000	0.4	2.07	420	~~41.89~~	52	66.9
	"	29.0	980	0.8	4.14	696	425	61	67.4
	"	39.5	950	1.2	6.21	948	618	65	67.7
	"	44.0	943	1.35	6.98	1056	689.4	65	67.9
	"	63.5	900	2.05	10.6	1524	999	66	67.0
	"	76.0	875	2.5	12.93	1824	1185	65	67.82
	"	87.5	846	2.9	15.00	2100	1329	63	67
	"	101.5	816	3.42	17.68	2436	1511	62	67.6.
	"	111.0	795	3.7	19.13	2664	1593	60	67.0
SHUT DOWM									

BLOCKED ROTOR TEST

I		TM	N-M TORQUE
10	0	.4	2.07
22	0	.75	3.88
31	0	1.05	5.43
39.5	0	1.3	6.72
49	0	1.65	8.53
67	0	2.25	11.6.

0.9.80.

(3)

ME	TEMP	VOLTS	AMPS	TORQUE	SPEED	~~I~~PIN	TNM	POUT	?
3	21.0	72	73	~~2.2~~ 2.17	~~2216~~ ?				
0	38.0	~~72~~	77	~~2.07~~	2330 ?				
UT	DOWN TO CHECK ZERO ON TM.								
2	48.0	72	81	2.45	3143	5832	12.47	4177	72
0	54.6	72	81	2.36	3200	5832	12.15	4072	70
02	56.7	80	93	2.65	3558	7440	13.7	5105	69
5	59.5	80	93	2.65	3572 [374]	7440	13.7	5125	69
0	63.0	80	94	2.62	3591 [376.1]	7520	13.55	5095	68
5	66.5	80	94.5	2.6	3632 [380.4]	7560		5113	68
20	70.0	80	95.0	2.6	3661	7600	13.44	5154	68

10.9.80.

(3)

ME	TEMP	VOLTS	AMPS	TORQUE	SPEED	~~I~~PIN	TNM	POUT	?
3	21.0	72	73	~~2.2~~ 2.17	~~2216~~ ?				
0	38.0	~~72~~	77	~~2.07~~	2330 ?				
UT	DOWN TO CHECK ZERO ON TM.								
2	48.0	72	81	2.45	3143	5832	12.47	4177	72
0	54.6	72	81	2.36	3200	5832	12.15	4072	70
02	56.7	80	93	2.65	3558	7440	13.7	5105	69
5	59.5	80	93	2.65	3572 (374)	7440	12.7	5125	69
0	63.0	80	94	2.62	3591 (376.1)	7520	13.55	5095	68
5	66.5	80	94.5	2.6	3632. (380.4)	7560		5113	68
20	70.0	80	95.0	2.6	3661	7600	13.44	5154	68

10.10.80 FRIDAY HEAT RUN @ 96 VOLTS.

START UP 10.49

×5.17 for T in Hmetres

AMPS	VOLTS	R.P.M. SPEED	TEMP	TIME	TM	ℓ.
		3886			3.1	
99	93	~~2207~~	16.5	10.56	~~276~~	
103	96	3874	24.0	11.00	3.05	
04	96	3936	31.0	11.05	2.95	
07	96	3998	38.0	11.10	2.95	
2	95.5	4061	47.0	11.15	3.0 (18.5)	62%.
4	94.5	4080	54.5	11.20	3.0 -	62%.
				11.25	- smoke from	

No load power input - earlier test on 15/9/80

I	V	RPM	TEMP °C	TIME.	
4.3	11	510	46.3		
5.2	24	1080	46.0		
6.1	32.6	1500	46.0		
6.5	38	1760			
7.1	46.6	2250	46.5		
7.5	55.0	2500	47.0	12.23	
7.5	59.6	2750	48.1		
7.7	64.0	3050	488		
7.8	68.2	3250	50.3		
7.9	72.6	3500	509		
7.9	81	3900	52		
~~8.0~~	85.4	4000	reading upone. space	12.38	Nominally constant speed at regular intervals; current reduces
7.8	85.4	4000	54.2	12.45	
7.6	85	4000	58	12.50	
7.4	85	4000	61.2	12.55	
7.2	85.4	4100	63.8	13.01	
7.2	85.0	4100	66.8	13.05	
7.2	86	4200	687	13.10	

-380-

Current reduces as temp speed increases

DYNAMOMETER DISCONNECTED.

TIME	TEMP	VOLTS	AMPS	TM	SPEED	PIN
4.40	31.5	80	17.5	.17	3423	1400
4.45	26.6 (5.4)	80	15.0	0.0	3426	1200
4.50	32.0 (4.5)	80	15.0	0.0	3486	1200
4.55	36.5 (4.2)	80	14.0	0.0	3545	1120
5.00	40.7 (3.8)	80	13.8	0.0	3568	1104
5.05	44.5	"	13.8	0.0	3626	1104
5.10	48.1 (3.6)	"	13.5	0.0	3641	
REDUCE SPEED						
	49.0	60	12.0	0.02	2779	
	50.0	48	11.0	0.02	2216	
	50.0	36	9.8	0.1		
	50.5	24	8.0	0.1	1072	
	50.0	12	6.5	0.1	630	

TORQUEMETER 0.0.

Note no load temperature rise. and speed increase.

Appendix III

Tests to Determine the Performance Characteristics of the Lee-Dickens 10 KW Disc Motor

1. Introduction

These tests were carried out during the period 5th November to 5th December 1980 on a second build of this particular motor.

For this build a new armature was fitted and a means of adjusting brush position incorporated.

A series of six 15 mm dia. holes were also drilled around the periphery of the casing in line with the disc armature to assist motor ventilation.

2. Test Rig and Instrumentation

The test rig was identical to that used for the first build of the motor. A Heenan & Froude Hydraulic Dynamometer provided the load. This was driven through a shaft which incorporated a torque meter and fly-wheel. The flywheel was originally incorporated in order to damp out any load fluctuations which might occur when operating the Dynamometer at the bottom end of its load range and was also available for carrying out any subsequent transient tests. The layout of the test rig is shown in Fig. 1.

Speed was measured by means of an electro-magnetic transducer placed adjacent to the coupling flange. This gave an output of eight pulses per rev. which was fed to a counter displaying RPM directly.

Current and voltage were measured using standard meters.

Motor temperatures were measured by means of thermocouples positioned at the following locations:

1. On the outside of the motor casing.

2. Adjacent to the outer race of the non-drive end bearing.

3. On the side of one of the permanent magnet pole pieces.

3. Tests and Results

Prior to carrying out load tests the brushes were first set to the optimum position. A series of preliminary tests were then carried out followed by the following main tests, the results of which are included in this report.

a) No Load Tests

These tests were carried out with the motor output coupling disconnected. Input power and speed were measured for a range of supply voltage. Tests were repeated at different temperature levels. The results are shown in Fig. 2.

b) Load Tests

During the preliminary tests it was found that the motor speed for any set voltage and motor load was extremely sensitive to temperature. To obtain consistent performance data therefore, all load tests were

carried out with the motor at high temperature where temperature changes were small over the period of each test.

Performance data at 24, 48, 72 and 84 volts are given in Figs. 4 to 7. Performance data at 48 volts is also given in Fig. 5 with the motor at a lower temperature.

Motor speed at 84 volts was in excess of the design speed of 4000 rpm therefore no tests were carried out at higher voltages.

c) Heat Run

The final test carried out was at 84 volts and a constant input current of 100 Amps (Power Input 8.4 KW), from cold. Initially, as temperatures increased, the speed increased, however part way through the test there was a period when the speed decreased before increasing again at the normal rate. (Fig. 8) Finally after 30 minutes running and with the motor casing at a temperature of 70°C smoke was emitted from the motor and the test was abandoned. Examination of the armature through one of the ventilation holes indicated that damage to the armature had occurred. It is considered that the period when speed decreased was associated with deterioration of the armature.

4. Discussion

The most significant result arising from these tests has been the large variation of motor speed with temperature. The characteristics of the permanent magnet material are such that a reduction of flux of 0.2% per °C would be expected which would directly affect the motor speed. Fig. 8 however indicates a much higher value than this.

A further related point which arises is that at 96 volts the speed would be approximately 4700 rpm compared with the design speed of 4000 rpm.

The measured performance data given in Figs. 4 to 7 indicates a progressive increase in peak efficiency with motor voltage. The first series of tests carried out at 84 volts gave a peak efficiency of 80%, however subsequent tests carried out just prior to armature failure gave higher efficiencies, approaching 87%. For the second tests the motor had been running for a long period at high temperature and the whole motor was probably at a higher temperature than during the first tests (this tends to be confirmed by the motor running at a higher speed). The reason for the higher efficiency was the higher speed since all other readings were identical.

The no-load test results of Fig. 2 have been processed on the basis that friction torque is independent of speed. This has enabled values of friction and windage power loss to be evaluated separately also the variation of friction loss with temperature has been determined as shown in Fig. 3.

The high value of bearing friction when cold was apparent during tests where, during the first 15 minutes of running, the bearing temperature always increased at a faster rate than any other temperature on the motor. It is considered that this is probably associated as much with bearing seal friction as friction in the bearing itself.

During the course of the tests it was not possible to stabilise temperatures below 70°C casing temperature at any load above 3-4 KW. Obviously a serious study of motor cooling is essential.

5. Conclusions

1. Due to speed limitations it was not possible to carry out any tests at voltages exceeding 84 volts.

2. The maximum power output at 84 volts was 8.5 KW at 120 amps. At this point the speed was 4200 rpm and with the motor at high temperature the efficiency was 85%. It is considered that running at this condition for even the short period of the tests caused damage to the armature.

3. The motor speed was found to be extremely sensitive to temperature. This is an aspect which requires further investigation.

4. Except for the high temperature test referred to in (2) all efficiencies were below 80% and generally efficiency was also found to be sensitive to temperature.

5. Temperature also had an effect on bearing friction losses. It is considered that a different type of bearing mounting arrangement and different bearing seals should be considered.

6. Motor cooling is completely inadequate and a serious study of this aspect is essential.

17th December, 1980.

10 KW Disc Motor Test Rig

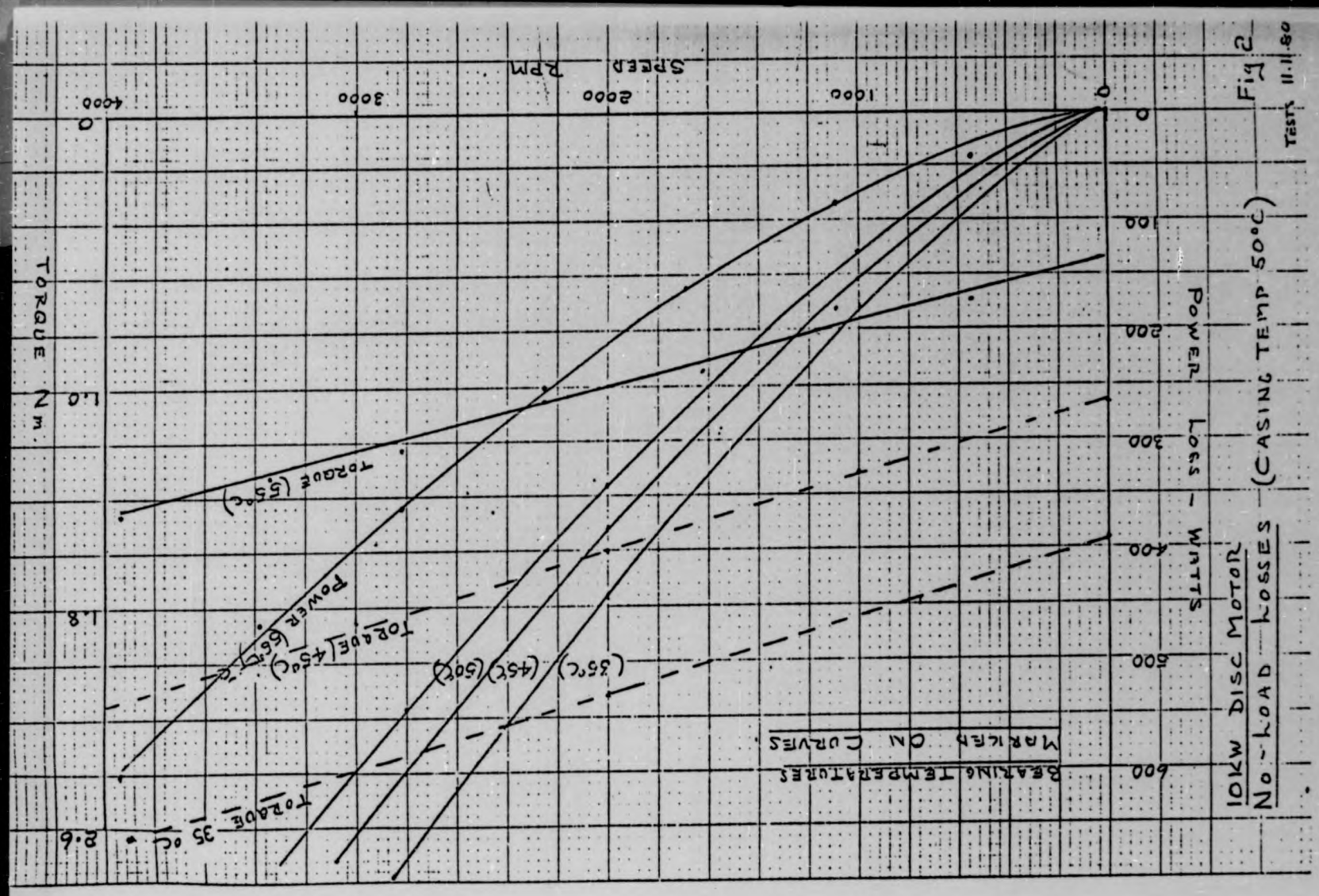
10KW DISC MOTOR
No-LOAD LOSSES (CASING TEMP 50°C)
Fig 2
Tests 11.11.80
POWER LOSS - WATTS
SPEED RPM
TORQUE Nm.
BEARING TEMPERATURES
MARKED ON CURVES
(35°C) (45°C) (50°C)
TORQUE 35 o/l = 2.6
TORQUE (45°C)
POWER (65°C)
TORQUE (50°C)

Fig

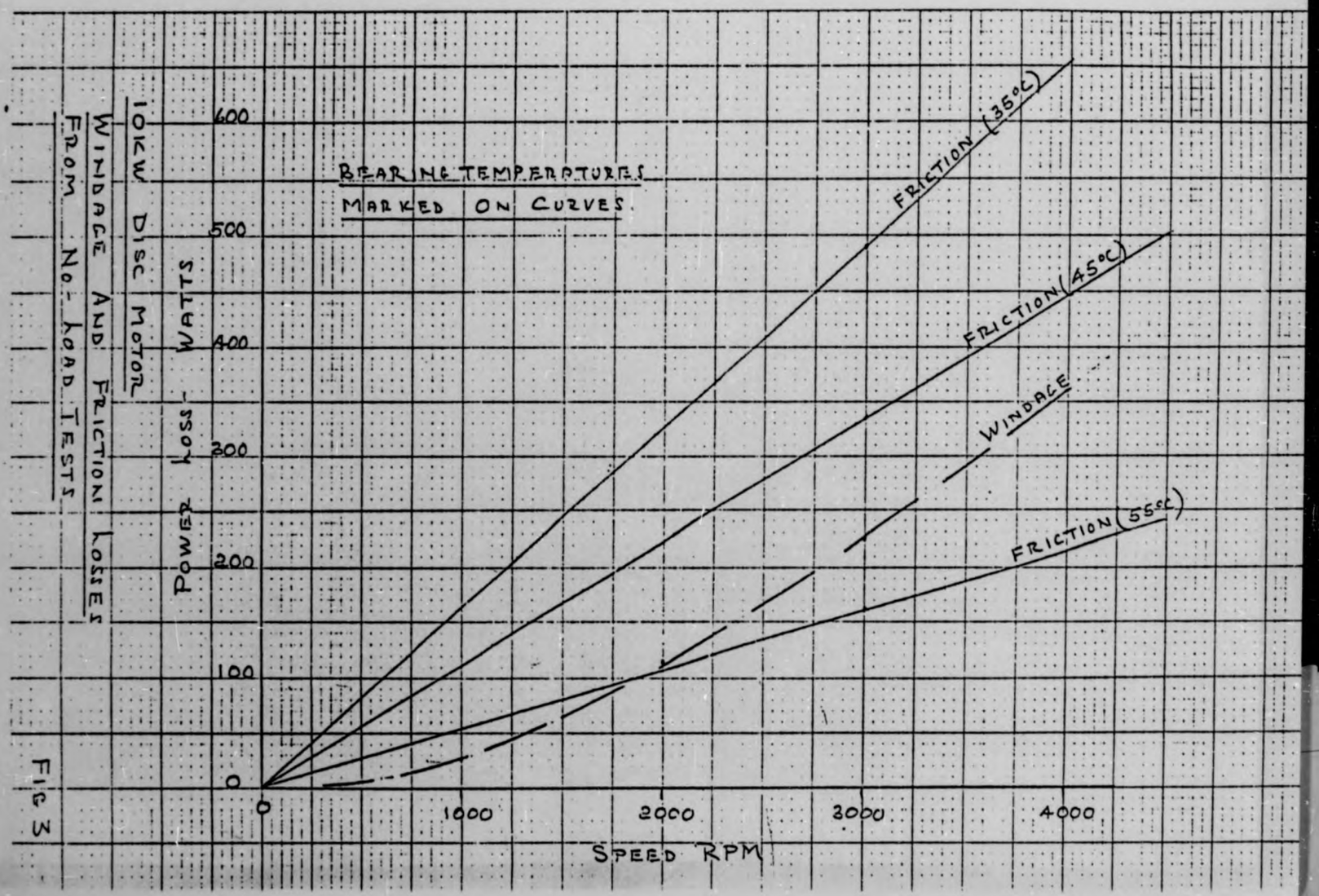

10KW Disc Motor

Windage and Friction Losses from No-load Tests

Fig 3

701

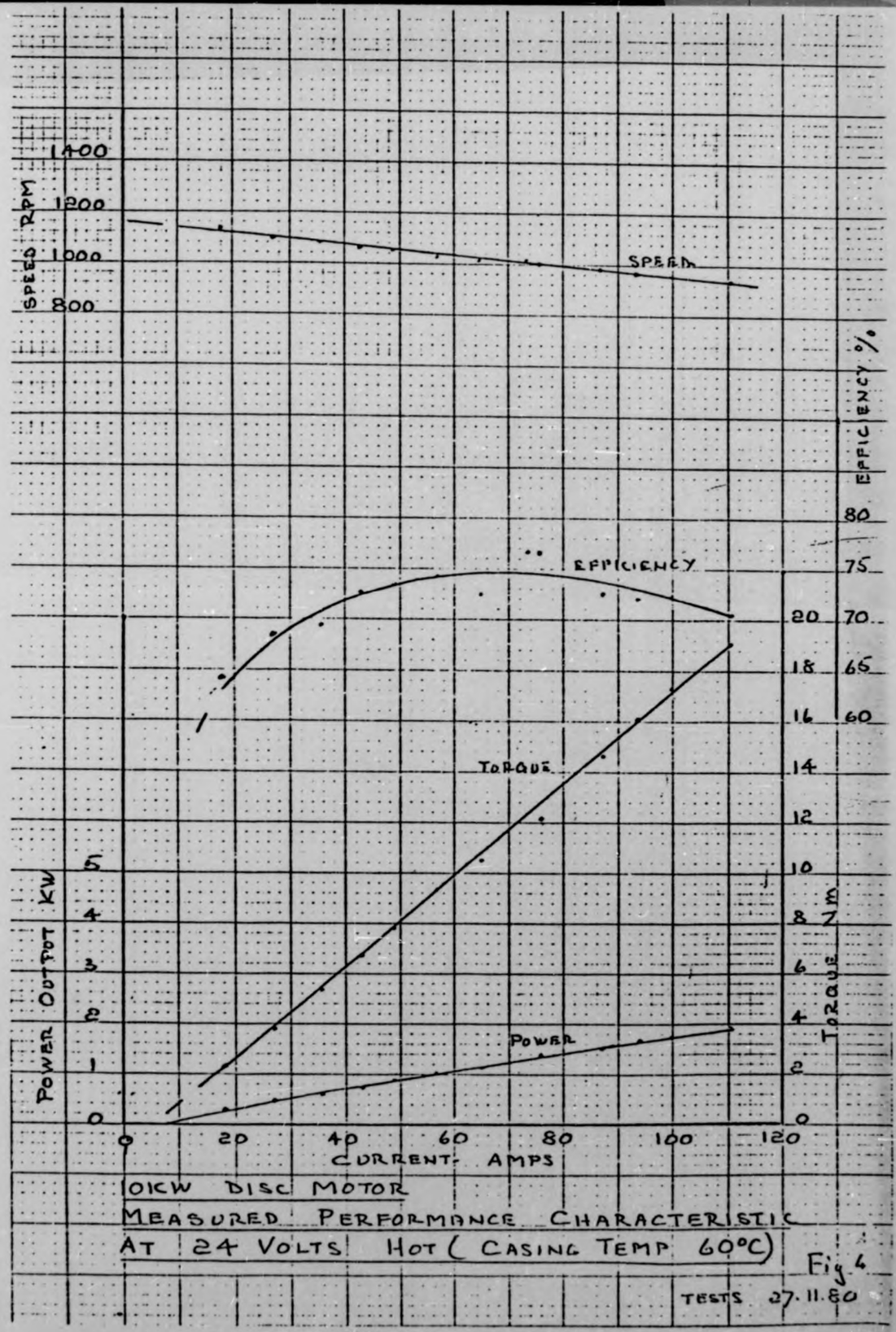

10KW DISC MOTOR
MEASURED PERFORMANCE CHARACTERISTIC
AT 24 VOLTS HOT (CASING TEMP 60°C)

Fig 4

TESTS 27.11.80

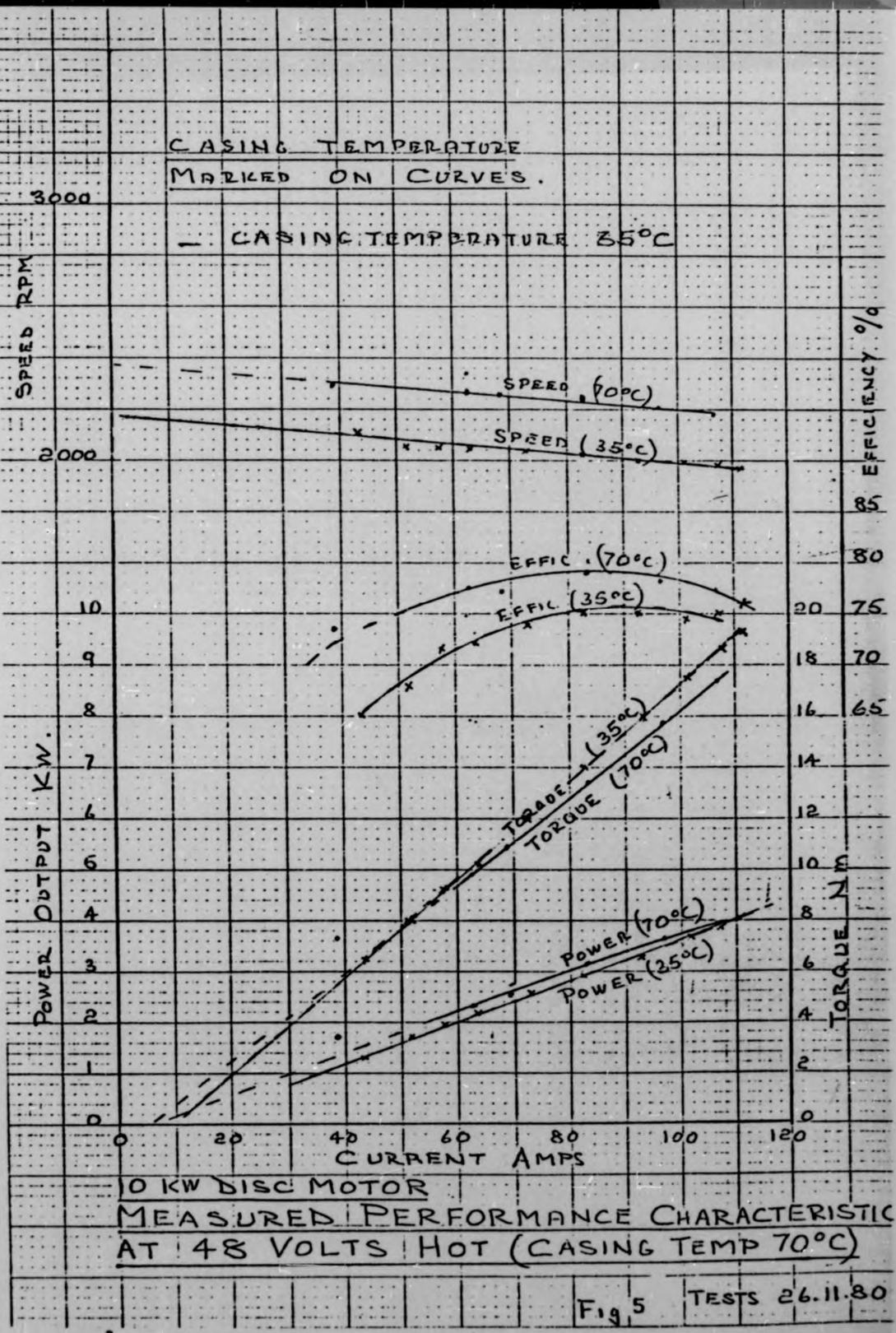

10 KW DISC MOTOR
MEASURED PERFORMANCE CHARACTERISTIC
AT 48 VOLTS HOT (CASING TEMP 70°C)

Fig 5 TESTS 26.11.80

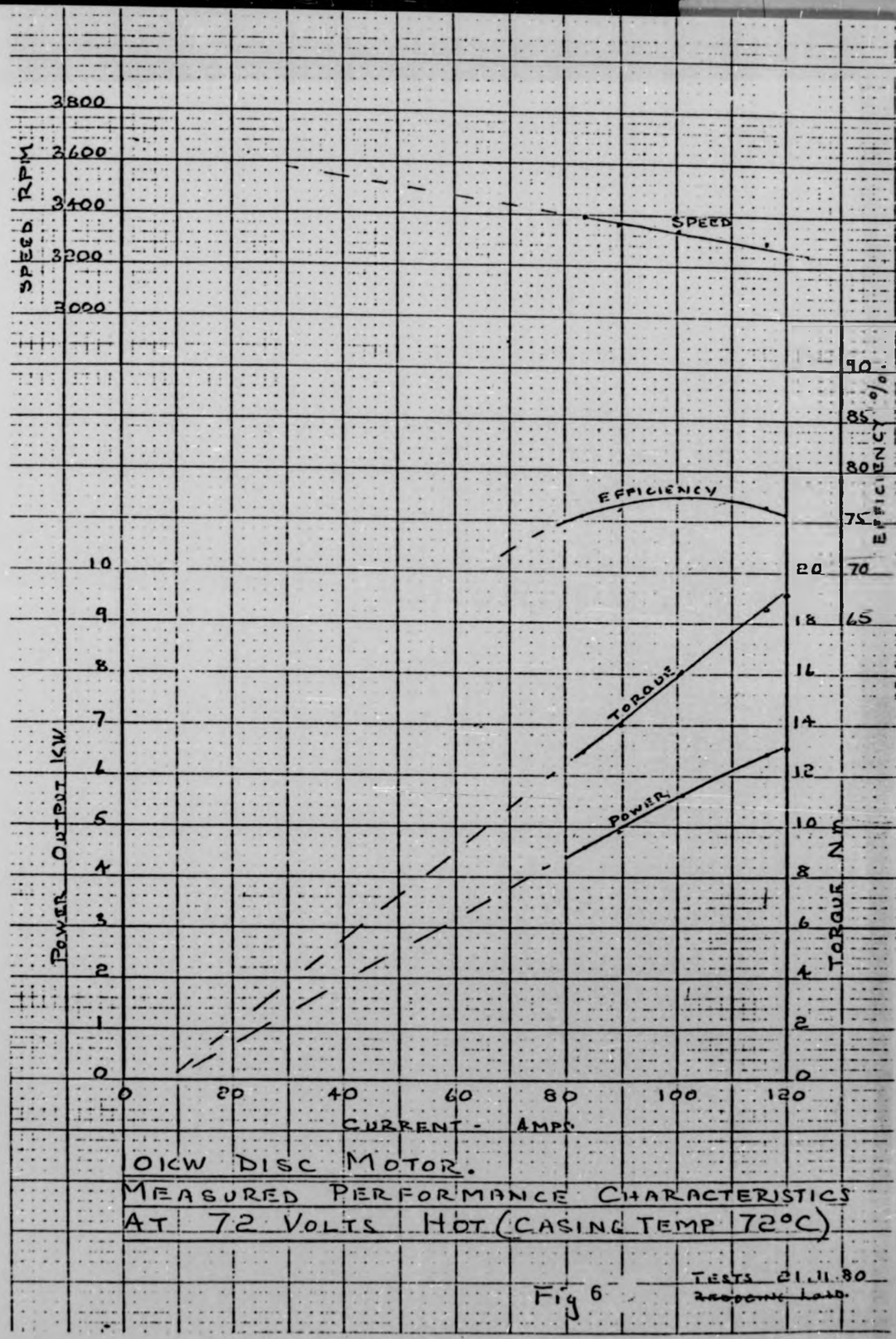

OICW DISC MOTOR.

MEASURED PERFORMANCE CHARACTERISTICS AT 72 VOLTS HOT (CASING TEMP 72°C)

Fig 6

TESTS 21.11.80
~~RESPONSE LOAD~~

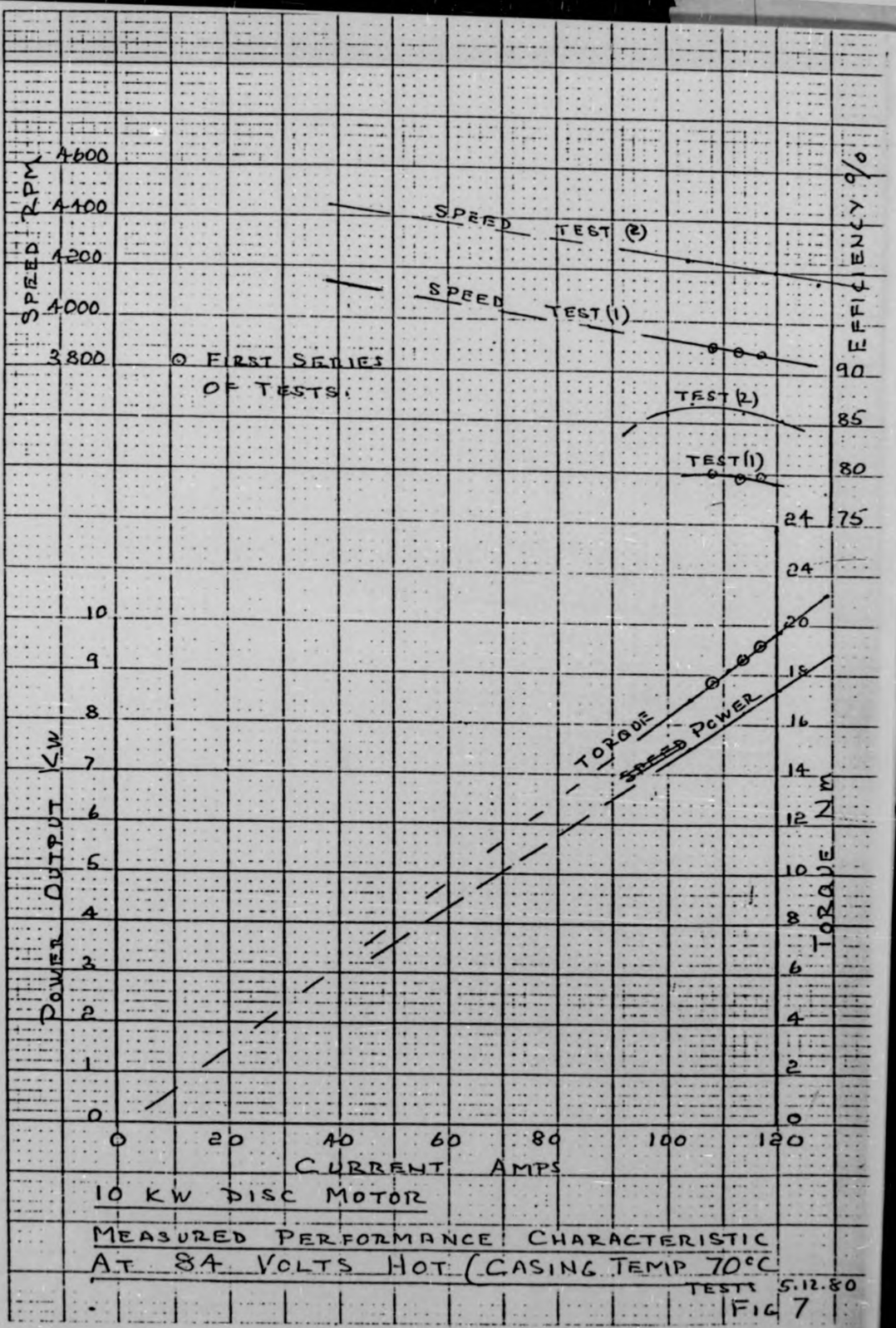

10 KW DISC MOTOR

MEASURED PERFORMANCE CHARACTERISTIC

AT 84 VOLTS HOT (CASING TEMP 70°C

TEST: 5.12.80

FIG 7

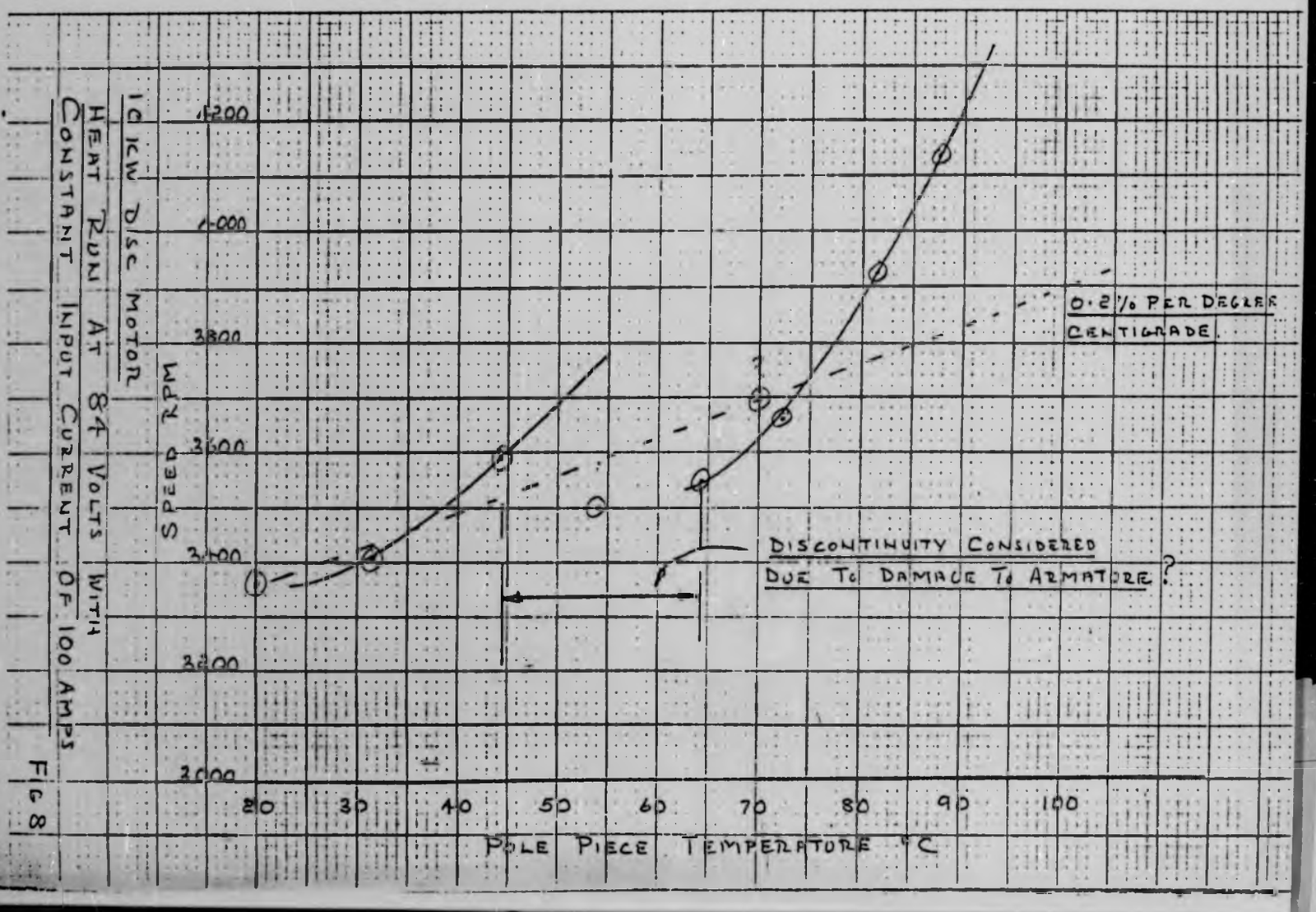

IC ICW DISC MOTOR

HEAT RUN AT 84 VOLTS WITH CONSTANT INPUT CURRENT OF 100 AMPS

Fig 8

Appendix IV

NeIGT (Neodymium-Iron-Boron) permanent magnet material and magnetic characteristics

Magnetic Characteristics	NeIGT 27	NeIGT 35
Peak Energy Density—(B_0H_0) MGO —kJ/M³	27 *216*	35 *280*
Residual Induction B_r—Gauss —mT	10800 *1080*	12300 *1230*
Coercive Force H_c—Oersted —kA/M	9600 *765*	9800 *780*
Intrinsic Coercive Force H_{ci}—Oersted —kA/M	10500 *835*	10200 *810*
Magnetizing Force H_s—Oersted —kA/M	35000 *2000*	35000 *2000*
Recoil Permeability	1.1	1.1

Material Characteristics		
Density—lb./cu. in. —g/cm³	.268 *7.4*	.268 *7.4*
Curie Temperature—°C	310	310
Operating Temperature—°C (Dependent upon operating slope and duty cycle)	up to *150*	up to *150*
Temperature Effects Of Induction For Magnets: Reversible—%/°C at B_0H_0 Irreversible—% to 125°C at B/H = 5	 −.125 < 3	 −.125 < 3
Mechanical Properties—Tougher than Alnico and $SmCo_5$; subject to less cracking and chipping.		

Note: All characteristics are shown for comparison purposes only. Operating values are determined by magnetic circuit design.

A—Axial, field parallel to pressing direction
I—Isostatic, preorient any direction

Demagnetization and Energy Product Curve

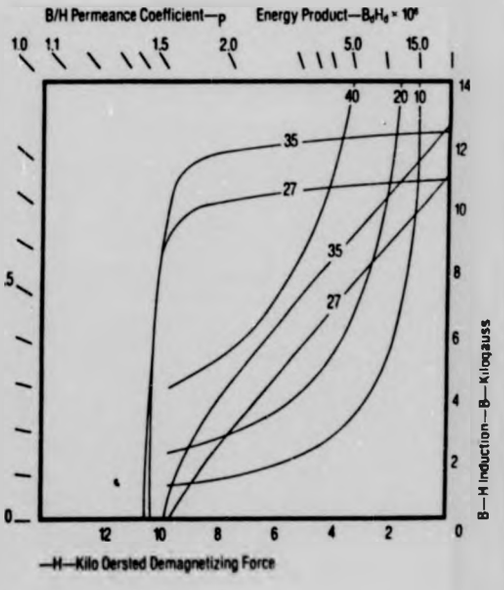

Appendix V Published Papers

The reprints submitted here have been published jointly with the author's supervisor and emanate from, or relate to, the work described in this Thesis. In order, the Papers are:

"Design and performance of D.C. disc armature motors for traction applications" presented at the Fifteenth Universities Power Engineering Conference, 3B2, Leicester, March 1980.

"Disc Armature Traction Motors" presented at the Drive Electric 80 Conference, October 1980.

"Design and Performance of a 10kW D.C. Disc Motor with Ferrite Magnets" presented at the International Conference on Electrical Machines, September 1982, Budapest, Hungary.

"Design and Performance of 10kW Disc Motor for Electric Vehicle Drives" presented at Drive Electric, Amsterdam, October 1982.

DESIGN AND PERFORMANCE OF DISC-ARMATURE D.C. MOTORS FOR TRACTION APPLICATIONS

M.R.N.Ali, A.E.Corbett, M.A.Özpolat (University of Warwick)
and C.S.Roerig (Moore Reed and Co Ltd).

1. Introduction

The disc-armature d.c. motor has potential for use in electric traction because of its high operating efficiency and good power density. This improved performance over conventional machines results from the elimination of all iron losses in the machine and the use of a multi-polar permanent-magnet field system. As the field is axial the active conductors have to be oriented radially, with circumferential end-windings, and the armature is thus constructed of individual pre-formed coils nested together to form a thin multi-layer disc (Fig.1). The coils are connected to a conventional commutator and the usual lap, wave and duplex windings are all possible. The complete assembly is encapsulated in epoxy resin for rigidity and mechanical strength and therefore there is no rotating iron in the motor. Furthermore the low inertia of the armature gives good dynamic response in applications where this is desirable[1]. A complete motor assembly is shown in Fig.2.

2. Magnet Materials

A wide range of magnetic materials is available for use in these motors, ranging from sintered ferrite to the more exotic rare-earth materials. Specifying which material to use depends largely on the motor application[2], but as the airgap of the machine is relatively large, comprising the complete disc thickness and a suitable running clearance on each side, materials with a high coercive force are usually the most appropriate. This is particularly the case in traction applications where the need for high mechanical strength under arduous duty cycles, and several layers of relatively heavy-gauge wire often lead to a large disc thickness. Ferrite materials are particularly suitable here because they have a high coercivity, and also the added advantage of being the cheapest material available. However, since the working flux density and the energy density are relatively low it is sometimes necessary to specify alternative materials although these generally cost much more.

The use of high remanence magnets means that it is easier to design an efficient machine, but because of the reduction in coercive force a large amount of the material will be needed when a large air gap is also required. For these reasons ferrite magnets are specified wherever possible and it has been found[3] that the cost advantage in doing so generally far outweighs the small reduction in motor efficiency. One method of reducing the effective airgap in the machine is to introduce iron powder into the epoxy resin used for encapsulating the armature.[4] However, this also introduces hysteresis and eddy-current losses into the machine and results in magnetic pull between stator and rotor.

3. Use as a Traction Motor

It was envisaged at an early stage that the motor would prove advantageous for battery traction applications, and the first prototypes were built for this purpose.[5,6] More recent work has involved designing and constructing prototypes for applications varying from an electrically driven moped to a high-performance hybrid car. One aspect of the work has been the comparison of disc-motor performance with that of a conventional series-wound traction motor. A small three-wheeled car has been converted to electric drive for evaluation of the motors. Typical efficiency curves are shown in Fig.3 and the benefits of disc-motor drive are apparent over all operating conditions.

In terms of vehicle performance an increase of 20% in steady-speed range may be expected when a disc-armature motor is used.

It has been found that in many battery traction applications an inefficient drive system can be replaced with a disc-motor correctly matched to a high-performance mechanical transmission. The benefit can be taken as extended range and/or reduced battery requirement.

The limited performance of electric vehicles has been the subject of much recent debate, and one solution is the hybrid electric vehicle. In one such vehicle, battery power is augmented by a diesel driven generator. Fig.4 shows a twin-rotor disc-motor which has been specially developed for a hybrid car. The two armatures operate independently in a common magnetic circuit and each armature drives one rear wheel of the vehicle through an efficient belt drive. Thus differential action is accomplished electrically, eliminating the need for the conventional final drive, a source of heavy losses in many electric vehicles.

4. Motor Design

The design of a d.c. disc- armature motor is a straightforward process. With reference to Fig.5 it can be shown that for maximum power from the machine the relationship $r_2 = \sqrt{3}\, r_1$ must be satisfied. Also, for a given magnet material, the actual power output is proportional to the cube of r_2. It is possible to derive an equation relating the speed, power and voltage of a motor to the optimum value of r_2. Other important factors to consider are the number of poles and coils to be used. Specifying too few poles leads to excessively long end-windings thereby increasing the associated I^2R loss. On the other hand, since for commutation reasons, a minimum number of coils/pole must be specified, a large number of poles can result in an excessive number of coils and commutator segments, and ultimately in impracticable solutions. Also, magnetic leakage increases with pole number. Even with these limitations a large number of feasible alternatives can be considered to meet a design specification. It would certainly be a tedious process to design by hand even several of these options for optimization over efficiency or power density, but fortunately digital computing techniques can be used to advantage here. Several programs have been written which ease the burden on the motor designer, and the most powerful version produces a series of alternative designs when given the power, speed and voltage requirement. In addition the designs for optimum efficiency and power density are output separately. It is also possible to specify in more detail parameters such as number of poles, number of coils, gauge of wire, any size limit, type of winding, magnet working point,etc. This would normally be a second stage of the procedure and the final step is the complete specification of one design with a set of predicted performance curves included in the output.

5. Motor Performance

An important factor in traction applications is the thermal behaviour of the motor, especially when related to conditions of overload. Conventional motors have a large mass of iron in the rotor to absorb the heat produced by the armature windings. By comparison the heat storage capability of a disc-motor is poor, and the thermal performance must be based upon how quickly heat from the armature can be dissipated. The use of permanent magnet means, of course, that there is no heating from field windings. The epoxy resin used for armature encapsulation must be able to withstand high temperatures without undue flexing, but it must also be able to accommodate expansion of the copper it surrounds. Good heat transfer results from the armature conductors being close to the surface of the disc and the large surface area presented by the disc geometry. The naturally induced radial airflow can assist in the cooling process.

Practical tests have involved temperature measurements while the motor is on load. This enables allowable temperature rise in the disc to be determined along with an assessment of permissible magnitudes and durations of armature current. Fig.8 gives results of a heat run on the motor shown in Fig.2 . The thermal time constant is about 60 minutes and this is shorter than in conventional machines of similar output. Results have shown that the motor is able to run continuously

with an armature temperature of 108°C which corresponds to twice the design current. As in conventionally constructed machines even higher overloads can be tolerated for shorter period of time - an important consideration in traction applications. No significant armature distortion or deflection has been noticed during testing.

6. Motor Control

The control of d.c. machines is a well-researched subject and in the field of battery electric vehicles there are several methods available.[7,8] Resistive control and battery switching have long been used although these are generally inefficient and unsophisticated. Developments in semiconductor technology have allowed the thyristor controller to provide an efficient if relatively expensive solution, but secondary effects related to battery and/or motor life and performance have yet to be accurately determined. This type of controller operates by switching the supply voltage across the motor for varying periods of time at frequencies typically in the range 300 - 1000 Hz. The inductance of the motor windings ensures that current flows continuously in them to give smooth, variable-speed operation.

Battery switching and resistive control may easily be applied to disc-armature motors, but when using chopper controllers account must be taken of the extremely low armature inductance. The switching element will be applied to what is almost pure resistance and the armature current will tend to follow the applied voltage waveform. The high degree of current ripple can have an adverse effect on the motor/controller combination, and indications are that controllers with normal switching frequencies will generally be incompatible with this type of machine. Specifying a much higher switching speed means that thyristors are no longer suitable and the high power switching transistor must be used. A controller of this type has been built for an electric car but for efficient operation the frequency has had to be limited to about 6 kHz. To give acceptable ripple it has been calculated that frequencies around 50-60 kHz are needed and therefore, unless suitable advances are made, it would appear that extra inductance will have to be added to the motor circuit when controllers of this nature are to be used.

7. Conclusions

The disc-armature motor has been shown to have significant advantages when used in traction applications. The efficiency and power density are improved over comparable d.c. machines and the motor performs well under conditions of overload. Care must be exercised when specifying the control system when chopper-type drives are to be used. Further work on various on-going projects will enable more experience of the traction use of the motor to be gained.

8. Acknowledgements

The authors gratefully acknowledge the support of Cableform Ltd, Lee-Dickens Ltd, and Moore Reed and Company Ltd.

9. References

1. Corbett, A.E., and Mohammad M.T., 1976. 'The disc-armature d.c. motor and its applications', IEE Conference Publication 136, Small Electrical Machines, 59-62.
2. Corbett, A.E. and Roerig C.S., 1978. 'Selecting permanent magnet materials for disc-armature d.c. motors', International Conference on Electrical Machines, Brussels, SP 4/2.
3. Corbett, A.E. and Roerig C.S., 1979. 'The economic design of disc-armature traction motors' Unpublished Report, University of Warwick.
4. Stott, G., 1971. 'Iron powder compacts for electromagnetic applications', M.Sc. thesis, University of Warwick.
5. Corbett, A.E. 1970, 'A disc armature d.c. motor', EMPO Conference, Dundee, 42.
6. Campbell, P. 1972, 'A new wheel motor for electric commuter cars', Elec Review, Vol. 190, 10.
7. Morrison, J.J.,'Electronic Control of Battery Electric Vehicles,'The Radio and Electronic Engineer, Feb. 1972.
8. Murphy, G.J., 'Alternative Approaches to Speed Control in Electric Vehicles' SAE paper 780292, 1978.

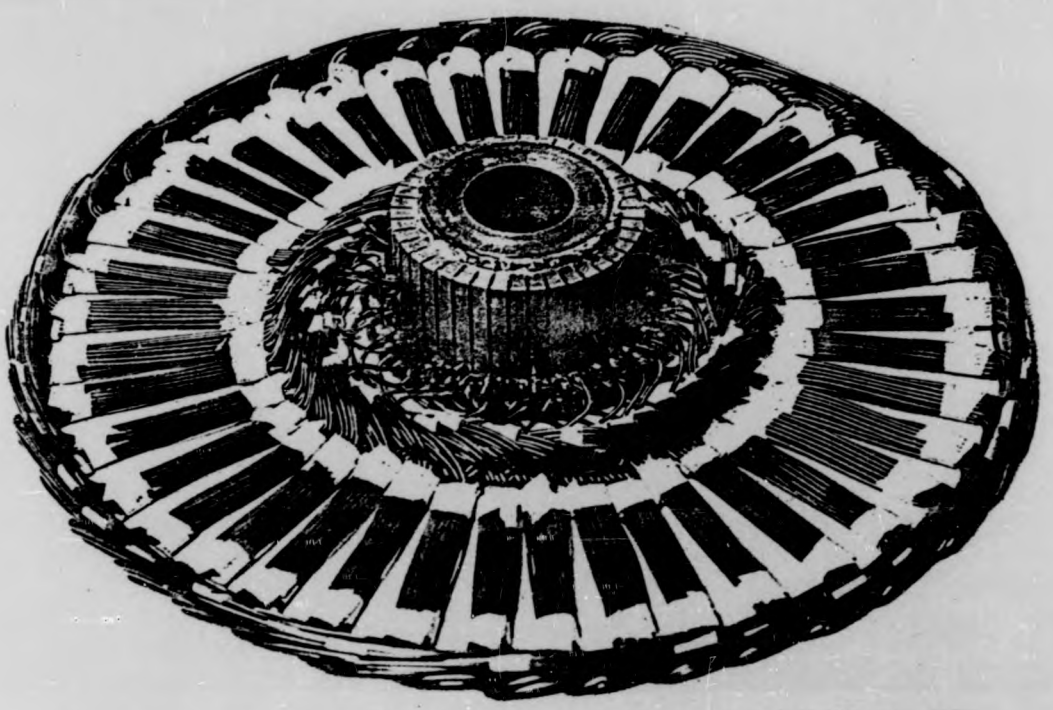

Fig. 1. Armature prior to moulding.

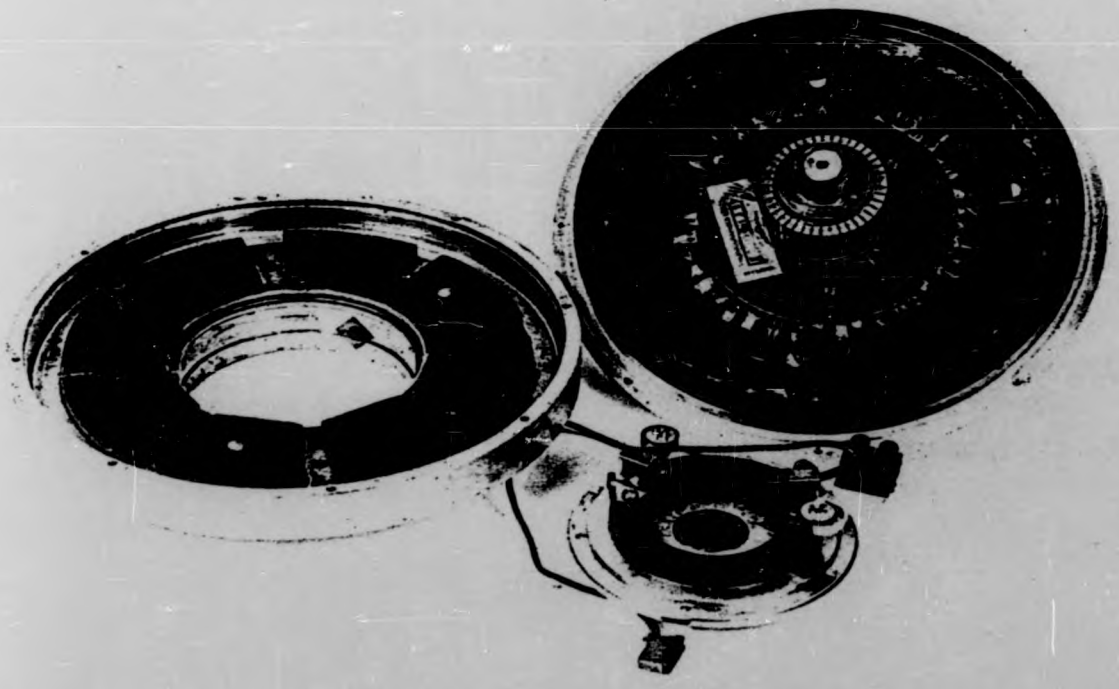

Fig. 2. Components of a typical disc-armature motor.

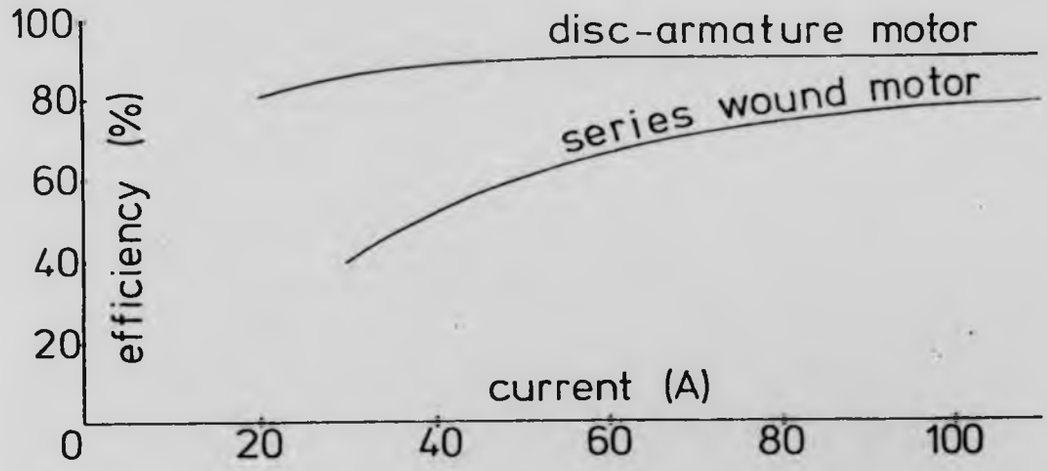

Fig. 3. Comparative efficiency curves

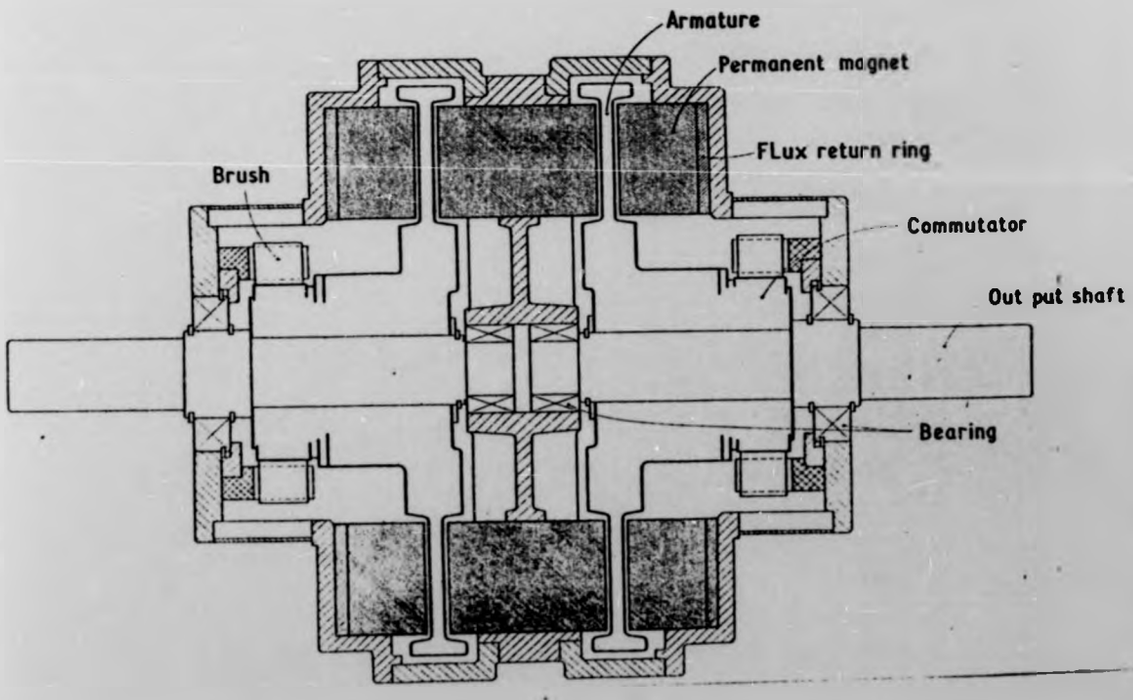

Fig. 4. Twin rotor disc-armature motor for hybrid car drive

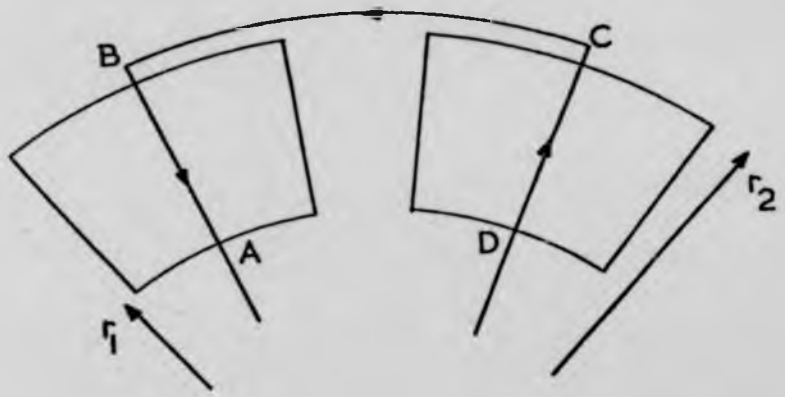

Fig. 5. Schematic of magnets with a single-turn coil.

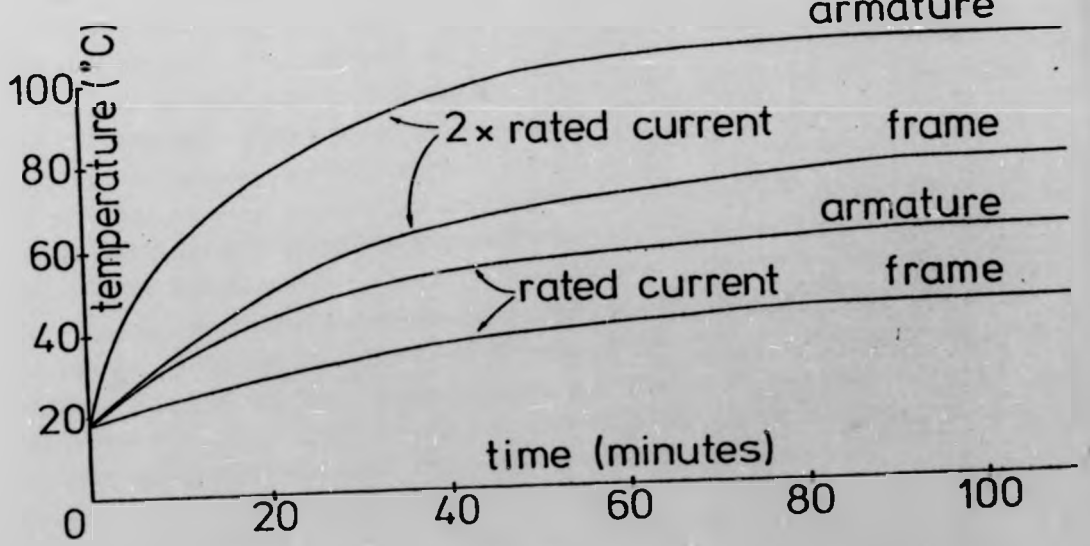

Fig. 6. Results of heat runs on disc motor

DISC ARMATURE TRACTION MOTORS

M.R.N. Ali, C. Anscomb and A.E. Corbett (University of Warwick)
C.S. Roerig (Moore Reed and Co. Ltd.)

1. INTRODUCTION

While the major limitation on electric vehicle performance remains that imposed by the lead/acid battery every effort must be made to ensure the most efficient use of the energy available for vehicle propulsion. On an energy per unit weight basis petrol can have up to 200 times that of a lead/acid traction battery[1] with obvious advantages for road transportation. Two parameters of the electric traction motor which have considerable bearing on the overall vehicle performance are the efficiency and power density (ratio of motor power to motor weight). The disc armature d.c. motor is superior in both respects to the conventional series wound motor which has been an almost universal choice for battery electric traction applications.

The topology of the machine is radically different from conventional machines in that the active conductors run radially and are encapsulated in a plastic material (e.g. epoxy resin) to form a thin disc. It is thus necessary for the working magnetic flux to be oriented in the axial direction. The machine is multipolar with typically 6 to 12 poles. As no iron is contained in the armature the associated losses are eliminated but the magnetic airgap tends to be relatively long which makes it appropriate to use permanent magnets to supply the magnetic field. The elimination of eddy-current and hysteresis losses combined with permanent magnet excitation lead to the high efficiency and power density mentioned above. The machine differs from the printed circuit axial field motor in that wound, multi-turn coils are used with conventional commutator and brushgear. This has the advantage of potentially higher reliability, especially under overload conditions, as the conductors are shielded from the elements. It is also possible to consider all the usual armature winding patterns (lap, wave etc.). After winding the individual coils (Fig. 1) they are nested together, connected to the commutator (Fig. 2) and the complete assembly is then encapsulated in a purpose-built mould. The stator assembly is made by fixing the segment magnets to steel flux-return rings which can form part of the motor case. A complete motor assembly is illustrated in Fig. 3.

2. MAGNET MATERIAL CHOICE

As with any permanent magnet machine the choice of magnet material depends heavily on the machine application[2]. A wide range of materials is available and the characteristic demagnetisation curves of a representative selection are shown in Fig. 4. Machines using materials of higher remanance (or higher working flux) tend to have higher values of efficiency but unfortunately these materials are usually very expensive. The relatively long airgap in the machine, especially in the traction versions, lends itself to materials of high coercivity although these do not provide a high working flux density. Clearly a compromise has to be sought but as the machine is inherently efficient it has been found possible[3] to produce designs using the cheapest material available (Barium Ferrite) which compare very favourably with similar designs[4] using the more expensive materials (Alnico and rare-earth $SmCo_5$). The ferrite material is worked well above the BH_{max} point on the demagnetisation curve (that point corresponding to optimum material utilisation) and although this means a larger amount of magnet material will be required the low cost of the material does not preclude this with the benefit apparent as a higher working flux density. However, as the flux is still less than that obtained using any other material a higher copper content in the armature must be specified to compensate. This in turn will lead to higher copper losses and thus the machine will tend to have a slightly reduced efficiency. While it is difficult to generalise here an impression of the difference in efficiency between an Alnico-magnet disc motor, a ferrite-magnet disc motor and a conventional series wound motor may be gleaned from Fig. 5, and although for the reasons stated the efficiency of the ferrite disc motor will never be as good as the alnico version the improvement over the series machine is quite dramatic. One method of reducing the effective length of the airgap in the machine, and thus the amount of magnet material required is to introduce iron powder into the epoxy resin used for encapsulating the armature[5]. However, this also introduces eddy-current and hysteresis losses and results in magnetic pull between stator and rotor.

3. USE IN BATTERY ELECTRIC TRACTION

In the original patent for the design of the machine[6] electric traction was mentioned as a specific application and the early prototypes were built for this purpose[7,8] although other, very different applications have also been found[9]. Of particular interest is the concept of motorised

wheel units[8] where the electrical machine is situated adjacent to the driven wheel and becomes part of the vehicle unsprung weight (Fig. 6). The unit should be as light as possible and thus the electric motor is designed to have a very high operating speed (in excess of 10,000 rev/min). Suitable gearing must, of course, be interposed between motor and road-wheel. More recent work has employed the more conventional layout of an inboard motor driving the wheels of the vehicle through reduction gearing. (Any solution involving direct drive of the road wheels generally necessitates the specification of a heavy and inefficient machine.)

Various projects have been established to demonstrate the benefits of drives using disc-armature motors. A machine rated at 96 V, 7.5 kW and 3400 rev/min has been built for evaluation in a small electric car based on the Reliant Robin. In this project the disc motor is being compared with an equivalent series-wound motor with both machines designed to drive through the existing 4-speed gearbox and rear axle. The disc motor employs magnets of the alnico type (Hycomax 3) which allow a moderately high air-gap flux density and lead to a very high motor efficiency (Fig. 5). Unfortunately the cost of alnico material has increased quite dramatically during the course of the project owing to a large increase in the world price of cobalt, and it is considered that magnet material of this type will not become widespread in traction motor usage. A machine using ferrite magnets has been developed for use in a hybrid sports car, the Dragonfly Nova (Fig. 7). The motor is rated at 96 V, 20 kW, 4000 rev/min and is novel in that two rotating armatures are used in a common magnetic circuit. The motor has two independent output shafts which power the rear wheels through belt-reduction gearing thereby eliminating the need for a mechanical differential gear. Significant savings in weight and cost result from adopting the twin-rotor arrangement rather than two separate motors. The vehicle also employs a disc-armature generator having many parts which are common to the motor.

Prototypes for lower power traction applications have been produced including machines rated at 12 V, 900 W, 2500 rev/min; 72 V, 1100 W, 2500 rev/min; 24 V, 130 W, 2000 rev/min and 20 V, 180 W, 4000 rev/min.

4. MOTOR PERFORMANCE

Although different in construction the disc armature motor obeys the same fundamental electromagnetic laws as any rotating electrical machine. As permanent magnets are used to provide a constant magnetic field the operating characteristics of the machine are quite straightforward.

Essentially, the rotational speed is proportional to the applied voltage and the torque developed is proportional to the current drawn. At any constant applied voltage the speed falls only slightly as the torque and current increase. The field distortion caused by armature reaction effects is negligible as the air-cored coils and large number of poles means that the demagnetising force per pole is quite small. Similarly, no permanent demagnetisation effects have been recorded with any motor of this type. The low inductance of the armature allows good commutation and thus machines with high rotational speeds may be considered, leading to high specific outputs. As the armature reaction field is negligible the brush position may be set on the neutral axis thus allowing regeneration and motor reversal to be accomplished easily. As can be seen from Fig. 5 the high motor efficiency is maintained over a wide range of power output.

An important factor in traction applications is the thermal behaviour of the motor especially when related to conditions of overload. Conventional motors have a large mass of iron in the rotor to absorb the heat produced by the armature windings. By comparison the heat storage capability of a disc armature motor is poor and the thermal performance must be based upon how quickly heat from the armature can be dissipated. The use of a permanent magnet field means, of course, that there is no heating from field windings. The armature encapsulation material must be able to withstand high temperatures without undue flexing, but it must also be able to accommodate expansion of the copper it surrounds. Good heat transfer results from the armature conductors being close to the surface of the disc and the large surface area presented by the disc geometry. The naturally induced radial airflow can also assist in the cooling process with forced cooling possible under particularly arduous conditions of operation. Extensive tests have been carried out on prototype machines in order to investigate the performance parameters thoroughly and accurately. These include measurement of armature and case temperatures under various loading conditions and it has been found possible[10] to operate the motor with armature temperatures in excess of 100^{o} C. It is necessary however to take into account the reduction in flux density at these temperatures, particularly in the case of ferrite magnets whose reversible coefficient of demagnetisation with temperature is approximately 10 times that of alnico materials.

5. MACHINE DESIGN

The design of a disc armature motor is based upon two fundamental relationships. With reference to Fig. 8 these are:

$$P \propto r_2^3 \qquad (1)$$

where P is the output power and r_2 the outer active radius (the outer radius of the magnet ring).

$$r_2 = \sqrt{3}\, r_1 \qquad (2)$$

where r_1 is the inner active radius. Equation (2) has been found[11] to yield the maximum power output for a given machine diameter. The constant of proportionality in equation (1) depends on such parameters as magnet choice, winding details, operating voltage etc., and it has been found possible[12] to derive an equation relating these factors to yield the optimum value of r_2 for a given motor speed, power, voltage, and magnet material. Having determined r_2 (and thus r_1) in this manner there are still many design possibilities available with wide variation in the number of poles and coils, for example. Specifying too few poles leads to excessively long end-windings thereby increasing the associated I^2R loss. On the other hand, since for commutation reasons, a minimum number of coils per pole must be specified, a large number of poles can result in an excessive number of coils and commutator segments and ultimately in impractical solutions. Also magnetic leakage increases with pole number. It would certainly be a tedious process to design by hand even several of these options for optimisation purposes, but fortunately digital computing techniques can be used to advantage here. Several programs have been written which ease the burden on the motor designer and the most powerful version produces a series of alternative designs when given the power, speed and voltage requirement. In addition, the designs for optimum efficiency and power density are output separately and once a given design has been chosen a set of predicted performance curves may additionally be produced.[13]

6. MOTOR CONTROL

There are several methods of controlling the speed of a battery electric vehicle ranging from the simple but inefficient resistive control to complex and expensive electronic chopper circuits. The choice of

controller rests very much with the envisaged application. For a vehicle which runs for the majority of the time at maximum speed a combination of battery switching and resistive control would probably be the best option; for those intended to operate on public roads alongside conventional i.c. engined vehicles an efficient electronic chopper may well be the most appropriate solution. While battery switching and resistive control may easily be applied to disc armature motors care must be exercised if a chopper controller is to be used. The extremely low value of armature inductance means that a high degree of current ripple will be likely at conventional switching frequencies. This is exactly the opposite condition to that found in the series wound motor whose inductance assists in sustaining a relatively constant motor current. The problem may be overcome by specifying a higher switching frequency although this entails using a power transistor instead of the more usual thyristor. There is, however, a maximum switching rate that may be used with transistors and research is continuing into this important area of application.

7. CONCLUSIONS

The disc-armature motor has been shown to have significant advantages when used in traction applications. The efficiency and power density are improved over comparable d.c. machines and the motor performs well under conditions of overload. The design of such motors is now a straightforward process using CAD procedures and, although selecting control methods requires some care, considerable benefits are nevertheless available for battery electric vehicles.

8. ACKNOWLEDGEMENTS

The authors gratefully acknowledge the support of Cableform Ltd., Electro Dynamic Construction Co. Ltd., Lee-Dickens Ltd., Moore Reed and Co. Ltd., and the Science Research Council.

9. REFERENCES

1. Charlesworth, G., 'The energy and resource implications associated with the widespread use of electric vehicles', 1st International Conference on Electric Vehicle Development, 1, 2 May 1977.

2. Corbett, A.E., and Roerig, C.S., 'Selecting permanent magnet materials for disc-armature d.c. motors', International Conference on Electrical Machines, Brussels, SP4/2 Sept. 1978.

3. Corbett, A.E., and Roerig, C.S., 'The economic design of disc-armature traction motors', Electric Vehicle Developments, 5, March 1980.

4. Campbell, P., 'Permanent-magnet motors for electric vehicles', Electric Vehicle Developments, 3, September 1979.

5. Stott, G., 'Iron powder compacts for electromagnetic applications' M.Sc. thesis, University of Warwick, 1971.

6. Carter, A.H. and Corbett, A.E., 'Electric motor', British Patent 1231782, 1971.

7. Corbett, A.E., 'A disc-armature d.c. motor', EM70 Conference, Dundee, 1970.

8. Campbell, P., 'A new wheel motor for electric commuter cars', Electrical Review, Vol. 190, 1972.

9. Corbett, A.E., and Mohammad, M.T., 'The disc-armature d.c. motor and its applications', IEE Conference Publication 136, Small Electrical Machines, 1976.

10. Ali, M.R.N., Corbett, A.E., Ozpolat, M.A., and Roerig, C.S., 'Design and performance of d.c. disc-armature motors for traction applications', Fifteenth Universities Power Engineering Conference, 3B2, Leicester, March 1980.

11. Corbett, A.E., 'Disc-armature motors', University of Warwick report, 1970.

12. Roerig, C.S., 'D.C. disc-motors', University of Warwick report, 1977.

13. Corbett, A.E., and Roerig, C.S., 'Computer-aided design of permanent magnet motors', First United Kingdom Conference on Permanent Magnets, London, June 1980.

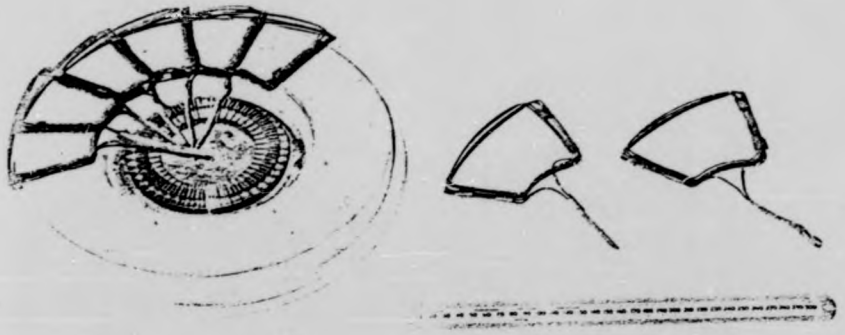

Fig. 1: Coils of armature winding

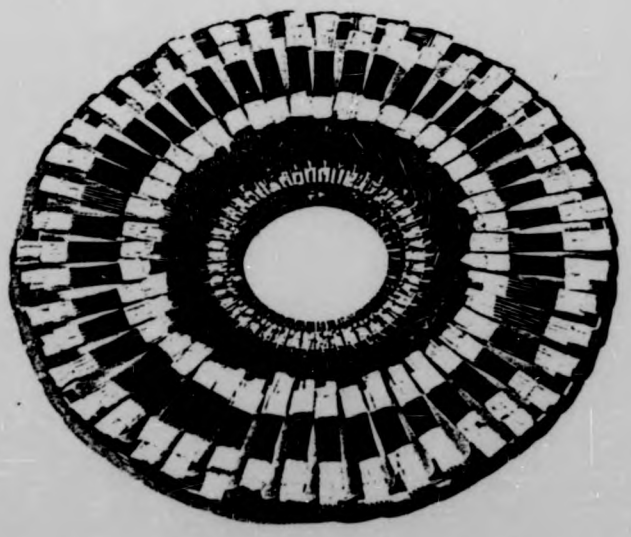

Fig. 2: Armature winding connected to commutator

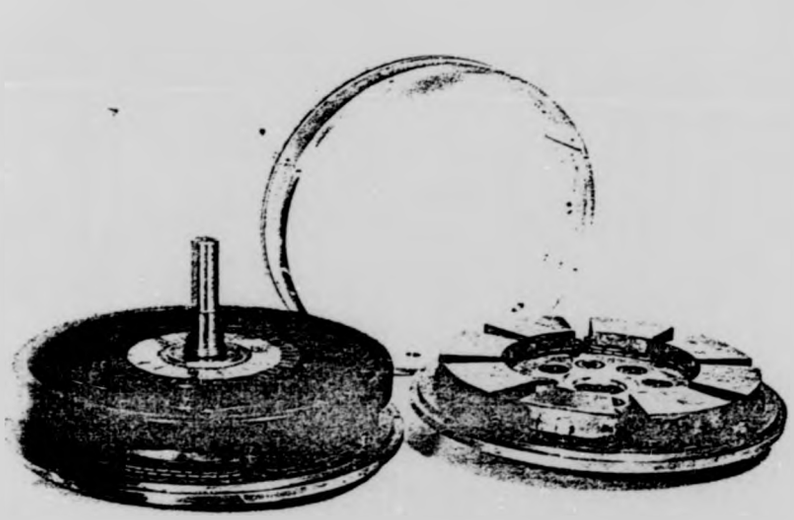

Fig. 3: Components of complete motor

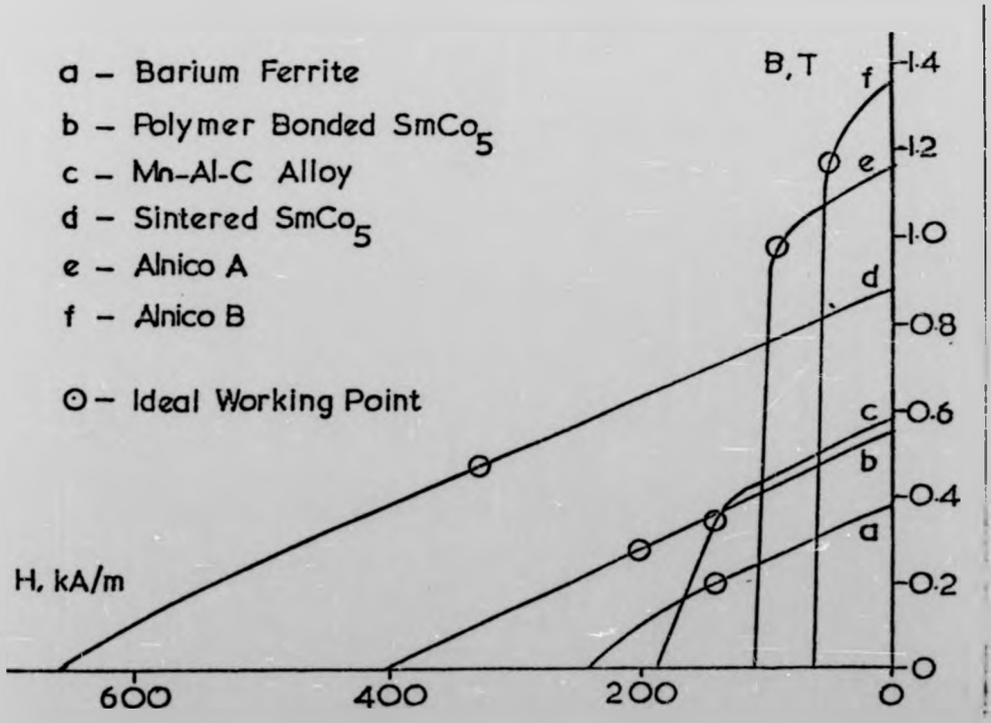

Fig. 4: Characteristics of permanent magnet materials

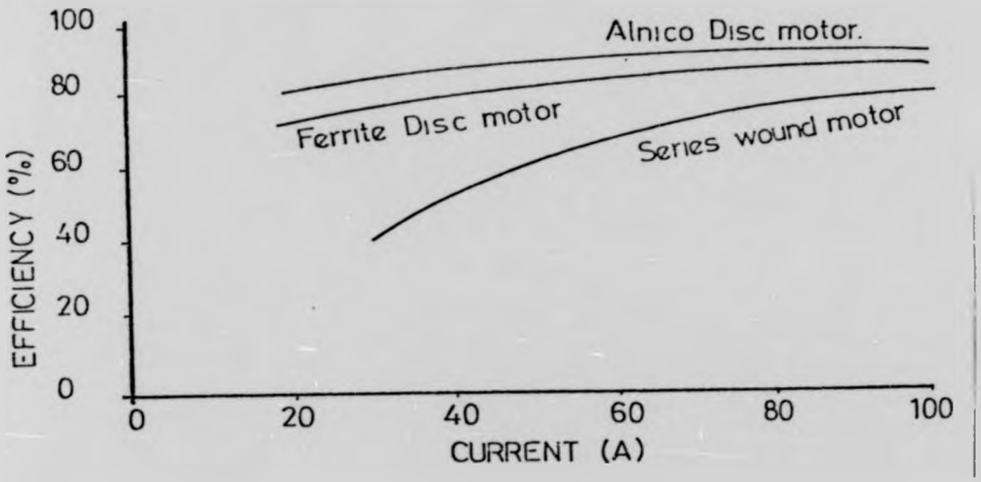

Fig. 5: Comparative motor efficiency characteristics

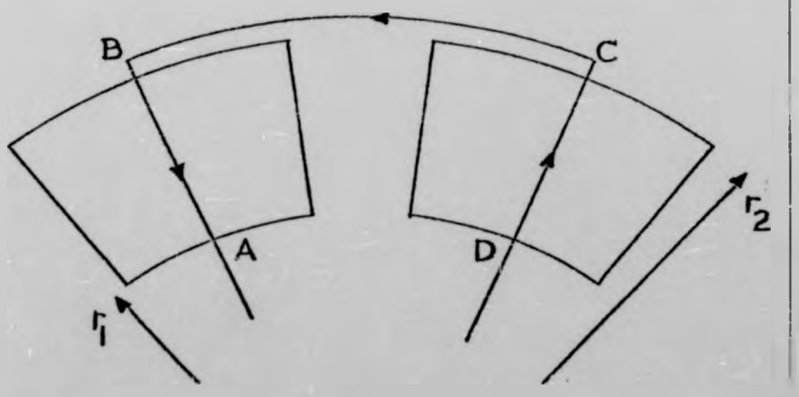

Fig. 8: Schematic of magnets with a single-turn coil

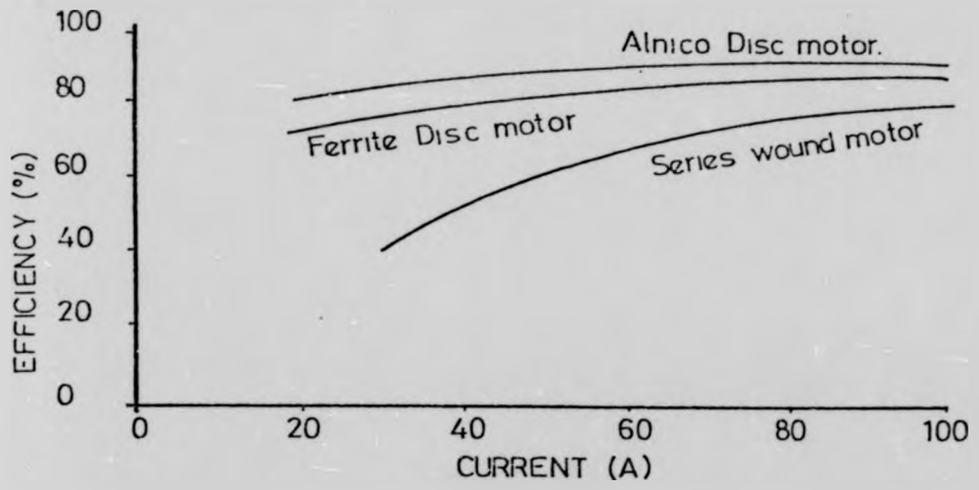

Fig. 5: Comparative motor efficiency characteristics

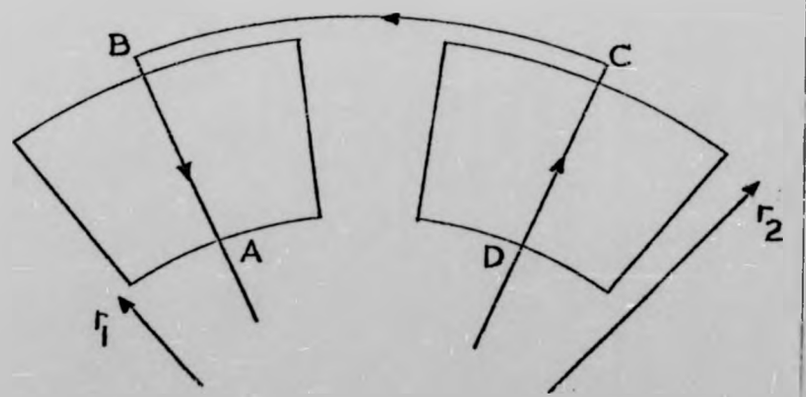

Fig. 8: Schematic of magnets with a single-turn coil

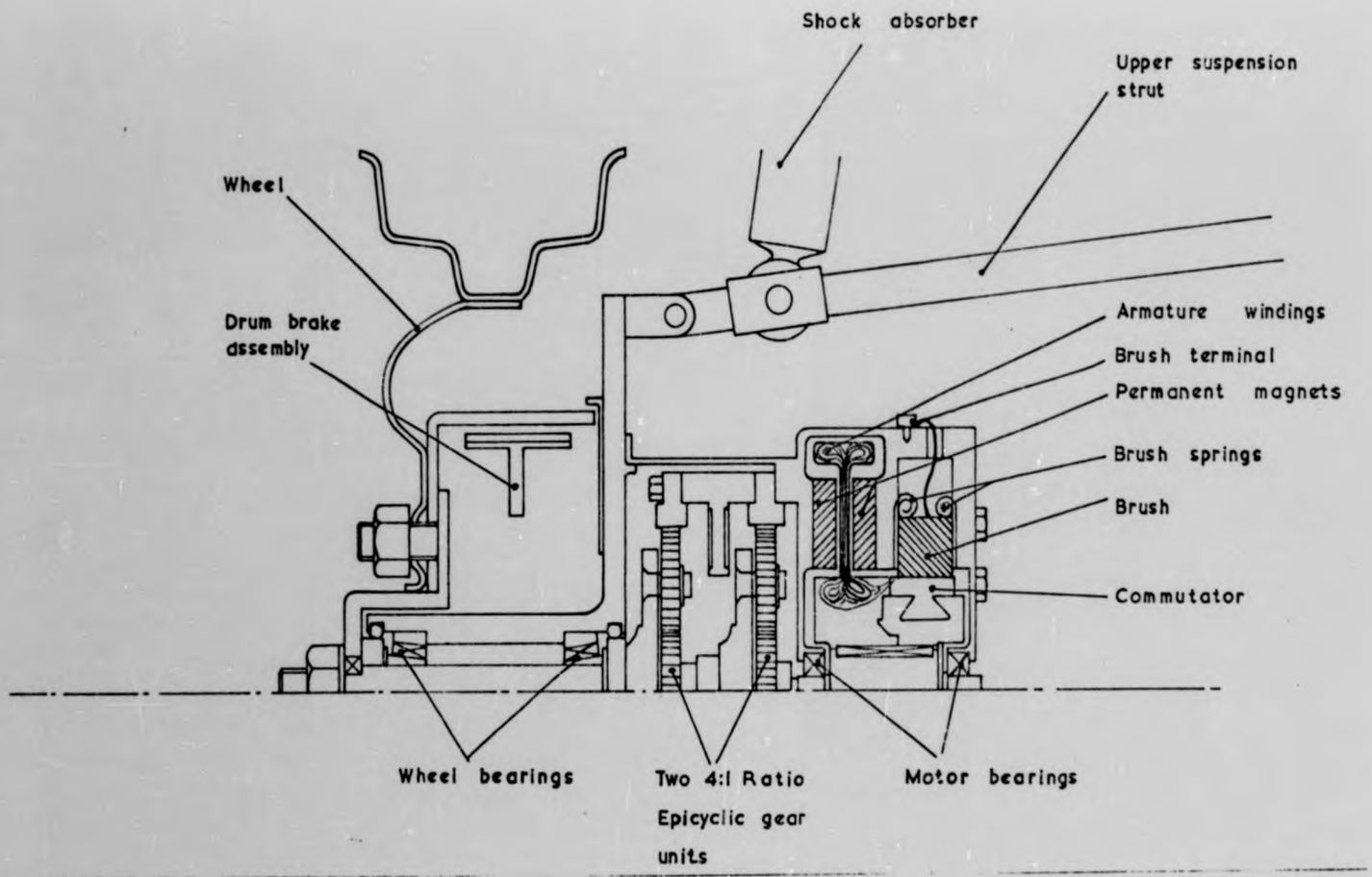

Fig. 6: Motorised wheel unit

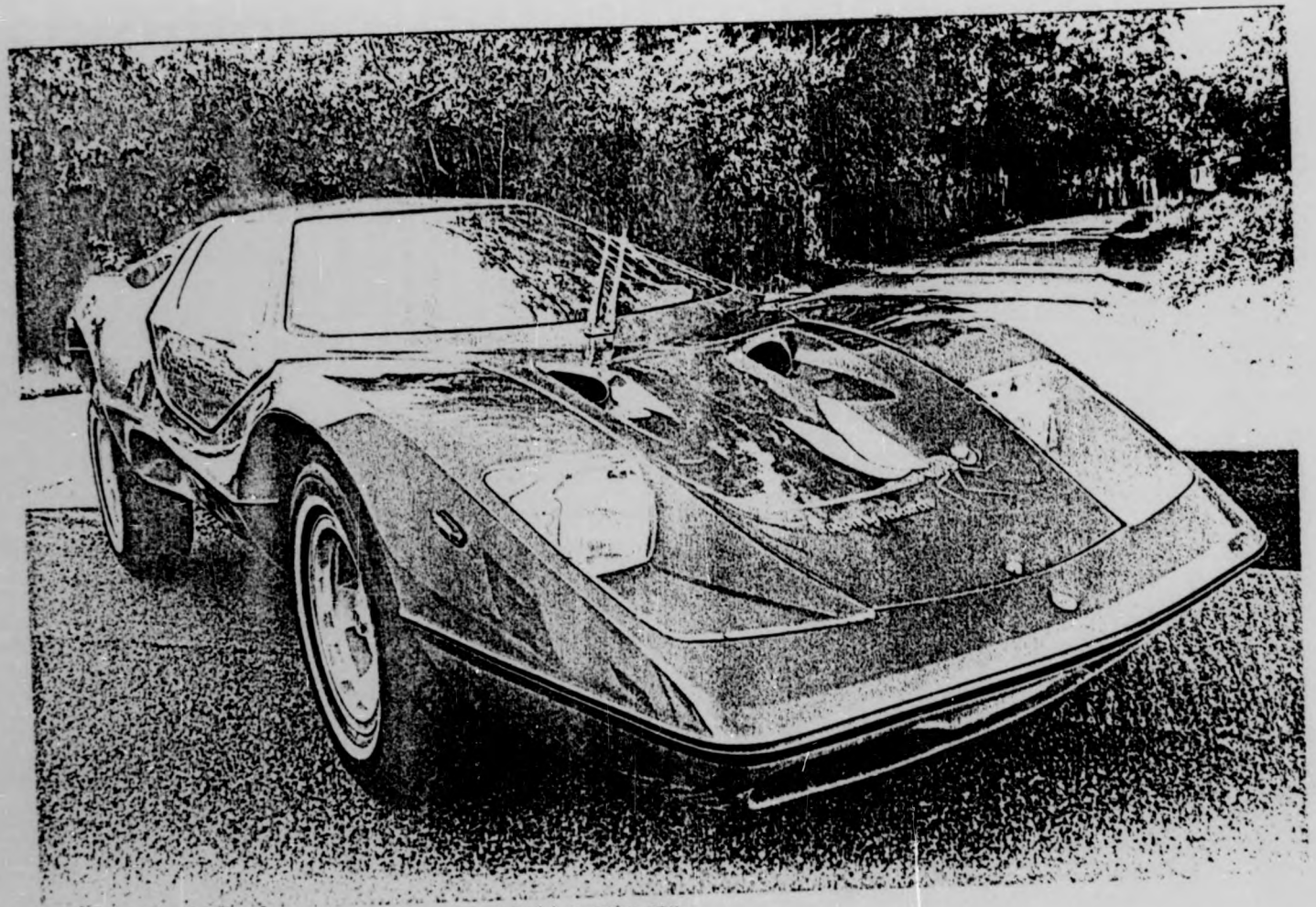

Fig. 7: The Dragonfly Nova hybrid sports car

DESIGN AND PERFORMANCE OF A 10 kW D.C. DISC MOTOR WITH FERRITE MAGNETS

M.R.N. Ali and A.E. Corbett
University of Warwick, UK

INTRODUCTION

Development of the axial-field, permanent-magnet, d.c. disc motor has demonstrated significant improvements over conventional machines in terms of efficiency and power density, giving the machine good potential for application in electric and hybrid vehicles. Furthermore the short axial length and high power-to-volume ratio of the machine facilitate the design of compact traction systems.

The essential difference between the d.c. disc motor[1] and its conventional counterpart lies in the disposition of the active conductors and the working magnetic flux: in the disc motor the magnetic flux is parallel to the shaft and the active conductors are perpendicular to it. This configuration lends itself well to high pole number designs, and the heavy steel yoke of conventional machines is replaced by thin-section steel flux return rings and a light alloy frame. Using permanent magnets it is practicable to employ a coreless armature construction which further promotes weight saving and means that no iron is subject to a varying magnetic flux. The absence of iron losses and elimination of the requirement for excitation power are both helpful in the quest for high efficiency.

MAGNETIC CIRCUIT

The axial magnetic field is produced by permanent magnet poles which are segments of a toroid, alternately magnetised and bonded to a steel ring to provide a magnetic path to adjacent magnets. The magnetic circuit is completed either by a second set of poles or a steel ring only on the other side of the air gap.

The air-gap length is determined largely by the choice of permanent magnet material. Fig. 1 shows demagnetisation curves of three magnetic materials which are commonly considered. Design studies have shown that if the selection of magnetic material is based on obtaining maximum power density for the machine then samarium cobalt should be specified. To achieve the highest flux density in the air gap alnico should be selected, but the length of the poles can be excessive owing to the relatively low coercivity. The main drawback of both samarium cobalt and alnico materials is that their costs are prohibitively high for many commercial applications.

In contrast, the cost of ferrite material is low enough to make it viable in spite of its low remanence and energy density. For economic use of magnet material it is general practice to work the material near to the point on the demagnetisation curve which gives $(BH)_{max}$, but in the case of ferrites it is beneficial in terms of overall cost effectiveness to work the material at higher values of flux density owing to the low cost and low density of the material. In this way acceptable air gap flux densities can be achieved without incurring excessive weight and cost penalties. However, since the flux density is still low in comparison with electromagnetically excited machines, a high copper content in the armature must be specified to compensate.

THE DISC ARMATURE

The armature has a coreless, disc-shaped winding, the wire-wound coils of which have an even number of layers and are encapsulated in a plastics material to form a rigid disc having no core loss (eddy current, hysteresis) since it is iron free. As in any electrical machine, the electrical loading is limited by the power loss in heating and the permissible temperature rise. The current density specified at the design stage depends on the method of cooling to be employed and the relative importance of efficiency and power density in the particular application.

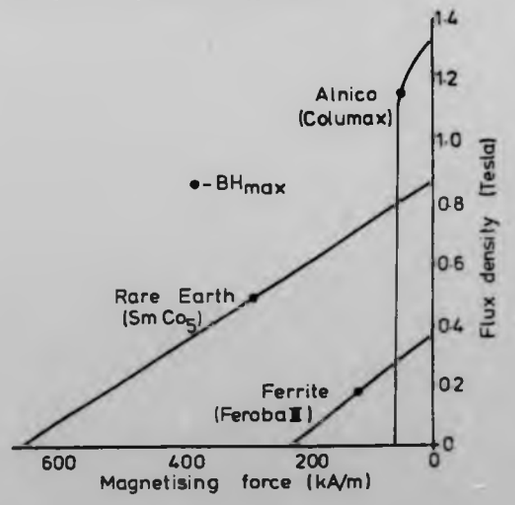

Fig. 1 : Demagnetisation curves.

DESIGN OPTIMISATION

The fundamental relationships of disc motor design are

$$P \propto r_2^3 \quad (1)$$

$$r_2 = \sqrt{3}\, r_1 \quad (2)$$

where P is the output power, and r_1 , r_2 are, respectively, the inner and outer active radii of the disc[3].

Equation (1) has a constant of proportionality which depends on parameters such as magnet material, winding connection, etc. and it is possible to determine the optimum value of r_2 for a given motor speed, power, voltage and magnetic material. Equation (2) must be satisfied in order to achieve the maximum power output for a given machine diameter.

A computer aided design procedure has been developed to generate design data and predicted performance characteristics. In the first stage of the design procedure the program produces a series of alternative designs for a specified power, voltage and speed, and highlights the two unique designs which give optimum efficiency and optimum power density[4]. The second stage of the procedure provides the facility for 'fine-tuning' the design parameters to meet the particular requirements of the application.

TWIN ARMATURE MOTOR

To illustrate the results which can be achieved from application of the above concepts and design philosphies a 96 V, 10 kW, 4000 rev/min motor is described. In fact a twin-armature version[5] rated at 20 kW has been developed for the drive of an experimental hybrid sports car. This machine (Fig. 2) comprises a common magnetic circuit which houses two disc armatures, each armature independently driving an output shaft which transmits power to a road wheel through belt-reduction gearing, thereby eliminating the need for a mechanical differential gear. Significant savings in weight and cost result from adopting the twin-rotor arrangement rather than two individual motors.

Since the machine has a constant magnetic field (at a given magnet temperature) the speed-voltage and torque-current characteristics are linear. Owing to the large number of poles (8), and the high mmf of the magnets, it is found that armature reaction has a negligible effect on the working magnetic field. There is no measurable shifting of the neutral axis, thus allowing the brushes to have a unique position for different loads including reversing and regeneration. This property coupled with low armature inductance leads to very good commutation.

Fig. 3 shows test results on the motor at the rated voltage of 96 V together with efficiency curves for other operating voltages. It is clear that the machine achieves high efficiency over a wide range of operating conditions and should show good energy economy in electric vehicle applications. The experimental results were obtained on a single-disc, self-ventilated version of the machine and in view of the modest temperatures attained on test it is concluded that it might be possible to achieve a further increase in efficiency by reducing the air flow and hence the resulting windage losses.

REFERENCES

1. Carter, A.H. and Corbett, A.E., 1971, 'Electric motor', British Patent 1231782, 1971.

2. Corbett, A.E. and Roerig, C.S., 1978, 'Selecting permanent magnet materials for disc-armature d.c. motors', ICEM, Brussels, SP4/2.

3. Ali, M.R.N. et al, 1980, 'Disc-armature traction motors', Drive Electric 80 Conference, London.

4. Corbett, A.E. and Roerig, C.S., 1980, 'Computer-aided design of permanent magnet motors', First U.K. Conference on Permanent Magnets, London.

5. Ali, M.R.N. et al, 1980, 'Design and performance of d.c. disc-armature motors for traction applications', Fifteenth Universities Power Engineering Conference, 3B2, Leicester.

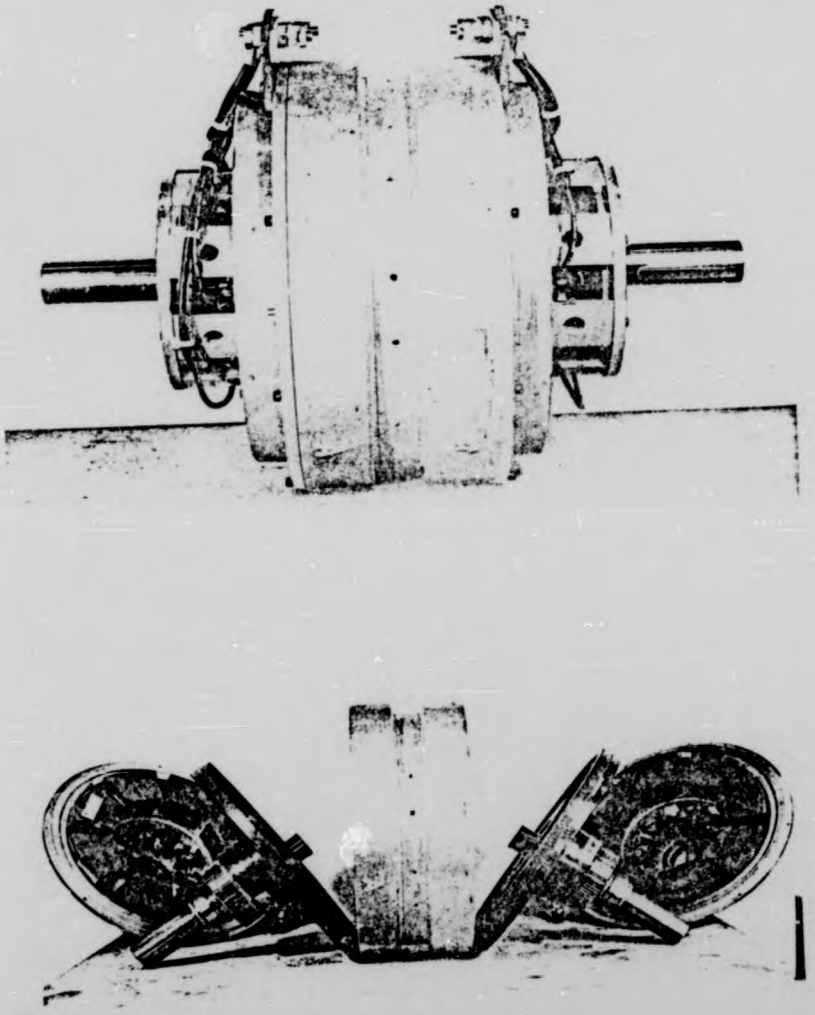

Fig. 2: 20 kW twin-armature disc motor (overall diameter 400 mm).

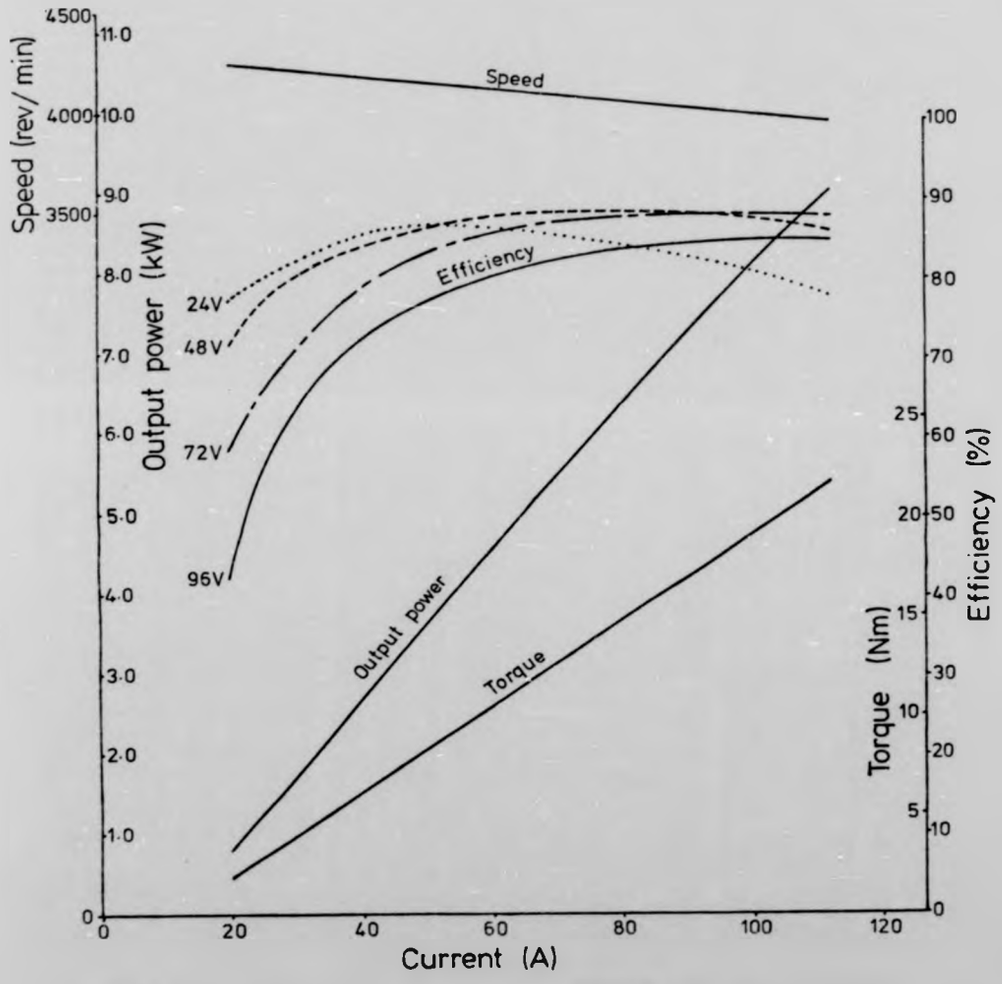

Fig. 3. : Test results of 10 kW disc motor showing [illegible] at 96V and efficiency at other voltages.

Note: The rating of the loading machine [illegible] motor on test to a figure slightly less [illegible].

DESIGN AND PERFORMANCE OF 10 kW DISC MOTOR FOR ELECTRIC VEHICLE DRIVES

M.R.N. Ali and A.E. Corbett, University of Warwick, Coventry, U.K.

INTRODUCTION

Owing to the limitation on range and performance imposed by today's lead acid batteries it is vital that the drive system components in electric and hybrid vehicles be designed for high efficiency. Even with present day batteries it is possible to build vehicles with acceptable range and performance if high efficiency can be achieved in the energy conversion process between battery and road wheels. To this end research at Warwick University has been directed towards developing high efficiency disc motors for traction applications[1]. Recently the disc machine has been applied to a hybrid car in which a twin armature motor provides tractive power while a single armature version of the same machine is employed as an engine-driven generator.

The disc motor, in addition to meeting the essential traction requirements of peak torque capability, high efficiency and high power density offers additional merits as compared to conventional traction motors. The short axial length and high power-to-volume ratio facilitate the design of compact traction systems. Reliability is high owing to the absence of a wound field and brush life is longer owing to the excellent commutation which results from low armature inductance.

CONSTRUCTION AND DESIGN OF DISC MOTOR

In the disc motor the working flux is produced by a multipolar system of permanent magnets. The magnets have a sector shaped pole face, being cut from an annular ring of the material. The magnet length depends on the type of permanent magnet material used and the airgap length. The poles are magnetised in alternative sequence and backed by a mild steel ring of the same ratio and sufficient thickness to provide a magnetic path to adjacent magnets without saturation. The part of the magnetic circuit which borders the other side of the airgap can be completed either by a second set of poles or a steel ring only. This configuration lends itself well to high pole number designs, and the heavy steel of conventional machines is replaced by thin-section steel flux return rings and a light alloy frame which gives appreciable increase to the power density of the machine.

The armature has a coreless, disc-shaped winding, the pre-formed wire-wound coils of which form two flat layers of active conductor having different lengths and levels to allow the individual coils to be nested together. The coils are connected to the commutator in the usual armature patterns (lap, wave etc.) and the complete assembly is then either encapsulated in plastic material using a steel mould or is wrapped with heat-curing glass-fibre tapes and dipped in varnish to give a "skeleton" construction. There is no iron in the armature and consequently no associated eddy current and hysteresis losses, and as the magnetic flux is provided by permanent magnet material there is no requirement for field-winding power and no associated heating. Eliminating stator losses and armature iron losses naturally leads to a relatively high efficiency machine.

CHOICE OF MAGNETIC MATERIAL

A wide range of magnetic material is suitable for use in the motors, ranging from sintered ferrite to rare earth-cobalt. Given that the airgap of the disc motor is quite large because it embraces the thickness of the armature disc as well as the necessary running

clearance on either side, magnetic material of high coercivity is needed, especially in traction applications in which high torque (and high armature currents) can result in high demagnetising fields. The ferrites exhibit high coercivity and owing to their low cost are well suited to the application in spite of their low remanence. The use of high remanence magnets enables motors of slightly higher efficiency to be designed, but, owing to the relatively low coercivity of these materials the amount of magnetic material is large when an air-gap of considerable span is needed. Fig 1 shows demagnetisation curves of three magnetic materials which are commonly considered. Design studies[2] have shown that if the selection of magnetic material is

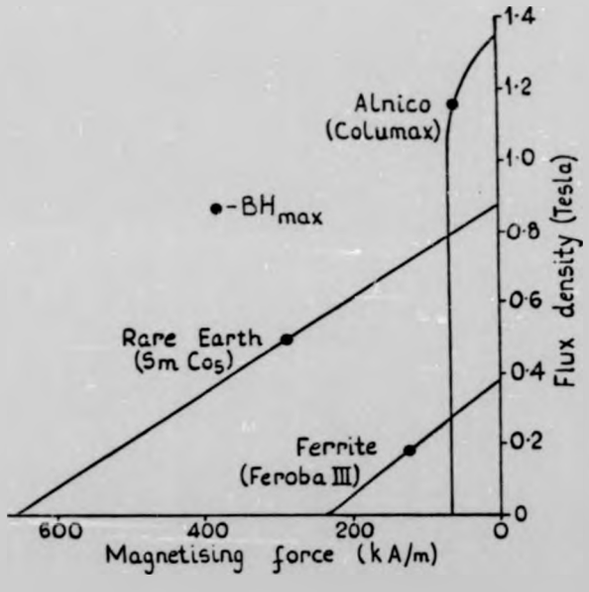

Fig. 1: Demagnetisation curves of some permanent magnet materials

based on obtaining maximum power density for the machine then samarium cobalt should be specified whereas to achieve the highest flux denisty in the airgap alnico should be selected. The main drawback of both samarium and alnico materials is that their costs are prohibitively high for many commercial applications. In contrast, the cost of ferrite materials is low enough to make it viable in spite of its low remanence and energy density.

For economic use of magnetic material it is general practice to work the material near to the point on the demagnetisation curve which

gives (BH) Max, but in the case of ferrites it is beneficial in terms of overall cost effectiveness to work the material at higher values of flux density owing to the low cost and low density of the material. In this way acceptable air gap flux densities can be achieved without incurring excessive weight and cost penalties. However, since the flux density is still low in comparison with electromagnetically excited machines, a high copper content in the armature must be specified to compensate. For this reason ferrite magnets have been listed in the specifications of the disc armature motor because the cost saving they represent is more significant than the small loss of efficiency of the motor.

One way of reducing the airgap in the magnetic circuit is to introduce iron powder in the epoxy resin which forms the armature encapsulant[3]. Unfortunately, this produces eddy-current and hysteresis losses and rotor-stator magnetic attraction, and consequently it is not usually specified.

PERFORMANCE AND CHARACTERISTICS OF THE MOTOR

Since the machine has a constant magnetic field (at a given magnet temperature) the speed-voltage and torque-current characteristics are linear. Owing to the large number of poles (8) and the high mmf of the magnets it is found that armature reaction has a negligible effect on the working magnetic field. There is no measurable shifting of the neutral axis, thus allowing the brushes to have a unique position for different loads including reversing and regeneration. This property coupled with low armature inductance leads to very good commutation.

Fig. 2 shows test results on a 10 kW, 4000 rev/min motor at the rated voltage of 96V together with efficiency curves for other operating voltages. It is clear that the machine achieves high efficiency over a wide range of operating conditions and should show good energy economy in typical traction duty cycles. The experimental results shown were obtained on a single-disc, self-ventilated "skeleton" version of the machine and in view of the modest temperatures attained on test it is concluded that it might be possible to achieve a further increase in efficiency by reducing the airflow and hence the resulting windage losses.

TWIN ARMATURE MOTOR FOR HYBRID CAR

Results of recent projects[4] on electric and hybrid vehicles clearly demonstrate the high penalty to be paid in power losses when using conventional transmissions, including 4-speed gearboxes, which have been primarily designed for i.c. engined vehicles. To avoid such a penalty, a twin armature disc motor with differential action has been developed for the drive of an experimental hybrid sports car[5]. This machine (Fig. 3 and Fig. 4) comprises a common magnetic circuit which houses two disc armatures, each armature mechanically driving an independent output shaft which transmits power to a road wheel through belt-reduction gearing, thereby eliminating the need for a mechanical differential gear. The twin armature motor and belt reduction gears have been carefully designed to fit within the limited span between the two road wheels in the space usually occupied by the differential rear axle drive. Significant savings in weight and cost result from adopting the twin rotor arrangement rather than two individual motors, and furthermore the absence of the differential gearbox cancels the associated mechanical losses and weight which has a positive effect on the overall efficiency and weight of the hybrid vehicle. The twin armature motor offers a simple and reliable traction system which needs less service and maintenance which, in turn, reduces the running cost. In addition to the twin armature disc motor, the vehicle is fitted with an on-board engine-generator set to provide the average power requirement while the batteries are specified to provide excess

motive power and to store surplus generated (included regenerative)

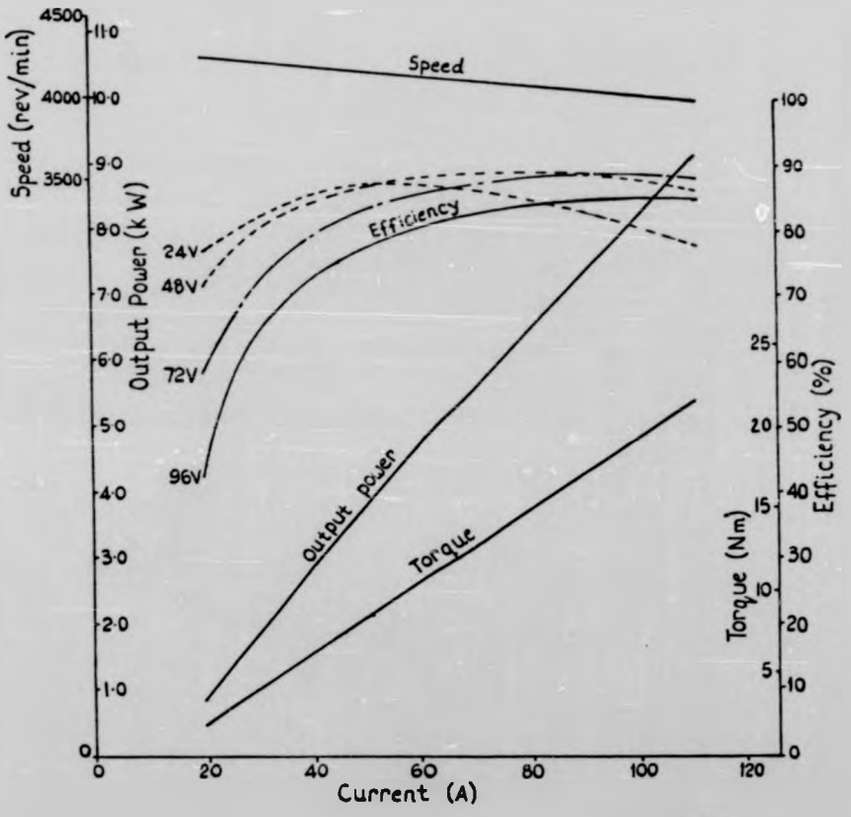

Fig. 2: Test results of 10 kW disc motor showing performance characteristics at 96V and efficiency at other voltages. (Note: The rating of the loading machine limits the maximum torque of the disc motor on test to a figure slightly less than the full-load value).

power. The vehicle is a series hybrid and the most suitable application is in frequent stop/start driving, such as city driving, or the duty cycle of delivery vehicles. A schematic diagram of the vehicle system is shown in Fig. 5, It consists of batteries, controller, twin

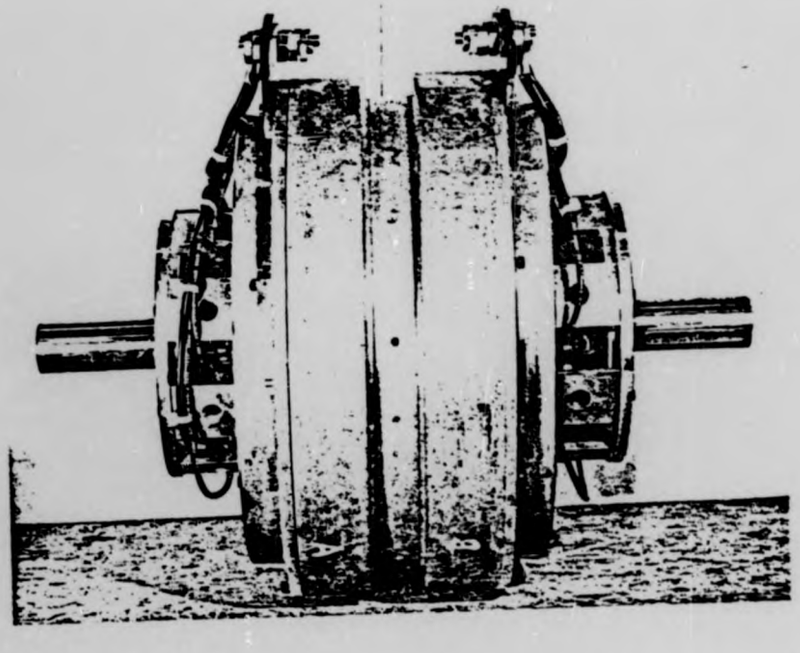

Fig. 3: Prototype twin armature disc motor

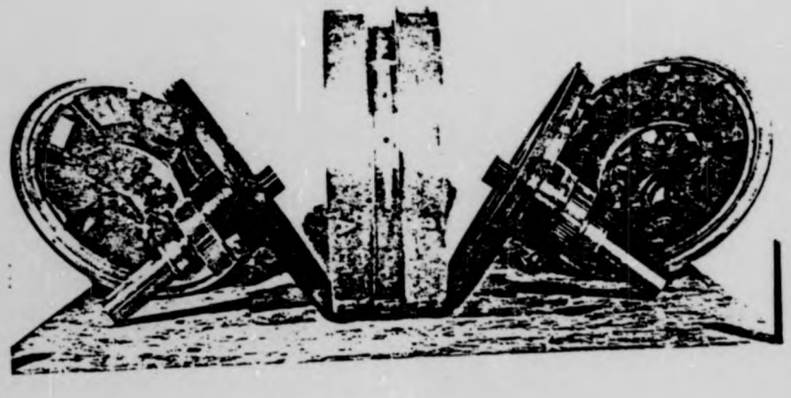

Fig. 4: Components of motor shown in Fig. 3

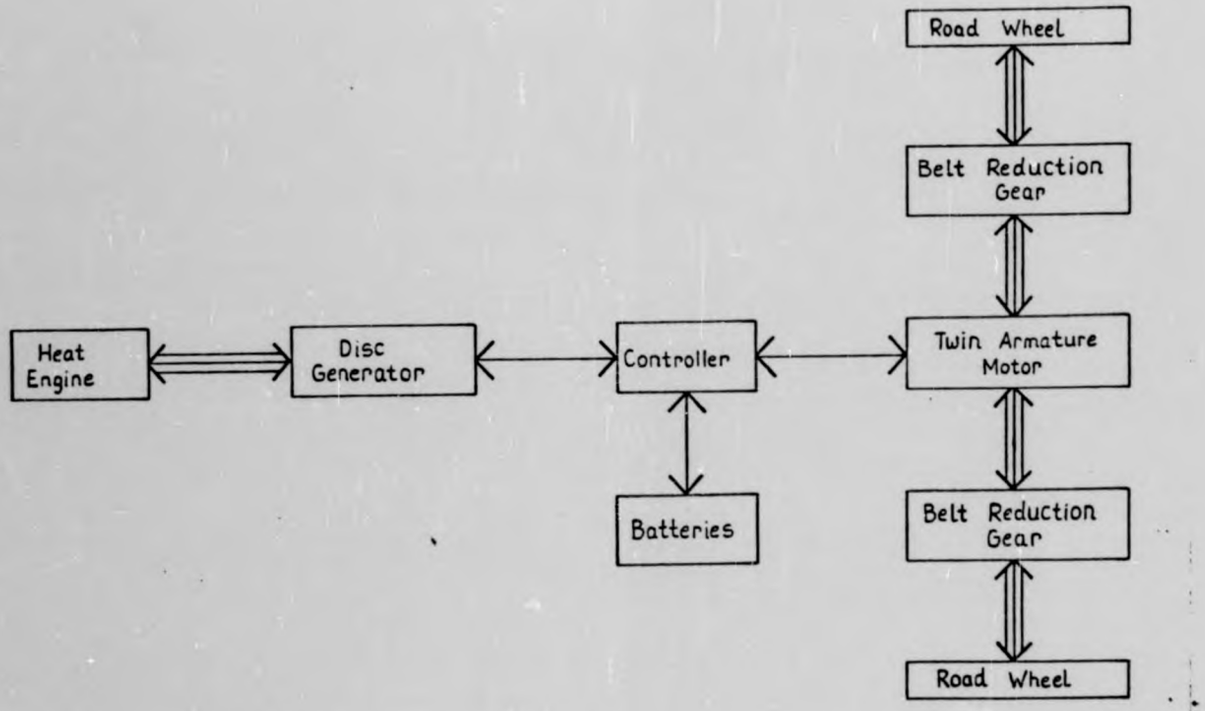

Fig. 5: Drive system of hybrid car with twin-armature disc motor drive

disc motor, disc generator-diesel engine, belt reduction gears and the road wheels. The engine is a twin-cylinder diesel unit suitably sized to meet the vehicle's average power requirement. The d.c. generator is identical mechanically to the single disc armature motor and the same components are used in its manufacture. The only significant difference is the design of the armature winding which is tailored to match the engine and battery characteristics. Owing to the short axial length of the disc generator it can be mounted on the engine as an overhung load thereby obviating the need for an elaborate bedplate and coupling arrangement. The disc armature adds to the flywheel effect of the engine. The end frame comprising the brushgear neatly closes the bell-shaped housing. Furthermore the disc generator is capable of acting as a starting motor for the engine, with direct drive. Indeed, the disc machine is capable of developing more than sufficient power to turn the engine from cold for sustained cranking. The generator output can be controlled electronically which requires semi-conductors of high power rating. Alternatively, it may be possible to achieve satisfactory regulation by speed control of the engine or even by varying the airgap mechanically (and hence the flux).

REFERENCES

1. Carter, A.H. and Corbett, A.E., 1971, 'Electric motor', British Patent 1231782, 1971.
2. Corbett, A.E. and Roerig, C.S., 1978, 'Selecting permanent magnet materials for disc-armature d.c. motors', ICEM, Brussels, SP412.
3. Stott, G., 1971, 'Iron powder compacts for electromagnetic applications', M.Sc. thesis, University of Warwick.
4. Corbett, A.E. and Roerig, C.S., 1981. 'Energy utilisation in electric vehicles', Electric Vehicle Developments, September 1981.
5. Lee, G.A. and Corbett, A.E., 1979, 'Development of a hybrid electric vehicle using high efficiency disc motors', EVDG Conference, London.